UNIVERSITY OF SOUTHAMPTON

FACULTY OF PHYSICAL SCIENCES AND ENGINEERING

Department of Electronics and Computer Science

Dynamic Rating for Improved Operational Performance

by

Rui Huang

Thesis for the degree of Doctor of Philosophy

August 2015

UNIVERSITY OF SOUTHAMPTON

ABSTRACT

FACULTY OF PHYSICAL SCIENCES AND ENGINEERING

Thesis for the degree of Doctor of Philosophy

DYNAMIC RATING FOR IMPROVED OPERATIONAL PERFORMANCE

by Rui Huang

Many power transmission systems are under pressure from increasing load demand as well as changes in power flows due to the evolution of the power market and the integration of renewable energy generations. At the same time, limited finance for installing new cables and the difficulties in reinforcement of existing circuits in urban areas incentivize transmission operators around the world to find ways to maximize the flexibility and usage of their existing transmission network. As a result, it is crucial to adopt new current rating methods which are able to optimize asset utilization, minimize risk and reduce the constraint costs incurred by transmission system operators.

Historically, most cable thermal ratings are continuous ratings, with fixed seasonal values for a certain cable circuit. They are based on worst-case assumptions and are not able to consider the real-time environmental conditions. The ignorance of the real-time change in environmental conditions, which control the rate of heat dissipation from the cable, makes continuous ratings generally conservative. However, the rating values can also be optimistic for some extreme situations such as thermal runaway in the soil around the cables, which might cause overheating.

Several dynamic rating systems have been applied to the existing underground cable in practice by using online monitoring data. Some worst case assumptions used in conventional cable rating standards have been removed. Such systems have been reported to deliver increases of 5-20% in cable current capacity. However, most existing dynamic rating systems can only determine a short-term rating at the current time step. It would be valuable for transmission operators to know the short-term rating in advance to assist in day-ahead planning.

To solve this problem, a predicted rating system, which is capable of providing network operators with accurate short term current ratings at the day ahead stage, has been developed in this work. This novel cable rating concept integrates a day-ahead load forecasting system into the dynamic rating system to provide the time-limited short-term rating calculated forward from any point within the next 24 hours.

Some shortcomings of existing rating methods for different kind of insulated cable installations have been detected and overcome. More suitable models have been built, compromising between accuracy and solution speed to fit them into the predicted rating system.

A day-ahead load forecasting system has been built by using the Support Vector Regression (SVR) method. Dynamic thermal models are used to translate the load prediction into thermal prediction 24 hours ahead. Thus, the time-limited short-term ratings can then be calculated 24hrs ahead, based on the predicted load data and cable temperature data. In addition, an error estimation system has been integrated to estimate the predicted conductor temperature error quickly, thus increases the reliability of the predicted rating system.

Utilizing this predicted rating system has the double benefit of reducing variations in dynamic ratings (which makes them difficult to plan with), while reducing the risk of thermally overloading the cable, thus prematurely ageing the dielectric.

For a large scale transmission network, the dynamic rating and predicted rating systems for all the cable circuits might require huge amounts of computation and very long solution times, which make their application impractical and infeasible. The idea of using a machine learning method, such as Support Vector Regression, has been shown to dramatically reduce the solution time for dynamic rating calculations.

Contents

Symbols and Abbreviations

ACF	autocorrelation function	
b	variable in convective heat transfer coefficient equation for forced cooling	
c	variable in convective heat transfer coefficient equation for natural cooling	
C	cost of error to determines the trade-off between the flatness and losses	
C_A	thermal capacitances of the conductor and the inner part of the dielectric	$Jm^{-1}K^{-1}$
C_B	thermal capacitances of the remainder of the cable	$Jm^{-1}K^{-1}$
C_E	constant in convective heat transfer coefficient equation from Electra 143	
Corrcoef	correlation coefficient of two group of data	
Cov	covariance of two group of data	
C_W	coefficient in Weedy forced cooling convective heat transfer equation for horizontal tunnel	
D_e*	external diameter of the cable	m
D_{tun}	diameter of inner tunnel surface	m
E	coefficient in IEC 60287 heat transfer equation on cable surface	
Error(t)	processed load error for *t* hour ahead prediction	A^2
F	coefficient in Weedy natural cooling convective heat transfer equation for horizontal tunnel	
f	frequency of the applied voltage	Hz
g	acceleration due to gravity	ms^{-2}
g_i	coefficient in IEC 60287 heat transfer equation on cable surface	
Gr	Grashof Number (ratio of buoyancy to viscous force acting on a fluid)	
h	heat dissipation coefficient	$Wm^{-2}(K)^{-5/4}$
h_{conv}	heat transfer coefficients for convection from the cable surface to ambient air	$Wm^{-2}K^{-1}$
$h_{conv,f}$	convective heat transfer coefficient forforced cooling	$Wm^{-2}K^{-1}$
$h_{conv,m}$	mixed convection heat transfer coefficient	$Wm^{-2}K^{-1}$

$h_{conv,n}$	convective heat transfer coefficient for natural cooling	$Wm^{-2}K^{-1}$
h_l	time lag in ACF	h
h_{rad}	heat transfer coefficients for radiation from the cable surface to ambient air	$Wm^{-2}K^{-1}$
h_t	total heat transfer coefficient from cable surface to ambient air	$Wm^{-2}K^{-1}$
h_{wall}	the convective heat transfer coefficient from air to tunnel wall	$Wm^{-2}K^{-1}$
$h_{wall,n}$	natural cooling convective heat transfer coefficient at the tunnel wall	$Wm^{-2}K^{-1}$
I	conductor current	A
k	thermal conductivity	$Wm^{-1}K^{-1}$
K	Kernel function	
k_{air}	thermal conductivity of the air	$Wm^{-1}K^{-1}$
K_{angle}	wind direction factor in IEEE 738 standard	
K_r	constantin in radiative heat transfer coefficient equation from Electra 143	
k_r	effective emissivity	
L	length of riser shaft	m
$L(t)$	hourly load at time t	A
m	variable in convective heat transfer coefficient equation for natural cooling	
p	coefficient in Weedy natural cooling convective heat transfer equation for horizontal tunnel	
P	variable in convective heat transfer coefficient equation for forced cooling	
Pr	Prandtl Number (ratio of kinematic viscosity to thermal diffusivity)	
R_{ac}	conductor AC resistance at the maximum operating temperature	Ωm^{-1}
Re	Reynolds Number, the ratio of inertial forces to viscous forces	
Re_{eff}	effective Reynolds Number for mixed convection	
Re_{eq}	equivalent Reynolds Number for natural convection	
T	temperature	K

$T(t)$	hourly temperature at time t	°C
T_0	constant temperature on the boundary	K
T_4	external thermal resistance of the cable	KmW^{-1}
T_A	thermal resistance of the dielectric	KmW^{-1}
$tan\ \delta$	tangent of the dielectric loss angle	
T_B	thermal resistances of the remainder of the cable	KmW^{-1}
T_{conv}	thermal resistances to simulate convection from cable surface to ambient air	KmW^{-1}
T_{in}	internal thermal resistance of the cable	KmW^{-1}
T_{rad}	thermal resistances to simulate thermal radiation from cable surface to ambient air	KmW^{-1}
U	phase voltage	V
U_{air}	air velocity	ms^{-1}
W_a	armour losses	Wm^{-1}
W_c	conductor losses	Wm^{-1}
W_d	dielectric losses	Wm^{-1}
W_s	sheath losses	Wm^{-1}
W_t	total heat generation	Wm^{-1}
x_i	input features for SVR training	
y_a	actual values in MAPE equation	
y_i	associated output value of x_i in SVR training	
y_p	predicted values in MAPE equation	
Z	coefficient in IEC 60287 heat transfer equation on cable surface	
α	smoothing factor in exponentially weighted moving average equation	
α_i	Lagrange multipliers	
α_i^*	Lagrange multipliers	

β	the volumetric thermal expansion coefficient	K^{-1}
γ	variable in RBF kernel function	
ε	allowed deviation in the SVR training	
η_c	correction factor of multi-cable in natural convective heat transfer coefficient equation for horizontal tunnel	
η_i	Lagrange multipliers	
η_i^*	Lagrange multipliers	
η_{wh}	correction factor of horizontal wall in natural convective heat transfer coefficient equation for horizontal tunnel	
η_{wv}	correction factor of vertical wall in natural coolingconvective heat transfer coefficient equation for horizontal tunnel	
θ_{amb}	ambient air temperature	°C
θ_{amb}^*	ambient air temperature	K
θ_c	cable conductor temperature	°C
$\theta_{c\_initial}$	initial cable conductor temperature	°C
θ_s	cable surface temperature	°C
θ_s^*	cable surface temperature	K
θ_{wall}	temperature of inside tunnel wall	°C
λ	sheath and armour loss factor	
λ_1	sheath loss factor	
λ_2	armour loss factor	
μ_{air}	dynamic viscosity of air	Pas
v	ratio of dry and moist soil thermal resistivity	
v_{air}	kinematic viscosity of air	m^2s^{-1}
ξ_i	slack variables of the upper training error of SVR model	
ξ_i^*	slack variables of the lower training error of SVR model	
ρ_{air}	density of air	kgm^{-3}

ρ_s	effective soil thermal resistivity	KmW^{-1}
σ	*Stefan-Boltzmann* constant	$Wm^{-2}K^{-4}$
σ_{load2}	standard deviations for predictive load^2 error	
σ_{tem}	standard deviations for conductor temperature error	
φ	angle between the wind direction and the cable axis	
Δx	slice separation of tunnel	m
$\Delta\theta_d$	temperature rise caused by dielectric losses	°C
$\Delta\theta_{ds}$	temperature rise caused by solar radiation	°C
$\Delta\theta_s$	excess of cable surface temperature above ambient temperature	°C
$\Delta\theta_x$	critical temperature rise of the boundary between the moist and dry zones above ambient temperature	°C

DECLARATION OF AUTHORSHIP

I, Rui Huang

declare that this thesis and the work presented in it are my own and has been generated by me as the result of my own original research.

Dynamic Rating for Improved Operational Performance

I confirm that:

1. This work was done wholly or mainly while in candidature for a research degree at this University;
2. Where any part of this thesis has previously been submitted for a degree or any other qualification at this University or any other institution, this has been clearly stated;
3. Where I have consulted the published work of others, this is always clearly attributed;
4. Where I have quoted from the work of others, the source is always given. With the exception of such quotations, this thesis is entirely my own work;
5. I have acknowledged all main sources of help;
6. Where the thesis is based on work done by myself jointly with others, I have made clear exactly what was done by others and what I have contributed myself;
7. Parts of this work have been published as:

Conferences

Huang, R.; Pilgrim, J.A.; Lewin, P.L.; Payne, D., "Dynamic Cable Ratings for Smarter Grids," *Innovative Smart Grid Technologies Europe (ISGT EUROPE), 2013 4th IEEE/PES*, pp.1-5, 2013.

Huang, R.; Pilgrim, J.A.; Lewin, P.L.; Scott, D.; Morrice, D., "Cable Tunnel Thermal Rating Prediction Using Support Vector Regression," *Probabilistic Methods Applied to Power Systems (PMAPS), 2014 International Conference on*, pp.1-6, 2014.

Huang, R.; Pilgrim, J.A.; Lewin, P.L.; Scott, D.; Morrice, D., "Use of Day-ahead Load Forecasting for Predicted Cable Rating." *Innovative Smart Grid Technologies Europe (ISGT EUROPE), 2014 5th IEEE/PES*, pp.1-6, 2014.

Huang, R.; Pilgrim, J.A.; Lewin, P.L.; Scott, D.; Morrice, D., "Managing Cable Thermal Stress through Predictive Ratings," *Electrical Insulation Conference (EIC), IEEE,* pp.110-113, 2015.

Huang, R.; Pilgrim, J.A.; Lewin, P.L.; Scott, D.; Blackwell, A; Morrice, D., "Predicted Rating System for Directly Buried Cables," *9th International Conference on Insulated Power Cables (Jicable)*, 2015.

Signed:.....

Date: .....

Acknowledgements

I would like to present my sincere appreciation to a number of people who have provided great supports in all aspects over my PhD. First, I would link to acknowledge National Grid and Tony Davies High Voltage Laboratory for funding all the work within my PhD thesis.

I would like to thank my supervisors Dr James Pilgrim and Prof Paul Lewin for their great patience, support and guidance during my PhD. They have provided invaluable enlightenment and inspiration in these three years so that I can finally start to write this thesis. I am grateful to my colleagues in the Tony Davies High Voltage Laboratory who support and motivate me day in and day out. Especially thanks to Dr Richard Chippendale for his help in modelling aspect; Stelios Christou, Dr Jack Hunter, Mike Smith and Neil Palmer for their assistance in setting up experimental work in the laboratory.

Finally I would like to acknowledge the support of my families and my fiancée. They are always backing me and encouraging me to finally go through these three years and finish writing this thesis.

Chapter 1: Introduction

Like the heart of the human body, electricity plays a basic but essential role in our modern life. Electricity networks, as per the arteries of the body, carry electricity to every single unit to make them function well. The electricity generation system and the electricity market has seen a great evolution in the last century, while the power transmission network has remained almost unchanged during the last 40 years.

1.1 Power transmission network

The integration of renewable energy generation, the increase of the load demand, even the rise of the number of electric vehicles are placing a lot of pressure and uncertainty on the existing power transmission system [1], [2]. Although there are a number of on-going power transmission network projects which will increase network capacity, it is difficult to keep pace with the growth in required transmission capacity. The opening of the transmission system to independent power operators, uncertainty concerning government regulation, rates and financing, and public opposition to new cable projects has also made cable capacity more of a concern when the underground cable becomes the bottleneck that limits the system transfer capability [3].

With limited finance for large scale network reinforcement schemes, and difficulties in siting new cables in cities, it is desirable for network operators to extend the service life of cables for as long as possible [4]. As a result, there is great pressure to increase current ratings on existing cable circuits. At the same time, they need to ensure that the system can still operate reliably under the higher load. To facilitate these demands, it is crucial to adopt new current rating methods capable of optimizing asset utilization with minimum risk.

1.2 Cable installations

A series of cable installations can be chosen to fulfil the requirements of utilizations. The most common scenario for installing underground cable is to lay them directly in the soil. The depth of buried cable varies depending on voltage level. In terms of installation cost, it is far more cost effective to shallow bury cables [5]. The most important heat transfer mode for buried cable systems is thermal conduction through the soil. As a result, to achieve the highest possible current ratings, cables buried underground are often installed in a region of imported backfill which has better thermal conductivity than the native soil [6]. A good backfill is not adversely affected by drying out and can have a thermal conductivity two or more times greater than the

native soil [7]. Figure 1.1 shows the temperature distribution of the cross-section of a buried single core three phase XLPE cable circuit.

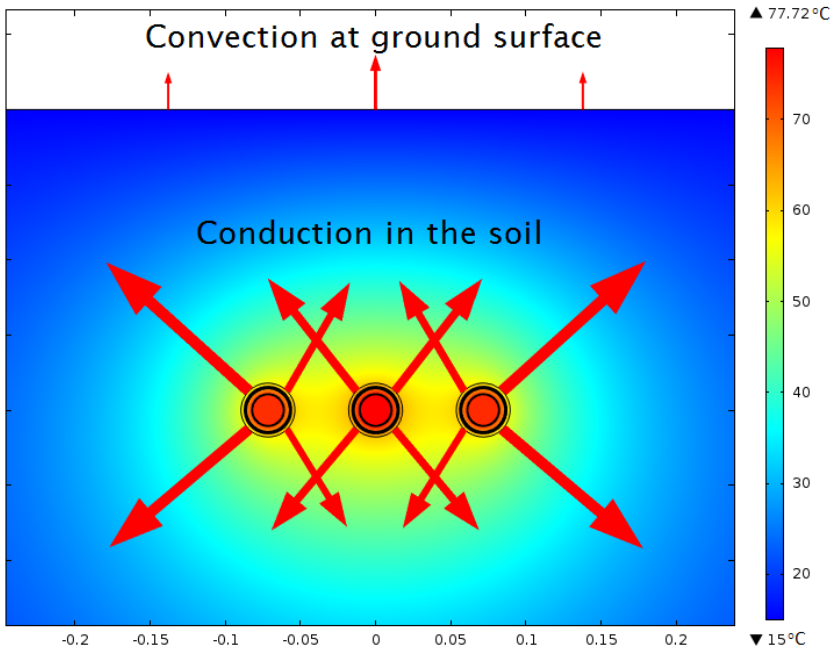

Figure 1.1 - Buried cable installation

Where cables are linked in substations, a short section of cable might be installed in air. The cables at the connection point with overhead lines are often installed in air outdoors via a protective riser to provide mechanical protection [7].

Cables are often installed in troughs in substations, with the troughs being flush with the ground surface. The cable is cooled through the natural convection in the air filling the trough and the ratings of such cable installations are highly dependent on the weather due to the proximity of the cables to the ground surface [8].

Another type of installation of cables in air is cables installed in tunnels. In generating stations, short tunnels are often used to convey a large number of cable circuits. Long tunnels are built for carrying major EHV transmission circuits which for various reasons cannot be carried overhead [7]. Tunnels are also commonly used for river crossings [9]. In UK, the popularity of cable tunnel installation has increased in recent years, especially in the London area with a large amount of the 132kV network installed in tunnels [10]. As the capital cost of such cable installation is higher than directly buried cable, system operators desire to optimize the rating, grouping and the number of circuits to fulfil a given transmission capacity. Figure 1.2 shows the cross-section of a typical cable tunnel. 2 three phase circuits are installed near to the tunnel wall. The installation means that heat generated within a cable is dissipated through radiation, convection and ultimately conduction.

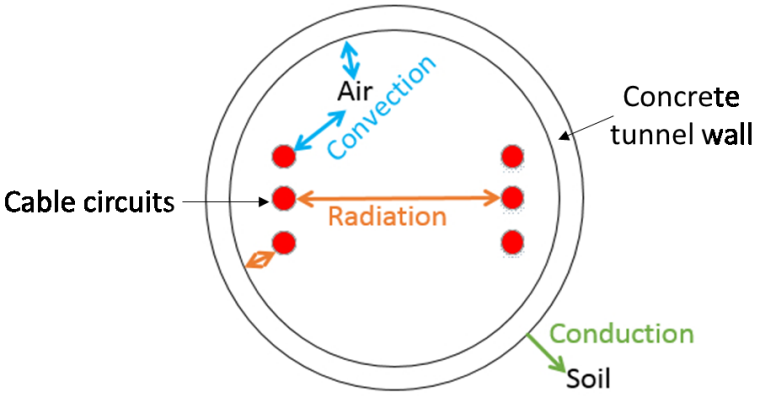

Figure 1.2 - Cables installed in tunnel

1.3 Rating of cables

For cable systems, the factor limiting the current carrying capacity is normally temperature. The maximum temperature of the underground cable is typically determined by the temperature limit on the insulation material (90°C for XLPE cable) due to the rise in irreversible degradation processes in the dielectric above this temperature. Thus, to calculate the cable current rating, the thermal field internal to, and around, the cable should be investigated. Heat is generated from the conductor, dielectric and sheath, with this thermal energy then being transferred toward the surrounding environment by conduction, convection and radiation depending on the installation types. Thermal models will be built to simulate the heat generation and transfer in cable system, thus, the cable ratings can be calculated by considering the critical temperature of the conductor.

Several kinds of different cable rating specifications are used for the transmission network operation. Presently, the most common thermal rating used for cable systems design is the continuous rating, defined as the maximum continuous current which can be carried through the cable without exceeding its maximum conductor temperature limit. However, a cable circuit will never operate at its continuous rating all of the time in the real world, as a result of the cycling usage (daily, weekly and seasonally) of the electricity and the necessary safety margin of current capacity for possible failures or outages.

Thus, the emergency rating for cable is introduced as a more practical rating tool for operation of the transmission network under constrained conditions. Based on a known preload level, the emergency rating is defined as the maximum current which can be carried through the cable for a certain period (for instance 6 hours) without exceeding its maximum temperature limit. Emergency ratings are able to estimate the highest cable current carrying capacity when the additional power flow needs to be carried under some special conditions, for instance when a

parallel circuit needs to be taken out for maintenance. Look up tables are usually used to check the emergency rating for different percentages of preload condition in different seasons.

The traditional methods used to calculate continuous ratings and emergency ratings have two major shortcomings: First, they have historically been conservative [11] due to being based upon worst-case assumptions. Walldorf et al. claim that by using both historical data and real time measurement, dynamic ratings can deliver increases of 5-20% in cable current carrying capacity [12]. Second, static cable rating methods do not consider the real-time change of environmental conditions such as soil thermal resistivity and ambient temperature, which control the rate of heat dissipation from the cable. As a result, there is a potential danger of underestimating the effects of long periods of dry weather. The power failure that affected the Auckland Central Business District in 1998 shows the difficulty in determining the soil thermal properties to determine a safe cable rating [13].

Such issues highlight the benefit of dynamic cable rating. The availability of online monitoring makes it viable to measure in real-time the current loading and relevant environmental data. These data are used in the dynamic thermal models for different cable installations to achieve dynamic ratings. Instead of using look up tables based on a conservative preload level to calculate emergency ratings, dynamic rating methods are able to fully consider the different scenarios of the initial condition depended on the historical data and calculate an accurate emergency rating based on the real-time temperature of the cable system. Thus, dynamic rating can help to remove uncertainties, maximizing asset utilization but without increasing risk.

1.4 Research motivation

As discussed in Section 1.3, traditional rating methods do not use real-time measurement data. These rating values, which are calculated from worst-case scenarios, normally give the system operators conservative results. In addition, in some extreme weather, the actual condition might be worse than the worst-case assumption, thus the potential risks of overestimating the rating also exist during operation.

The use of conservative cable ratings for the power transmission system can lead to constraints being imposed on circuit flows which are not in reality required, which causes a large amount of the unnecessary constraint costs. On the other hand, the potential risks of overestimating the cable rating under some extreme conditions might result in the degradation of the dielectric due to overheating. As a result, it is vital for system operators to implement new current rating methods capable of optimizing asset utilization and reducing the risk at the same time. In addition, the constraint costs of the transmission grid could be further reduced if the real-time

cable ratings can be reliably predicted in advance, allowing better integration with operational planning.

In order to achieve this, it is necessary to evaluate the existing methods of cable rating for different installations, and remove the assumptions in the models which might cause conservatism or potential risk in the cable ratings. Furthermore, to predict the cable rating, methods should be developed to assess the uncertainties of different factors which might affect the cable rating in advance.

1.5 Contribution of this thesis

As the response to the research motivation presented in Section 1.4, the contributions to the state of the art made in this thesis can be summarized in two main parts of the field of dynamic cable ratings.

1. The most important contribution in this work is to announce a novel cable rating concept, Predicted Cable Rating, which combines a day-ahead load forecasting system with the dynamic thermal model to predict the short-term emergency cable rating forward from any point within the next 24 hours. Such accurate short term current ratings at the day ahead stage has the dual benefits for network operators of reducing variations in dynamic ratings (which makes them difficult to plan with), while reducing the risk of thermally overloading the cable. In order to achieve precise predicted ratings, the following targets were addressed:
    - Accurate dynamic thermal models for different cable installations were developed from standard methods. In this work, a group of dynamic thermal models for a variety of common cable arrangements (directly buried cable, cable in air and cable tunnel) have been built and compared to find the models with best compromise between the accuracy and solution speed. Several enhancements have been delivered which make these dynamic thermal models able to take into account the real time measurement data (load and environmental data) to perform more precise and reliable cable ratings.
    - A day-ahead load prediction system. Support Vector Regression (SVR) technique was applied to build the load prediction system after the analysis and comparison of several load prediction models. A comprehensive analysis was done to choose a group of most appropriate input features for the SVR models. This load prediction system is able to predict the load demands for the next 24 hours at each step. Test results show that the Mean Absolute Percentage Error (MAPE) for this load prediction system is less than 1.5 and 4 for 1hr-ahead and 24hr ahead prediction respectively.

- A predicted rating error estimation system was built by using the exponentially weighted moving average (EWMA) equation and Multiple Linear Regression (MLR) technique. This system is able to estimate the predicted rating error by using the actual and predicted load data without the dynamic thermal model. It has been implemented in the predicted rating system in order to quickly detect the predicted rating errors and replace the predicted rating by real-time rating value if the error estimation is higher than a set limit. Such function is important in the predicted rating system in order to make it reliable and give system operators confidence to implement the system on their network.

2. A further contribution to the technical state of art has been made by the novel development of SVR models to estimate thermal status of a cable directly without using dynamic thermal models. Such a method is able to perform a fast rating calculation for the cable system. One of the outstanding examples is for the cable tunnel installation, where the SVR method is able to reduce the solution time for the rating calculation from 2 minutes by using dynamic thermal model to less than 2 seconds. A series of comprehensive analyses have been done to choose the most suitable input features for SVR models to calculate the emergency ratings for different cable installations. In addition, a SVR rating prediction system for cable in air is built by combining the input features of the day-ahead load prediction model and the input features of emergency rating calculation model. Thus, the 24hr-ahead rating prediction can be achieved by using the SVR model directly without the dynamic thermal model.

1.6 Thesis structure

This chapter has outlined the background of developing new cable rating methods for the power transmission grid. These methods should be applicable to different kinds of cable installations. In order to optimize the utilization of the power transmission grid, it is imperative to obtain accurate and reliable real-time cable ratings. Thus the system operators are able to run the existing grid in the most efficient and reliable manner.

Chapter 2 presents a comprehensive review of published cable rating methodologies. Critical reviews of the traditional rating methods and existing dynamic rating methods are included in this chapter, which identifies the shortages of these methods and proposes some potential approaches for the improvement of cable ratings.

With the purpose of building dynamic rating systems, Chapter 3 introduces three dynamic thermal models for different cable installations (directly buried cable, cable in air, cable tunnel), which are able to take into account the measured load and environmental data to calculate the real-time temperatures and ratings. These models are constructed by using the finite difference

method, with the results compared to a more detailed FEA model, and the traditional rating standards. The comparison results prove that these dynamic thermal models outperform the traditional rating standards and benefit from shorter solution time than FEA models.

In order to predict the day-ahead emergency cable ratings, a 24hr-ahead load forecasting system is required. Chapter 4 presents the construction of day-ahead load forecasting system. It details a load prediction system by using Support Vector Regression (SVR) method to estimate the next 24 hours' loading in hourly steps. Comprehensive tests of input features of the SVR model have been presented and finally a group of the most appropriate features were chosen to perform the best load prediction results. In addition, the challenges of extending the SVR method to transmission circuit load prediction are also presented.

Chapter 5 introduces a novel cable rating algorithm, Predicted Cable Rating, based on the integration of the load forecasting model introduced in Chapter4 into a dynamic rating system. The day-ahead Predicted Cable Rating is able to provide the time-limited emergency rating calculated forward from any point within the next 24 hours. This can help transmission operators make day-ahead plans and reduce their constraint costs. The predicted rating algorithm has been applied in buried cable, cable in air and cable tunnel dynamic rating systems respectively. Predicted results are presented for all the cases and demonstrated by the rating values obtained by direct solution of the thermal model. In addition, an error estimation system based on the exponentially weighted moving average equation is used to estimate the predicted conductor temperature error quickly without using the dynamic thermal model.

Chapter 6 presents validation results from a laboratory test installation. A 33kV single-core single-phase XLPE cable was used to test the thermal response to a step input current; to a given input load profile and to a rating value after a given input load profile. By comparing the experimental results with the result from dynamic thermal model for cable in air, it can been found that the dynamic thermal model can obtain accurate cable temperature and thermal ratings. An example application of the predicted rating algorithm has also been demonstrated to show its ability to provide precise day-ahead rating predictions.

To examine ways of calculating ratings more quickly, Chapter 7 proposes a method to derive ratings directly via an SVR model. This is achieved by pre-training the SVR models using the results from the dynamic thermal models. After fully testing the input features in the SVR models, the most suitable models have been identified for different cable installations. The results calculated by the SVR models are examined by the direct solutions from the dynamic thermal models.

The final chapter summarises the rating methods developed in this work, highlights the benefit of these improvements and discusses the potential to further develop the techniques proposed in this thesis.

Chapter 2: A review of Cable Rating Methodologies

Thermal rating is the major factor that limits the current carrying capacity of HVAC cables. As a result, numerous researchers all over the world have focused their interest on this area. Several International Standards have been published by the International Electrotechnical Commission (IEC) since 1969 [14]. The Institute of Electrical and Electronics Engineers (IEEE) has published over 3000 ampacity tables for power cables since 1994 [15]. Besides these standards, lots of additional research has been published to propose solutions to specific cable rating problems, and to remove the imprecise assumptions in the traditional rating methods. This chapter presents the key issues for cable thermal rating problems. The traditional rating methods and existing dynamic rating methods are introduced and compared, with their key assumptions and restrictions being identified.

2.1 Rating of cables

The majority of AC cables have a thermally limited current rating. Hence the major criterion for cable rating is the conductor temperature. As a result, it is important to investigate the thermal field around the cable system.

There are three major heat sources in the cable system itself, two of which depend on the load current in the circuit and one on its operating voltage. The joule loss (W_c) is the most significant loss, which is generated by the electrical resistance of the conductor, it can be calculated by

$$W_c = I^2 R_{ac} \tag{2.1}$$

where I is the conductor current (A) and R_{ac} is the resistance (Ωm^{-1}) at the maximum operating temperature. For AC operation allowance must be made for skin and proximity effects in the calculation of R_{ac} [16]. The losses in the metal sheath (W_s) and armour (W_a) also depend on circuit current. They occur due to circulating currents being induced in the metallic cable sheath and armour, and through eddy current losses due to the skin and proximity effects. The magnitude can be defined using

$$W_s + W_a = \lambda I^2 R_{ac} \tag{2.2}$$

where λ is defined as the sheath and armour loss factor [7]. The voltage dependant losses are the dielectric losses (W_d). Dielectric losses occur through the flow of current and the accumulation of charge in the insulation, the losses are defined according to

$$W_d = 2\pi f C_d U^2 \tan\delta \tag{2.3}$$

where U is the phase voltage (V), f is the frequency of the applied voltage (Hz), and tan δ is the tangent of the dielectric loss angle.

The heat generated in cables will dissipate to the surrounding environment by three modes: conduction, convection and radiation. For directly buried cables, the major means of heat dissipation is conduction through the soil around the cable. For cables in air, the convection and radiation from cable surface to the air dominate. The convection at the cable surface can be classified into natural convection and forced convection according to the air speed on the cable surface. In addition, the solar radiation might heat up the cable surface when the cables are installed outdoors and directly exposed to the sun. For cables installed in tunnels, the heat will leave the cable through radiation from the cable surface to the tunnel surface, convection from the cable surface to the air in the tunnel, and from air in the tunnel to the tunnel surface. Then the heat travels through the soil surrounding the tunnel by conduction. In addition, if the cable or tunnel system is shallow buried, the convection and solar radiation on ground surface will also have influence on the cable rating.

2.2 Traditional rating methods

Current rating methods for electric power cables have a long history, with some of the concepts presented in early published papers by Kennelly [17] and Mie [18] still used in today's standards. In 1957, Neher and McGrath published their paper which successfully summarized most of the important prior ampacity work [19]. The technique that they describe is based on energy balance in the conductor and analysis of heat flow in an equivalent thermal circuit.

2.2.1 IEC standards

Using techniques common with the Neher and McGrath paper, IEC 60287 was published as the standard approach for calculating the continuous ratings of cable circuits [14]. It provides a series of one-dimensional, steady state models, which can adapt to different cable structures, laying arrangements and environment types to allow calculation of static rating and steady state temperature. Section 2.1 of the IEC 60287 standard provides a method for calculating both the internal and external thermal resistances in different cable formations and surrounding environments, including in free air, directly buried, in buried pipe, in buried troughs and in ducts [20].

The rating calculations in this standard are all based on some assumptions. The most significant one is to simplify the three dimensional cable with a one dimensional thermal-electric analogue model (detailed in Section 3.2.2). To simplify the three dimensions into two dimensions, the

standard assumes the hotspot in the cable circuit is known and there is no heat flow in the longitudinal direction from this hotspot. To further simplify the model into one dimension, the thermal parameters of the surrounding environment are adjusted to include the deviations from the two dimensions. Furthermore the standard assumes that the ground surface is isothermal and the surrounding soil environment possesses uniform thermal resistivity. These imprecise worst case assumptions make the traditional continuous rating results either conservative [21] or unreliable [5], [22]. Some researchers use FEA methods to build more accurate models and have formed some comparisons with the IEC standard, showing a 14% over-rating for the isothermal ground surface model at shallow burial depths [5]. For deeper burial and lower conductor temperature, the ground surface boundary condition has less effect. As a result the IEC 60287 standard may not be suitable for shallow buried cables with a high conductor temperature. The standard adopts a two-zone model in which the moist soil is assumed to have uniform thermal resistivity and the boundary between dry and moist soil is assumed as a stated critical isotherm. It is easy to implement but can oversimplify the problem [23].

IEC 60853-2 outlines the calculation for transient and cyclic ratings for cable operating at voltages greater than 36kV and emergency ratings for cables of all voltages [24]. It is based on the IEC 60287 standard and the work by Goldenberg [25], setting an equivalent thermal circuit with a one-dimensional transient model. Because the methods of calculating the thermal resistances are as per IEC 60287, the assumption of uniform soil thermal resistivity and diffusivity and isothermal ground surface is retained. In addition, all cables are assumed to see the same load cycle which limits the application of this standard to more straight forward installations. Work by Freitas et al. [23] compares the conductor temperature from four different transient simulations (dry soil, two-zone, moist soil and moisture migration) and presents two results showing that the IEC 60853 model forces a decrease of load for safety and that the degree of soil saturation plays an important role on the current carrying capacity.

2.2.2 Cigré methods

Cigré study committee 21 (HV Insulated Cables, now termed B1) has published several technical reports presenting different methods for specific cable installations. Cigré Electra 24 [26] and Electra 44 [27], as a supplement of IEC 60853, provide methods for calculating rating factors for cyclic loads (load factor less than 100%) and for calculating the cable response to an applied step function in load. They approximate the internal thermal components of a single-core cable by reducing them to a one dimensional thermal equivalent circuit having two lumped resistance/capacitance cells, and treat the surrounding soil by an analytical method. This method is acceptable within the ±3% temperature accuracy limitations given for duration of transient and cable types.

Cigré Electra 66 [28] provides a guideline for obtaining the rating of a forced-cooled cable system via a numerical method. Cigré Electra 87 [29] presents a computer method for the calculation of the response of single-core cables to a step function thermal transient. In this computer method, the thermal circuit is refined by increasing the number of cells, which is difficult to solve by hand calculation. In addition, for groups of cables, the losses affected by mutual heating are accurately taken into account. Cigré Electra 104 [30] outlines the rating calculation of forced cooled cables for thermal transients and cyclic loads.

Electra 143 [31] is the standard method published by Cigré for calculating the temperature in ventilated cable tunnels. However, this method has some limitations, such as the constant tunnel cross section, constant voltage level and current, plus an assumption that the air speed in the tunnel is high enough to create turbulent flow.

2.2.3 Improvements of cable thermal model from other works

The review of existing cable rating methods above highlights a number of areas where traditional cable rating methodologies appear hardly capable of matching the actual cable operation. The assumptions in traditional models might lead to either optimistic or pessimistic rating results in the system. Many individual works have been published which propose improvements in cable rating technology by overcoming the assumptions in traditional rating models. The universal environmental thermal parameters and isothermal ground boundary condition are two major assumptions which attracted interest from researchers. Furthermore, the additional ventilation facilities are more and more commonly used, which requires extra thinking about the integration of the cooling system into the thermal model. The thermal limit of cable joints should also be considered as it might be the bottleneck of the whole cable circuit.

2.2.3.1 Environmental thermal parameters

The environmental thermal parameters are vital to obtain accurate cable ratings. In IEC standards, the soil thermal parameters are assumed to be constant at the worst case scenario, which is historically conservative. Some systems [32], [33] measure these thermal parameters prior to the commissioning of the cable and use these values in the thermal model to calculate the cable temperature and rating. However, these values can vary during the operation of the system which might result in a risk of the cable system. Generally, two approaches have been introduced in the literature to obtain the real-time ambient thermal parameters. First, [34]–[36] show that the thermal resistivity of soil can be directly measured by using a separate equipment. Then the real-time measurement values can be applied to the cable thermal model. Second, if the temperature measurement is available in the cable system, it is possible to adapt the ambient

temperature parameters by comparing the measurement data with results from the cable thermal model [37], [38]. In this case, it is assumed that the temperature deviation between simulation and measured data is from the errors of thermal parameters. Thus, these parameters are updated until the temperature deviation is within an expected range.

2.2.3.2 Ground boundary condition

In IEC standards, the ground boundary is assumed to be isothermal. However, many works have proved that this assumption is not always suitable in real cable systems. Lewin demonstrates the influences of solar radiation and convection heat exchange at the ground surface, calculating a more accurate rating method for power cables buried in surface troughs [8]. Swaffield uses FEA software to build a more accurate model and shows that the isothermal ground surface boundary condition will result in up to 14% over-rating at shallow buried depth [5]. The author of [39] found that the isothermal ground boundary can underestimate the conductor temperature by 6.5% and 4% for 0.5m and 1m deep buried cable system respectively.

2.2.3.3 Additional cooling system

Due to higher rating requirements from the high demand areas, about 16% of the transmission cable circuits in the UK have additional cooling systems [40]. The cooling system can be performed by natural or forced fluid (air or liquid) flow in the tunnel or pipe. Many conventional standards are not able to take into account the effects of additional cooling systems.

The author of [41] investigates the accuracy of the Electra 66 method for calculating the cable rating for forced cooled cable circuits with water pipes. The heat transfer problem is defined for 2-D slices and solved iteratively at steps along the length of cable route, with the water properties and heat-transfer coefficient varying with water temperature along the route. Pilgrim [9] presents a revised method for calculating the rating of cable circuits installed in ventilated cable tunnels based on Electra 143, but removing the restriction that all the cable circuits in the tunnel can only operate in the same load cycle.

2.2.3.4 Cable joints

The failure rate of cable joints are normally higher than the cable itself during high voltage type tests, partial discharge test and real operations [42]. However, it has been proved by researches that the a proper designed cable joint do not present a limiting factor on the circuit ratings [40], [43]. This is because that cable core-to-core spacing is designed to be sufficiently large in the joint without external cooling. Some joints are design with external cooling system [40], [43] to

make sure they are not the thermal bottleneck of the circuit. As a result, the rating model of cable tunnel is not considered in this thesis.

2.3 Dynamic rating algorithm and existing systems

Given the pressure to increase cable capacity without undue risk, new rating methods which are able to take into account load history and real-time measurement of parameters instead of the worst-case environment are strongly desirable.

Dynamic cable rating methods are based on real-time measurements of load and environmental data and use accurate dynamic thermal models which can apply these data. As a result, the parameters which are measured by the system and the usage of these parameters in models to calculate cable ratings are two of the most important factors in evaluating dynamic cable ratings.

2.3.1 Dynamic rating algorithm

Real-time cable loading is measured by system operators during their real-time operation, which can be used for the calculation of heat generation from cable. In some new cable circuits, distributed temperature sensing (DTS) technology has been implemented [33], [35], [44]–[46]. It allows the real-time monitoring the temperature in or around the cable through its longitudinal direction. The DTS optic fibre can be applied on the cable surface or in the cable screen[45]. Since the conductor temperature is the limitation of cable thermal rating, dynamic thermal models are still necessary to obtain the conductor temperature. In addition, cable ratings are not measurement values, they are calculated by dynamic thermal models according the real-time temperature and loading.

Figure 2.1 shows the flow charts of the continuous cable rating calculation (a) and the dynamic cable rating calculation (b). Instead of using set worst case assumptions, the real-time load and environmental data are used to update the parameters for the thermal models in the dynamic rating system. Based on the real-time cable temperature calculated by the dynamic thermal model, the real-time ratings can be obtained at each time step.

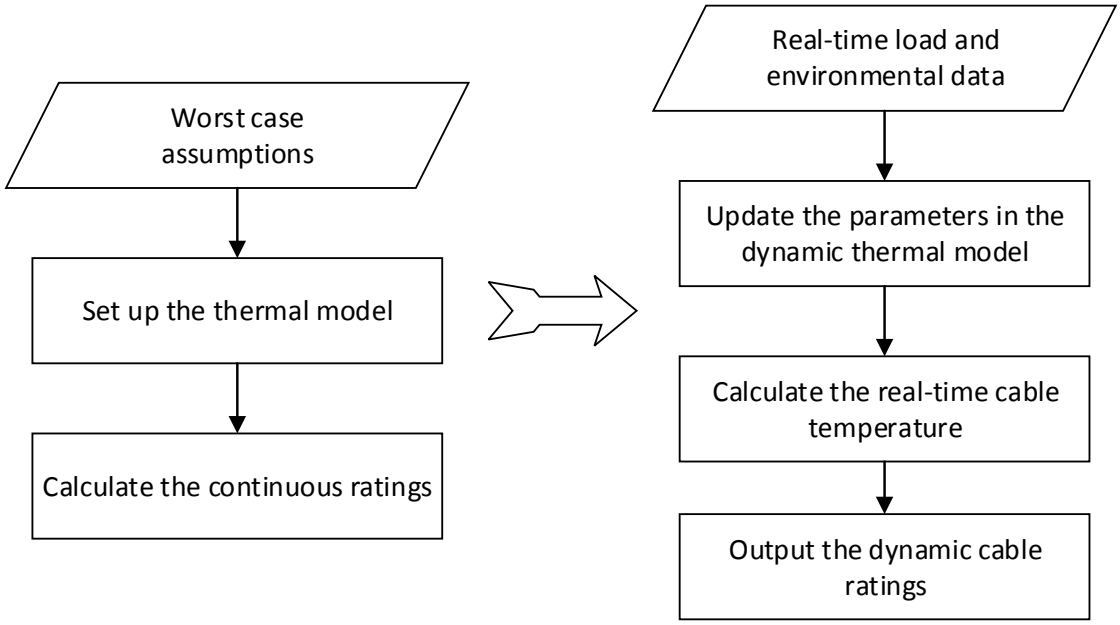

Figure 2.1 - Continuous cable rating vs. Dynamic cable rating

2.3.2 Existing dynamic rating systems

Several dynamic rating systems have been installed and are in service for different network operators around the world. Most of them are providing benefits by increasing the load capacity and reducing risk to the transmission networks [21], [32], [37], [47]. In this section, some existing dynamic rating concepts are introduced and analysed to identify their key limitations.

2.3.2.1 National Grid Circuit Thermal Monitor

National Grid has previously installed a system which is able to provide on-line continuous monitoring and overload thermal ratings of cables based on system measurements and real-time thermal modelling. The stored data can also help the operator to plan future operations [48]. The calculation model is based on the use of superposition as described in Cigré Electra 87 and recommended in IEC 60853. It can model a 2-dimensional slice through a buried cable circuit with natural cooling or forced cooling using separate cooling pipes. It can also model uniform surrounding soil characteristics or two-layer resistivity caused by the use of backfill material or soil dry-out. In addition, the mutual heating effects, including the influence by adjacent double circuits carrying different loads can be calculated in the model.

The dual layer thermal resistivity is calculated using a boundary element method which does not consider moisture migration in the soil. Although a finite element model is chosen to validate

this dual resistivity method and the result shows good agreement, the finite element model does not take moisture migration into account. In addition, there is no temperature measurement facility to monitor the cable surface temperature, as a result both the cable surface temperature and conductor temperature have to be calculated by the model at every step. Even a small error will affect the next step and the accumulation of these errors can have a very negative effect on the accuracy of the cable rating calculation. At the ground surface, only the air real-time temperature is included in the model, but the heat convection and solar radiation are ignored and the ground surface is assumed to be isothermal.

2.3.2.2 Dynamic Rating for High-Pressure Fluid Filled Circuit by USi

This project uses a dynamic rating system and slow fluid circulation system to upgrade the 300 hour emergency rating of four parallel 69 kV high-pressure pipe-type cable circuits by 13%, from 102 MVA to 115 MVA [49].

The effective soil thermal resistivity is derived by comparing measured and computed pipe temperatures until the temperature differences are minimized. The computed pipe temperatures are based on measured load currents using a dynamic thermal model of the four parallel cable feeders including the effects of soil thermal resistance and capacitance. It also takes into account the depth and spacing of each pipe and mutual heating effects between these four pipes. After the soil thermal resistivity has settled, it is taken along with the ambient soil temperatures, depth and pipe spacing, and all these parameters are used to compute current ratings for each hot spot section and the rating of the worst location is selected.

The method in this paper suggests that comparing the surface temperature by direct measurements with dynamic thermal modelling to obtain the equivalent soil parameters is convenient to obtain effective soil thermal resistivity and cable ratings. But the surface temperature change is not only dependent on the soil thermal resistivity but also dependent on other environment parameters, i.e. ambient temperature. As a result, the soil thermal resistivity calculated may not be accurate.

2.3.2.3 Probabilistic Cable Rating by Queensland University of Technology

The paper describes an on-line monitoring system for obtaining daily values of soil thermal parameters, illustrating the daily variations that can happen and the data analysis procedures to gain a monthly probability distribution of thermal resistivity and consequently to obtain a probabilistic cable rating [35].

The authors of [35] state that soil moisture content is the most important factor in determining soil thermal resistivity and this in turn depends on the local rainfall. The transient sphere

technique was developed for measuring the soil thermal resistivity and diffusivity [34]. They are installed in backfill adjacent to the cable and in native soil to measure the thermal resistivity under actual operating conditions and to correlate these values with rainfall for a given location. Four years of measurement data are analysed to establish a quantitative link between rainfall and soil thermal resistivity. This provides an opportunity for short-term prediction of cable rating and enables the user of rainfall statistics to predict seasonal or monthly soil thermal resistivity probability distributions for long-term use. These results show that the system is able to help operators to make their cable systems more efficient and provide opportunities to delay the reinforcement of existing cable systems [36].

Although it is a good way to measure soil thermal characteristics, the method described in the paper is not a real dynamic rating. The author links soil moisture content with rainfall and soil thermal resistivity with soil moisture content, then uses the measurement data to calculate the relationship between rainfall and soil thermal resistivity and cable rating directly. However, in the real dynamic rating, the soil thermal resistivity is not totally dependent on rainfall and the cable rating is also not totally dependent on soil thermal resistivity.

2.3.2.4 MAXAMP Dynamic Rating System by Kinectrics

A dynamic feeder rating system, MAXAMP, has been developed by Kinectrics Inc., Toronto, Canada [37]. The system is able to compute the maximum current that the cable can carry for the specified conditions and the maximum duration of a given overload condition before the conductor maximum temperature is reached.

The MAXAMP system can perform calculations for steady state ratings and real-time emergency ratings. The calculation method for the steady state rating is based on the Neher and McGrath paper and IEC 60287, while the dynamic emergency rating is based on the IEC 60853 standard.

For real-time rating calculation, the measurements of cable surface temperature, ambient temperature and cable loading must be taken into account. Historical load data for a default period of 24 hours is used to establish an initial temperature distribution for the calculation of the variables (a minimum of about 6 hours of history is required in order to obtain accurate results). The cable surface temperature is used to calculate the effective soil thermal resistivity. It is evaluated from the following equation:

$$\rho_s = \frac{1}{\nu T_4'|_{\rho_s=1}} \cdot \frac{\theta_s - (\nu - 1)\Delta\theta_x - \theta_{amb}}{nW_c(1 + \lambda_1 + \lambda_2) + W_d} \qquad (2.4)$$

where θ_s is the measured cable surface temperature (°C); $\Delta\theta_x$ is the critical temperature rise of the boundary between the moist and dry zones above ambient temperature (°C); v is the ratio of dry and moist soil thermal resistivity (set to 1 if soil dry out is ignored); n is the number of conductors; W_d are the dielectric losses (W); T_4' is the external thermal resistance of the cable (KmW^{-1}); λ_1 and λ_2 are the sheath loss factor and armour loss factor respectively. The DFR system also uses Gear and Adam-Moulton predictor-corrector integration algorithms [50] to allow the time step and iteration order able to automatically change depending on signal variation and required accuracy.

This paper mainly focuses on the algorithmic approach to data analysis, especially on optimizing the integration time step. However the basic method for rating calculation is still based on the IEC 60287 and IEC 60853 standards. Although the soil thermal resistivity can be updated every 24h or every step, the equation for soil thermal resistivity is only suitable for the steady-state rating but not real-time rating.

2.3.2.5 Combined FEM and Distributed Temperature Sensing dynamic rating

This paper describes a combined technique of FEM and a gradient-based optimization algorithm to estimate the thermal parameters of the soil surrounding the cable system [51]. This method requires the distributed temperature sensor to be installed to measure the cable surface temperature. Cable load and DTS measurement temperature are collected at the hot spot over a period of time. The measurement data are then used to estimate the unknown parameters in the cable model.

The rating method is based on the DTS system, FEM model and a gradient-based optimization algorithm. Although the soil temperature and soil thermal resistivity are assumed to be uniformly distributed in the FEM model which is not true in practical circumstances, the DTS helps to reduce the error from these assumptions by using the optimization algorithm. The real-time measurement data is compared with the result from the FEM model in every step, and the equivalent uniform soil temperature and soil thermal resistivity are updated by the optimization algorithm to limit the difference to an acceptable range.

2.3.2.6 DCRS by USA Energy System Research Centre

An online dynamic cable rating system (DCRS) has been developed by the Energy System Research Centre in the USA [32]. Using temperature sensors, cable surface temperature and transformer temperature can be monitored and transferred to the dynamic rating system. In addition, DCRS can extract real-time temperature forecast data from a weather station. With all the required information collected, the DCRS provides real-time cable rating estimation.

The forecasting temperature information is first used in DCRS for dynamic cable rating prediction. The DCRS extracts and updates the forecasting temperature information from the website for dynamic rating calculations. An example of the conductor temperature results is shown in Figure 2.2:

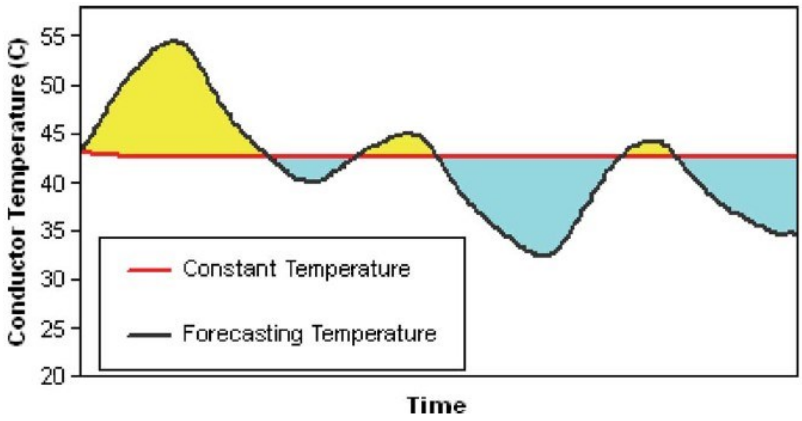

Figure 2.2 - Conductor temperature forecasting for constant and forecasting temperatures [32]

Figure 2.2 shows that the conductor temperature may be overestimated or underestimated by constant temperature assumption, therefore it is necessary to include forecast temperature information for better cable rating prediction.

2.3.2.7 EPRI Dynamic Rating System DTCR

The development of the EPRI Dynamic Thermal Circuit Rating (DTCR) system was begun in 1991 [3]. It requires various monitored parameters including ambient soil temperature, load and soil thermal resistivity. The method used in the dynamic rating for underground cable module in DTCR is based on the paper by Neher and McGrath, the IEC 60287, and the IEC 60853 standards. In addition, an "additive wave method" is used in DTCR to track the response of conductor temperatures to a constant heat input. DTCR examines the load at intervals less than 0.5 hours, each time the load changes, a new temperature response "wave" is launched. The total temperature response at a given time is the summation of all the previous temperature response functions from each change in the heat due to load change and conductor resistance change by temperature. The DTCR system is able to "look back" hundreds of hours in the loading history, making extensive computations for conductor temperature due to the long earth thermal time constant. It also mentions the usage of load demand forecasting to predict the cable rating in the flowchart, but no detail was presented in the report [52].

2.3.2.8 KEMA and NUON Dynamic Rating System in Netherlands

In 2005 Netherlands energy company NUON implemented a pilot dynamic rating project for underground cable and overhead lines to explore and obtain experience for further dynamic rating implementations all around the grid [53].

The dynamic rating system is used to calculate the future loading possibilities without using glass fibres for temperature measurements [54]. In this project, thermal models are used to assess the thermal situation of the component in operation. Temperature measurements are still important but are only used to verify the accuracy of the thermal models.

The load information is forwarded to the model every five minutes, and new weather data is forwarded to the model every twenty-four hours by the Energy Management System (EMS). In the KEMA dynamic thermal model for the power cable, a ladder network of thermal resistances and capacitances is used to represent the cable [42]. A group of equations are deduced by the dynamic models. These models are mainly based on the IEC 60853 standard, but the model in this system is able to perform calculations based on constantly varying input data [55]. The online data used for these models is the actual load delivered by the EMS. In addition, the soil temperature which is deduced from an investigation towards both the theoretical behaviour and other temperature measurements in the Netherlands is taken into account.

2.3.2.9 Valcap and AdapPro Dynamic Rating System in Denmark

The Danish transmission system operator Energinet.dk is running a dynamic rating system, called “Valcap” which is supplied by the cable manufacturer NKT cables [46]. Valcap is based on a combination of a DTS system and an IEC based dynamic rating system for power cables. The optical fibre is integrated in the cable screen or applied on the cable surface so that the temperature profile along the cable can be continuously measured by the DTS system with a spatial resolution of about 1-2m. AdapPro is a self-learning system, which uses the transmitted load current of the cable and the measured temperatures to verify the thermal parameters in the calculation model continuously. Such facility makes the model self-adaptive by taking into account the changing environment, thus the accuracy of the cable rating can be improved.

2.3.2.10 Real-time ampacity estimation (R-TAS^{TM}) in Korea

In Korea, LS Cable Company started its R-TAS^{TM} project in 2001, tested the system in 2003 and finally applied this real-time ampacity estimation system on two real cable circuits (Shinyangjae-Gwachon and Bukbusan-Nambusan) in 2005 [44]. This system includes three modules: Distributed Temperature Sensor (DTS), Conductor Temperature Monitoring (CTM), and Dynamic Rating System (DRS). DTS was installed every 4km with a spatial resolution of 2

meters and temperature accuracy within ±1.5°C. CTM was used to calculate the conductor, insulation and sheath temperature of maximum 50km cable length at 2 minute intervals by using the DTS and load current data. DRS was designed to estimate the continuous rating and emergency rating at the cable conductor hotspot. As the hotspot location might change with time, the cable conductor temperatures for the entire cable route are calculated. The cable temperature calculation is based on the IEC standard, thus the assumptions in the IEC standard also exist in this system.

In the Shinyangjae-Gwachon project, the application of the R-TAS^{TM} system increased the continuous rating current and 4hr emergency rating current by 5.8% and 18.3% respectively. While in the Bukbusan-Nambusan project, the real-time measurement system found that the tunnel hotspot temperature is 46.1°C which is higher than the designed value of 40°C. According to this result, the continuous rating of this circuit is de-rated by 12.5% and a tunnel ventilation system is planned to be installed for this circuit in 2007.

2.3.2.11 Electrothermal coordination (ETC) from DTU and Energinet.dk

The work from DTU and Danish TSO Energinet.dk built an Electrothermal coordination (ETC) system for their cable based transmission grids [45]. ETC system is able to consider the current based load conditions and the thermal behaviour of the components at the same time. The dynamic thermal model is based on thermoelectric equivalents (TEEs), which has similar principle with the IEC standards. However, this model utilizes a division of the surround soil into 100 zones, the insulation into 10 zones and the cable jacket into 3 zones. As a result, it can obtain more precise cable temperatures than the IEC standards. The ground surface is assumed to be isothermal and the conductor losses and sheath losses are calculated as described in IEC 60287. However, these two losses are temperature dependent, which means the losses calculated in this system are conservative.

The novelty of this work is to connect the cable temperature calculation and load flow simulations for the transmission system. The AC-balanced load flow calculations are performed by DigSilent Power Factory (DSPF) which is used by the Danish TSO. The load current of each cable is then used in the thermal cable models to calculate the real-time temperature. In addition, the temperature dependent electrical resistivity of the cable is calculated and used in the next load flow calculation. Instead of using current levels as the criterion in the system reliability, the thermal limits are used for the operating criteria. With a simple case study, the author showed the ETC system is more economic and flexible than the existing systems.

2.4 Development Requirements

Section 2.1 introduced the major factors of heat generation and transfer in different kinds of cable installations. However, most of the traditional rating methods introduced in Section 2.2, especially IEC standards, are based on a number of imprecise assumptions which may not match the heat transfer phenomenon in reality. The main reasons for the continuing use of the continuous rating by transmission operators are the lack of actual knowledge of the cable environment and the limitations of thermal models. In order to apply the dynamic rating method, more accurate models are required. At the same time, these models must be able to take into account the real-time load and environmental data instead of using the worst case assumption. However, most of the existing dynamic rating systems introduced in Section 2.3 are still based on the model from IEC standards which have been proved to be unreliable in some cable installations.

In order to overcome these problems, thermal models for three kinds of cable installation, including directly buried cable system, cable installed directly in air and cable installed in tunnel system have been investigated. Several thermal models for each kind of cable arrangement have been built and tested with the real-time load and environmental data to find suitable dynamic thermal models for dynamic rating system. This is discussed further in Chapter 3.

On the other hand, most of the existing dynamic rating systems can only perform the emergency cable rating from the present time step. However, transmission operators also need to know the emergency rating in advance to assist in day-ahead planning. In order to predict the emergency cable rating forward from the future time steps, the thermal status of the cable at future time steps should be predicted. Thus, environmental and load forecasting systems are required to be integrated into the dynamic rating system. Based on the dynamic thermal models, the environmental and load forecasting data can be translated into the thermal prediction of the cable. The load forecasting and predictive cable rating are discussed further in Chapter 4 and Chapter 5 respectively.

Chapter 3: Dynamic Thermal Models for Predicted Ratings

This thesis proposes a novel rating prediction method based on the integration of a load forecasting system into a dynamic rating method. This day-ahead Predicted Cable Rating provides the time-limited emergency rating calculated forward from any point within the next 24 hours to assist in day-ahead planning for transmission operators. In order to obtain reliable rating values, accurate dynamic thermal models for different kinds of cable installations are a prerequisite.

Dynamic thermal models operate on real-time measurements of environmental conditions, equipment temperature, and circuit loading. As a result, the parameters which are measured by the system and the usage of these parameters in models to calculate cable temperature are two of the most important factors in evaluating dynamic thermal models. In cable systems, the temperature won't change suddenly but gradually from one temperature to another temperature (e.g. 20°C to 90°C). Thus, the thermal time constant of the cable system, which represents the time required for the cable system to transition from the state maintained at a certain temperature to a different temperature in this manner (a standard value of the time to make 63.2% of the total temperature change), is used to describe the speed of thermal responsiveness for different cable installations. Normally for the same cable sample, the thermal time constant, from shortest to longest, are cables in air, tunnel cables and buried cables. As a result, for each kind of cable installation, a different dynamic thermal model is required.

In this section, the idea of predicted rating is introduced and dynamic thermal models for three kinds of cable installations (directly buried, in air and cable tunnel systems) have been analysed and tested to find the most appropriate models for use in the predicted rating system.

3.1 Requirements of predicted rating

The ideal of predicted rating is based on the dynamic thermal models for each kind of cable system, day-ahead temperature forecasting data and load predictions, the predicted rating system can be implemented.

An example of the predicted rating concept is presented in Figure 3.1. The current time step t is at hour 48. The hourly load predictions from 48hr to 72hr (blue dash line) are generated from the load prediction system. Based on these load prediction data, the cable temperature can be predicted during this period. If the 12hr ahead 6hr emergency rating is required, the predicted

cable temperature at (t+12, 60 hours) will be used to calculate the 6hr emergency rating, the maximum step current the cable can carry from 60hr to 66hr. When the time step comes to (t+12), the predicted error estimation system will obtain an estimation of the error in the predicted rating very rapidly (within 0.1 second). In this case, the predicted rating overestimates the 6hr emergency rating by 22A, if this value is higher than the set limit, the predicted rating values will be replaced by the real-time rating value. It should be noted that the whole procedure of 24hr-ahead predicted rating will be processed at every hour (can be modified according to the operational requirement) in the system. As a result, the predicted ratings will be updated by more accurate values at each hour. This is a crucial step in making the method more user friendly for system operators, who presently are not able to plan the operation of the system based on instant values of rating.

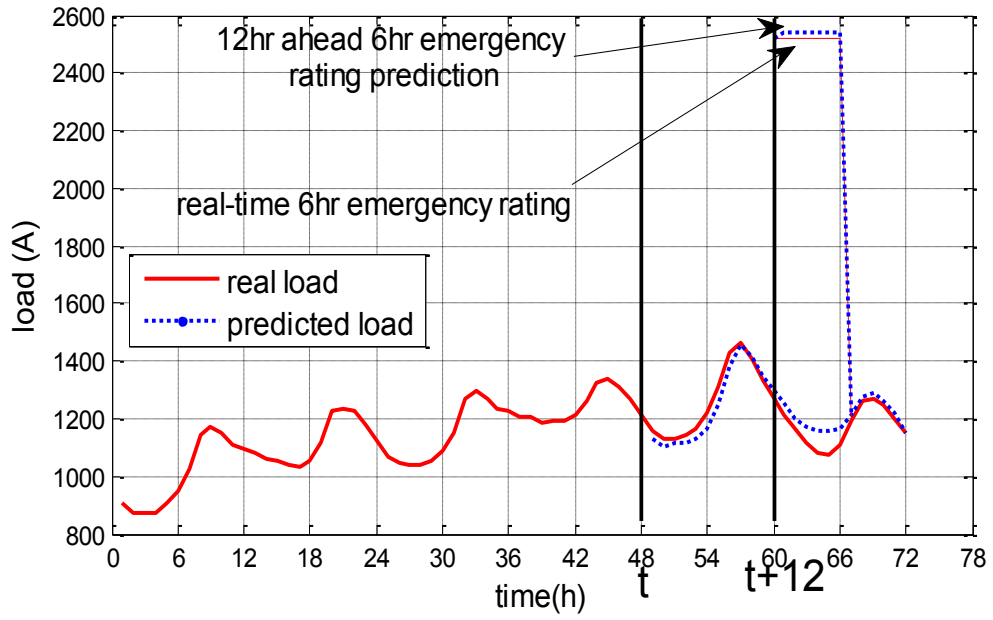

Figure 3.1 – Illustrative predicted rating example

From this example, some requirements for the predicted rating system can be recognised. First, dynamic thermal models for different kinds of cable installations should be built. These models should be able to take into account the real-time measurement data and the predicted data, update the thermal parameters and heat losses which are essential to calculate the temperature response of the cable in each step. In order to function well in the predicted rating system, these dynamic thermal models should be precise and fast in cable temperature and rating calculations. Thus, the suitable models should reach a compromise between the accuracy and solution speed.

Second, in order to predict the cable rating 24 hours ahead, the day-ahead ambient temperature and load information are needed at each time step. In this work, the ambient temperature forecast data is assumed to be available. A load prediction system is required to forecast the

day-ahead load demand. This system should be able to forecast the load of cable circuit for the following 24 hours and update the prediction at each step.

Third, in order to reduce the risk of predicted rating system, a rating error estimation function should be integrated in the system. This function should be able to estimate the prediction rating error without using the dynamic thermal model to perform a fast and reliable error estimation. When the estimated rating error is higher than a set value, the predicted rating value in the system will be replaced by the real-time rating value.

This Chapter lays emphasis on finding dynamic thermal models which are suitable for the predicted rating systems for buried cable, cable in air and cable tunnels.

3.2 Directly buried cable

Most existing dynamic rating methods for buried cable are based on the IEC 60287 and IEC 60853 standards. However, according to the tests in this section, the poor performance of IEC models in real-time conditions shows that they are not the ideal base thermal models for a dynamic rating system for buried cables. As a result, a more suitable thermal model should be found to perform a better dynamic rating. This section includes the in-depth analysis of the IEC 60853 and Finite Difference Method (FDM) transient models to evaluate their applicability in the dynamic rating algorithm for buried cables. An FEA model is built as a benchmark, as it allows the study for more complex thermal environments around the cable, which are able to offer an improvement over the simpler analogue approaches by removing assumptions. In addition, such tools have been used by many authors to examine problems related to cable ratings [5][40][56].

3.2.1 Example circuit of directly buried cable

The properties of a 275kV XLPE cable are shown in Table 3.1. Thermal properties of the materials are from [24].

Table 3.1 - Buried Cable Properties

Component	Outer Diameter (mm)	Material	Thermal Conductivity (W/m·K)	Volumetric Heat Capacity (MJ/m^3K)
Conductor	65.0	Copper	400	3.45
Conductor screen	68.6	Semicon	0.286	2.4
Dielectric	112.6	XLPE	0.286	2.4
Dielectric screen	115.8	Semicon	0.286	2.4
Screen/Bedding	121.0	Copper/Semicon	44.1	2.4
Sheath	128.4	Lead	35.3	1.45
Outer Sheath	139.6	PE	0.286	2.4

Three single-phase cables are buried 500mm below the ground surface with 400mm phase spacing in a flat configuration. The heat generation from the cable is calculated using the IEC 60287 standard [14]. All the soil has the same thermal parameters and is treated as a uniform medium with thermal resistivity of 1.5 KmW^{-1} and volumetric heat capacity of 1 $MJm^{-3}K^{-1}$. The cable has semi conductive conductor screen and dielectric screen layers, their thermal property are assumed to be the same with XLPE (as shown in Table 3.1) due to the lack of actual values.

3.2.2 Thermal model based on IEC 60853-2

The analytical method, IEC 60853-2 [24], is the most widely used base model around all the existing dynamic rating systems for underground cable[3], [37], [48], [54]. An equivalent 2-cell, one dimensional thermal circuit is used to calculate the temperature rise internal to the cable (Figure 3.2). The hypothesis of Kennelly [17] and an attainment factor are used to calculate the temperature rise of the rated cable resulting from adjacent cables and ambient conditions (Figure 3.3). Summing these two parts then gives the total conductor temperature rise above ambient.

The first section of Figure 3.2 includes the heat sources (W_C) from conductor losses; thermal resistance (T_A) of the dielectric along with the thermal capacitances (C_A) of the conductor and the inner part of the dielectric; the thermal resistances (T_B) and capacitances (C_B) of the remainder of the cable are represented in the second section which already takes account of the extra losses occurring in the sheath. If the cable is installed in a duct or pipe, the duct or pipe is also included in the second section of the thermal circuit. If the cable is installed in air, the second section includes everything as far as the free air.

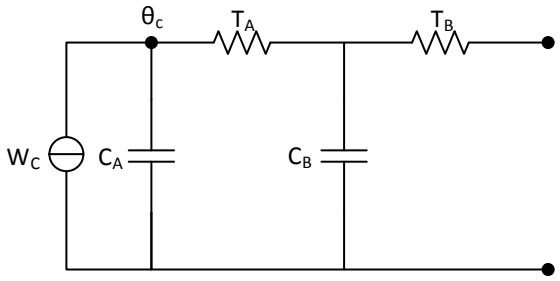

Figure 3.2 - Thermal circuit to calculate the temperature rise in the internal parts of the cable in IEC 60853-2

To calculate temperature rise from the influence of the surrounding soil, the IEC 60853-2 standard assumes that the cables are line heat sources with the internal thermal properties equal to that of the ambient soil. The hypothesis of Kennelly is used to consider the ground surface by assuming that this surface is isothermal. As a result, the conductor temperature rise from heat

sources external to the rated cable can be calculated as the sum of the temperature rise caused by the adjacent cables and the fictitious images of the rated cable and all the adjacent cables placed symmetrically with the ground surface (Figure 3.3). The fictitious image cables are assumed as negative heat sources with the same heat magnitude of their counterparts.

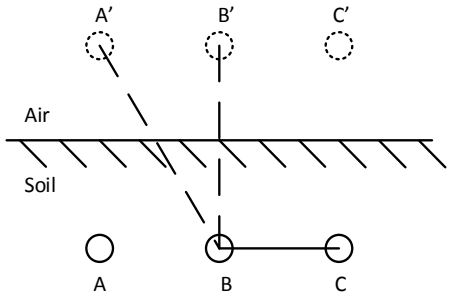

Figure 3.3 - Kennelly hypothesis to calculate the temperature rise due to the external parts of the cable in IEC 60853-2

The original IEC 60853-2 can only calculate the transient thermal response to a step current which is not suitable for the dynamic rating calculation. In order to consider the cable temperature response to the load current varying with time, the temperature rise is calculated using a numerical convolution technique. The following equation describes the integration procedure:

$$\theta_c(t) = \theta_{c\_initial} + \sum_{t=1}^{t \le m} d\theta\big(W_t(t), W_t(t-1)\big) \qquad (3.1)$$

where $W_t(t)$ represents the total heat generation from the t^{th} step loading at the integration step, $d\theta(W_t(t), W_t(t\text{-}1))$ is the temperature change caused by the loading difference between 2 adjacent steps. In IEC 60853-2, this temperature change is combined from two parts (internal cable and external environment); $\theta_{c\_initial}$ is the initial cable conductor temperature (°C) and $\theta_c(t)$ is the cable conductor temperature (°C) at time t; m is the total time steps.

3.2.3 Thermal model based on Finite Difference Method (FDM)

Nowadays, the whole thermal equivalent circuit can be easily computed by using the Finite Difference Method (FDM). Cigré Electra 87 [29] presents a FDM method for the calculation of the thermal transient response of single-core cables to a step function. The thermal circuit is refined by increasing the number of cells, although the assumption that the heat flow is radial both inside and outside the cable domains remains. Thus, the transient heat conduction in the cable and soil are solved using the FDM for both time and space domain.

This section discusses the thermal equivalent circuit in great details in order to construct an accurate thermal model for buried cables. In addition, the real-time load current input of the cable is able to be considered in this thermal model in order to calculate the real-time cable temperature. The thermal-electric analogue circuit for the example buried cable circuit in Table 3.1 is presented as Figure 3.4. The material of the conductor screen and insulation screen of this cable circuit is a conductive XLPE compound, as a result, these two layers are assumed to have the same thermal properties as the XLPE insulation. The conductor losses, sheath losses and armour losses are calculated per IEC 60287 standard. There are still some assumptions incorporated in this model: the ground surface is isothermal by using the Kennelly hypothesis; thermal properties of the ambient soil and cable components are assumed to be constant which ignores any change in the thermal properties from moisture migration in the soil; the thermal field occupied by adjacent cables and image cables are assumed to be the same with soil; the metallic parts in the cables are regarded as isothermal by assuming negligible thermal resistances.

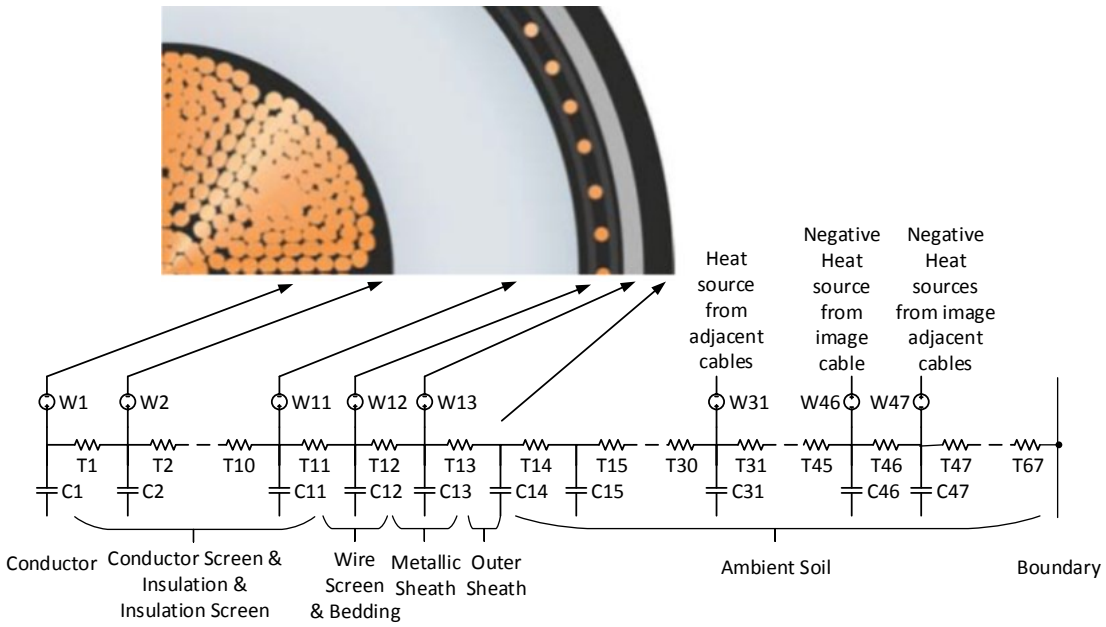

Figure 3.4 – Thermal-electric analogue circuit for buried cables

In the FDM model, the components in each cell of the thermal circuit are regarded as isothermal. In order to obtain more accurate solutions, the thick layers or the layers with high thermal resistance need to be divided into more layers to fully represent the shape of the temperature profile in the radial direction. In this model, the numbers of layers in the cable insulation and ambient soil have been tested and the results suggest that 10 layers of insulation and 50 layers of ambient soil should be sufficient to obtain an accurate temperature result in transient studies. Thus, the first 14 layers are used to represent the internal parts of the cable from the conductor to the cable surface. In order to simulate the 2D boundary condition in 1D

FDM model, two issues have been considered. First, three additional layers are placed in the soil in order to consider the heat generated from adjacent cables and image cables. The image cables are used to simulate the isothermal ground surface by the hypothesis of Kennelly. Second, the external boundary of the soil is 20 meters away from the rated cable and set as a constant temperature according to the typical soil temperatures in different seasons. The 20 meters external boundary is sufficiently far away from the cables so that there is no appreciable change in temperature at such distance.

3.2.4 FEA model for directly buried cable

A 2D model has been built in commercial FEA software as a comparator to the IEC 60853 and FDM models themselves, and the dynamic rating model based upon them. The thermal field domain of this model is shown in Figure 3.5. The cross section of buried cable geometry is symmetric. Although the sheath loss coefficients of the two outer cables are slightly different, the effect on the conductor temperature results of the rated cable is negligible (less than 0.05°C in steady-state), so the sheath loss coefficients are set as same value for both outer cables. Thus, it is only necessary to model half of the cross section by setting the left side boundary condition as symmetry. It provides benefits in terms of saving the computation time. The right side boundaries are set as thermal insulation, and extended 10m in the x-direction from the centre-line of the cable group, which is sufficiently far away from the cables that there is no appreciable change in temperature with distance. Both the symmetry and thermal insulation boundary conditions can be represented by:

$$\boldsymbol{n} \cdot (k \nabla T) = 0 \tag{3.2}$$

where k is the thermal conductivity ($Wm^{-1}K^{-1}$) and T is the temperature (K). This equation specifies that the temperature gradient across the boundary must be zero because there is no temperature difference across the boundary.

The ground surface condition is able to include both convection and solar radiation. In order to compare with the IEC and FDM models, the ground surface is assumed to be isothermal in this test. At the depth of 10m from the ground surface, the bottom boundary is specified isothermal at a temperature of 10°C. The isothermal boundary condition can be described by:

$$T = T_0 \tag{3.3}$$

where T_0 is the constant temperature (K) on the boundary.

All the soil has the same thermal parameters and is treated as a uniform medium. The thermal conductivity of the screen/bedding layer is determined by the mixture rule [57] to obtain an

equivalent value of two kinds of components. According to this rule, the equivalent thermal conductivity and volumetric heat capacity of the screen/bedding layer are calculated by sum of the two thermal properties of components (copper and semicon) multiplied by their volume fraction. The heat generation from the cable is calculated using the IEC 60287 standard and the construction and settings within the FEA model is as per [5].

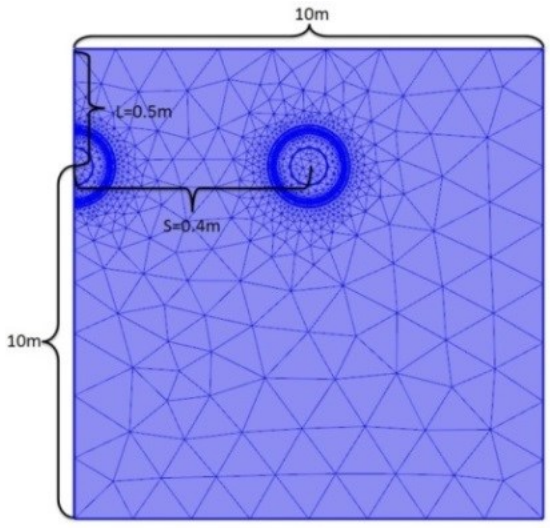

Figure 3.5 - Geometry of the FEA model for buried cable

3.2.5 Test results for directly buried cable

Figure 3.6 shows the conductor temperature difference between the FEA model and models using IEC 60853 and FDM respectively. It presents results for a 24hr transient of the given cable circuit in Section 3.2.1, after the application of a 1400A step load. The initial temperature of the cables and ambient soil is set as 20°C, the soil thermal resistivity 1.5 KmW^{-1} and the soil volumetric heat capacity is 1 $MJm^{-3}K^{-1}$.

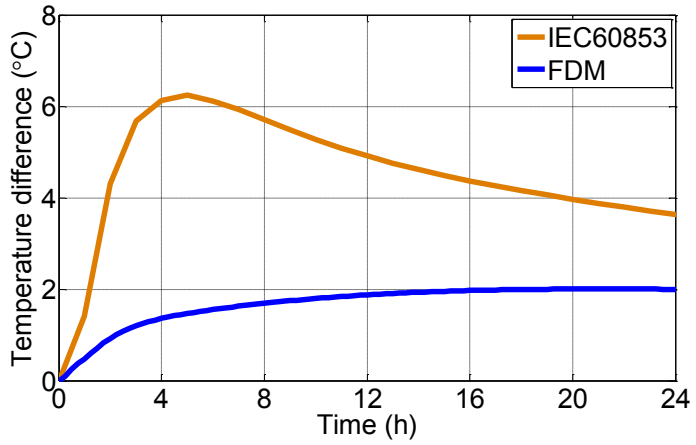

Figure 3.6 - Conductor temperature difference compared to FEA model

In Figure 3.6, the temperature difference between the IEC and FEA models rises sharply in the first 5 hours, peaks at about 6.2°C and then decays after 5 hours. Comparing the difference between the IEC and FEA models, the difference between the FDM and FEA model is much smaller over the first 24 hours, the maximum difference being only 2°C. The FDM method shows a much better fit to the FEA model as it represents more realistically the rate at which heat dissipates from the cable surface into the soil. As a result, using the FDM model instead of the IEC 60853 model as a basic transient calculation model within the dynamic rating calculation has the potential to improve the performance of the whole system. To test this supposition, two dynamic rating models have been implemented in Matlab.

3.2.5.1 Dynamic cable temperature

Figure 3.7 shows the conductor temperatures calculated by the models over a 1 week period. In this test, the cable geometry is as per Table 3.1. As expected, the FDM dynamic thermal model matches very well with the FEA model. The maximum difference between these two models is only 0.4°C which is much better than the 4.1°C seen in the IEC 60853 based model. In addition, the mean absolute difference between the FDM and FEA model is 0.09°C compared to 1.83°C between the IEC 60853 based model and the FEA model.

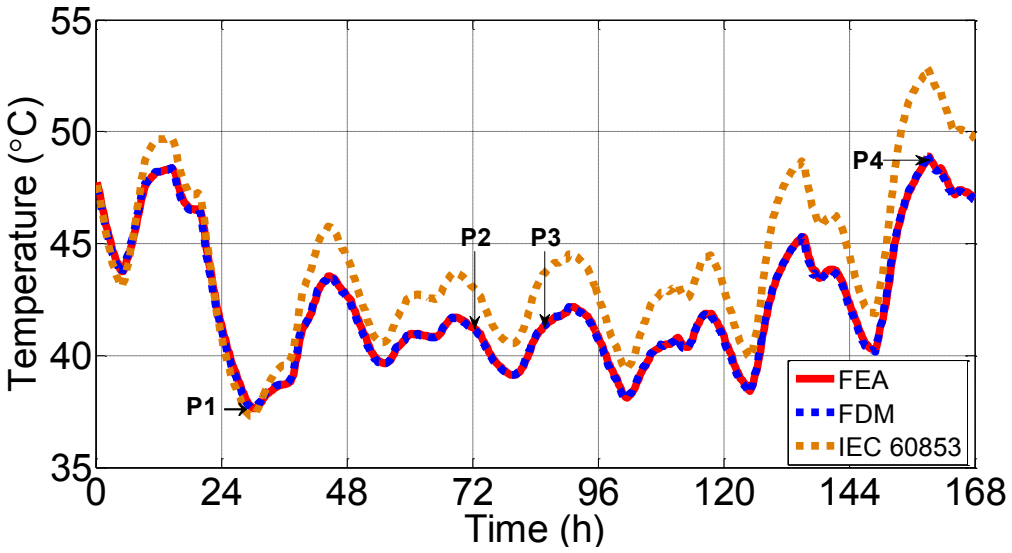

Figure 3.7 - Conductor temperature of FEA, IEC based and FDM models

The solution time for the FDM model is shorter than the IEC based model which gives the FDM model further advantage in practical usage. The reason for the longer solution time in the IEC based model is that the superposition method in the model needs to consider the temperature rise due to the historical load at each step. The long thermal time constant for the buried cable requires a very long period of historical data (at least two weeks), resulting in longer solution times and higher memory usage. However, the solution for the FDM model proceeds via the

creation of a matrix equation for each node in the thermal-electric analogue circuit, and a tridiagonal matrix algorithm is used to solve the temperature in the matrix. As a result, only the temperature matrix from the previous step is needed to solve the equation at the current step which makes it faster than the IEC based model. Using a PC of 3.40GHz i7 CPU and 16GB RAM, it takes 96 seconds to solve the transient thermal model for one year (365 days, 1 hour/step) by using the FDM model compared to 649 seconds by using the IEC based model and 2422 seconds by using FEA model.

3.2.5.2 Dynamic cable ratings

To test the benefits from using the improved FDM model, four points which present a low level loading, two mid-levels loading and a peak loading point are chosen (Table 3.2, Figure 3.7) as the starting points for an emergency rating calculation.

Table 3.2 - Parameters for four starting points

Parameters	**Point1**	**Point2**	**Point3**	**Point4**
Time (h)	28.5	72	81	158.5
Load (A)	324	1008	1008	1476
Temperature (°C)	38.2	41.3	40.0	48.61

Table 3.3 shows the 1hr, 6hr and 24hr emergency ratings, which indicate the maximum current which can be carried by the circuit for the relevant time periods from the given starting points. For comparison, the 'winter' continuous rating is 1692A using an ambient temperature of 10°C and the 'summer' rating is 1454A at an ambient temperature of 30°C, these two rating values are calculated from the FEA model.

Table 3.3 – Emergency Rating for Different Models

Model		Benchmark FEA(A)	IEC 60853 based model(A)	FDM model(A)	Improvement from IEC to FDM
Emergency ratings of **Point 1**	1hr	4457	4182	4349	3.75%
	6hr	2852	2431	2693	9.19%
	24hr	2251	2082	2148	2.93%
Emergency ratings of **Point 2**	1hr	4398	4044	4276	5.28%
	6hr	2806	2436	2710	9.76%
	24hr	2252	2092	2167	3.33%
Emergency ratings of **Point 3**	1hr	4490	4084	4317	5.19%
	6hr	2825	2447	2726	9.88%
	24hr	2290	2097	2174	3.36%
Emergency ratings of **Point 4**	1hr	4189	3741	4024	6.76%
	6hr	2742	2379	2646	9.74%
	24hr	2257	2069	2148	3.50%

The data shown in Table 3.3 demonstrates that improvements in emergency rating of up to 10% can be obtained through the use of the FDM thermal model instead of the IEC model. A rating improvement of this magnitude could be vital in mitigating costly generation constraints where an adjacent circuit is under outage. The reason for the improvement in 6hr rating being larger than the 1hr and 24hr rating can be seen with reference to Figure 3.6, where the maximum error of the IEC 60853 standard occurs 5 hours in to the transient, owing to an overestimated conductor temperature rise from the environment.

The comparison results among these three models show that the FDM model is able to provide precise transient temperature and emergency rating results close to FEA model while using much shorter time than both FEA and IEC based model. Thus, the FDM model is chosen as the dynamic thermal model in predicted rating system for buried cable.

3.3 Cable in air

For cables installed in air, where changes in cable temperature occur quickly due to the short time constant, using dynamic cable ratings which take fully into account load history and real-time measured environmental parameters instead of the worst-case environment could dramatically improve the ratings of existing cable systems.

Heat transfer phenomena are more complex for cables installed in air than for those installed underground, and proper handling of these situations requires the solution of a set of energy balance equations. Among these equations, the convective heat transfer coefficient at the cable surface is the most uncertain one due to the various influences from air temperature, viscosity, density, velocity and flow angle. As a result, this section focuses on testing the existing heat transfer coefficients on three base models with real-time input data, in order to find a suitable base model for the dynamic rating system. These models and results will be used to generate test cases for comparison with experimental data in Chapter 6. The properties of the cable used in this test are the same as the buried cable (Table 3.1 in Section 3.2.1).

3.3.1 Base thermal model analysis

1. IEC based model

IEC 60287 is theoretically able to calculate the steady-state rating for cables laid in free air both with and without solar radiation. Based on a large number of tests on various cables configurations which were carried out in the UK during 1930s, Whitehead and Hutchings [58] deduced the following equation that represents the total thermal dissipation from cable surface to air:

$$W_t = \pi D_e^* h(\Delta\theta_s)^{5/4} \quad (3.4)$$

where D_e* is the external diameter of the cable (m), h is the heat dissipation coefficient on cable surface ($Wm^{-2}(K)^{-5/4}$), and $\Delta\theta_s$ is the excess of cable surface temperature above ambient temperature (K). Thus, the equivalent thermal resistance T_4 external to the cable can be expressed as:

$$T_4 = \frac{1}{\pi D_e^* h(\Delta\theta_s)^{\frac{1}{4}}} \quad (3.5)$$

The values of heat transfer coefficient, h, were obtained from these experiments and fitted with the following analytical expression:

$$h = \frac{Z}{(D_e^*)^{g_i}} + E \quad (3.6)$$

where constants Z, E and g_i which are related to cable diameter for various cable arrangements are given in Table 2 in IEC 60287. Surface temperature rise above ambient, $\Delta\theta_s$, can be obtained iteratively by considering the energy balance equation at the cable surface ((3.7) for cables protected from direct solar radiation and (3.8) for cables directly exposed to solar radiation):

$$\theta_c - \theta_{amb} - \Delta\theta_s + \Delta\theta_d = \frac{\pi D_e^* h(\Delta\theta_s)^{\frac{5}{4}} T_{in}}{1 + \lambda_1 + \lambda_2} \quad (3.7)$$

$$\theta_c - \theta_{amb} - \Delta\theta_s + \Delta\theta_d + \Delta\theta_{ds} = \frac{\pi D_e^* h(\Delta\theta_s)^{\frac{5}{4}} T_{in}}{1 + \lambda_1 + \lambda_2} \quad (3.8)$$

where θ_c is cable conductor temperature (K); θ_{amb} is ambient temperature (K); $\Delta\theta_d$ is the temperature rise caused by dielectric losses (K); $\Delta\theta_{ds}$ is the temperature rise caused by solar radiation (K); λ_1 and λ_2 are sheath and armour loss factors respectively; T_{in} is the internal thermal resistance of the cable. After the value of T_4 for cable in air has been calculated, cable temperature and ratings can be obtained by the normal procedure as referred to IEC 60287 and IEC 60853 standards.

This method tries to embody heat convection, radiation, conduction and mutual heating in a single heat transfer coefficient. However it restricts the use of the model to natural cooling. Furthermore this experimentally based equation is over-simplified and cannot fulfil all the circumstances of cable geometries and arrangements. Morgan has shown that exponent ¼ in (3.5) and heat transfer coefficient h in (3.6) varies with the temperature rise of the cable surface [59]. This is because a larger temperature rise of the cable surface will cause further reduction in

air density, which will lead to greater air velocity. As a result, the heat transfer on the cable surface will be faster, which gives an increase in h.

2. Thermal model based on FDM

In common with the application on buried cables, the Finite Difference Method (FDM) can be used to build a dynamic thermal model for cable in air. Instead of considering the conduction of heat through the soil as for buried cables, the cable in air model takes into account the convection and radiation from cable surface to ambient.

In order to simulate the heat transfer on the cable surface in the FDM model, one node outside the cable is used to represent the ambient air by assuming the ambient temperature matches the air temperature. Only one axial slice of the cable needs to be modelled if no longitudinal temperature variation is assumed. Unlike the IEC standard, this FDM model is able to divide the heat transfer coefficient into two parts: convection and radiation, which are represented by T_{conv} and T_{rad} respectively in Figure 3.8.

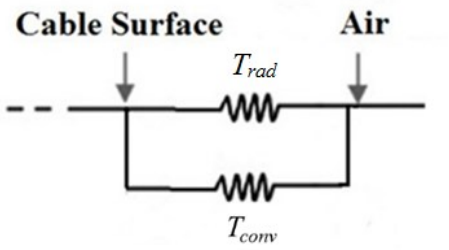

Figure 3.8 - Thermal network from Cable surface to ambient air

T_{conv} and T_{rad} are thermal resistances (KmW^{-1}) to simulate convection and thermal radiation from cable surface to air respectively. T_{conv} and T_{rad} can be calculated by following equations from Electra 143 method [31].

$$T_{conv} = \frac{1}{\pi D_e^* h_{conv}} \tag{3.9}$$

$$T_{rad} = \frac{1}{\pi D_e^* h_{rad}} \tag{3.10}$$

where h_{conv} and h_{rad} are the heat transfer coefficients ($Wm^{-2}K^{-1}$) for convection and radiation from the cable surface to air respectively. In the FDM model, these two values are calculated by the following equations:

$$h_{conv} = \frac{k_{air} C_E (Re)^{0.65}}{D_e^*} \tag{3.11}$$

$$h_{rad} = \sigma K_r k_r \left(\theta_s^{*2} + \theta_{amb}^{*\,2}\right)\left(\theta_s^* + \theta_{amb}^*\right) \tag{3.12}$$

$$Re = \frac{U_{air} D_e^*}{\nu_{air}} \tag{3.13}$$

where Re is the Reynolds Number, the ratio of inertial forces to viscous forces; k_{air} is the thermal conductivity of the air ($Wm^{-1}K^{-1}$); U_{air} is the air velocity (ms^{-1}); v_{air} is the kinematic viscosity of air (m^2s^{-1}); C_E is the experimentally determined constant referred in Table I in Electra 143 [31]; σ is *Stefan-Boltzmann* constant ($Wm^{-2}K^{-4}$); K_r is a constant linked to cable installation and k_r is the effective emissivity defined by Weedy and El Zayyat in Electra 143; θ_s^* and θ_{amb}^* are cable surface temperature and ambient air temperature in K. Note that the thermal resistance T_{conv} and T_{rad} are in parallel in the circuit of Figure 3.8, and according to parallel circuit theory and (3.9-3.10), an equivalent thermal resistance for T_{conv} and T_{rad} can be derived. Thus, a total heat transfer coefficient h_t can easily be obtained from (3.14):

$$h_t = h_{conv} + h_{rad} \tag{3.14}$$

The convective heat transfer coefficient T_{conv} from Electra 143 is only used for forced cooling due to the assumption that the air velocity is sufficiently high that turbulent flow occurs. In addition, the exponent 0.65 and the value of C_E in (3.11) were proved to vary with Reynolds Number by Morgan [60]. With Reynolds Number ranges from 0.4 to 4×10^5, the value of C_E decreases from 0.989 to 0.0266 and the exponent term (equal to 0.65 in (3.11)) will increase from 0.330 to 0.805. These changes will make the heat transfer coefficient fit the experimental curve better [60].

3. FEA model

To test the precision of the FDM model, an FEA model is built as a benchmark. This model uses a heat transfer coefficient on the cable surface to simulate the heat transfer between cable and air. The geometry is shown in Figure 3.9. In common with the buried cable, the cable cross section geometry is symmetric, it is only necessary to model half of the cable by setting a symmetrical boundary condition at left side. The heat generation from the cable is calculated using the equations in IEC 60287 standard but improved by the consideration of temperature dependent conductor and sheath losses.

The equations to calculate the heat transfer coefficient for convection are common with the equations used in FDM model. Thermal radiation on the cable surface is simulated by the 'Surface-to-Ambient Radiation' FEA model, with real time air temperature input according to:

$$q_{rad} = k_r \sigma \left(\theta_s^{*4} - \theta_{amb}^{*\,4}\right) \tag{3.15}$$

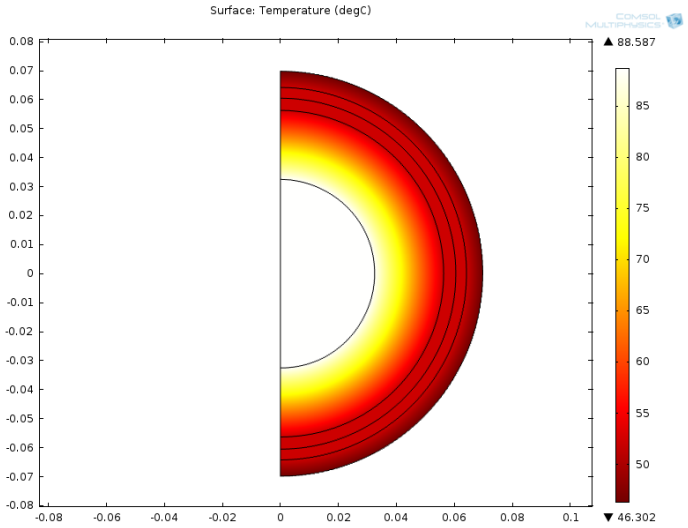

Figure 3.9 - Geometry of FEA model for cable in air

3.3.2 Heat transfer coefficients

In addition to the heat transfer coefficient from IEC 60287 standard and the Electra 143 methods which have been introduced above, two other methods to calculate heat transfer coefficient on the cable surface are presented here: Morgan's equations and the IEEE 738 standard. Unlike the IEC 60287 standard or the Electra 143 method which can only be applied to natural cooling or forced cooling condition, two new methods can be used in both two circumstances.

1. Morgan's equations

Morgan presented a thermal rating model for overhead-line conductors including both natural and forced cooling equations and a method to consider solar radiation [60].

The heat transfer coefficient for radiation at the cable surface h_{rad} is calculated by (3.12) (the same method as in Electra 143). For the natural cooling model, the heat transfer coefficient of convection $h_{conv,n}$ is calculated by:

$$h_{conv,n} = \frac{k_{air} c (Gr \cdot Pr)^m}{D_e^*} \tag{3.16}$$

where *Gr* is the Grashof Number (ratio of buoyancy to viscous force acting on a fluid) and *Pr* is the Prandtl Number (ratio of kinematic viscosity to thermal diffusivity). The value of coefficients *c* and *m* are given from Table 2 in [60] with various ranges of Rayleigh Number (*Gr*·*Pr*).

For the forced cooling model, the heat transfer coefficient of convection $h_{conv,f}$ is calculated by:

$$h_{conv,f} = \frac{k_{air} b (Re)^p}{D_e^*} \tag{3.17}$$

The values of coefficients b and p for various ranges of the Reynolds Number are taken from Table 3 in [60]. It can be noticed that the equation to calculate convective heat transfer coefficient in Electra 143 uses the same method as (3.17), but fixes the value of p to 0.65.

When the air velocity is at a low level, both natural and forced convection might need to be considered. For this natural cooling, an equivalent Reynolds Number for natural convection Re_{eq} is first calculated by:

$$Re_{eq} = \left[\frac{c(Gr \cdot Pr)^m}{b}\right]^{1/p} \tag{3.18}$$

The natural convective flow is vertical to the cable surface, and if the direction of the forced convective flow is at an angle φ with respect to the natural flow, the effective Reynolds Number for mixed convection Re_{eff} is given by:

$$Re_{eff} = \left[\left(Re_{eq} + Re \cdot cos\varphi\right)^2 + (Re \cdot sin\varphi)^2\right]^{0.5} \tag{3.19}$$

Thus the mixed convection heat transfer coefficient $h_{conv,m:}$

$$h_{conv,m} = \frac{k_{air} b \left(Re_{eff}\right)^p}{D_e^*} \tag{3.20}$$

The heat transfer coefficient obtained from Morgan's method can be used in the FDM and FEA models to consider natural, forced and mixed convection to determine the cable rating in free air. In addition, Morgan has shown that the natural cooling can be ignored when the cable surface temperature rise above ambient temperature does not exceed 20K and the air velocity exceeds $1 m \cdot s^{-1}$ [61].

2. IEEE 738 standard

The IEEE 738 standard is used to calculate the Current-Temperature relationship of bare overhead conductors [62]. The mathematical models of this standard are based upon the House and Tuttle method [63] and the modification by East Central Area Reliability Coordination Agreement (ECAR) [64]. Although it is a standard for bare overhead conductors, the methods to calculate convection rate and radiation rate at the cable surface with transient environmental factors can be referred to and applied to models for cable in air.

The forced convective heat transfer coefficient is calculated by (3.21-3.22) [62]. Equation (3.21) applies at low air velocity and (3.22) applies to high air velocity, at any air velocity, the larger of the two values is used.

$$h_{c1} = \frac{k_{air}\left[1.01 + 0.0372\left(\frac{U_{air}\rho_{air} \cdot D_e^*}{\mu_{air}}\right)^{0.52}\right]K_{angle}}{\pi \cdot D_e^*/1000} \tag{3.21}$$

$$h_{c2} = \frac{k_{air}\left[0.0119\left(\frac{U_{air}\rho_{air} \cdot D_e^*}{\mu_{air}}\right)^{0.6}\right]K_{angle}}{\pi \cdot D_e^*/1000} \tag{3.22}$$

where ρ_{air} is the density of air (kgm^{-3}); μ_{air} is the dynamic viscosity of air (Pas). It should be noticed that the unit for D_e^* in IEEE standard is in mm. K_{angle} is the wind direction factor calculated by:

$$K_{angle} = 1.194 - cos\varphi + 0.194cos2\varphi + 0.368sin2\varphi \tag{3.23}$$

where φ is the angle between the wind direction and the cable axis. The natural cooling heat transfer coefficient can be obtained by:

$$h_{conv,n} = \frac{0.0205\rho_{air}^{0.5}D_e^{*0.75}(\theta_s - \theta_{amb})^{0.25}}{\pi \cdot D_e^*/1000} \tag{3.24}$$

The radiated heat transfer coefficient is:

$$h_{rad} = \frac{0.0178D_e^*k_r\left[\left(\frac{\theta_s + 273}{100}\right)^4 - \left(\frac{\theta_{amb} + 273}{100}\right)^4\right]}{(\theta_e - \theta_{amb})\pi \cdot D_e^*/1000} \tag{3.25}$$

where k_r is the emissivity of cable surface. θ_s is cable surface temperature (°C) and θ_{amb} is the ambient temperature (°C). All the variables in Equations (3.21-3.25) can be found from Table (2-7) in the IEEE 738 standard [62]. This standard considers the different air densities with the various elevations of cable above sea level, which do not appear in other methods.

All the models and heat transfer coefficient equations introduced above have been coded in Matlab or built in Comsol software. In order to compare results of each model and heat transfer coefficient, real-time input data are applied to all the models, with the results obtained presented in the following section.

3.3.3 Test results for cable in air

The load data used in this test is from the Medway cable circuit. It contains 60 days' half-hourly load data from 01/03/2007 to 29/04/2007. According to the test, the thermal time constant is less than 2 hours for cable protected from direct solar radiation under the constant input current and ambient conditions used in this report. When the cable is directly exposed to solar radiation, 3 days are needed to reach the constant daily cycle due to the daily solar pattern. As a result, 7 day constant load calculated from average load value of these 60 days represents a sufficient initial condition. The real-time environmental inputs considered in this test include air temperature, wind speed, wind direction and solar intensity. In common with the load data, the first 7 days are a constant average value to build up an initial condition. Among these four real-time inputs, the first three are from a weather station in Chatham [65], close to the Medway circuits. Air temperature is measured half hourly; wind speed and direction data are the average value per day. Although daily wind speed and direction data is not sufficient enough for real-time cable temperature calculation, the input step in the model is set as 15mins to make sure the model can be applied with more frequent input data.

The natural cooling models mentioned before have been applied with real-time input data to calculate the conductor temperature and cable ratings. Similar tests have been applied for forced cooling models with the results shown in Appendix 1.

3.3.3.1 Dynamic cable temperature

Five natural cooling models have been built with real-time input data to test their performance:

1) IEC 60287 & IEC 60853 model (IEC)
2) FDM model with natural cooling heat transfer coefficient from Morgan (FDM_Morgan)
3) FDM model with natural cooling heat transfer coefficient from IEEE 738 (FDM_IEEE738)
4) FEA model with natural cooling heat transfer coefficient from Morgan (FEA_Morgan)
5) FEA model with natural cooling heat transfer coefficient from IEEE 738 (FEA_IEEE738)

The results are shown in Figure 3.10. In order to display the data clearly, Figure 3.10 only presents the results for the first 23 days and the time interval of the temperature data plotted in Figure 3.10 is at every 4 hours which is sufficient for presenting the trend of the data. From Figure 3.10, the following features can be observed. First, with the same heat transfer coefficient, the conductor temperature results from the FDM model and FEA model match well. The maximum conductor temperature difference between the FDM model and FEA model using Morgan's heat transfer coefficient and IEEE 738 heat transfer coefficient are 0.5°C and 0.48°C respectively. However, the much shorter solution time makes the FDM method preferable in the transient simulation. Second, the IEC model is not able to consider the time factor and altitude factor of solar radiation. As a result, in the first 7 days when the inputs are constant, daily

patterns seen in other models due to time and altitude factors of solar radiation could not be observed from the IEC model. In addition, compared to the other four models, the difference in conductor temperature between the IEC model and any other model is the largest. (During 67 days' simulation, the maximum difference between IEC and Morgan: 11.76°C; maximum difference between IEC and IEEE 738: 11.57°C). Third, Morgan's heat transfer coefficient is more conservative than the IEEE 738 method, leading to the conductor temperature being 1.19°C higher on average during the 67 days' simulation. The maximum temperature difference between these two methods is 2.72°C.

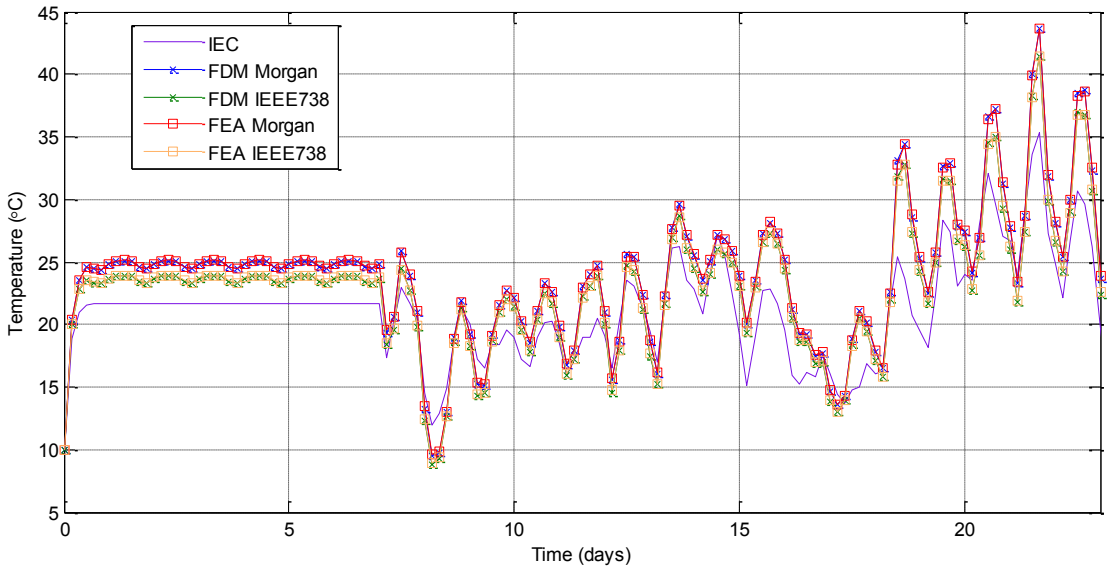

Figure 3.10 - Conductor temperatures from different natural cooling model

This section shows that the FDM model for cable in air is able to obtain precise transient cable temperature compared with the FEA model with the same heat transfer coefficient on the cable surface. However, the two convective heat transfer coefficients for natural cooling on the cable surface used in this section are from empirical equations, with unknown accuracy. As a result, a lab experiment will be used to demonstrate the accuracy of the FDM model for cable in air in Chapter 6.

3.3.3.2 Dynamic cable ratings

The thermal time constant for cables installed in air is much shorter than for directly buried cable. So the emergency rating calculation for cable in air is usually for a short term and requires fast calculation. Four sets of emergency rating data have been calculated for cable in air by natural cooling. In each set, the one-hour, four-hour and six-hour duration are assessed for the emergency rating. Figure 3.11 shows the real-time load input data and four chosen points to calculate the emergency rating:

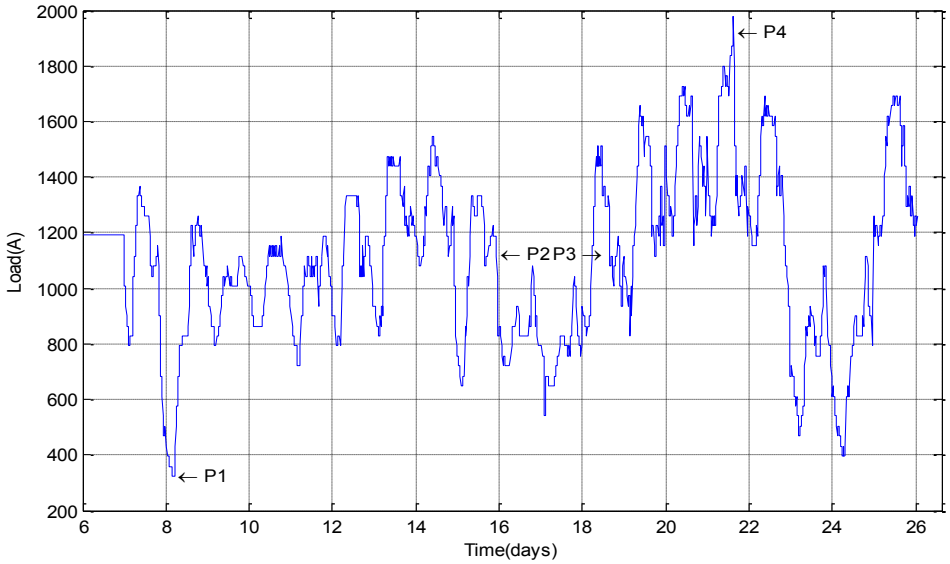

Figure 3.11 - Four chosen points to calculate emergency ratings for cable in air

Four points in Figure 3.11 present a low level load, two mid-levels of loading and a peak loading point. These four points as shown in Table 3.4 were chosen as the starting points for emergency ratings.

Table 3.4 - Four starting points to calculate the ratings for cable in air

Parameters	**Point1**	**Point2**	**Point3**	**Point4**
Time (h)	4:00a.m.	4:30p.m.	5:30a.m.	3:00p.m.
Load (A)	324	1116	1116	1980

Three models including the IEC model, FDM_Morgan model and FDM_IEEE 738 model are used to calculate emergency ratings for the natural cooling case. The ambient temperature is assumed as a constant value of 10°C and the intensity of the direct solar beam on a surface normal to the beam is assumed as 1000Wm^{-2} as this value is recommended in [20] when the solar radiation condition is unknown. Emergency rating results are shown in the Table 3.5:

Table 3.5 - Emergency rating for point 1-4 in natural cooling models

Ratings	**1hr rating (A)**			**6hr rating (A)**			**24hr rating (A)**		
Models	IEC	FDM_ Morgan	FDM_ IEEE738	IEC	FDM_ Morgan	FDM_ IEEE738	IEC	FDM_ Morgan	FDM_ IEEE738
Point 1	6104	5462	5487	3743	3230	3291	3537	2979	3066
Point 2	5952	4968	5005	3728	3182	3248	3537	2979	3066
Point 3	6273	5255	5283	3758	3204	3267	3537	2979	3066
Point 4	6046	4476	4569	3734	3138	3214	3537	2979	3066

From these tables, it is possible to identify the following features:

I. The results from FDM_Morgan model and FDM_IEEE738 model are similar, with those from the FDM_IEEE738 model being slightly higher. The result from the IEC model is much higher than the other two models. The reason can be found from Figure 3.10, as the IEC model does not satisfactorily account for the solar radiation. As a result, if the IEC method is used in the dynamic rating system, the rating will be overestimated.

II. Although point 2 and point 3 are at the same preload level, the emergency ratings are different. This is because of the loading history before the test point. For point two, the loading is reducing while the heat built up by the previous loading still has influence on the conductor temperature. This is the opposite of the situation at point three.

3.4 Tunnel cables

The number of cable tunnels with forced ventilation has significantly increased in the UK. In order to maximize the operational benefit from these assets, accurate real-time and advance cable ratings are essential. Because the bulk air velocities in the tunnels and the tunnel inlet temperature can vary with time, considering the real-time fluctuation of convection values from cable surface to air and from air to tunnel wall is vital to dynamically rate the cable. The dynamic thermal model used in this work is based on [9]. The convective heat transfer coefficient has been updated, taking both natural and forced convection into account.

3.4.1 Example circuit of tunnel cables

Two cable circuits are installed in a ventilated tunnel, each of the circuit includes three single phase 400kV XLPE cables. The properties of the cable are shown in Table 3.6. The phase separation is 0.5m, the heat generation from the dielectric losses is calculated using the IEC 60287 standard, while the conductor losses and the sheath losses are temperature dependent.

Table 3.6 - Cable properties

Component	Outer Diameter (mm)	Material	Thermal Conductivity (W/mK)	Volumetric Heat Capacity (MJ/m^3K)
Conductor	64.5	Copper	400	3.45
Dielectric	119.3	XLPE	0.286	2.4
Screen/Bedding	128.3	XLPE	0.286	2.4
Sheath	131.3	Aluminium	250	2.5
Outer Serving	142.5	PE	0.286	2.4

The tunnel system has three sections, two of which are riser shafts. The geometry of each section of the tunnel and the cable arrangement in the tunnel sections are shown in Figure 3.12 and Figure 3.13. The volumetric heat capacity of the rock is 2 $MJm^{-3}K^{-1}$ and the thermal resistivity of the surrounding rock is 1 KmW^{-1}. An isothermal boundary condition of 10°C is set 15m away from the tunnel centre. The air velocities can range from 0ms^{-1} to 4ms^{-1} in tunnel section 2.

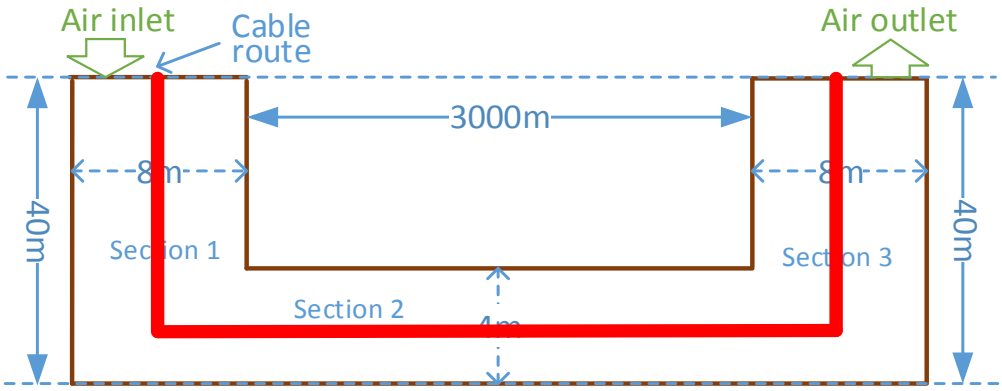

Figure 3.12 – Tunnel geometry

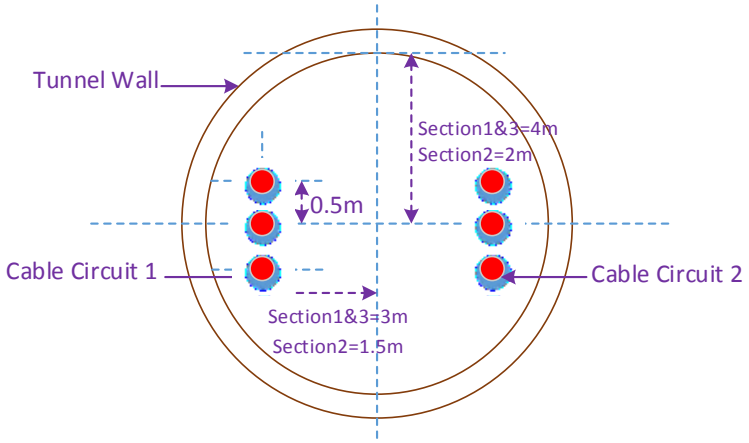

Figure 3.13 - Cable arrangement in the tunnel sections

3.4.2 Dynamic thermal model

Cigré Electra 143 is a numerical method widely used for calculating cable ratings for tunnel installations [31]. It uses a one-dimensional thermal circuit to represent slices through the tunnel cross-section based on a lumped parameter thermal-electrical analogue approach. The cable itself is modelled by a 5 node radial thermal network. Three further nodes are used to model the air within the tunnel and tunnel wall. Soil around the tunnel is modelled by dividing it into a set of annular rings with an equivalent number of nodes in the thermal network. In order to

represent the full tunnel, a number of axial divisions with equal size are used to take account of axial heat flow due to bulk air movement. However, this method has some limitations, such as the constant tunnel cross section, identical current for individual circuits, plus an assumption that the air speed in the tunnel is high enough to create turbulent flow.

The thermal model from Pilgrim et al [9] removes the restriction that different cable circuits can only operate in the same load cycle. In this model, FDM technique is used to simulate each cable in the tunnel. Each of the cables is represented as a thermal network by ten nodal points including thermal resistances, thermal capacitances and heat sources. The location of each node is shown in Table 3.7. Compared with the Electra 143 method, this model subdivides the dielectric area and adds more nodes in the thermal circuit to consider each component in the cable.

Table 3.7 - Nodal locations

Node	Location
1	Conductor (isothermal)
2	Outer surface of conductor screen
3-5	1/3, 2/3 values of dielectric and dielectric outer surface
6	Outer surface of Dielectric screen
7	Outer surface of bedding/screen wires
8	Outer surface of sheath
9	Log mean radius of serving
10	Outer surface of cable

The thermal network for the tunnel in this model is made to allow the consideration of air temperature rise from all the individual cables (Figure 3.14). A group of thermal resistances ($R10_n$) are defined to simulate the heat convection from each cable surface (node 10_n) to the air in the tunnel (node 11). Moreover, another group of thermal resistances (R_{rn}) directly connecting each cable surface (node10_n) to the tunnel wall (node12) are used to represent the heat transfer by thermal radiation between cable surface and tunnel surface. R11, between nodes 11 and 12, simulates the heat transfer from air in the tunnel to the tunnel wall by convection. To consider the heat transfer in the axial direction due to the air movement through the tunnel, the whole tunnel is divided into several slices and a thermal resistance R_{ax} is used to define the axial heat transfer between slices. The soil surrounding the tunnel is divided into m annular rings using the method in [31].

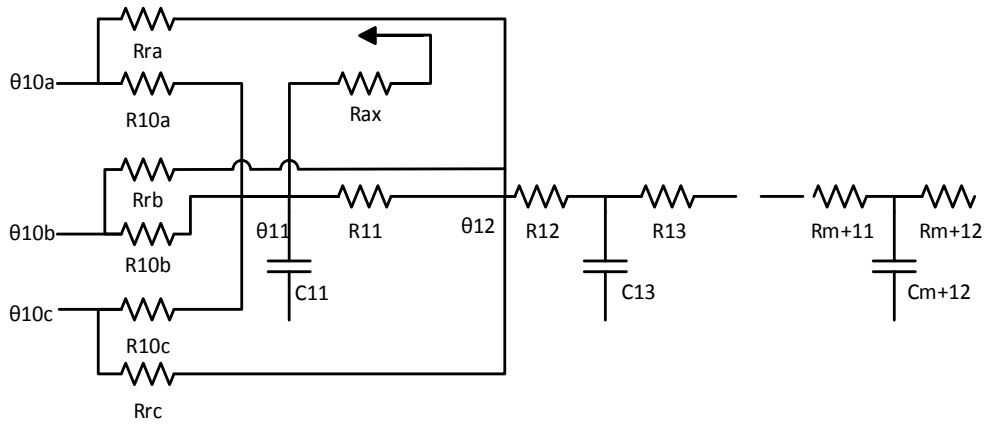

Figure 3.14 - The thermal network for the tunnel and ambient

The values of thermal resistances (KW^{-1}) for R_{10n}, R_{rn} and R_{11} are calculated by following equations:

$$R_{10n} = \frac{1}{\pi D_e^* h_{conv} \Delta x} \tag{3.26}$$

$$R_{11} = \frac{1}{\pi D_{tun} h_{wall} \Delta x} \tag{3.27}$$

$$R_{rn} = \frac{1}{\pi D_e^* h_{rad} \Delta x} \tag{3.28}$$

where h_{conv} and h_{rad} are the convection and radiation heat transfer coefficients from cable surface to air respectively ($Wm^{-2}K^{-1}$). The h_{wall} is the convective heat transfer coefficient from air to tunnel wall ($Wm^{-2}K^{-1}$). Δx is the slice separation (m); D_e^* is the diameter of cable surface (m); D_{tun} is the diameter of inner tunnel surface (m). In the model from Pilgrim [9], these three values are calculated by the following equations from the Electra 143 method:

$$h_{conv} = \frac{k_{air} C_E (Re)^{0.65}}{D_e^*} \tag{3.29}$$

$$h_{wall} = \frac{0.023 k_{air} (Re)^{0.8} (Pr)^{0.4}}{D_{tun}} \tag{3.30}$$

$$h_{rad} = \sigma K_r k_r [(\theta_s + 273)^2 + (\theta_{wall} + 273)^2][(\theta_s + 273) + (\theta_{wall} + 273)] \tag{3.31}$$

$$Re = \frac{U D_e^*}{\nu} \tag{3.32}$$

where θ_{wall} is the tunnel wall temperature (°C); U is the air velocity in tunnel (ms^{-1}); ν is the kinematic viscosity of air in tunnel (m^2s^{-1}); C_E is the experimentally determined constant referred to Table I in Electra 143.

As this method uses the same heat transfer coefficients, h_{conv} and h_{wall}, as the Electra 143 model, the inherent limitation in these two coefficients restricts the model to cases of forced convection. As a result, both the Electra 143 model and Pilgrim's model could not be applied to the tunnel cables where the ventilation system is controllable. In order to overcome this limitation and obtain the benefit from controllable ventilated tunnel, a new method has been implemented in this work to calculate the heat transfer coefficients, h_{conv} and h_{wall}, which makes them capable to consider both the natural and forced convection in the tunnel.

3.4.3 Modification of heat transfer coefficients

In order to fully account for the natural convective cooling in the model, an updated model has been built. The original heat transfer coefficients in Electra 143 are updated by considering natural cooling and the different values at different phases under varied cable arrangements. By combining this series of heat transfer coefficients, the dynamic thermal model is able to consider the natural, forced and mixed convection to determine the cable rating in either ventilated or unventilated tunnel systems. This permits the consideration of the full range of possible fan speeds. The updated heat transfer coefficients for both horizontal tunnel and riser shaft are briefly introduced in this section.

3.4.3.1 Horizontal tunnel

Both the natural and forced convective heat transfer coefficients for cable surface are updated in horizontal tunnel. The natural convective heat transfer coefficient is added for the tunnel wall.

1) Cable surface

For horizontal tunnels, the natural and forced convective heat transfer coefficient on the cable surface can be defined as follows:

$$h_{conv,n} = \eta_c \eta_{wh} \eta_{wv} \frac{k_{air} F (Gr \cdot Pr)^p}{D_e^*} \tag{3.33}$$

$$h_{conv,f} = \frac{k_{air} C_W (Re)^{0.65}}{D_e^*} \tag{3.34}$$

where η_c, η_{wh} and η_{wv} are the correction factor for multi-cable, horizontal wall and vertical wall effects respectively, they are obtained from Table 1 in [66]. The values of coefficients C_W, F and p can be found from Table 6.2 in [67]. The values are related to different cable phases in different kinds of cable arrangements. Pr is the Prandtl number which is set as a constant (0.719) in this test; Gr in this case can be defined as:

$$Gr = \frac{g\beta(\theta_s - \theta_{air})D_e^{*3}}{v^2} \quad (3.35)$$

where g is the acceleration (ms^{-2}) due to gravity; β is the volumetric thermal expansion coefficient (K^{-1}); θ_s and θ_{air} are the cable surface temperature and tunnel air temperature respectively (°C); v is the air viscosity ($kgs^{-1}m^{-1}$).

2) Tunnel wall

The natural convective heat transfer coefficient at the tunnel wall $h_{wall,n}$ can be represented using relations for the heat flux to a vertical cylinder under Laminar flow condition [7] [68]:

$$h_{wall,n} = \frac{k_{air}0.59(Gr \cdot Pr)^{0.25}}{D_{tun}} \quad (3.36)$$

where D_{tun} is the tunnel inside diameter (m); Gr in this case is defined as:

$$Gr = \frac{g\beta(\theta_{air} - \theta_{wall})D_t^{\,3}}{v^2} \quad (3.37)$$

where θ_{wall} is the temperature of inside tunnel wall (°C).

3.4.3.2 Riser shaft

For vertical tunnels (riser shafts), the forced convective heat transfer coefficient is the same as in the original Electra 143 method, while the natural convective heat transfer coefficient are added from Morgan [60] and Dyer's [69] work.

1) Cable surface

The natural convective heat transfer coefficient on a cable surface is defined as:

$$h_{conv,n} = \frac{k_{air}c(Gr \cdot Pr)^n}{L} \quad (3.38)$$

$$Gr = \frac{g\beta(\theta_e - \theta_{air})L^3}{v^2} \quad (3.39)$$

where L is the shaft length (m); the values of coefficient c and n can be found from the Table 10.4 in [7].

2) Tunnel wall

The natural convective heat transfer coefficient on the inside of the tunnel wall is defined as:

$$h_{wall,n} = \frac{k_{air}Nu}{0.5D_{tun}} \quad (3.40)$$

$$Nu = \begin{cases} \dfrac{(Gr \cdot Pr)}{400} & if\ (Gr \cdot Pr) < 200 \\ 0.35(Gr \cdot Pr)^{0.28} & if\ (Gr \cdot Pr) \geq 200 \end{cases} \quad (3.41)$$

$$Gr = \frac{g\beta(\theta_{air} - \theta_{wall})(0.5D_{tun})^4}{Lv^2} \quad (3.42)$$

3.4.4 Benchmarking tests for the updated model

In order to validate the performance of the updated model, a series of comparisons under different ventilation rates have been taken against Pilgrim's model (named original model in this section). The cable and tunnel installation and thermal parameters can be found in Section 3.4.1. The tunnel air inlet temperature is set as 20°C, with a constant current input of 1500A per phase. The resistances of the conductor and sheath are temperature dependant, which are calculated by the temperature results from the previous iteration until it is converged. The results are compared for tunnel air velocities ranging from 0-4ms^{-1} in tunnel section 2 and are shown in Table 3.8.

Table 3.8 - Steady state results for tunnel cable models

Air Velocity at Section 2(ms^{-1})	**Section**	**Max Conductor T (°C)**		**Max Tunnel Air T (°C)**	
Model		**Original**	**Updated**	**Original**	**Updated**
0	1	NA	66.62	NA	46.56
	2	NA	83.98	NA	68.31
	3	NA	66.62	NA	46.56
1	1	38.50	38.30	20.28	20.28
	2	54.35	54.29	39.81	39.83
	3	56.28	56.45	39.90	39.92
2	1	36.33	36.30	20.14	20.14
	2	44.51	44.50	31.14	31.14
	3	46.96	47.01	31.23	31.23
3	1	35.27	35.27	20.10	20.10
	2	40.43	40.43	27.72	27.72
	3	42.82	42.85	27.80	27.80
4	1	34.60	34.60	20.07	20.07
	2	38.19	38.19	25.91	25.91
	3	40.44	40.47	25.97	25.97

At the unventilated condition, the updated model shows much higher temperature than all of the ventilated conditions. This is because the natural convective cooling has very small effect for the heat dissipation on cable surface. The thermal radiation between cable and tunnel wall dominates (higher than 93%) the heat transfer under unventilated conditions. For the ventilated condition, the maximum conductor and air temperature from the updated model and the original

model match very well, with the conductor temperature difference within 0.17°C and the air temperature differences within 2 decimal places.

3.4.5 Dynamic rating results

Six typical test points have been chosen to calculate the 6hr emergency rating and are presented in Figure 3.15. Point 1 is at the load trough (1611A, 60.68% of the steady-state rating); Point 2 and 3 are at the same preload level of 75.25% (1998A); Point 4 and 5 are at the same preload level of 84.07%; Point 6 and 7 are at the same preload level of 90.06%. The dynamic rating results from these points can be used to compare with the ratings calculated by the different pre-fault levels.

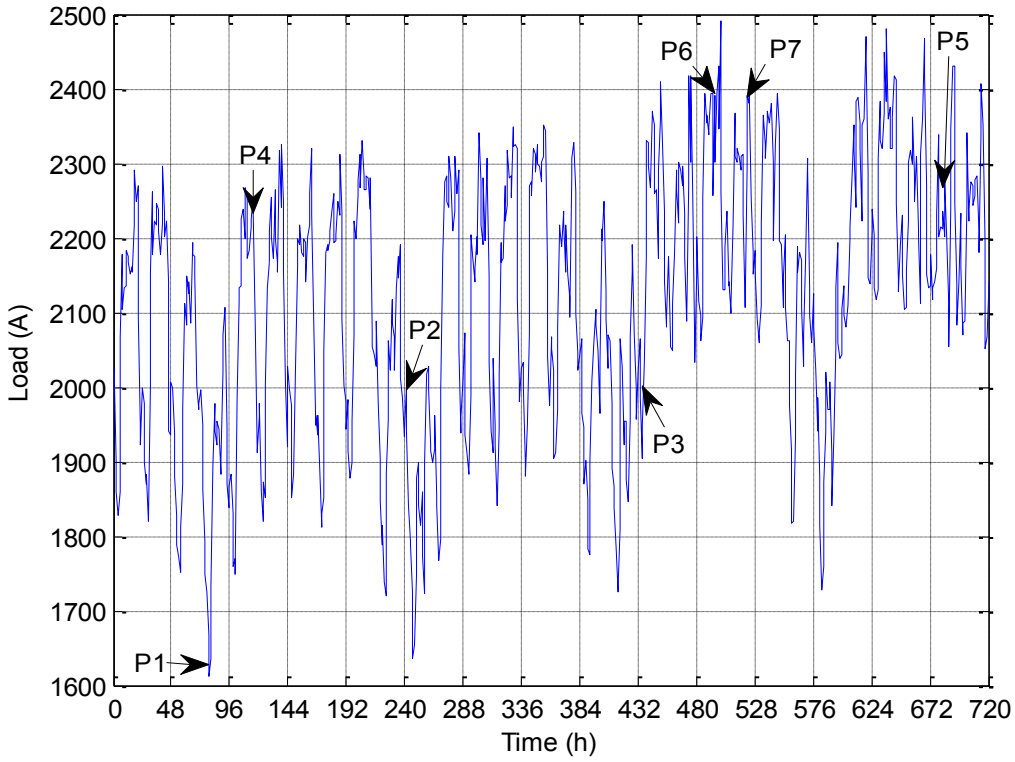

Figure 3.15 - Test points for 6hr emergency rating for tunnel cables

Assuming the load of both two circuits is the same, the emergency rating for both circuits simultaneously is calculated. The inlet air temperature is assumed as a constant value (equal to the temperature of the current point) during the next 24 hour in the rating calculation. The 6hr emergency ratings for six typical points are calculated by only considering the pre-fault level and by the dynamic model respectively. Results are shown in Table 3.9.

Table 3.9 - Dynamic rating results for tunnel cables

Point	Hour	Load (A)	Preload level (%)	Air T (°C)	6hr Emergency Rating (A)	
					Pre-fault	Dynamic
1	495	2391	90.06	8.3	3012	3169
2	522	2391	90.06	4.3	3012	3200
3	116	2232	84.07	10.8	3109	3183
4	678	2232	84.07	8	3109	3250
5	241	1998	75.25	6.3	3233	3223
6	430	1998	75.25	11.2	3233	3243
7	79	1611	60.68	8.5	3394	3233

At Point 1 and Point 2, the preloads (2391A) are only 1A higher than the 90% preload level (2390A) and the inlet air temperature are 8.3°C and 4.3°C respectively. Thus, the emergency rating results can be referred to the results with pre-fault percentage of 90%. The seasonal 6hr emergency rating with 90% pre-fault level is 3012A for spring/autumn, while the dynamic ratings in Table 3.9 are 3169A and 3200A. Compared to the spring/autumn rating value, 157A and 188A increase can be obtained from the dynamic rating values which consider the real-time data.

The same situation can be found from the rating results at Point 3 and Point 4 when compared to the spring rating (3109A) with 84% pre-fault level, 74A and 141A improvement in 6hr emergency rating can be obtain at Point 3 and Point 4 respectively. The reason for the improvement is the assumption in the initial condition that the cable tunnel reaches its steady state condition at pre-fault load level in the seasonal rating calculation. While for Point 1 to Point 2, the initial cable temperatures are lower than the steady state temperature of their corresponding pre-fault load as the historical load level for the previous period is lower than the pre-fault load (Figure 3.16).

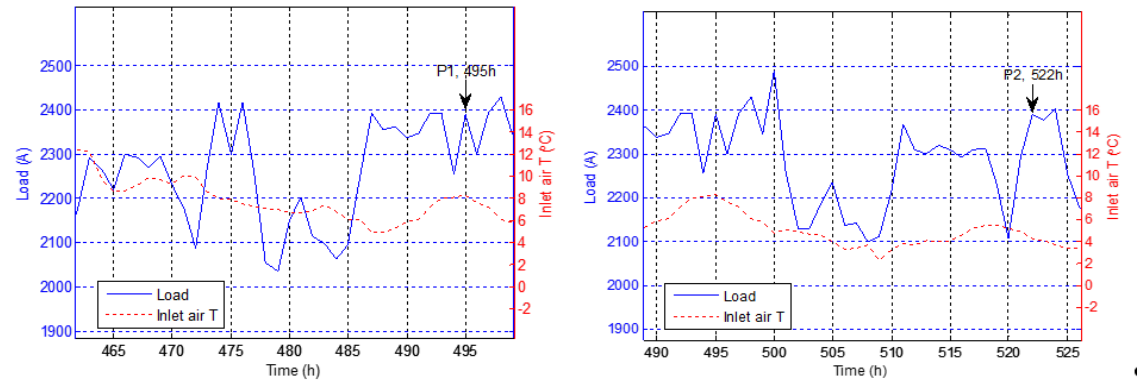

Figure 3.16 - Real time load and inlet air temperature at Point 1&2

However for Point 5 (preload 1998A, 75.25%), the historical load level for a previous period is higher than the pre-fault load (Figure 3.17). As a result, the 6hr emergency ratings (3223A for Point 5) is lower compared to the 6hr rating result under the 75% pre-fault condition (3233A for spring).

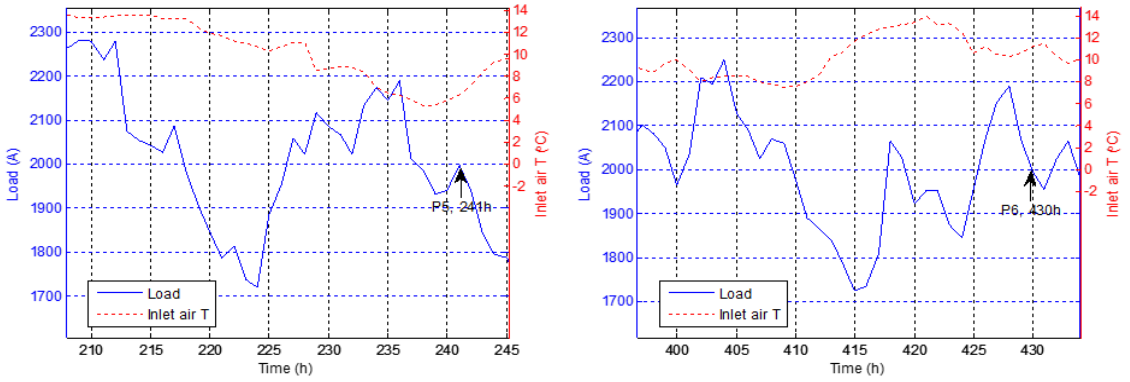

Figure 3.17 - Real time load and inlet air temperature at Point 5&6

Figure 3.18 shows the historical load and inlet air temperature before Point 3 and Point 4. The real time load at these two points is the same (2232A), while the 6hr emergency ratings have 67A difference (Point 4 higher than Point 3). There are two reasons, first is the inlet air temperature at point 3 (8°C) is lower than point 4 (10.8°C); second is that the historical load level of Point 4 is higher than the level of Point 3 which makes the initial cable temperature at Point 4 higher.

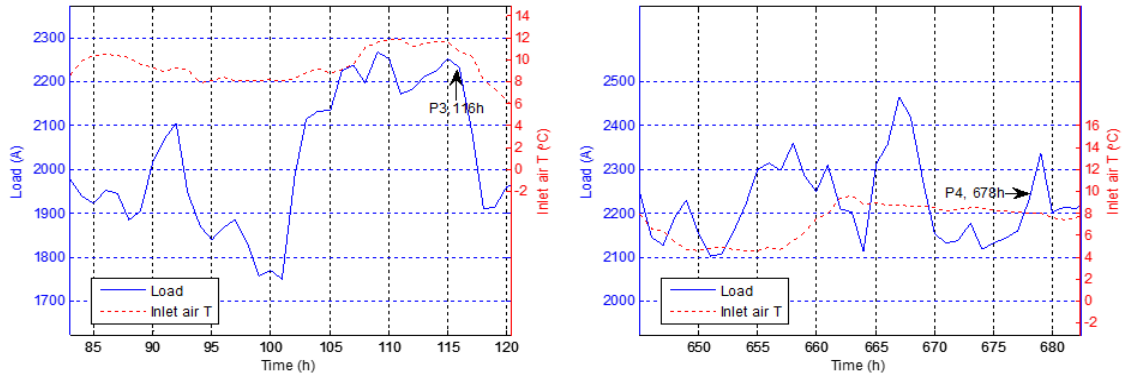

Figure 3.18 - Real time load and inlet air temperature at Point 3&4

For some more critical conditions, Point 7 (1661A), there is a sharp decrease in circuit load before that point (Figure 3.19).

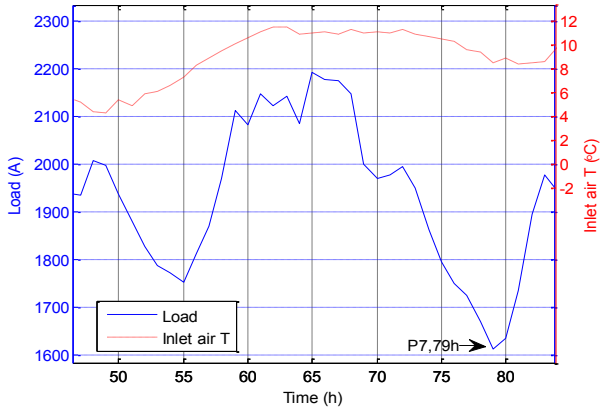

Figure 3.19 - Real time load and inlet air temperature at Point 7

The emergency rating of Point 7 might be lower than the rating of the points which have higher initial load. For example, Point 6 (1998A) in Figure 3.17 and Point 4 (2232A) in Figure 3.18 have 6hr emergency ratings of 3243A and 3250A respectively. While for Point 7 (1661A), which has lower initial current than Point 4 & 6, the 6hr emergency rating is only 3233A, lower than Point 6 and Point 4.

It is clear that the current method to find the emergency rating from the pre-fault table might underestimate the cable ratings by only considering the pre-fault level. To obtain an accurate rating, the historical load and inlet air temperature should be considered in a dynamic thermal model and emergency ratings should be calculated based on the real time cable tunnel temperatures obtained from the dynamic thermal model.

3.5 Summary

This chapter embodies an essential step towards developing a dynamic rating system for different cable installations. By comparing the different kinds of dynamic thermal models, it is possible to examine and select the most appropriate model for each cable installation. In this chapter, a series of dynamic thermal models have been built for buried cable, cable in free air and tunnel cables by finding suitable compromises between the accuracy and the solution speed of the model. Thus, they can be suitable for usage in predicted rating systems.

Several models have been investigated for different cable installations, with the finite element based models used as the benchmarks for different installations. For directly buried cables, the finite difference method (FDM) is used to build the dynamic thermal model to compare with the IEC standard and the FEA model. For cables in free air, the model built from the IEC 60853-2, FDM and FEA methods have been tested with different heat transfer coefficients on the cable surface under both natural cooling and forced cooling conditions. Compared to the IEC

standard, the FDM models match better with the FEA model. In addition, having similar temperature and rating results with the FEA models, the FDM models require much shorter solution time. Having shown the ability to achieve an accurate and fast solution, the dynamic finite difference method has been chosen to use in the dynamic rating system for further analysis.

For the tunnel cables, a model has been built based on Pilgrim's model in [9]. The restriction of the original model that can only apply to ventilated tunnel has been removed. Thus, the new model can be applied to both the ventilated and unventilated tunnel cables. In addition it can be used for the analysis of controllable ventilation system.

Chapter 4: Load Forecasting for Predicted Rating

Accurate load forecasting is essential to electrical utilities in the competitive environment created by the electrical industry deregulation. It can help electrical utilities to plan the purchasing and generating of electrical power, load switching and infrastructure development. However, there is no evidence in the literature of load forecasting being used in cable rating algorithms. In the predicted rating concept developed within this work, a day-ahead load forecasting system is integrated to generate cable emergency ratings 24 hours ahead. The load prediction can then be used in the dynamic thermal model of cable to predict the cable temperature 24 hours ahead in order to get the initial condition at the point of time which rating is calculated. Compared to most existing dynamic rating systems, which can only perform the emergency cable rating at the current time step, the 24hr-ahead predicted rating is clearly value to transmission operators to assist in day-ahead planning, as in many circumstances the environment may be more benign than assumed by offline rating analysis. If this is the case, constraint costs could be minimised. In this Chapter, typical techniques for day-ahead load forecasting are introduced and analysed. A comprehensive test for input features of one selected method, namely the use of Support Vector Regression (SVR) for load prediction is presented. The load predictions from the SVR model were compared with the other two models with the results showing the superiority of the SVR technique for day-ahead load forecasting.

4.1 Load prediction methodologies

Day-ahead load prediction is within the concept of Short Term Load Forecasting (STLF). Normally, the STLF process should consider factors, such as time, weather, historical load and possible types of customer. The time factors include the time of year, the day of week and the hour of day. The load patterns show a great difference between weekdays and weekends (holidays). Weather conditions might be the most important factors in the STLF as the temperature-load pattern can be clearly obtained from most of the data. The historical load information can be used to consider the autocorrelations in the load pattern. The electrical utilities might have different classes of customers, such as residential, industrial or commercial usages. The load patterns for these three kinds of customers are different. In addition, the load demand might be more and more sensitive to the electricity price in the future when the concern of the cost increase from customers.

Most existing load forecasting systems only consider the time of day, the day of week, historical load and temperature information as there is not enough data for other features. A lot of techniques have been developed and adopted for dealing with STLF. The general procedure to

build a load prediction model is shown in Figure 4.1. The historical weather and load data are used to build and train the prediction model. After the model being completed, the input features at each step (normally including historical load and weather data, and weather forecasting data) are used in the model to obtain the prediction results.

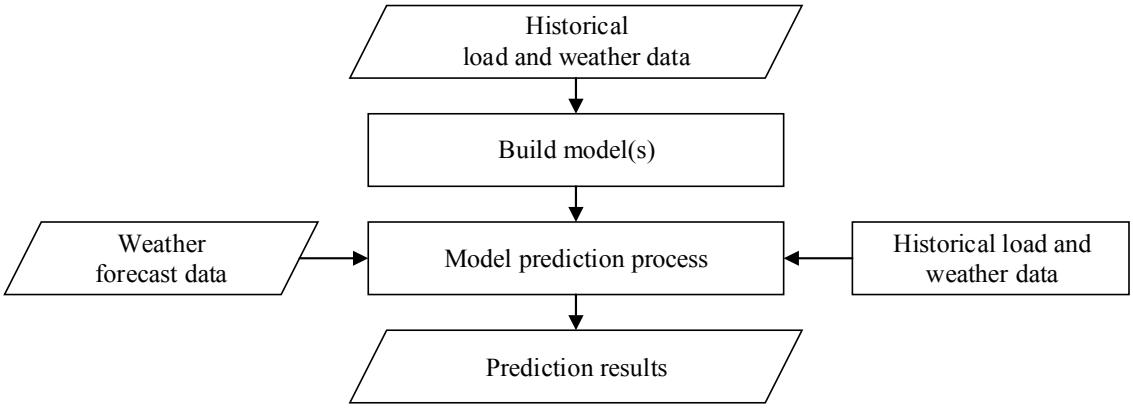

Figure 4.1 - Flowchart of short term load forecasting

The existing STLF models can be mainly classified into two groups: Statistical methods and Artificial Intelligence methods. The statistical approaches mainly include regression analysis, similar day analysis and time series analysis. The Artificial Intelligence based approaches include the Artificial Neural Network (ANN), fuzzy logic (FL) and Support Vector Regression (SVR) [70], [71]. In addition, some hybrid techniques [72], [73], [74], [71] also have been studied and adopted to the load prediction problems.

4.1.1 Similar day analysis

The similar day analysis is based on a search engine to find the historical data with similar characteristics to the forecast day. The characteristics selected from similarity checks can be weather, day of the week and the historical load curve. Instead of only one similar day's load, the forecast can include the information of several similar days by using a linear combination or regression procedure. The range of searching history can be from one year to several years. A demand trend coefficient might need to be used to take into account the demand increase during the previous years. In practice, it is difficult to define the length of the search history, the number of the similar days and the number of characteristics in the search engine to get the best prediction results. As a result, the similar day analysis is not able to provide accurate load forecasting according to [75]. However, the similar day analysis becomes popular when it is implemented with other prediction methods. It can be used as the first stage in the hybrid models to process input data [76] or select the input models.

4.1.2 Multiple Linear Regression method

Regression methods, as one of the earliest and widest applied techniques in the STLF field, have been well known for a long time. The relation of load demand and other factors such as weather, day type and hour of day can be modelled by regression technique. Tao et al. [77] presented a benchmark model by using Multiple Linear Regression for the STLF. Their model incorporates deterministic influences such as hour, day, month and trend, stochastic influences such as historical load and exogenous influences such as temperature. Regression models have the ability to explicitly identify possible causal relationships between input features and output results. However, Multiple Linear Regression methods might have difficulty when dealing with complex nonlinear relationships. They require an explicit knowledge of these relationships by the model developer and might require complex transformations of input features. In addition, appropriate transformations might not always fit the model and the complex nonlinear relationships might not be recognized by model developers.

4.1.3 Time series method

Time series models for STLF are based on the assumption that the load data have an internal structure, such as autocorrelation (daily, weekly and seasonal) and trend. This method has been used for decades for STLF [78], [79]. Different kinds of models have been developed, including ARMA (autoregressive moving average), ARIMA (autoregressive integrated moving average), ARMAX (autoregressive moving average with exogenous variables) and ARIMAX (autoregressive integrated moving average with exogenous variables). ARMA and ARIMA use the time and load as the only input features. However, the load demand generally has strong relation with the weather, which makes ARIMAX a preferred option for the STLF [80][81]. Authors in [82] introduce a method combining the regression techniques with ARIMA models for STLF. The regression method is used to forecast the peak and trough load and remove the weather-dependent trend from the load series. ARIMA is then applied to produce the load curve and adjust the prediction value based on the peak and trough load.

4.1.4 Artificial Neural Networks (ANN)

ANN has been widely studied and applied in the STLF area since 1990 [83] and become a heavily published research field [84], [22], [85], [86]. An ANN is a non-linear interconnected assembly of artificial neurons. It is an essentially non-linear circuit that has the demonstrated capability to do non-linear curve fitting. In the STLF area, ANN was expected to deal with the nonlinear relationship between the load and weather variables and be adaptable to new data. The ANN based model in [85] has been compared with a regression based model in [87] (both these

two models were developed from the same utility). The analysis of peak and hourly load prediction showed that the ANN model offered improved accuracy in both peak and hourly load forecasting. These results reflect the advantages of the ANN approach in detecting the complex nonlinear relationships between variables. In addition, the possible interactions between input features can be detected by ANN model without requiring knowledge from model developers.

However, there are some inherent limitations existent in an ANN model. It is a black box model which has limited ability to clearly identify possible underlying relationships. The training data are set up for the network by the developer and then essentially the network trains itself and determines the importance of each input features by placing different weights on them. In this way, the developer could not identify the values of different input features, thus, the model might contain some lower value input features which might be harmful to the prediction results or to the efficiency of the calculation. In addition, ANN techniques are prone to over-training and over-fitting. When the iterative training in ANN results in an over complex model for the problem, this model might generally have poor predictive performance. As a result, many issues remain to be solved in ANN models. The training parameters, such as learning rates, number of hidden layers and nodes, and momentum terms are difficult to determine. Thus, it is difficult to conclude that one has developed the best possible ANN model for STLF.

4.1.5 Gradient Boosting Machine

The Gradient Boosting Machine is a machine learning method which generates an accurate prediction model in the form of an ensemble of several weak prediction models [88], [89]. Gradient Boosting Machines have previously performed well in load prediction as two of the top five groups in the GEFCom 2012 load forecasting competition use this technique [90], [91].

Lloyd combined the gradient boosting machine with other two methods (Gaussian process regression and multiple linear regression) and presented the final prediction model as the ensemble (weighted average) of the predictions from three separate methods in GEFCom 2012 [91]. The ensemble of different uncorrelated predictions will have lower variance than each one prediction separately. Taieb and Hyndman [90] used separate models for different forecast distances, the gradient boosting technique being applied to build each model.

4.1.6 Support Vector Regression (SVR)

The Support Vector (SV) algorithm is a nonlinear generalization algorithm developed in Russia during the 1960s [92] [93]. It can be included in the framework of statistical learning theory, which has been developed over last four decades [94][95].

Unlike ANN, which tries to define complex functions of the initial input feature space, SVR implements a nonlinear mapping of the input feature data into a high dimensional feature space by using kernel functions. Then SVR applies a 'kernel trick' to solve the high dimensional problem in a new space (for details refer to Section 4.2). Thus, the problem of selecting an architecture for an ANN is replaced in SVR by selecting a suitable kernel [96]. The computational complexity of SVR is independent of the dimensionality of the input space in contrast to that of ANN [96]. The over-fitting problems in ANN model is reduced in SVR by allowing a deviation from the target function and actual obtained values. It can be further reduced by taking advantage of structural risk minimization during the training stage in SVR. The lower likelihood of over-fitting is the main reason that SVMs often outperform ANNs in practice [70], [71], [97]. The potential input data can be explicitly identified and analysed by testing the SVR model to obtain a set of the most appropriate input features.

With these advantages, SVR is a promising technique for data prediction and has shown great capability in the application of STLF. Chen et al. won a load prediction competition in the EUNITE 2001 [70] by using SVR method. The improved performance compared with regression and time series methods in [98] also shows the advantage of the SVR technique in the STLF area.

4.1.7 Summary

Much work on the subject of STLF has been published during recent decades, but there is no single model or algorithm which is superior for all situations. This is because the features of geographic, climatologic, social characteristics, economic and the mixture of customers are unique in the data from different utilities. Different kinds of models and corresponding input features might be suitable for different data, which require the testing to select the most suitable model or algorithm by using real data.

From previous reviews, the SVR technique has presented several inherent advantages compared with other algorithms. To construct an SVR model for STLF, one of the vital questions is to find the most appropriate input features. However, nothing is known in an a priori situation that could detect which set of input features is most suitable for a given dataset. As a result, the sensitivity investigation of the SVR model to a number of potential input features is required.

It is noteworthy that most of the publications concerning the SVR STLF system did not include sensitivity tests for different input features. They directly used a set of given input features, without proving their applicability for the STLF, in the SVR model. In order to find the most suitable input features in SVR STLF model for a given dataset, especially for the implementation in the predicted rating system, a comprehensive test of input features for the

SVR model is presented in following sections of this Chapter. Such procedures of sensitivity test can be used as a guideline to find the most appropriate input features for other datasets in the future.

4.2 Support Vector Regression (SVR) technique

Regression is dealt within SVR by solving the optimization problem:

$$min_{\omega,b,\xi_i\xi_i^*}\left[\frac{1}{2}\omega^T\omega + C\sum_{i=1}^{n}(\xi_i + \xi_i^*)\right]$$

subject to:

$$\begin{aligned} y_i - (\omega^T\phi(x_i) + b) &\leq \varepsilon + \xi_i^* \\ (\omega^T\phi(x_i) + b) - y_i &\leq \varepsilon + \xi_i \\ \xi_i\,, \xi_i^* &\geq 0, i = 1, \ldots, n \end{aligned} \tag{4.1}$$

where (x_i, y_i) are given training data for the SVR, x_i are input features, y_i are the associated output value of x_i. ξ_i and ξ_i^* are slack variables of the upper and lower training error respectively subjected to the ε-insensitive tube $|\omega^T\Phi(x_i)+b-y_i|\leq\varepsilon$ (Figure 4.2). The points on the ε-insensitive tube are so-called Support Vectors. The cost of error C determines the trade-off between the flatness and losses to avoid under-fitting or over-fitting problems.

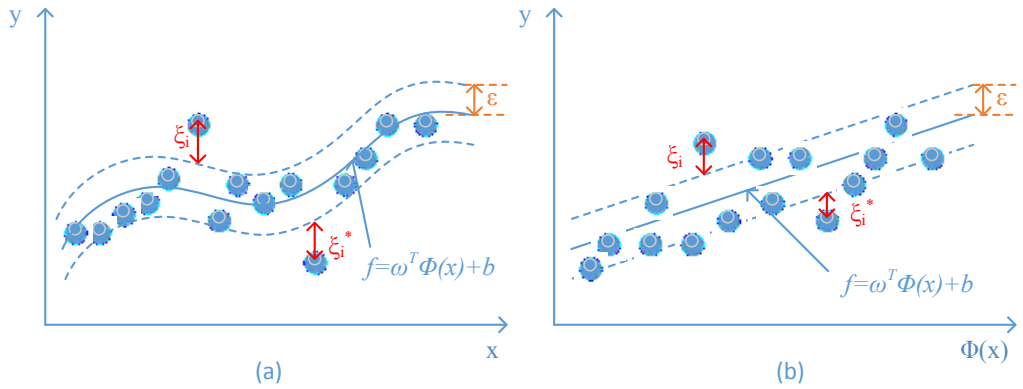

Figure 4.2 - ε Insensitive tube for SVR

The objective function in (4.1) implies that the goal of SVR is to find a function *f(x)* with a deviation no larger than ε from the actual targets y_i for all the training data which at the same time makes the function *f(x)* as flat as possible. While some times this kind of function is not feasible or we might want to allow some errors, two slack variables ξ_i and ξ_i^* are introduced to deal with this problem. After determining the tube ε (Figure 4.2), the SVR only considers the

data on the tube or outside the tube to minimize the objective function. Thus, fewer points are calculated in the model which makes the model faster. At the same time, by allowing a deviation ε, the over-fitting problem which usually happens in other methods can be prevented. For a non-linear case, the function Φ is used to map x_i to a higher dimensional space to make it linear (Figure 4.2(b)). This makes SVR more flexible to treat a wider range of regression problems.

The object function (4.1) is transferred into a Lagrange function and solved using the Lagrange duality method:

$$L = \frac{1}{2}\|\omega\|^2 + C\sum_{i=1}^{n}(\xi_i + \xi_i^*) - \sum_{i=1}^{n}(\eta_i\xi_i + \eta_i^*\xi_i^*) - \sum_{i=1}^{n}\alpha_i(\varepsilon + \xi_i - y_i + \omega^T\phi(x_i) + b) - \sum_{i=1}^{n}\alpha_i^*(\varepsilon + \xi_i^* + y_i - \omega^T\phi(x_i) - b)$$

subject to:

$$\eta_i, \eta_i^*, \alpha_i, \alpha_i^* \geq 0 \tag{4.2}$$

where L is the Lagrangian and η_i, η_i^*, α_i, α_i^* are Lagrange multipliers. By performing the partial derivatives of L with respect to the primal variables ω, b, ξ_i and ξ_i^*:

$$\begin{cases} \frac{\partial L}{\partial b} = \sum_{i=1}^{n}(\alpha_i^* - \alpha_i) = 0 \\ \frac{\partial L}{\partial \omega} = \omega - \sum_{i=1}^{n}(\alpha_i - \alpha_i^*)\,\phi(x_i) = 0 \\ \frac{\partial L}{\partial \xi_i^{(*)}} = C - \alpha_i^{(*)} - \eta_i^{(*)} = 0 \end{cases} \tag{4.3}$$

By substituting (4.3) into (4.2), a dual optimization problem can be constructed:

$$max_{\alpha,\alpha^*}\left[-\frac{1}{2}\sum_{i,j=1}^{n}(\alpha_i - \alpha_i^*)(\alpha_j - \alpha_j^*)K(x_i, x_j) - \varepsilon\sum_{i=1}^{n}(\alpha_i + \alpha_i^*) + \sum_{i=1}^{n}y_i(\alpha_i - \alpha_i^*)\right]$$

subject to

$$\sum_{i=1}^{n}(\alpha_i - \alpha_i^*) = 0, 0 \leq \alpha_i, \alpha_i^* \leq C, i = 1, \ldots, n \tag{4.4}$$

In addition, from (4.4) we can know that α_i and α_i^* are equal to 0 for all the points except Support Vectors. A part of (4.3) can be rewritten as:

$$\omega = \sum_{i=1}^{n}(\alpha_i - \alpha_i^*)\,\phi(x_i), thus, f(x) = \sum_{i=1}^{n}(\alpha_i - \alpha_i^*)\,\phi(x_i)^T\phi(\mathrm{x}) + b \qquad (4.5)$$

In this format, *f(x)* can be represented by a linear combination of the training patterns $\Phi(x_i)$. As a result, to predict the value of new points, we only need to calculate the inner products of new point $\Phi(x)$ and the training patterns $\Phi(x_i)$. Moreover, except for Support Vectors, α_i and α_i^* are all zero, so only the inner product of the new point and the points of Support Vectors need to be calculated.

While solving the problem in the higher dimension may result in dealing ω with a huge vector variable from the inner products of new point $\Phi(x)$ and the training patterns $\Phi(x_i)$, instead, a Kernel function is used in SVR to deal with its dual problem. The *K* in (4.4) is the Kernel function with $K(x_i,x_j)=\Phi(x_i)^T\Phi(x_j)$. Normally, the Radial Basis Function (RBF) kernel is employed in the test, assuming $\Phi(x_i)^T\Phi(x_j)=e^{-\gamma(x1-x2)2}$. Thus, the regression problem can be solved efficiently without knowing the inner product of $\Phi(x)$.

4.3 SVR model test for 24hr-ahead prediction

This section focuses on short-term load forecasting (STLF), in particular on predicting a day-ahead hourly load profile, which means that at each hour, the next 24hrs of load is forecast. The test aims to find a group of the most appropriate input features in the SVR model to obtain the prediction results as precise as possible. The data used in this section is from Global Energy Forecasting Competition 2012 [99], it has the hourly load data from a US utility and the hourly temperature data from the weather station. The data contains 4years' hourly load and ambient temperature data from 01/01/2004 to 31/12/2007.

4.3.1 Evaluation criteria in the test

To compare the result of predicted values and real values of load, two criteria have been used in this test. As a general standard to judge the accuracy of load prediction, the mean absolute percentage error (MAPE) is used as one of the criteria. MAPE has been widely used to judge model performance for load prediction [71], [99], [100].

$$MAPE = \frac{100}{n}\sum_{i=1}^{n}\left(\left|y_a(i) - y_p(i)\right|/y_a(i)\right) \qquad (4.6)$$

where y_a are the actual values, y_p are the predicted values and *n* is the total number of samples.

Since the aim of this load prediction system is its use in the predicted cable rating, the other criterion to assess is the cable conductor temperature error resulting from this load prediction error. In this chapter, the dynamic thermal model for cable tunnels presented in Section 3.4.3 is used to demonstrate the load prediction results. The raw load demand data are given in the unit of MW. In this test, they are linearly scaled to appropriate ranges for different cable installations in order to give a reasonable cable temperature level in practice. This criterion will be represented by the probabilities of conductor temperature errors being contained within ±2°C and ±3°C for different prediction horizons, as these kinds of temperature errors for a short time period would not have any significant impact on the service life of the cable (an XLPE cable may be overloaded up to 105°C during emergency [101]).

4.3.2 SVR models

The Matlab tool box LIBSVM [97] is applied to train the SVR by using the load and temperature data from 2004 to 2006 and predict the day-ahead load demand in 2007.

Two parameters, the cost of error C and the γ in RBF kernel, need to be allocated by the SVR training. To define the best values of these two parameters, a 'grid-search' method [13] for C and γ is applied. Various groups of C and γ are gradually tested. Inside each test, the procedure known as cross-validation is used. The three years training dataset is first split into three segments (one year per segment), and then each segment is tested by the SVR model which was previously trained by the other two segments sequentially. Thus, each year's load demand is predicted once by the other two years to prevent over-fitting problems. Finally, the pair of C and γ with minimum total error are chosen and used in the whole model trained by 3 years' data to predict the test dataset.

4.3.3 Input features test

The initial investigation of the historical load demand indicates that there are clear seasonal, weekly and daily patterns within the data. High demand can be found in the winter and summer due to the power consumption of heating and air conditioning respectively. The seasonal patterns imply that the load demand has a solid link with ambient temperature. The relation between temperature and load demand has been widely demonstrated in the literature [71], [77]. In the test data, a negative correlation (-0.6443) between load demand and temperature can be observed when the temperature is lower than 13°C, while when the temperature is higher than 13°C, a positive correlation (0.7348) can be found.

1. Basic Model (M1)

First, a basic model was built by applying a factorial experimental test with the input features of hour, weekday, season number and hourly temperature. The result showed that the model with all these features, named M1, presented the best accuracy. The MAPE for 24hr-ahead load prediction is 5.6 approximately and the probabilities of conductor temperature errors of the tunnel cables being contained within ±3°C are 99.96%, 91.65% and 78.61% for 1hr, 4hr and 24hr-ahead prediction respectively. It is interesting that the MAPE is almost constant from 1hr-ahead to 24hr-ahead predictions. The reason for this phenomenon is that this basic model is only based on same features which do not relate to the time horizon of the load prediction, so the prediction results do not have a relation with the number of hours ahead. However, the cable temperature errors rise with the increase of the prediction horizon, which is because the cable temperature errors relate to the accumulation of all the load errors in the prediction horizon.

2. Features from Autocorrelation of the data (M2)

Previously, the model is only provided with inputs for temperature and calendar, which leads to the assumption that the loads in adjacent hours are independent from each other. However, it is normally advantageous to the accuracy of the short term prediction to include the time series feature in the model [70], [71], [102]. In order to capture the time series characteristic in the load, past load demand and temperature data are considered to be encoded in the input features.

In practice, the load at one point in time has a strong relation with the loads at the same point in time of previous days. The autocorrelation function (ACF) of n (hourly) load data observations $\{x_1, \ldots, x_n\}$ can be calculated by (4.7) to find the correlations for data values at varying time lags.

$$ACF(h_l) = \frac{\hat{\gamma}(h_l)}{\hat{\gamma}(0)} \tag{4.7}$$

where h_l=0,1,…,n-1, is the time lag, $\hat{\gamma}$ is the sample autocovariance function (ACVF) which is given by:

$$\hat{\gamma}(h_l) = \frac{1}{n}\sum_{t=1}^{n-h}(x_{t+h_l} - \bar{x})(x_t - \bar{x}) \tag{4.8}$$

where $\bar{x}$ is the sample mean.

Autocorrelation of 1 at the lag hour of t corresponds to exactly the same value at every time interval of t. Smaller autocorrelation values indicate poorer correlation between data at every time interval of t. The autocorrelation results for all the load data is shown in Figure 4.3, which represents the similarity of the load data as a function of the time lag between themselves.

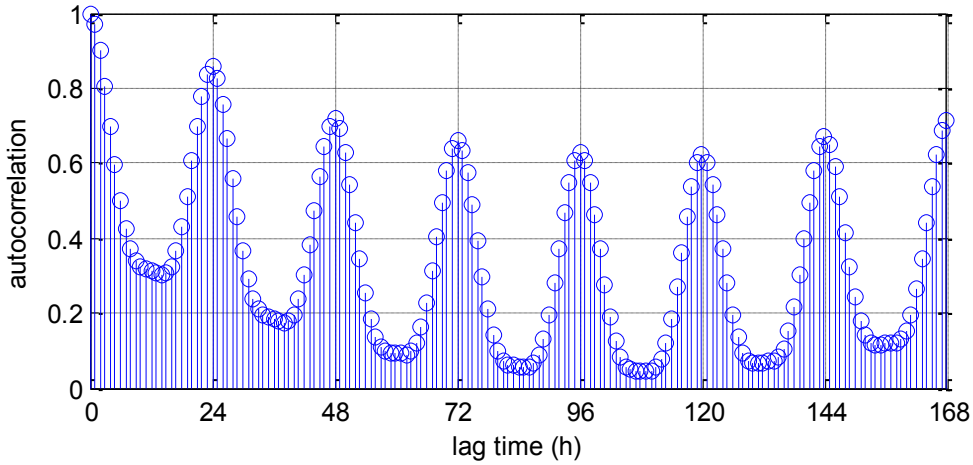

Figure 4.3 - Autocorrelation of one week for all load data

Figure 4.3 implies that the load at one point in time has a strong relation with the loads at the same point in time of previous days. In addition, if we scrutinize Figure 4.3, another feature can be observed: the autocorrelation between the present load and the loads adjacent to the load at the same time of the previous day are very high as well.

Figure 4.4 shows the correlation between hourly load and maximum load of the last day. The high correlation values for most hours of the day imply that the load might have strong relation with the maximum load of the preceding day. Hence, the maximum load of the previous day is added in the model for the next group of tests.

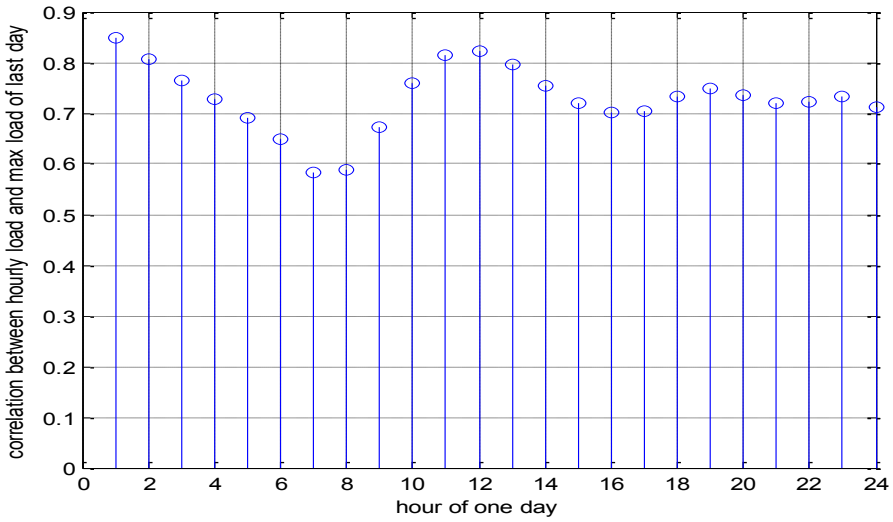

Figure 4.4 - Correlation between hourly load and max load of last day

According to the analysis of autocorrelation and correlation of the load data, tests have been done to gradually add the input features of the same hour load and temperature data of

preceding seven days, and the loads adjacent to the same hour load of previous day. Test results show that the model with addition input features of the same hour load and temperature data of the preceding day, the maximum load of preceding day, the loads adjacent to the same hour load of previous day (lag hour from the point to predict: 25 and 26) and the temperature information earlier than the predicting hour (lag hour from the point to predict: 1 and 2) has the best results. Thus, these new input features are added in model M1. The new model is named M2. With this new model, the MAPE reduces from 5.6 in M1 to less than 4 from 1hr to 24hr prediction horizons. At the same time, the probability of 24hr-ahead conductor temperature prediction errors being contained within ±2°C increases from 64.5% in model M1 to 84.5% in model M2.

3. Workday and weekend/holiday (M3)

In addition, obvious differences can be observed in the load characteristic between workdays and weekends/holiday days. Such a phenomenon will cause a discontinuity in the time series, leading to the use of separate models for the two day types. As a result, two independent models were built for workdays (M3_W) and weekends/holidays (M3_H) respectively. These two models were combined in one system (M3) by using a simple switching operation according to different day types. The input features of these two models were chosen through the test and presented in Table 4.1 with the other two models. *L* and *T* are the hourly load and temperature respectively, *t* means the hour to be predicted, (*t-n*) means *n* hour before the hour to predict.

Table 4.1 - Test sheet for time series (include the max load of previous day)

Model	***T(t)*** **Hour Weekday Season**	***L (t-24) T (t-24)***	***L (t-48) T (t-48)***	**max *L* of last day**	***L (t-25)***	***L (t-26)***	***T (t-1)***	***T (t-2)***
M1	√							
M2	√	√		√	√	√	√	√
M3_W	√	√	√	√	√	√	√	√
M3_H	√	√		√	√	√	√	√

Test results show that M3 has improvement over the previous steps' models. The probability of conductor temperature errors being contained within ±2°C increases from 84.5% in model M2 to 84.7% in model M3.

4. Multiple models for 24hr-ahead prediction (M4)

In the previous tests, only one or two (workday and weekend/holiday) models are used for all the day-ahead prediction. However, if a series of models can be applied for different hour-ahead predictions, the advantage of knowing more recent load information for shorter term load prediction (i.e. 1hr ahead prediction) can be implemented in the models.

Based on M3 which includes two models, different groups of models are tested to perform the 24hr-ahead prediction (Table 4.2). Each group has two models from M3 initially. One feature of the closest load data, *L(t-24/group_no)*, is added in the models in each group to involve the recent load information. *L* is the hourly load data; *t* is the hour of the load to be predicted; *group_no* is the number of the model group; *(t-24/group_no)* means the hourly load data *(24/group_no)* hours before the hour to predict.

Table 4.2 - Multiple models for the 24hr-ahead load prediction

Number of groups	Number of models	Hours ahead to be predicted in each group	Added feature in each group
2	4	one group for continual 12 hour	*L(t-24/group_no), group_no=1,2*
4	8	one group for continual 6 hour	*L(t-24/group_no), group_no=1,2,3,4*
6	12	one group for continual 4 hour	*L(t-24/group_no), group_no=1,2,...,6*
12	24	one group for continual 2 hour	*L(t-24/group_no), group_no=1,2,...,12*
24	48	one group for each hour	*L(t-24/group_no), group_no=1,2,...,24*

The test results for different prediction horizons by using different number of models are shown in Figure 4.5. By using more models, the prediction result from 1hr-ahead to 13hr-ahead improves due to the use of more recent load information in the model. The performances of 14hr-ahead to 24hr-ahead prediction do not have clear enhancement. As a result, it is worth applying a larger number of models for 1-13hr ahead prediction but fewer models for 14-24hr ahead prediction. A new system was built by using the system with 24 groups of models as a benchmark and limiting the MAPE differences between the new system and the benchmark system to smaller than 0.1 for 1-24hr ahead prediction. Thus, a new system with 10 groups of models was created, named M4, as shown in Table 4.3. MAPE results for M4 are shown in Figure 4.5.

Table 4.3 – Group details of model M4

Group Number	Corresponding ahead hours	Group Number	Corresponding ahead hours
1	1	6	6-7
2	2	7	8-9
3	3	8	10-13
4	4	9	14-17
5	5	10	18-24

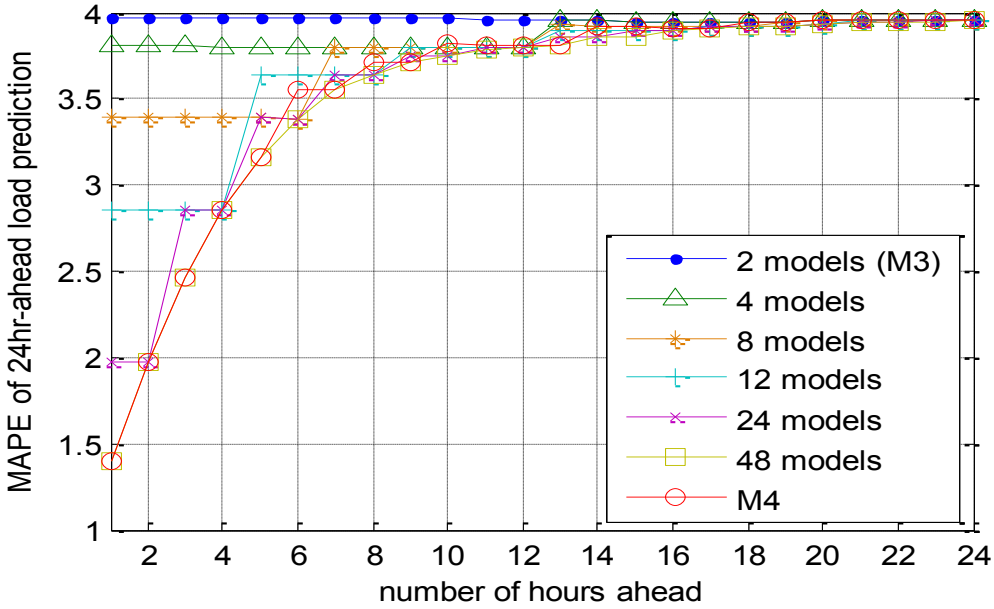

Figure 4.5 - MAPE for 24hr-ahead load prediction by multiple models

The usage of M4 not only shrinks the complexity of the prediction model, but also slightly reduces the solution time for one year test from 724 seconds for 48 models to 709 seconds. At the same time, no significant influence of the prediction accuracy can be observed from M4. Compared to M3 (704 seconds), M4 does not have a significant increase of the solution time as the simple switching operation before the SVR prediction would not affect the solution speed.

Figure 4.6 shows the advantage of using multiple models in the prediction by comparing the conductor temperature error caused by the load prediction error between model M3 and M4. The probabilities of conductor temperature errors being contained within ±2°C for M4 are higher than that for M3 for 1-24hr-ahead prediction, especially for 5hr-ahead prediction, the probability increases from 90.97% in M3 to 96.10% in M4. In addition, M4 will show more advantage over M3 in the cable temperature accuracy of longer prediction horizons for the cable installation with longer thermal time constant (for example, directly buried cable). This is because the large load prediction errors at the 1-13hr ahead load prediction from M3 will have greater accumulated effect for the cable temperature error long prediction horizons when the thermal time constant is longer.

For a comparative study, Table 4.4 presents the probability of conductor temperature errors being contained within ±2°C and ±3°C from the test results of all models. Model M4 presents greater performances (higher probability of conductor temperature error contained within ±2 and ±3°C) than any other models in all of the prediction result. In addition, model M4 is superior to model M3 in 1-4hr ahead prediction. As a result, model M4 is selected as the model used for day-ahead load prediction in this work.

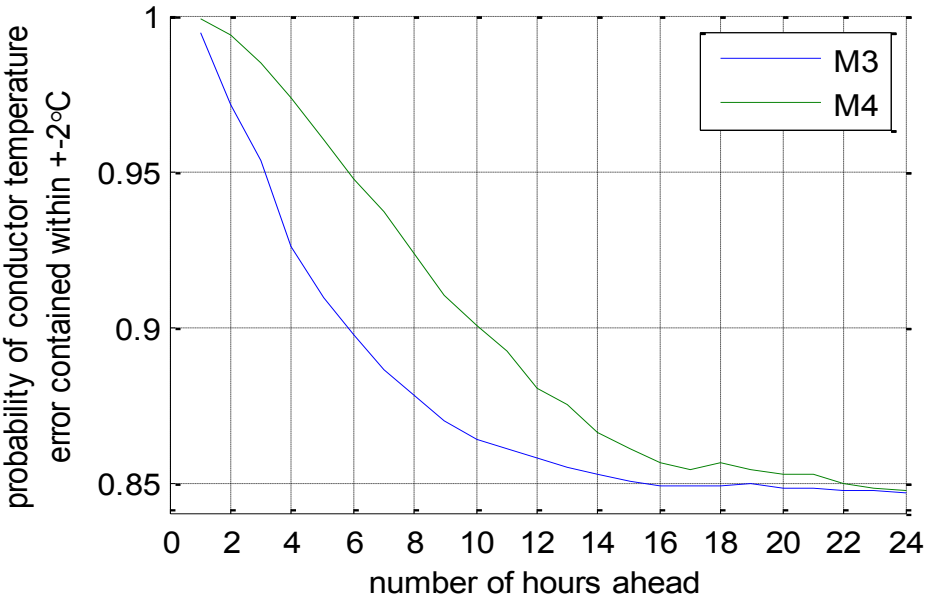

Figure 4.6 - Probability of cable temperature error being contained within ±2°C for M3 and M4

Table 4.4 - Probability of Conductor Temperature Errors Being Contained Within ±2°C and ±3°C in all Models

Model	1hr ahead		4hr ahead		24hr ahead	
	error within ±2°C	error within ±3°C	error within ±2°C	error within ±3°C	error within ±2°C	error within ±3°C
M1	98.22%	99.96%	78.67%	91.65%	64.48%	78.41%
M2	99.53%	100.00%	91.77%	97.42%	84.45%	94.52%
M3	99.53%	100.00%	92.65%	97.42%	84.72%	94.84%
M4	99.94%	100.00%	97.42%	99.02%	84.82%	94.86%

4.3.4 Test for the length of training data

The test in Section 4.3.3 have decided the most suitable input features for the day-ahead load prediction model of the given data set. All the SVR load prediction models in those tests are built by using 3 years' training dataset. In order to decide the minimum requirement of the train data, different lengths of the training dataset for SVR models have been tested in this section.

An ideal training dataset for SVR model should include sufficient features to represent the relation between input and output data. Since load demands has different features for each season, at least one year length of the training data should be used to build the SVR load prediction model. As a result, one year training data is used as the minimum unit. The first SVR model is built by the training data of the most recent year (2006), then gradually increase the

length of train data of SVR model to two years (2005 and 2006) and three years (2004 to 2006) for the other two models. These three SVR models with different length of training datasets are used to test the data in 2007. The MAPE results for these three SVR models are presented in Figure 4.7. It shows that, the SVR model built by 3 years' training data has the lowest mean absolute percentage errors (MAPE) for 1-24 hour ahead load demand predictions in the test of the data from 2007. Thus, this SVR load prediction model built by 3 years' train data is used for the further analysis in this thesis.

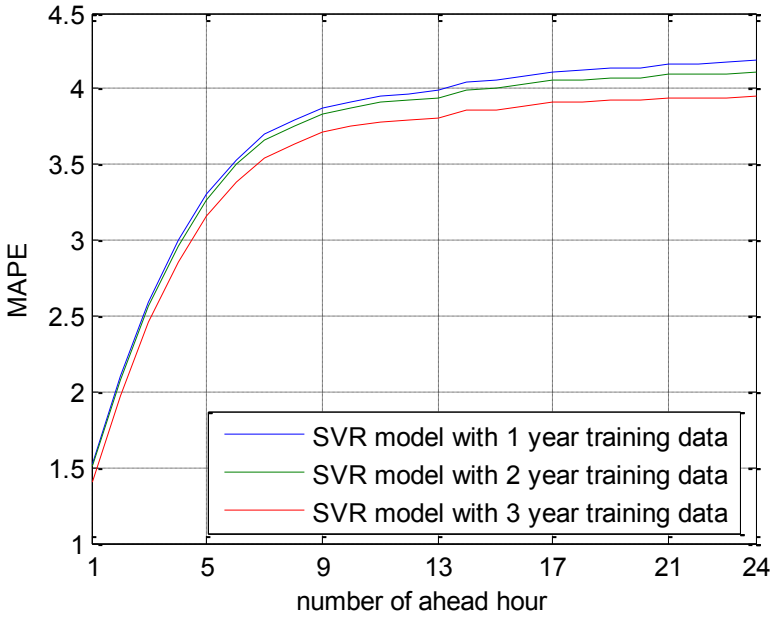

Figure 4.7 – Test results for SVR models with different length of training datasets

4.3.5 Benchmark models

In order to evaluate the day-ahead load prediction results from SVR model, two typical methods have been chosen to compare with the SVR, namely Multiple Linear Regression (MLR) and Gradient Boosting Machine (GBM). First, Multiple Linear Regression has been used to build a benchmark model for short term load forecasting using the principles presented by Tao [77], which have served as a benchmark for a US and a Canadian utility since 2009. It was also used as a benchmark for load forecasting competition in GEFCom 2012 [99] and was among the top four winners during the competition [103]. Second, Gradient Boosting Machine showed its advance in the short term load forecasting by occupying two places of the top five winners in GEFCom 2012 [90], [91], [99]. The same data used in SVR test have been applied to these two methods with the results of the MAPE for day ahead load forecasting being compared with the SVR model.

4.3.5.1 Multiple Linear Regression (MLR) model

The Multiple Linear Regression benchmark model for short term load forecasting considers the linear trend (*Trend*), temperature (*Tem*), calendar variables *(Hour, Day. Month*) and the interaction effects between these factors. The model [77] can be written as:

$$\begin{aligned} E(load) = {} & \beta_0 + \beta_1 \times Trend + \beta_2 \times Day \times Hour + \beta_3 \times Month + \\ & \beta_4 \times Month \times Tem + \beta_5 \times Month \times Tem^2 + \beta_6 \times Month \times Tem^3 + \\ & \beta_7 \times Hour \times Tem + \beta_8 \times Hour \times Tem^2 + \beta_9 \times Hour \times Tem^3 \end{aligned} \tag{4.9}$$

It should be noted that the usage of 3rd order polynomials for temperature is to consider the relation between load and temperature shown in Figure 4.8. A negative correlation between load demand and temperature can be observed when the temperature is lower than 13°C, while when the temperature is higher than 13°C, a positive correlation can be found.

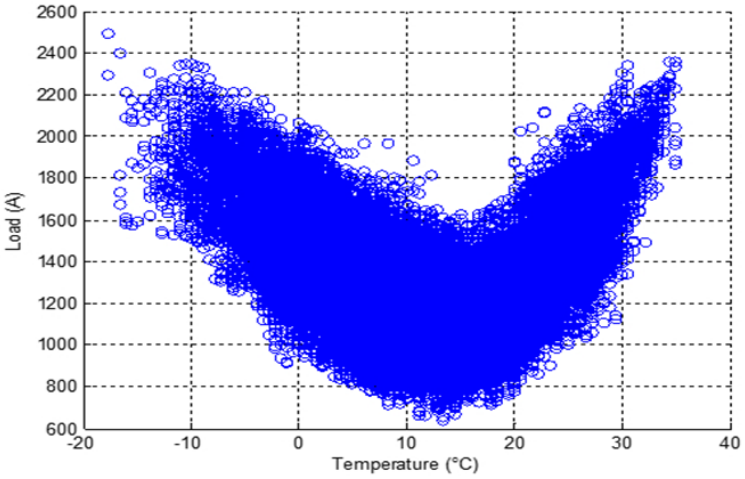

Figure 4.8 – Relation between load and temperature

One of the fundamental assumptions in this benchmark model is that the loads in adjacent hours are independent of each hour as the model does not include the historical load features. The only factor that affects the accuracy with a longer prediction horizon is the precision of temperature forecasting. However, the temperature forecasting in this test is assumed to be available by using the real-time temperature directly. Thus, the load forecasting accuracies of different prediction horizons are almost undistinguishable.

The same training (hourly load and temperature from 2004 to 2006) and testing (hourly load and temperature in 2007) data used in SVR test have been applied to test this MLR benchmark model. Although [77] claims that the MAPE is about 5 for day ahead hourly load forecasting, the MAPE of the same MLR model applied by new testing data in this work appears to be 10.9. The big increase of the load prediction error from MLR model by applying different testing data

indicates that the original MLR benchmark model in [77] may not be reliable when dealing with different input data.

As shown in Section 4.3.3, the addition of historical load and temperature features can improve the prediction accuracy dramatically. An updated MLR model has been built, based on the original MLR model in [77] and the analysis of new input features for MLR model. The result shows that, by adding nine input features presented in Table 4.5, the MAPE of day-ahead hourly load prediction by MLR model could be immediately reduced from 10.9 to 6.0. However, the MAPE for 24hr-ahead load prediction from SVR model is 3.96, which is still significant lower than the errors from the updated MLR model.

Table 4.5 – Adding input features for updated MLR model

Temperature	*T(t-1), T(t-2), T(t-24*), *T(t-48)*
Load	*L(t-24), L(t-48),* max *L* of last day, *L(t-25), L(t-26)*

4.3.5.2 Gradient Boosting Machine (GBM) model

The Gradient Boosting Machine was used by several teams in the GEFCom 2012 load forecasting competition and won two places in the top five of the competition [90], [91]. The details of input features and model parameters of [90] are presented in the paper, which makes it possible to be compared with the SVR model.

The GBM model in [90] uses 24 separate models for the prediction of each hour of the day, and each model has 43 input features which are concluded in Table 4.6.

Table 4.6 – Input features for Gradient Boosting Machine (GBM) model

Category	Features
Calendar effects	Time of year; Day of week; Hour of day
Load (*L*)	*L* of previous 12 hours; Same hour *L* of previous 2 days; Max and Min *L* of previous day; Avg *L* of previous 7 days
Temperature (*T*)	*T* of previous 12 hours; Same hour *T* of previous 2 days; Max and Min *T* of previous 2 days; Avg *T* of previous 1, 3 and 7 days

The main features are historical temperature and load (up to a week earlier) and present temperature. In addition, the model includes the consideration of the calendar effects. The *mboost* package [104]in R[105] was used to build and test model in [90]. To replicate the same GBM model for the comparison study with SVR model, the same package is applied in this

work. The same load and temperature data for training and testing used in the SVR model have been applied to this GBM model and the output day-ahead load prediction MAPE is found to be 5.3. Although the MAPE for day-ahead load prediction from GBM model is lower than that from MLR model, it is still higher than the SVR model in this work.

These two benchmark models (MLR and GBM models) are based on the concept of one day ahead load forecasting while the SVR model in this work is able to predict the load from 1hr ahead to 24hr ahead. A series of SVR models have been applied for different hour-ahead prediction to take advantage of knowing more recent load information for shorter term load prediction (i.e. 1hr ahead prediction in Figure 4.5). The same idea was applied to the MLR and GBM models to obtain more precise short term load prediction and the MAPE of different hour ahead load prediction are shown in Figure 4.9. The results indicate that the SVR model outperforms both the GBM and MLR models from 1hr ahead to 24hr ahead prediction. Thus, the SVR model is used for the analysis in the rest of this thesis.

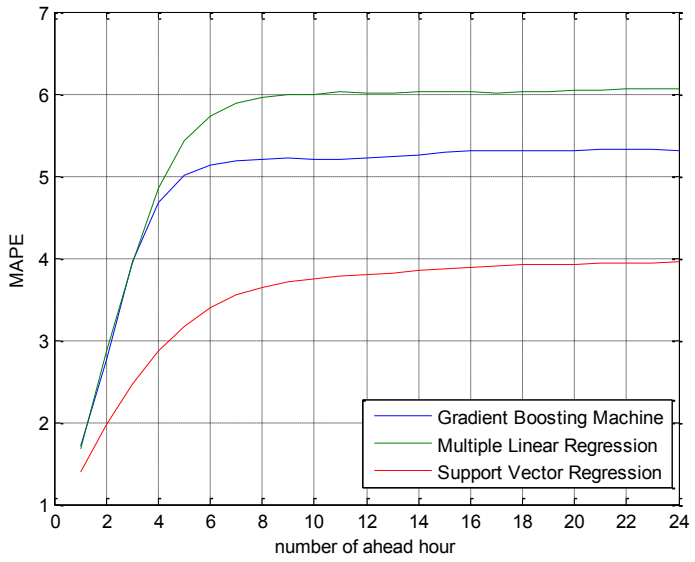

Figure 4.9 – Comparison of MAPE for day-ahead load prediction

4.4 Limitations

At the present time, the load prediction methods have been used to forecast the local load demand in an area, which is under the assumption of only one circuit feeding into a local area without power generation. However, the loading of one transmission circuit relates to a lot of factors as shown in Figure 4.10.

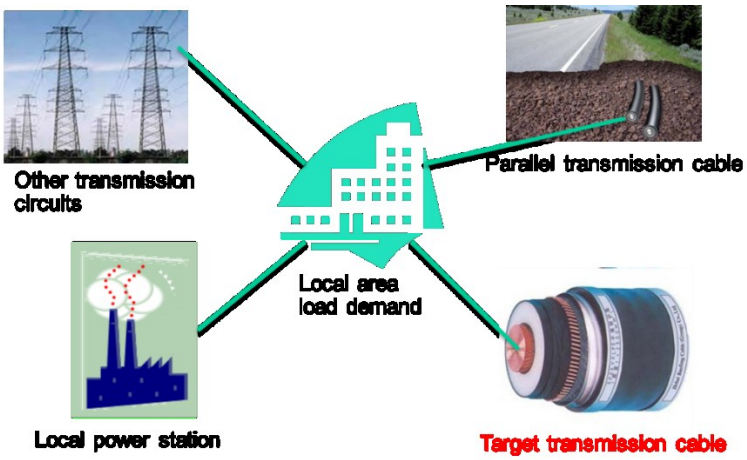

Figure 4.10 - Framework of the load prediction for transmission circuit

Large amounts of information is required for the load prediction of transmission line, including:

- The load demand of the area that the cable circuit will feed
- Loading of other adjacent circuits
- The power generated by stations connected into network adjacent to the cable circuit in question.

A long term dataset which includes all the above information are needed for SVR training, so it will be an extremely large dataset requiring heavy computation. However, this thesis mainly focuses on the application of predicted cable ratings and the methods to integrate the load prediction into the dynamic rating system to perform the rating prediction. As a result, these local load demand prediction results will be used to show proof of concept in the following chapters.

4.5 Summary

A day-ahead load prediction system has been built by using Support Vector Regression (SVR). With the assumption of only one circuit feeding into a local area without power generation, a comprehensive test of SVR model has been done to find a best way for the 24hr-ahead load prediction. Emphasis is placed on selecting inputs to the feature vector to keep computational time as low as possible, while delivering high quality predictions. With the appropriate input features of history load and temperature data, the MAPE of the SVR load prediction model can be 1.45 for 1hr ahead prediction and 3.95 for 24hr ahead prediction. Applying this load prediction into an example cable tunnel model, the probability of cable conductor temperature error being contained within ±3°C for 1hr, 4hr and 24hr ahead prediction can be found to be 100%, 98.98% and 94.48% respectively. The comparison in this section shows that the prediction results from SVR model outperform results from the models built by other two

popular techniques used in short term load forecasting tasks: Multiple Linear Regression and Gradient Boosting Machine. As a result, the day-ahead load prediction model built by SVR is used for the analysis in the rest of this thesis.

Chapter 5: Predicted Rating Test Results

In the previous two chapters, dynamic thermal models for three kinds of cable installations and an SVR day-ahead load prediction system are detailed. With these two systems, the day-ahead Predicted Cable Rating can be achieved to provide the time-limited emergency rating calculated forward from any point within the next 24 hours to assist in day-ahead planning for transmission operators. In this chapter, the predicted rating algorithm is applied to buried cable, cable in air and tunnel cable systems with the results compared to the ratings obtained by direct solution of their thermal model at the time concerned.

5.1 Predicted rating system

Based on the dynamic thermal models for each kind of cable system introduced in Chapter 3 and the day-ahead load prediction system presented in Chapter 4, the predicted rating system can be implemented by the structure shown in Figure 5.1.

The real-time load and environment data are measured and used in the dynamic thermal model to update the thermal parameters and heat losses which are essential to calculate the temperature response of the cable in each step. With this real-time temperature and historical load information, the normal dynamic rating can be obtained. In order to predict the cable rating 24 hours ahead, the day-ahead ambient temperature and load information are needed at each time step. In this work, the ambient temperature forecast data is assumed to be obtained from a nearby weather station. A load prediction system has been built based on the Support Vector Regression technique to forecast the next 24hours' load at each step.

Based on the real-time cable temperature results from the thermal model, these day-ahead prediction data are used to estimate the cable temperature 24 hours ahead. Thus, the predicted rating which provides the time-limited emergency rating calculated forward from any point within the next 24 hours can be performed.

In addition, a rating error estimation system will be detailed in this Chapter (Section 5.5). It is based on the exponentially weighted moving average (EWMA) equation and multiple linear regression (MLR) techniques and used to estimate the prediction rating error quickly without using the dynamic thermal model. When the estimated rating error is higher than a set value, the predicted rating value in the system will be replaced by the real-time rating value. Thus, the risk can be reduced in the whole system.

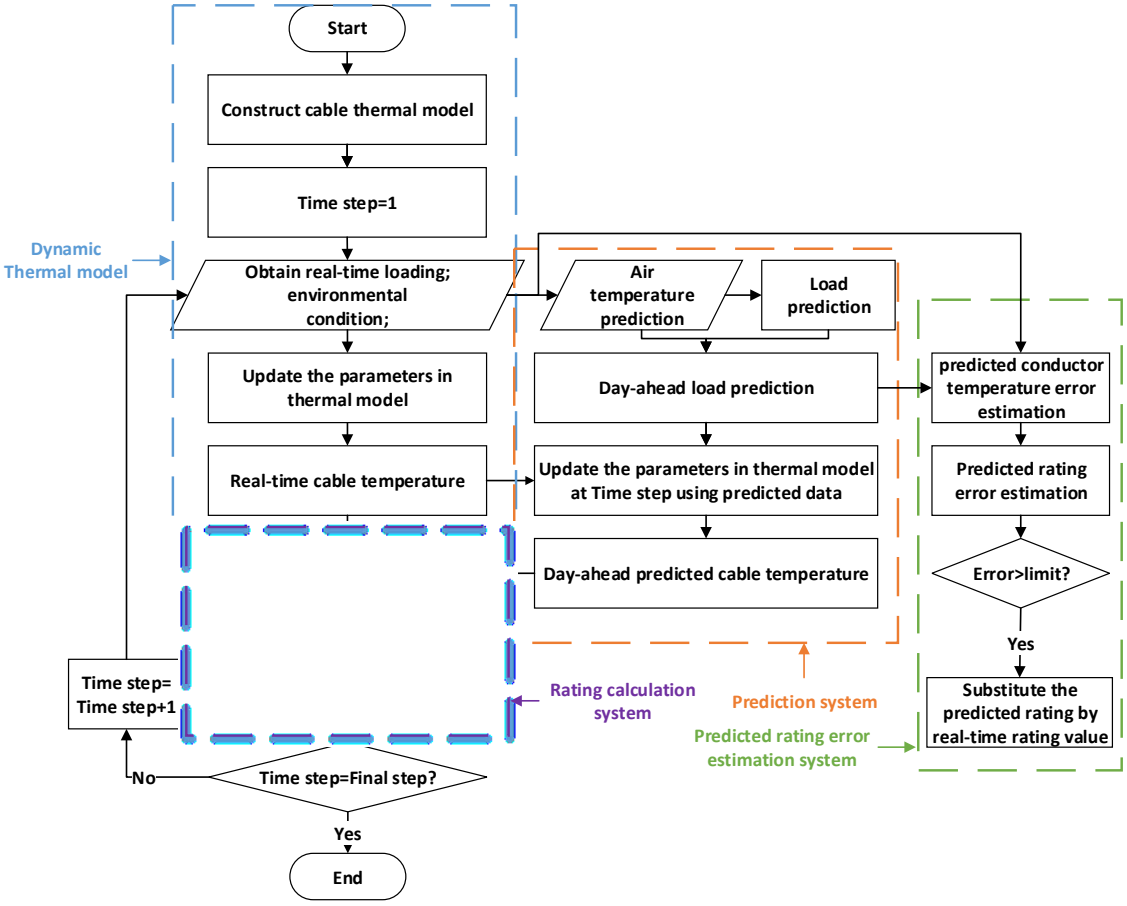

Figure 5.1 - Predicted cable rating algorithm

5.2 Predicted rating test for directly buried cable

In the tests of this section, the dynamic thermal model used is that which has been introduced in Section 3.2.3. The cable parameters can be found from Table 3.1 and the thermal environment is common with Section 3.2.1. The load prediction system and prediction results from Chapter 4 are applied as the conductor current, while the load data are linear scaled into the range from 0A to 1500A. This current level results in an average conductor temperature at about 45°C during the test, which can represent the realistic load level of this buried cable system. Figure 5.2 presents the real-time conductor temperatures and 6hr emergency ratings for a one year test.

It is clear that the conductor temperature and 6hr emergency rating have a negative relationship between each other, where a higher conductor temperature gives a lower emergency rating of the cable. Within this one year test, the 6hr emergency ratings range from 2360A to 2900A. In order to see the distribution of 6hr emergency ratings during the one year test for buried cable, the histogram plot of the 6hr emergency ratings throughout the test is presented in Figure 5.3. The distribution of the 6hr emergency ratings shows that most of the rating values are located

between 2650A and 2850A, as the result of a majority of cable conductor temperatures being within the range from 40°C to 50°C (Figure 5.4).

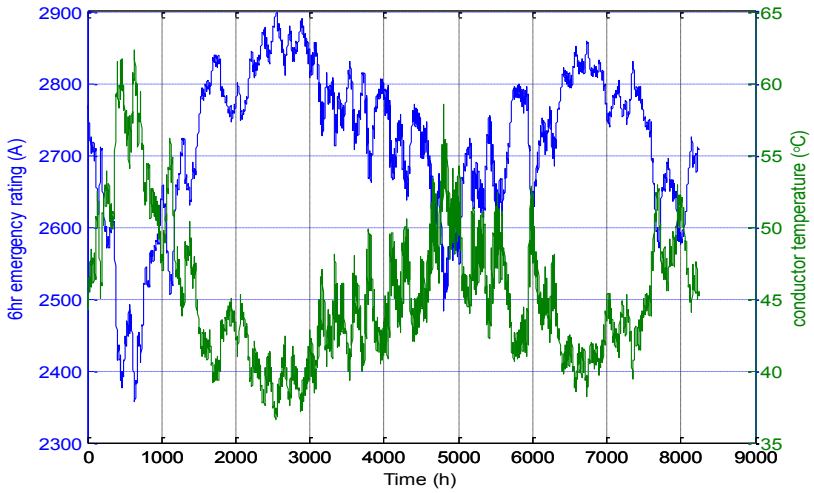

Figure 5.2 – Real-time temperature and 6hr emergency ratings for buried cable

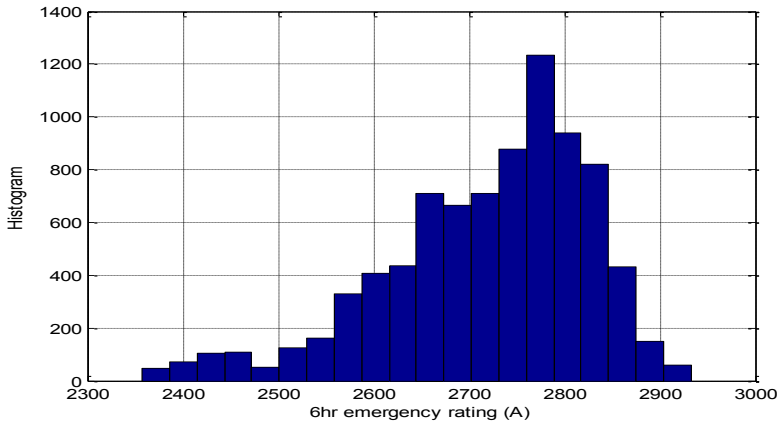

Figure 5.3 – Histogram of 6hr emergency rating for buried cable

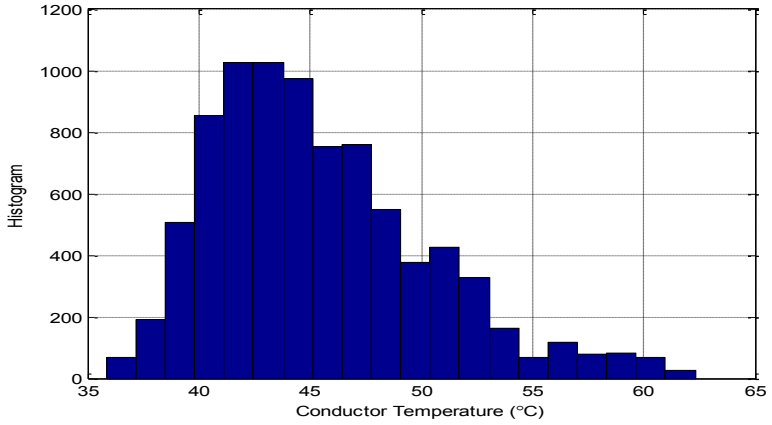

Figure 5.4 – Histogram of conductor temperature for buried cable

A test has been implemented to demonstrate the predicted rating for the buried cable. Assuming that the load before the original point (0 hour) in Figure 5.5 is known, the load from 0 hours to 24 hours is predicted by using the SVR models introduced in Section 4.3. Conductor temperatures based on the real data (red line) and predicted data (blue line) can be calculated by the dynamic thermal model and are presented in Figure 5.5.

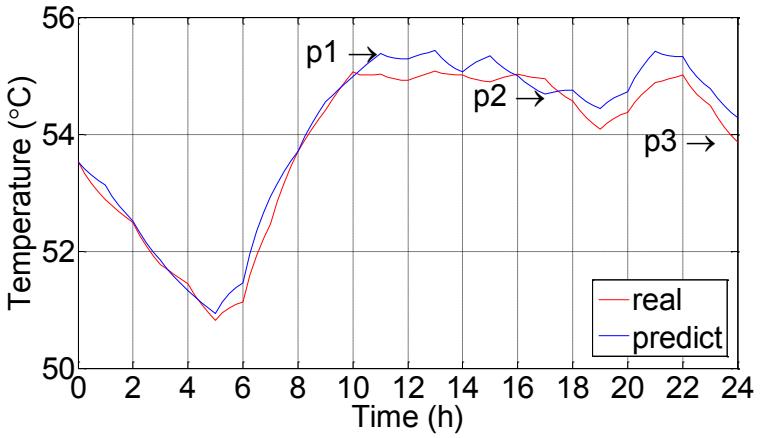

Figure 5.5 - Result of temperature prediction based on predicted load

Three points of in these 24 hours have been chosen to calculate emergency ratings and the results are shown in Table 5.1. Compared with the emergency rating calculated by the real load data, it can be found that precise predicted emergency rating forward from any point in the next 24 hours can be obtained based on the accurate load prediction and historical data. The maximum difference between real and predicted emergency ratings is 16A, 4A and 2A for 1hr, 6hr and 24hr ratings respectively. The absolute percentage errors for 1hr, 6hr and 24hr predicted ratings are only 0.42%, 0.16% and 0.1% respectively. It is worth noting that the maximal errors all happen at Point 3 in this case. This is because Point 3 is the latest predicted point (24 hours), the cable temperature error at this point has accumulated all the load prediction errors from 0 hour to 24 hours.

Table 5.1 - Forward emergency rating prediction results

Point	**P1**		**P2**		**P3**	
Time	11a.m.		5p.m.		12p.m.	
	real	**predict**	**real**	**predict**	**real**	**predict**
load (A)	1482.5	1457.9	1357.5	1309.4	1222.5	1251.7
T (°C)	55.0	54.9	54.9	54.7	53.9	54.3
1hr Emergency rating (A)	3750	3747	3744	3747	3776	3760
6hr Emergency rating (A)	2522	2521	2512	2511	2514	2510
24hr Emergency rating (A)	2097	2097	2092	2092	2091	2089

To consider the reliability of the predicted cable rating, some statistical methods are applied in the analysis within this section. The load prediction system from Section 4.3 has been implemented into the dynamic thermal model for buried cables, and obtained 6hr emergency rating predictions from 1hr ahead to 24hr ahead for a whole year. The rating prediction results were then compared with the real ratings (direct solution from the dynamic thermal model with the actual load). The predicted rating errors were calculated as the difference between the predicted ratings and real ratings (real values-predicted values). The results are shown in Figure 5.6 in the form of Cumulative Distribution Function (CDF), which represents the probability of the predicted rating errors being less than a certain value. It can be seen that most of the 6hr emergency rating prediction errors are being contained within ±5A, ±30A and ±50A for 1hr ahead, 4hr ahead and 24hr ahead predictions respectively.

For a predicted rating system, an overestimate of the rating value could place the cable system at risk. In other words, we do not need to worry about the situation when the predicted value is lower than the real rating value as the load will not exceed the actual rating and no thermal damage will occur. As a result, only the left part in the following figures showing the negative errors will really place the system in a risk. The reliability of the predicted rating system is defined by allowing a 20A overestimate of the cable rating (pink dash line in Figure 5.6), which is the approximate measurement error of a current transformer during 2000A loading. Such level of the overestimation of the 6hr emergency rating can only result in about 0.8°C of the conductor overheating at the end of 6 hours. For 1hr ahead prediction, the reliability of the 6hr emergency rating prediction errors stays at 100%. Then the reliability decreases as the prediction horizon grows. For 24hr ahead prediction, the reliability of the predicted rating system is still higher than 94%.

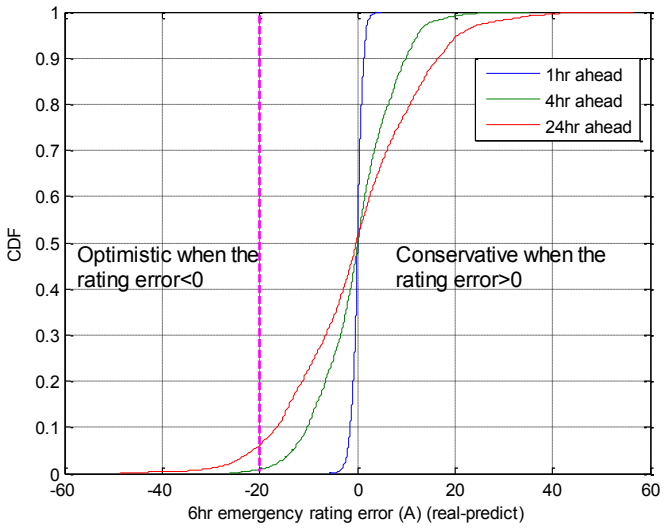

Figure 5.6 – CDF of 6hr Emergency Rating error for different hour ahead prediction

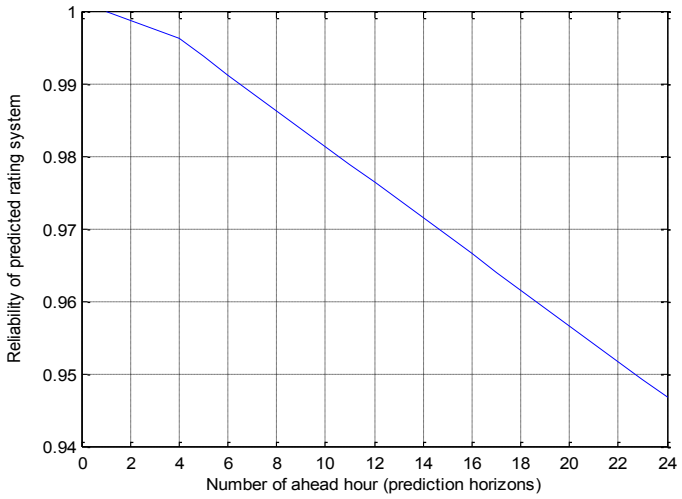

Figure 5.7 – Reliability for different hour ahead predicted rating

5.3 Predicted rating test for cable in air

In the predicted rating test for the cable in air, a 33kV single phase XLPE cable with 630mm^2 copper conductor is used with the geometries and properties shown in Table 5.2. A 10 meter sample of this type of cable will be tested with the experimental validation results of the prediction ratings shown in Chapter 6. The thermal parameters for the Aluminium wire armour are calculated by the rule of mixtures. According to this rule, the equivalent thermal conductivity and volumetric heat capacity of the armour are calculated by sum of the two thermal properties of components (Aluminium and PP) multiplied by their volume fraction.

Table 5.2 – Geometries and properties for cable installed in air

Component	**Outer Diameter (mm)**	**Material**	**Thermal Conductivity (W/m·K)**	**Volumetric Heat Capacity (MJ/m^{3}K)**
Conductor	30.40	Copper	400	3.45
Conductor screen	31.60	XLPE	0.286	2.4
Dielectric	52.27	XLPE	0.286	2.4
Dielectric screen	53.47	XLPE	0.286	2.4
Copper tape screen	53.62	Copper	400	3.45
Inner sheath	59.132	PVC	0.2	1.7
Fabric tap bedding	60.51	Fabric	0.130	2
Armour	65.51	Al/PP	1.449	2.286
Outer Sheath	72.40	PVC	0.167	1.7

The FDM dynamic thermal model with Morgan's natural cooling heat transfer coefficient is used, assuming that the cable is protected from direct solar radiation. The real-time load input and load prediction values from Section 4.3 are linearly scaled into the range from 0A to 1200A

in this test to make them closer to the actual values of the load carried by this cable circuit. The 24hr-ahead air temperature prediction is assumed to be available and perfect in this test in order to provide the ambient temperature input for the FDM model during the prediction.

Figure 5.8 and Figure 5.9 present the real-time conductor temperatures with 1hr emergency ratings and 3hr emergency ratings respectively during a one year test. The comparison between these two figures indicates that the magnitude and fluctuation of the 1hr emergency ratings are larger than those of 3hr emergency ratings. Within this one year test, the 1hr emergency ratings vary from around 1600A to 2300A, while the 3hr emergency ratings only range from 1475A to 1635A approximately. This is because the short thermal time constant of this cable (2.95 hours for 1400A constant conductor current and 20°C ambient air temperature which results in a steady-state conductor temperature of 82°C from the FDM model) makes the 3hr emergency ratings close to the value of continuous rating for this cable circuit.

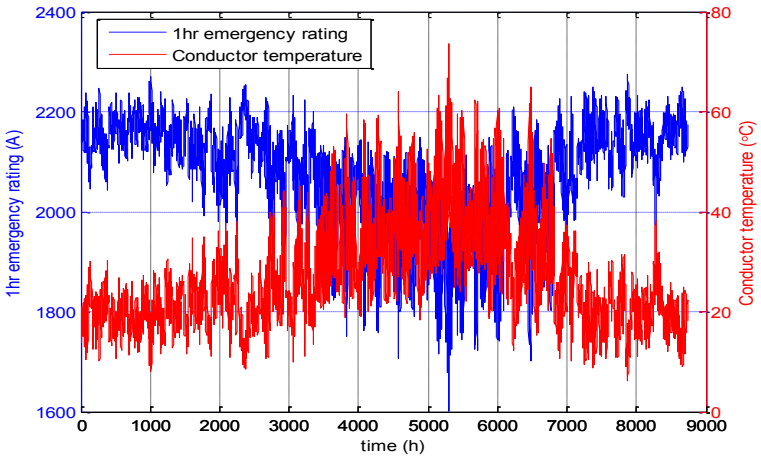

Figure 5.8 - Real-time conductor temperature and 1hr emergency ratings for cable in air

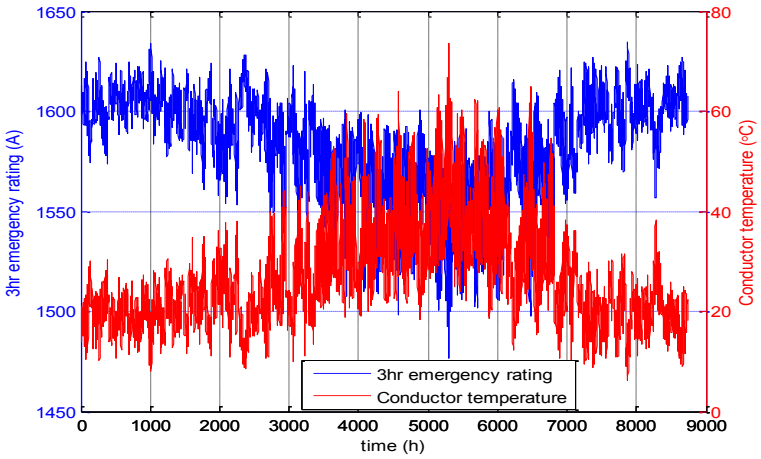

Figure 5.9 – Real-time conductor temperature and 3hr emergency ratings for cable in air

A typical whole week's 1hr-ahead and 24hr-ahead conductor temperature predictions are calculated by the FDM dynamic model and are presented in Figure 5.10. Compared with the actual conductor temperature values from direct solution of the thermal model, the 1hr-ahead conductor temperature prediction results are better than the 24hr-ahead prediction. The maximum conductor temperature differences between predicted values calculated by the load prediction result from SVR and actual values are 4.1°C and 5.4°C for 1hr-ahead and 24hr-ahead predictions respectively.

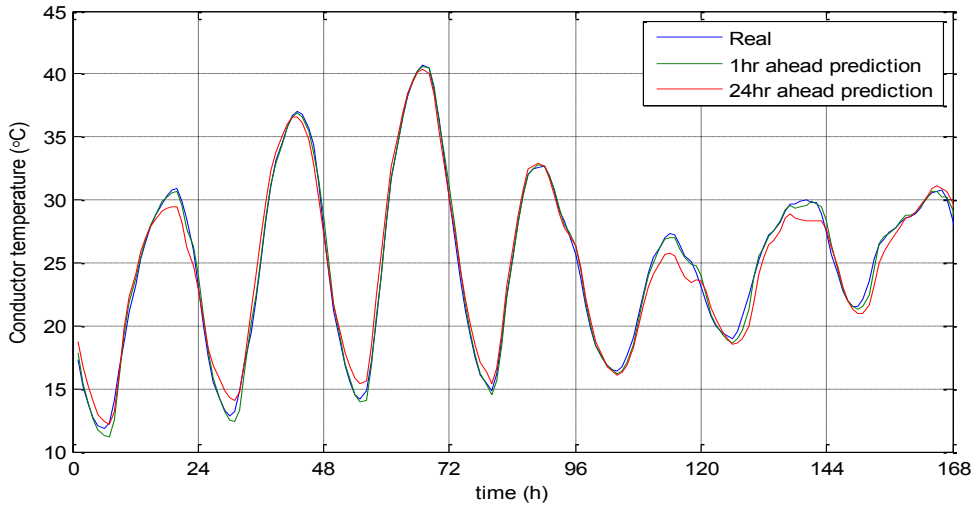

Figure 5.10 – Typical conductor temperature prediction result for cable in air

Based on the load prediction, ambient air temperature prediction and cable temperature prediction from the dynamic thermal model, day-ahead predicted ratings can be obtained. Due to the relatively short thermal time constant of cable installed in free air, only the 1hr and 3hr emergency rating (the maximum current the cable can carry over the next hour or three hours without exceeding the thermal limit) is calculated in this case. Predicted rating values are compared to the actual ratings obtained by direct solution of the thermal model at the time concerned. Figure 5.11 and Figure 5.12 show the Cumulative Distribution Function (CDF) of the errors in 1hr and 3hr emergency rating prediction. They present the probability of the predicted rating error being less than a certain value from different prediction horizons.

The analysis of the results shows that the predicted ratings from further prediction horizons have higher prediction errors. For example, the 24hr ahead predicted ratings have higher errors than the 1hr ahead predicted rating results, which can be inferred from Figure 5.11 and Figure 5.12 that the 1hr emergency rating errors and 3hr emergency rating errors are located within the range of ±100A and ±25A respectively for 24hr ahead prediction. Most of the 1hr emergency rating errors and 3hr emergency rating errors from 1hr ahead prediction are contained within ±25A and ±5A respectively.

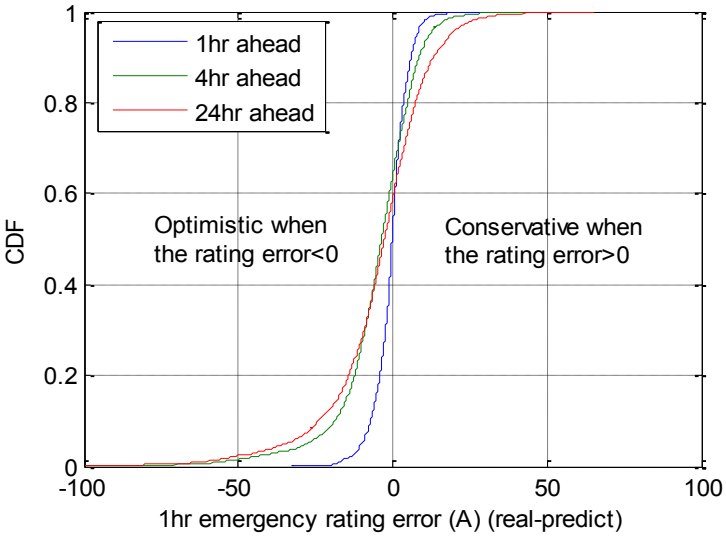

Figure 5.11 – CDF of 1hr Emergency Rating error for different hour ahead prediction

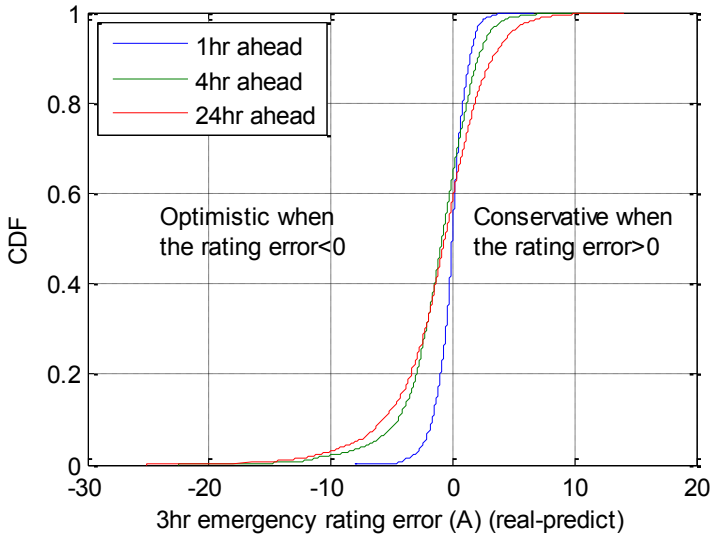

Figure 5.12 – CDF of 3hr Emergency Rating error for different hour ahead prediction

By allowing a 20A overestimate of the cable rating, which is the approximate measurement error of a current transformer during 2000A loading, the reliability of the predicted rating system can be obtained from Figure 5.13. Such overestimate of the rating only results in a suitably small level of conductor overheating at about 1.7°C at the end of 3 hours. It can be noticed that the reliability of the predicted rating system reduces with increasing prediction horizon due to more uncertainty during the longer prediction. In addition, the prediction for 3hr emergency ratings has higher reliability than the 1hr emergency rating prediction. The reliability of the 3hr emergency rating is higher than 99.6% for 1-24hr ahead prediction, while for the prediction of 1hr emergency ratings, the reliabilities for 1hr ahead and 24hr ahead prediction are about 99.5% and 87% respectively. This is because of two reasons. First, 3hr emergency ratings

are normally lower than the 1hr emergency ratings, the average 3hr emergency rating and 1hr emergency rating are 1581A and 2069A respectively. Second, the short thermal time constant for this cable circuit makes 3hr emergency ratings more stable than 1hr emergency ratings as the 3hr emergency rating is closer to the value of the continuous rating.

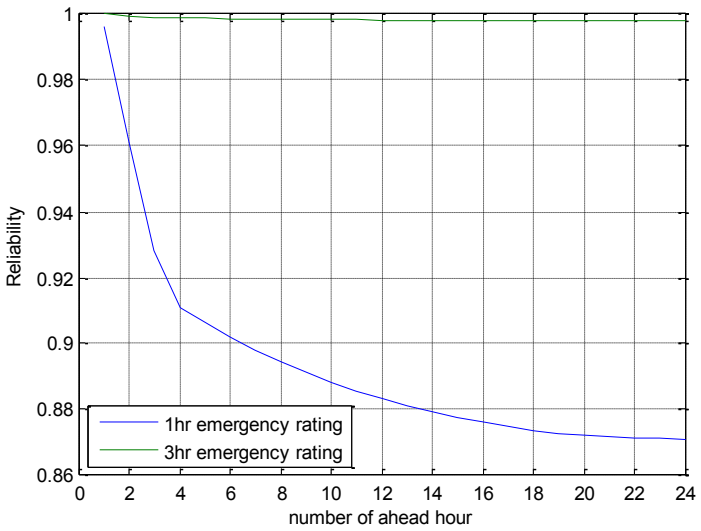

Figure 5.13 – Reliability for different hour ahead predicted rating

5.4 Predicted rating test for tunnel cables

In this section, the predicted rating algorithm is applied to the cable tunnels. By using the 24hr ahead load prediction results, the conductor temperature of the cable can be calculated 24hr ahead through the dynamic thermal model. Figure 5.14 shows an example of the 24 hour load prediction error and the error of the temperature calculated by the load prediction from SVR. The y-axis at the left side and right side show the load prediction errors and conductor temperature errors respectively. The positive value means the predicted load and conductor temperature are higher than the real values, which will result in a conservative cable rating, while the negative values on both y-axis will cause an optimistic cable rating.

The error of temperature has a 1-2 hour lag from the load prediction error due to the thermal time constant of the cable. In addition, the point with the largest error of load prediction does not always result in the largest error of temperature calculation. The greatest negative deviation of the temperature is at P1 in Figure 5.14, while it happens at P2 for the load prediction. This is because the temperature calculation will accumulate the influence of the error from the previous steps. Although the magnitude of the negative error at P1 is not as large as the error at P2, the error of the previous 6 hour of P1 are all negative, resulting in a large negative temperature error

at P1. While for P2, a period of positive error dominates its previous steps, offsetting the effect from the negative error, resulting in a very small temperature error at P2.

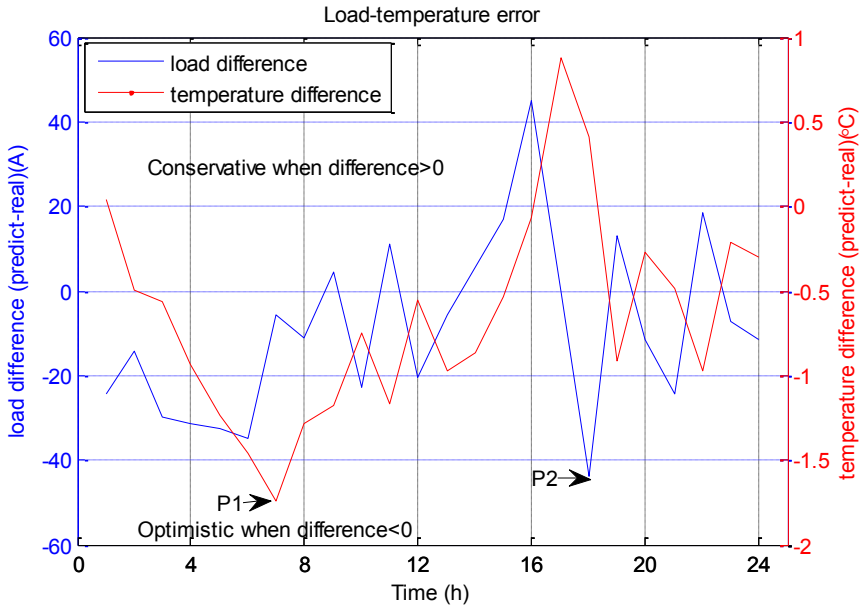

Figure 5.14 - Load prediction and conductor temperature error for a day

The day-ahead predicted cable ratings can be obtained from the dynamic thermal model based on the load prediction results. Two scenarios of the predicted rating are considered for the tunnel cables. Scenario one, the load of both two circuits is the same and the emergency rating for both circuits simultaneously is calculated. In scenario two, one circuit is under outage and the other circuit's emergency rating is calculated.

In both scenarios, the ventilation system is assumed to be fully working all the time (ventilation speed 4m/s at tunnel section two). Figure 5.15 and Figure 5.16 show the probability of the predicted 6hr and 24hr emergency rating error being contained within ±20A for different prediction horizons in Scenario One and Scenario Two. The blue bars and red bars show the results of the prediction of 6hr emergency and 24hr emergency ratings respectively.

Similar results can be observed from these two scenarios. Except for the 1hr ahead predicted rating (100% for 6hr and 24hr emergency rating in both scenarios), the probability of predicted 24hr emergency rating errors being contained within ±20A is higher than that of the predicted 6hr emergency ratings. For 6hr emergency ratings, the probabilities of the error being contained within ±20A are higher than 99% for the 4 hour ahead prediction, and higher than 93% for the 24 hour ahead prediction in both scenarios. For both scenarios, the probabilities of the 24 hour ahead predicted 24hr emergency rating errors being contained within ±20A are all 100%. This is because the 24hr emergency rating of this fully ventilated tunnel cables only ranges from 3020A to 3120A for both scenarios. Such small fluctuation of 24hr emergency ratings means that the

initial cable temperature only has a small effect on the 24hr emergency rating of this tunnel cables.

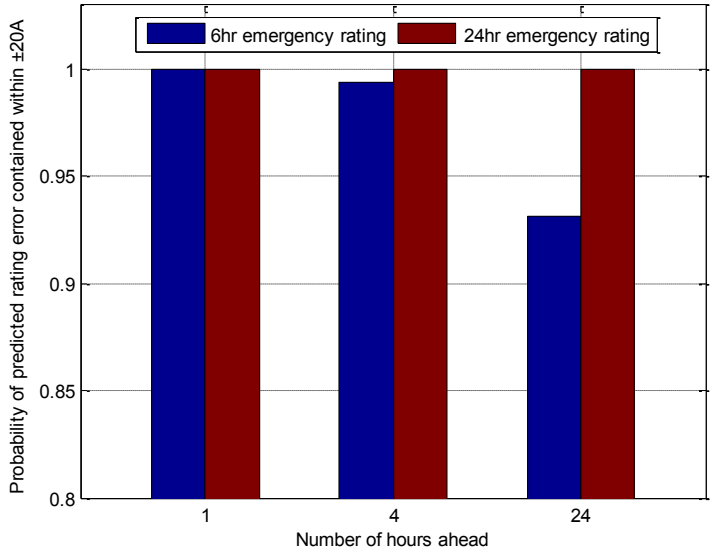

Figure 5.15 - Probability of the predicted rating error contained within ±20A (Scenario One)

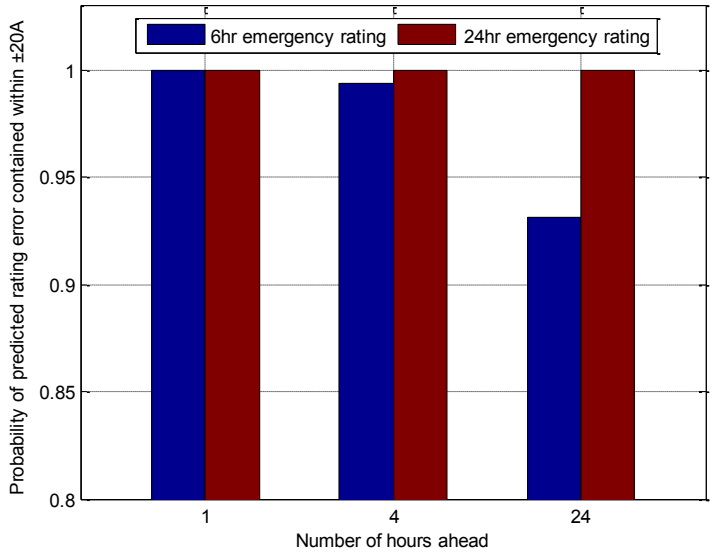

Figure 5.16 - Probability of the predicted rating error contained within ±20A (Scenario Two)

According to Figure 5.15 and Figure 5.16, the accuracy of the predicted 24hr emergency rating is very good, while the accuracy of the predicted 6hr emergency rating is relatively poor. Hence, some further analysis was applied to the predicted 6hr emergency rating. Figure 5.17 and Figure 5.18 show the accuracy of different hour ahead predicted 6hr emergency ratings by presenting the probability of the error being contained within ±20, ±30, ±50 and ±80A in Scenario One and Scenario Two respectively.

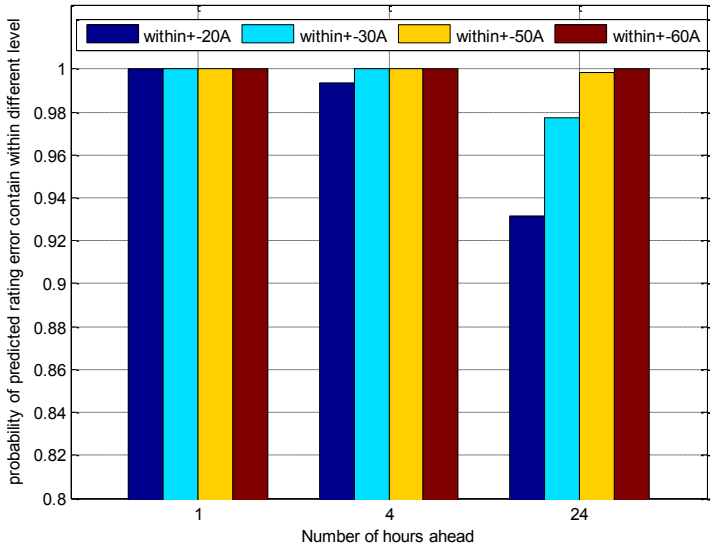

Figure 5.17 – Distribution of error of the predicted 6hr emergency rating (Scenario One)

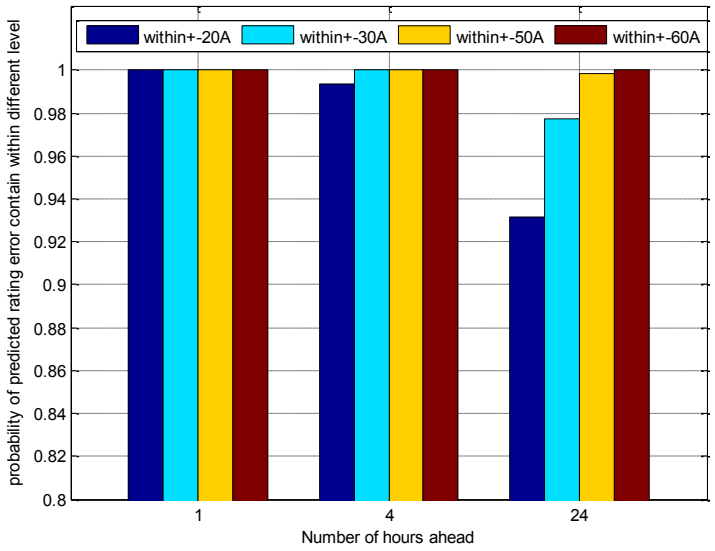

Figure 5.18 – Distribution of error of predicted 6hr emergency rating (Scenario Two)

The results from Scenario One and Scenario Two are again very similar. For the 1 hour ahead 6hr emergency rating prediction, the error in the predicted rating is 100% within ±20A in both scenarios. Predicting further ahead, the accuracy will reduce due to the accumulated error in the load prediction. The probability of the predicted rating error being contained within ±20, ±30 and ±50A reduces from around 99 %, 100 % and 100% for 4hr ahead to 93 %, 97% and 99 % for 24hr ahead respectively in both scenarios. To check the reliability of this predicted rating system, two cumulative distribution plots (Figure 5.19 and Figure 5.20) have been drawn to

describe the probability that the error of the predicted rating (real rating minus predicted rating) is less than a certain value.

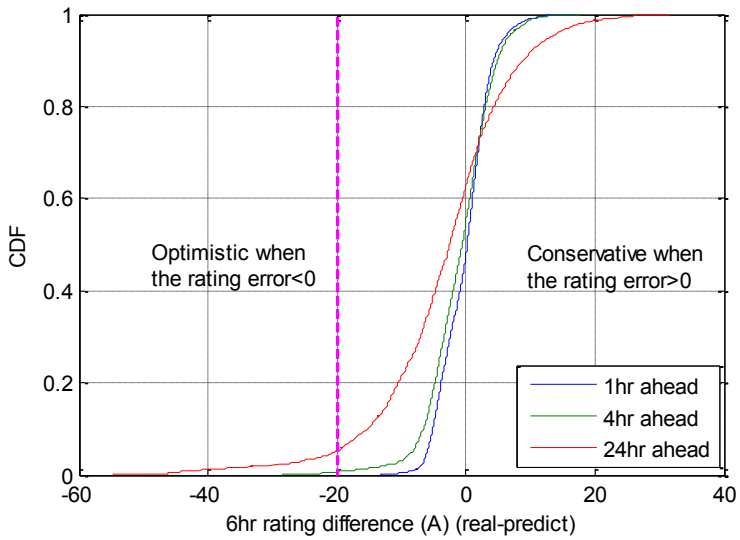

Figure 5.19 - CDF of 6hr Emergency Rating error for different hour ahead prediction (Scenario One)

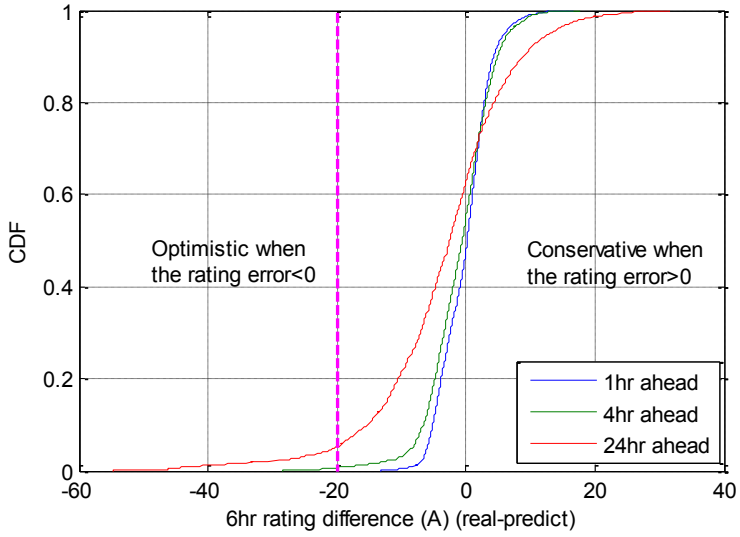

Figure 5.20 - CDF of 6hr Emergency Rating error for different hour ahead prediction (Scenario Two)

As per Section 5.3, by allowing a rating overestimate of 20A, the reliability of different hour ahead predicted rating can be obtained in Figure 5.21. The reliabilities of the predicted rating in Scenario One and Scenario Two are very similar. For the predicted 6hr emergency rating, the reliability of 1-6hr ahead predictions are about 99% in both scenarios, and the reliability of 12hr ahead and 24hr ahead predictions are higher than 97.5% and 94.9% respectively.

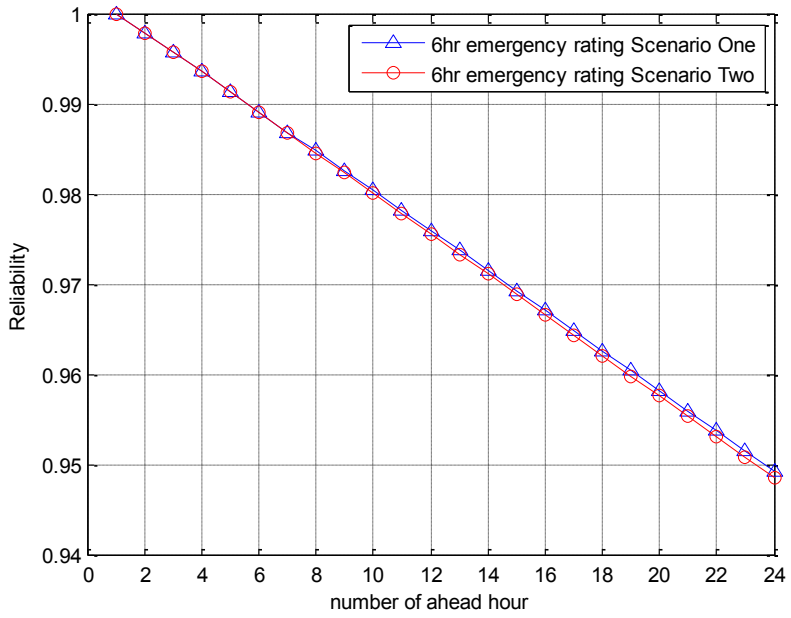

Figure 5.21 - Reliability for different hour ahead predicted rating

5.5 Error estimation system for predicted rating

During the predicted rating process, the load prediction error will result in a cable temperature prediction error, hence the rating prediction will deviate from the real rating value. This predicted rating error can only be calculated when the real-time load is known, in other words, the predicted rating error cannot be obtained until the step of the emergency rating is actually applied. As a result, a method to quickly detect the possible rating prediction errors is vital to the predicted rating system to prevent any risk in the cable circuit. However, the procedure of calculating the real rating by using a conventional dynamic rating technique at each step and then comparing the real-time rating results with the predicted rating result might be very time consuming, especially for more complex cable installations and the transmission systems with a large amount of cable circuits. For example, the calculation of a 3hr emergency rating for tunnel cable system takes about 2.3 seconds by the dynamic thermal model from Section 3.4. For a transmission grid with 200 cable circuits, it takes almost 8 minutes to calculate the errors of all the predicted ratings after the emergency rating having been applied. This speed of the error checking might increase the risk of overheating on cable circuits.

To quickly detect the possible rating errors, as well as building confidence to implement the predicted rating algorithm, it is important to integrate an error estimation system which can detect the predicted rating errors quickly. Such a predicted rating error estimation system is built in this section by investigating the relationship between the loads, conductor temperatures and

rating prediction errors. The load data and predicted rating data from tunnel cables system, which represents the most complicated of the three systems in this Thesis, are used to demonstrate this error estimation system for predicted rating.

5.5.1 Structure of error estimation system

The structure of the predicted rating error estimation system is presented in Figure 5.22. In order to estimate the predicted rating error quickly without using dynamic thermal model, this system aims to estimate the predicted rating error by only using the real-time and predicted load data. Thus, the relation among load prediction errors, cable temperature errors and predicted rating errors need to be analysed.

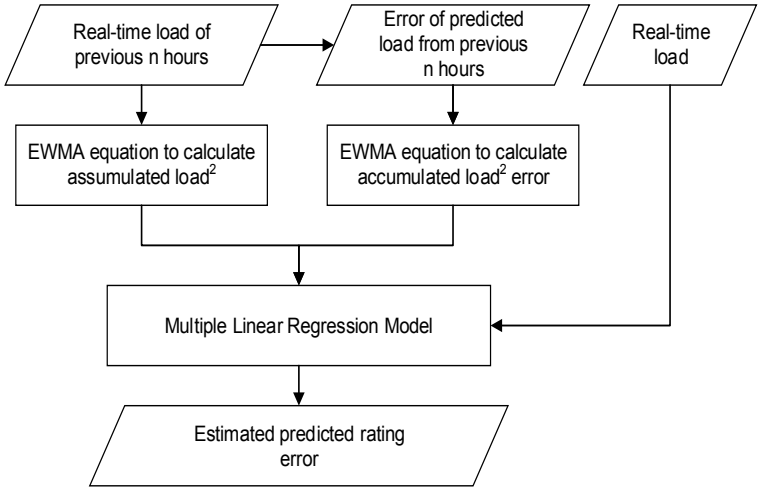

Figure 5.22 – Structure of predicted rating error estimation system

After the real-time load data have been measured, the load prediction error can be calculated. It is clear that the cable temperature is not only affected by the present load, but also by the preceding load history. For different hour ahead predictions, the cable temperature error depends on the accumulated error from all the previous load predictions. An exponentially weighted moving average (EWMA) equation is applied in Section 5.5.2 to fully consider the accumulated error of the load prediction.

The EWMA equation is also applied in Section 5.5.3 to calculate the relation between conductor temperature and historical load data. After obtaining the relation between load and conductor temperature, and between predicted load errors and conductor temperature errors, a simple Multiple Linear Regression (MLR) model is used in Section 5.5.4 to link the load data after processing and predicted rating errors directly.

5.5.2 Load error vs. Temperature error

The heat generated by the conductor losses are the dominant mechanism in cross-bonded cable circuits and are proportional to the square of the load when the temperature dependant resistance change is ignored. In addition, the conductor temperature rise due to the internal heat losses has a roughly linear relation with the heat generated inside the cable in each step's calculation as shown in Figure 5.23. This figure shows the conductor temperature rise at one step, based on the steady state of 1000A load current, has a linear relationship with the different load^2 data. As a result, at the first step, we use the load^2 error to find its correlation with conductor temperature error.

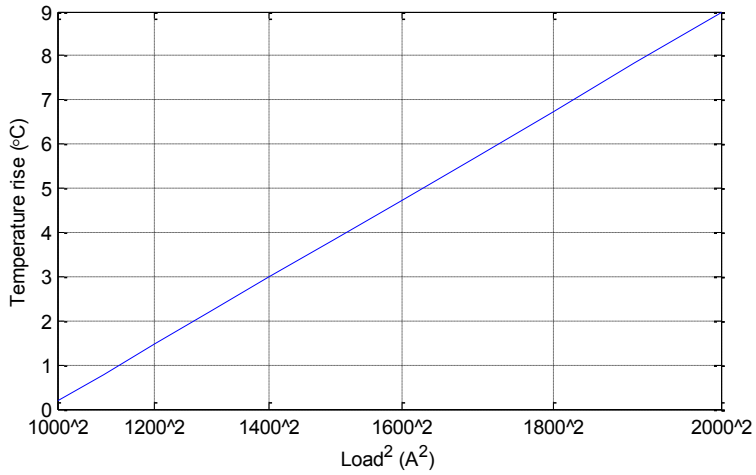

Figure 5.23 – Relation of conductor temperature rise at one step with load^2

The correlation of load^2 errors and conductor temperature errors can be used to define the degree of linearity. This value can be computed using the following expression:

$$Corrcoef(load^2, tem) = \frac{Cov(load^2, tem)}{\sigma_{load^2}\sigma_{tem}} \quad (5.1)$$

where *Cov (load^2, tem)* is the covariance of the load^2 error and conductor temperature error; σ_{load2} and σ_{tem} are the standard deviations for load^2 error and temperature error. *Corrcoef* =1 corresponds to a perfect linear correlation while *Corrcoef* =0 represents no correlation at all, the intermediate values show the degree of partial correlation. The values of correlation between error of load^2 and the error of conductor temperature are shown in Table 5.3.

Table 5.3 – Linear correlation between load^2 and conductor temperature prediction errors

Number of ahead hour	**1**	**4**	**24**
correlation coefficient	0.9999	0.9514	0.8779

For the 1hr ahead situation, the load^2 prediction errors and conductor temperature errors are almost linear with the correlation of 0.9999. The temperature error has an almost linear relation with load^2 error. For the 4hr and 24hr ahead cases, the correlation between load^2 prediction errors and conductor temperature errors becomes smaller, reducing to 0.9514 and 0.8779 for 4hr and 24hr ahead prediction respectively. The reason is that the cable temperature is not only affected by the present load, but also by the preceding load history. For different hour ahead prediction, the temperature error depends on the accumulated error from all the previous load predictions. Only considering the load prediction error at the present step is not enough to obtain an accurate temperature error.

The thermal capacity of the cable installation will result in an exponential decay of the response of conductor temperature over time to a given heat input. As a result, more recent load errors have a stronger influence on conductor temperature error. To fully consider the accumulated error of the load prediction, an exponentially weighted moving average (EWMA) equation is applied. It is able to summarise all the previous temperature response functions from each load^2 prediction error, and the weighting for each older error decreases exponentially over time:

$$Error(t) = \frac{\sum_{k=1}^{t} \alpha^{k-1} \varepsilon(t-(k-1))}{\sum_{k=1}^{t} \alpha^{k-1}} \tag{5.2}$$

where *Error(t)* is the processed load error for *t* hour ahead prediction; ε (*t*) is the prediction error of load^2 for *t* hour ahead and α is the smoothing factor (α<1).

By using this exponentially weighted moving average equation, the summation of all the previous temperature response functions from each load^2 prediction error can be considered, at the same time, the weighting for each older error decreases exponentially over time.

The smoothing factor α has been tested for different prediction horizons. It is determined by using values from 0.3 to 1 in increasing steps of 0.05. Results are shown in Table 5.4, the values of α with best correlation in each case are chosen for further test. The correlations between conductor temperature errors with the load errors after processing for different prediction horizons are all higher than 0.9989, showing that almost perfect linear relations can be found after the load error has been processed by the exponentially weighted moving average equation. In addition, simply setting α as 0.8, which puts emphasis (more than 80% of weighting) on the preceding 5 hours of load^2 errors, can also make sure that the correlations are all higher than 0.9989 for every hour ahead prediction. The correlations between conductor temperature errors and three kinds of load errors for different hour ahead prediction are shown in Figure 5.24.

Table 5.4 - Test results of smoothing factor α

Ahead hour number	α	Correlation	Ahead hour number	α	Correlation
1	0.7	0.9999	**13**	0.75	0.9990
2	0.7	0.9999	**14**	0.8	0.9990
3	0.7	0.9999	**15**	0.8	0.9991
4	0.7	0.9998	**16**	0.8	0.9991
5	0.75	0.9997	**17**	0.8	0.9991
6	0.75	0.9997	**18**	0.8	0.9990
7	0.75	0.9997	**19**	0.8	0.9990
8	0.75	0.9997	**20**	0.8	0.9990
9	0.75	0.9996	**21**	0.8	0.9990
10	0.75	0.9995	**22**	0.8	0.9990
11	0.75	0.9994	**23**	0.8	0.9989
12	0.75	0.9992	**24**	0.8	0.9989

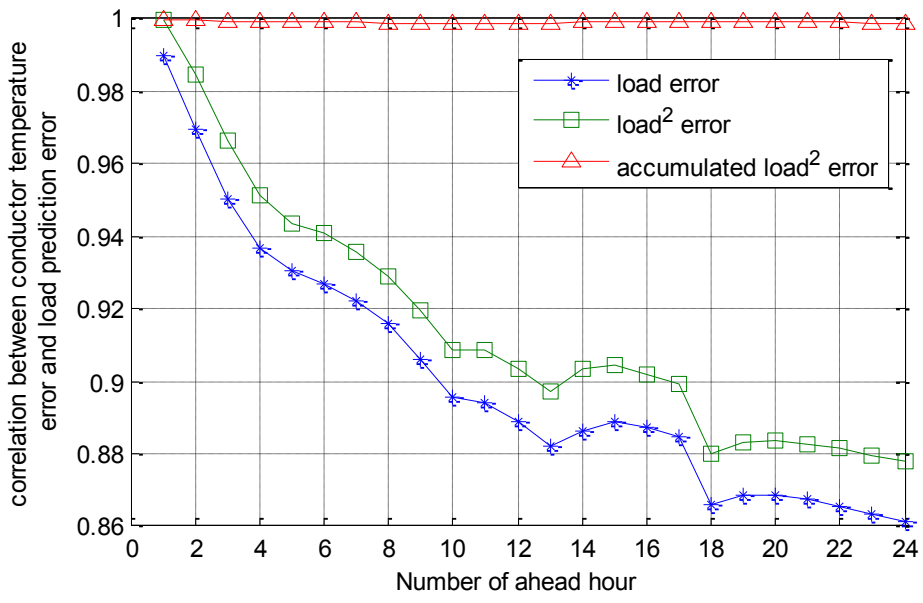

Figure 5.24- Correlations between conductor temperature errors and load errors for different prediction horizons

5.5.3 Load vs. conductor temperature

The EWMA equation is also applied to calculate the relation between conductor temperature and historical load data. In this case, ε (t) is the load^2 for t hour ahead. A grid search has been

used to find the best value of α and the required length of historical load data to be considered. The correlation between the conductor temperature and accumulated load calculated by the weighted moving average equation is used as the criterion to choose the best parameters. Figure 5.25 shows the values of correlation between conductor temperature and accumulated load calculated by weighted moving average equation with different length of historical data and values of α. The best correlation value is 0.9031 when the value of α is 0.6 and 12 hours of historical load data is taken into account. However, the length of historical data does not make a large difference when it is longer than 7 hours, which results in a correlation coefficient of 0.9013, only 0.0018 smaller than the best value. This is because the weights given to the historical load data older than 7 hours are smaller than 0.03 with the decaying factor α (0.6), meaning that they won't have much influence on the result of the EWMA equation. Thus, α equal to 0.6 and the length of historical data equal to 7 hour are chosen to get a relation between conductor temperature and accumulated load data shown in Figure 5.26.

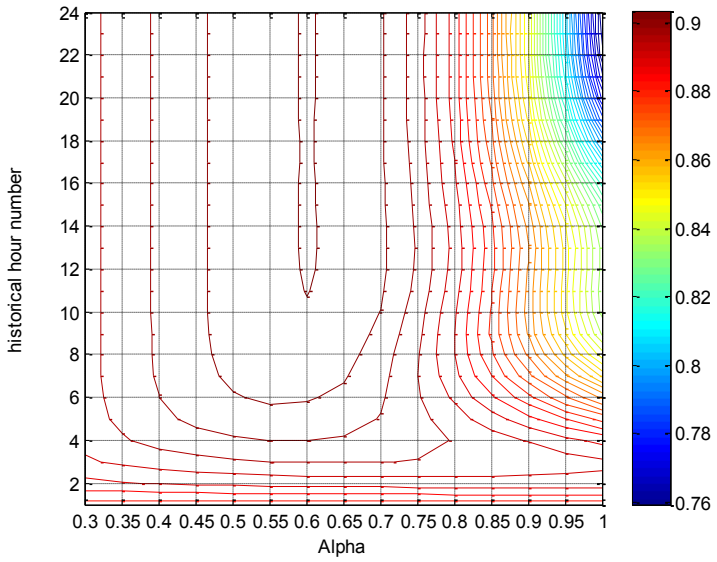

Figure 5.25 - Correlation between conductor temperature and accumulated load from different historical hour number and α

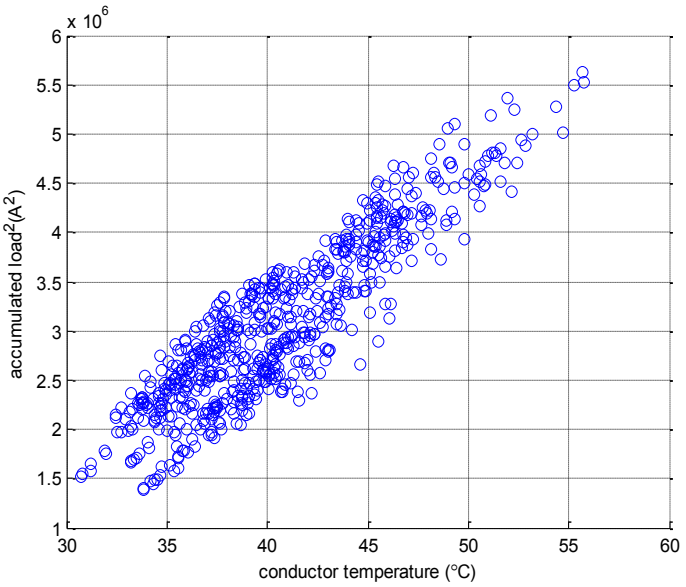

Figure 5.26 - Relation of accumulated load^2 vs. conductor temperature

5.5.4 Predicted rating error

In this section, the rating error is linked directly with the load error without using the dynamic thermal model for the cable system. The rating of the cable is mainly dependent on two factors: load and temperature. Section 5.5.2 to 5.5.3 show the methods of representing the conductor temperature prediction errors and real-time conductor temperature by only using the load prediction data and real-time load data. In addition, the data analysis show that the linear relations exist among load prediction errors and conductor temperature errors, hence it is believed that the predicted rating errors also have good correlation with the load prediction error and other load and temperature factors of the cable.

The Multiple Linear Regression method (MRL) [106] is one of the simplest, earliest and fastest regression techniques which have been used extensively in practical applications, such as capital asset pricing models, load prediction model and epidemiology models [107]. It is normally used to model the relationship between two or more features and a response variable by fitting a linear equation to observed data. In this section, MLR is chosen to model the relation between the load prediction, real-time load data and their corresponding predicted rating errors.

In order to test the different input features for the MLR model, the Mean Absolute Error (MAE) and maximum error of the 1hr, 4hr and 24hr ahead predicted 6hr emergency rating are used as criteria in the test.

As shown in Figure 5.22 and Table 5.5, the result from the EWMA equation for accumulated load^2 and accumulated load^2 error are used as input to the MLR model, as they represent the

initial cable temperature and the cable temperature prediction error of the initial condition when calculating the emergency rating respectively. In addition, the real load at the step before calculating the emergency rating is also used as an input since it is also a parameter that affects the initial condition of the rating calculation.

Table 5.5 – Input features for predicted rating error estimation

Model	accumulated load^2 error	real load	accumulated load^2
M1	√		
M2	√	√	
M3	√	√	√

Temperature error which is represented as accumulated load^2 error is used as the only input in Model M1 as it decides the difference of the initial condition when calculating the emergency rating. The mean absolute error of real predicted rating error and the error estimated by M1 are only around 3-5A in Table 5.6, showing that there is a strong relation between the rating errors and the initial temperature error. However, the maximum error may reach about 19A, as the difference of the initial condition is not the only factor that will influence the rating error.

In Model M2, the real load at the step before calculating the emergency rating, which is also a parameter that can affect the initial condition of rating calculation, is added as an input feature of the MLR model.

In Model M3, the initial temperature which is represented by the accumulated load^2 is added to the input of Model M2. This is because at the different level of initial temperature conditions, even the same temperature may result in different level of rating errors. High initial temperatures normally have smaller rating error than low initial temperatures when the temperature errors are the same.

The mean absolute error (MAE) and maximum error reduce from Model M1 to Model M3 (Table 5.6). As a result, Model M3 is finally chosen as the model to estimate the error of the predicted rating. With Model M3, we can estimate the predicted rating error within acceptable deviations by only using the real load and predicted load data. This rating error estimation procedure has been applied to one of the periods with the worst load prediction outcome. The results for different hour ahead prediction are shown in Figure 5.27 and Figure 5.28, which present the predicted rating error and its estimated value from the predicted error estimation system (Model M3) for 1hour and 24 hour ahead prediction respectively. These results show that the system for predicted rating error estimation can perform accurate predicted rating error

estimation by only using the real load and predicted load data. The accuracy of this system can be shown by displaying the CDF of the estimated deviation in Figure 5.29. The x-axis of Figure 5.29 presents the deviation of the predicted rating error estimation given by the estimated error minus the real error values. The y-axis shows the probability of the deviation being lower than the corresponding x-axis value. The probabilities of the deviation of estimated 1hour, 4 hour and 24 hour ahead predicted rating error being contained within ±4A are 98.95%, 99.25% and 86.00% respectively. The deviation of estimated 1-24hr ahead predicted rating error are all within the range from -12A to 6A.

Table 5.6 – Test results of predicted rating error estimation models

Model	**MAE (A)**			**Max Error (A) (predicted-real)**		
	1hr ahead	4hr ahead	24hr ahead	1hr ahead	4hr ahead	24hr ahead
M1	3.45	3.65	4.12	14.63	13.96	-15.34
M2	3.14	3.25	3.73	-12.47	-12.03	-15.68
M3	1.52	1.48	2.22	5.81	6.18	-10.25

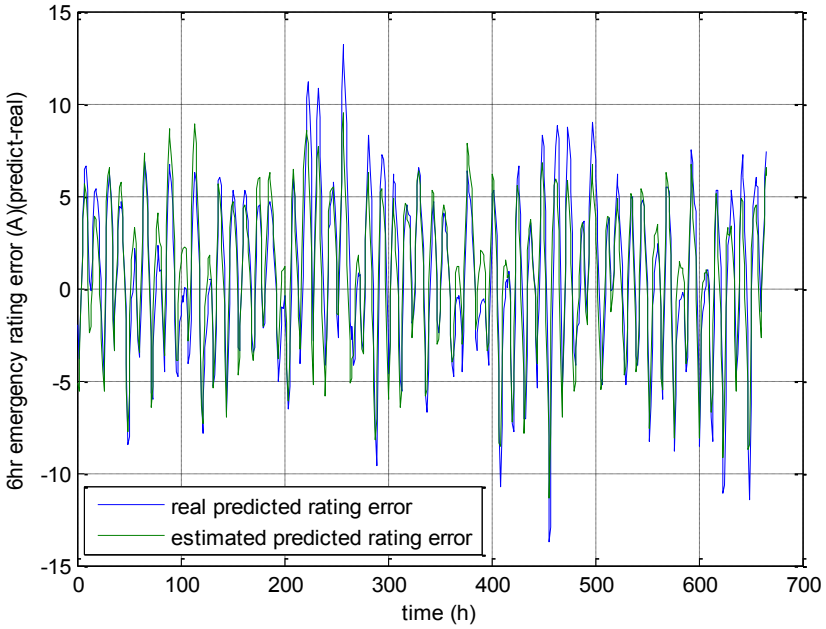

Figure 5.27 – 1hr ahead predicted rating error and its estimated values

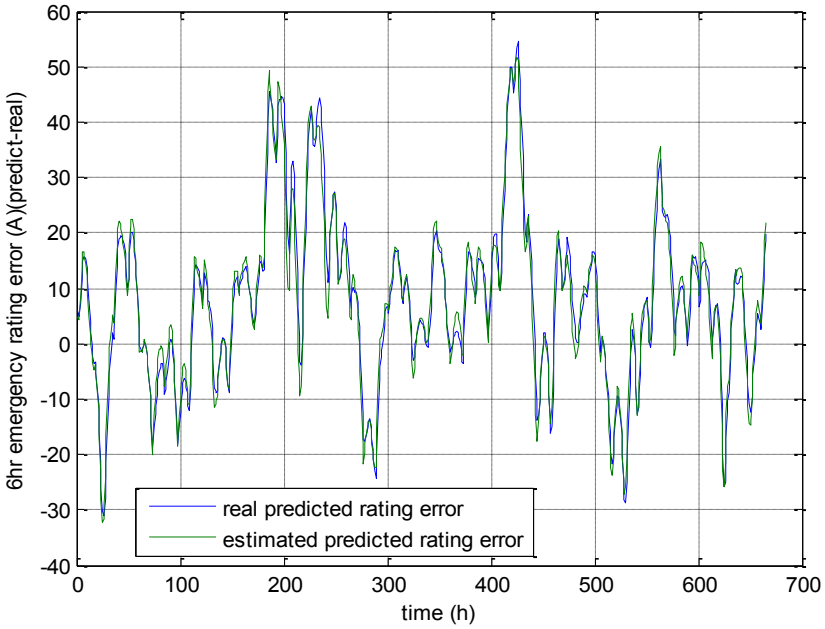

Figure 5.28 - 24hr ahead predicted rating error and its estimated values

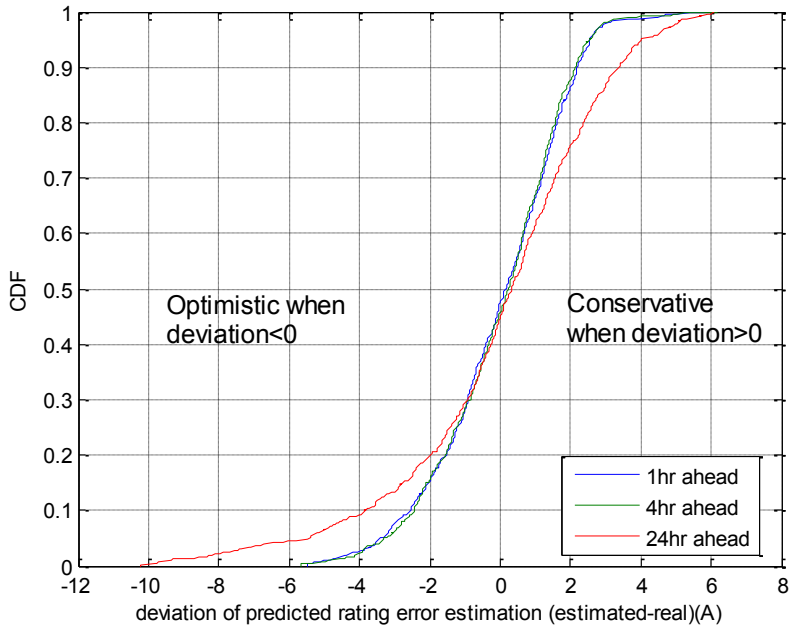

Figure 5.29 - Deviation of the predicted rating error estimation

It should be noted that, this system is able to estimate all the predicted rating errors for a transmission network with 200 tunnel cable circuits within 0.04 second. Compared against the 8 minutes by using the conventional dynamic thermal model, this system dramatically reduces the system response time when a dangerous rating error is detected.

5.6 Summary

In order to deliver valuable rating predictions to help with the day ahead planning for network operators, this Chapter has presented the tests results of Predicted Cable Ratings within the simulation scope. The Predicted Cable Rating system introduced in Chapter 3 was applied into three kinds of cable installations including buried cable, cable in free air and tunnel cables, with the load prediction results from Chapter 4. The predicted rating results, calculated from the load prediction results and dynamic thermal models, were compared with the real ratings (the direct solution from the dynamic thermal model using the actual load data). The predicted rating error is then defined as the difference between the predicted rating values and the real rating values.

After applying predicted rating systems to different cable installations, the test results show that accurate and reliable rating predictions can be obtained from 1hr ahead to 24hr ahead prediction horizons. Really positive results can be achieved when applying the predicted rating system on the test sample with different cable installations. For buried cables, all the 6hr emergency rating prediction errors are being contained within ±50A from 24hr ahead prediction, which is only about 1.8% of the average rating values. Furthermore, for 1hr ahead and 4hr ahead prediction, all the errors of the 6hr emergency rating prediction can be reduced to within ±5A and ±30A respectively. For the cable sample installed in free air, all the 3hr emergency rating prediction errors are contained within ±9A, ±15A and ±25A for 1hr ahead, 4hr ahead and 24hr ahead prediction respectively, which are all less than 1.6% of the average 3hr emergency rating values. For tunnel cables, the predicted rating errors of 6hr emergency rating are contained within ±14A, ±30A and ±55A for 1hr ahead, 4hr ahead and 24hr ahead prediction respectively.

In order to rapidly detect the predicted rating errors, an error estimation system for predicted rating is developed in this Chapter. It applies the exponentially weighted moving average equation to build up a linear relation between conductor temperature errors and accumulated load^2 errors. Then the Multiple Linear Regression technique was used to construct a regression model to estimate the predicted rating errors by using accumulated load^2 error, real-time load and accumulated load^2 directly without using the dynamic thermal model. This system is essential to the reliability of the predicted rating system, as it can estimate the predicted rating error quickly by only using the real-time and predicted load data, which dramatically reduces the processing time for a cable system when a dangerous rating error is detected.

Chapter 6: Experimental Validation of Models

In order to ensure that the Predicted Rating System is applicable to real operating cables, this Chapter details the progress made to demonstrate predictive rating applications through the use of a laboratory experiment. A heat cycle experiment for a cable in air is used with real-time current and ambient air temperature measured within a series of tests and used as inputs to the dynamic thermal model. The cable temperature results from the models are then compared with the measured temperatures from thermocouples to demonstrate the accuracy of the models.

6.1 Design of experimental setup

The cable sample used in this experiment is a 10m length of 33kV single phase XLPE cable with 630mm^2 copper conductor with the details of geometry and thermal property referring to Table 5.2. Two terminated ends of the conductor have been electrically connected to create a loop. Six cable rollers are used to support the cable 15cm above the ground surface. Single-point-bonding is used to prevent circulating current. The cable is installed indoors in the high voltage laboratory (Figure 6.1), without influence from wind and solar radiation, although ambient air temperature may fluctuate.

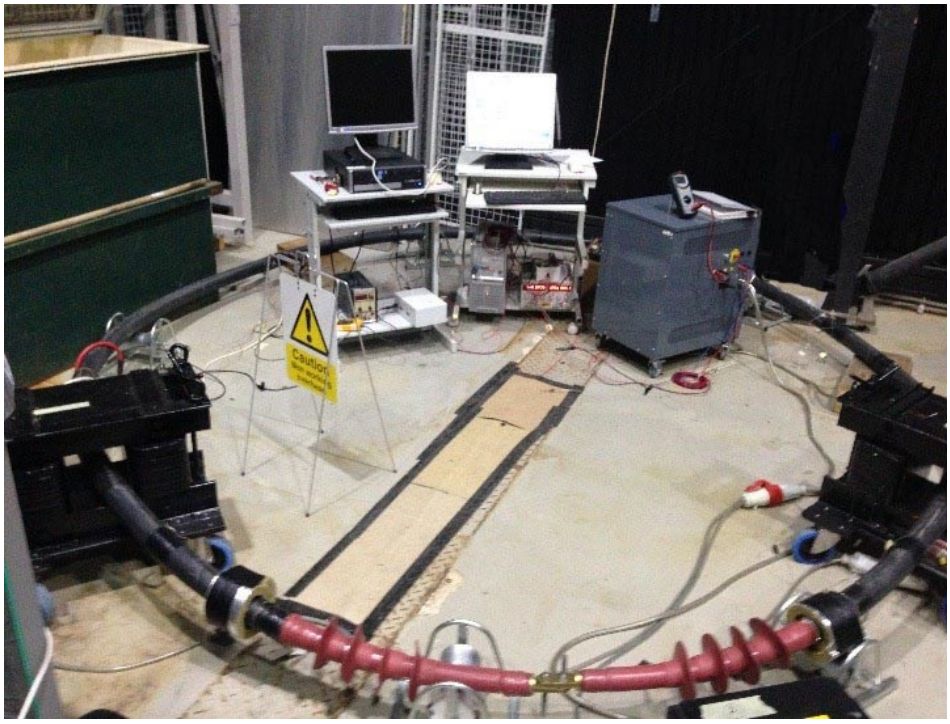

Figure 6.1 – Laboratory experiment

Figure 6.2 presents the details of this experimental setup, which includes the heating system (Variac and CTs), Current measurement system, thermal measurement system and data acquisition system.

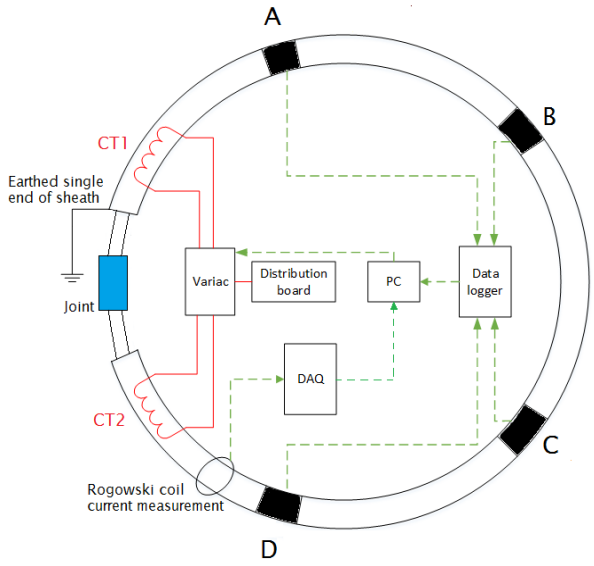

Figure 6.2 – Experimental setup

The heating system includes a motorized Variac transformer and two current transformers (CT). The motorized Variac is controlled by a computer to generate the input current to the primary windings of both CTs. The CTs then induce a much higher current in the secondary side which is formed by the single short circuit turn of the test cable. Each CT can generate up to 980A secondary current in this experiment. By including a system to control the motor in the Variac, the system can vary the input current to the CT according to a designed load profile. Thus, the desired daily load cycles can be generated in the cable loop. The current in the conductor is measured by a Rogowski coil and sent to the computer via a Data Acquisition system (DAQ). It is then recorded and used to adjust the current output from the Variac according to the target current value.

Thirty-three thermocouples are placed directly onto the conductor, armour and surface at four test sites of the cable (A-D in Figure 6.2) as well as the ambient air to measure the real-time temperature data. At each test site, the locations of thermocouples are shown in Figure 6.3. C1 is placed directly contact with conductor from the top of the cable; F1 – F4 are at cable surface; A1, A3 and A4 are placed directly contact with armour. The armour temperature measurements are able to show the temperature distribution from conductor to armour and from armour to cable surface. The measurements of multi test sites allow the influence from the conditions of cable installation and the cable end effects to be quantified. T type thermocouples were used in this experiment, with an associated precision of 0.4°C. In order to get an adequately high

resolution reading of the temperature data, all of the thermocouples are connected to a data acquisition system from Campbell Scientific which includes a CR1000 data logger and a 32 channel relay multiplexer. This system collects data from the thermocouples at one minute intervals and stores to a computer on five minutes intervals. The maximum, minimum and average temperature for conductor, armour and surface of the cable are calculated from all the measurement data for the following analysis.

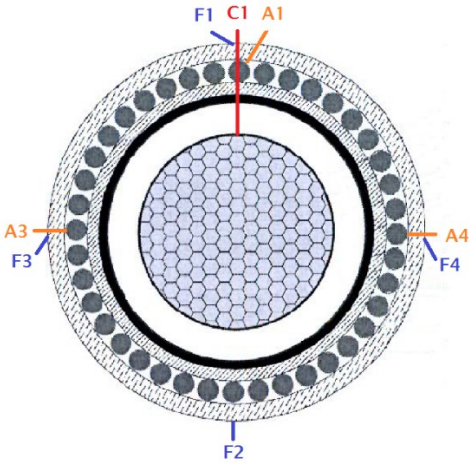

Figure 6.3 – Position of thermocouple locations at each test site

Details of the experimental control flowchart can be found in Appendix 2.

6.2 Demonstration of FDM dynamic thermal model

The FDM model for cable in air, which was introduced in Section 3.3, can be specified for the test cable as the thermoelectric circuit in

Figure 6.4. In this model, the number of layers in the cable insulation has been tested and the results suggest that 10 nodes of the insulation layer should be sufficient to obtain an accurate temperature result in transient studies. Except for the insulation, one node has been placed on each cable layer. Thus, twenty-four nodes have been placed from the conductor surface to the cable surface, with the locations defined in Table 6.1.

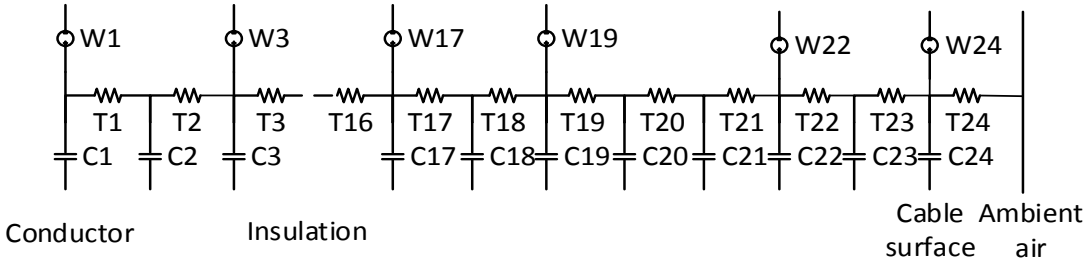

Figure 6.4 – Thermoelectric circuit for the test cable

Table 6.1 – Location of nodes in thermoelectric circuit

Node	Location	Node	Location
1	Conductor surface	20	Midway through PVC sheath
2	Conductor screen surface	21	Outer surface of fabric tap bedding
3-17	Insulation	22	Outer surface of wire armour
18	Insulation screen surface	23	Log mean radius of PVC outer sheath
19	Midway through copper tape screen	24	Cable surface

The heat sources in the cable are represented by W1 (conductor losses), W3-W17 (dielectric losses), W19 (sheath losses) and W22 (armour losses), which are calculated based on IEC 60287. It should be noted that no dielectric losses are present in this test as no voltage is applied to the cable. The conductor losses in this model are improved to be temperature dependant. As the cable is protected from the solar radiation in the lab, W24 which takes into account the heat from solar radiation is negligible. T1-T23 are used to simulate the thermal conduction between the nodes in the cable. T24 is the thermal resistance to represent convection and radiation from the cable surface to ambient free air. In this work, they are considered by natural convective heat transfer coefficient $h_{conv,n}$ from (3.16) and heat radiation coefficient h_{rad} from (3.12). C1-C24 are the thermal capacitances at each node. Initially, the cable model is built with the geometries and thermal parameters according to Table 5.2 which are given by the cable manufacturer and IEC 60853. This initial model is named FDM 1.0 model in the following part of this thesis.

6.2.1 Thermal response to step input (Test 1)

In order to characterize the steady-state behavior of the cable, the first test was designed to obtain the thermal response to a step current input in the cable. This test aims to have an 80-85°C conductor temperature at the steady-state so 1400A, calculated from the FDM 1.0 model, is used as the magnitude of the step current input. The thermal time constant for this cable sample with constant current and ambient air temperature of 1400A and 20°C is 2.98 hours according to the FDM model. This step current is applied for 2 days (48 hours) on this cable sample which is sufficient to make the cable conductor temperature reach and stay at the steady-state. Figure 6.5 presents the results of the comparison between FDM 1.0 model and experimental data in Test 1. It is apparent in Figure 6.5 that the FDM 1.0 model overestimates the conductor and armour temperatures by about 8°C and 4°C respectively in steady-state (compared to the average measurement data). However, the cable surface temperature from the model shows a good match to the average measured data.

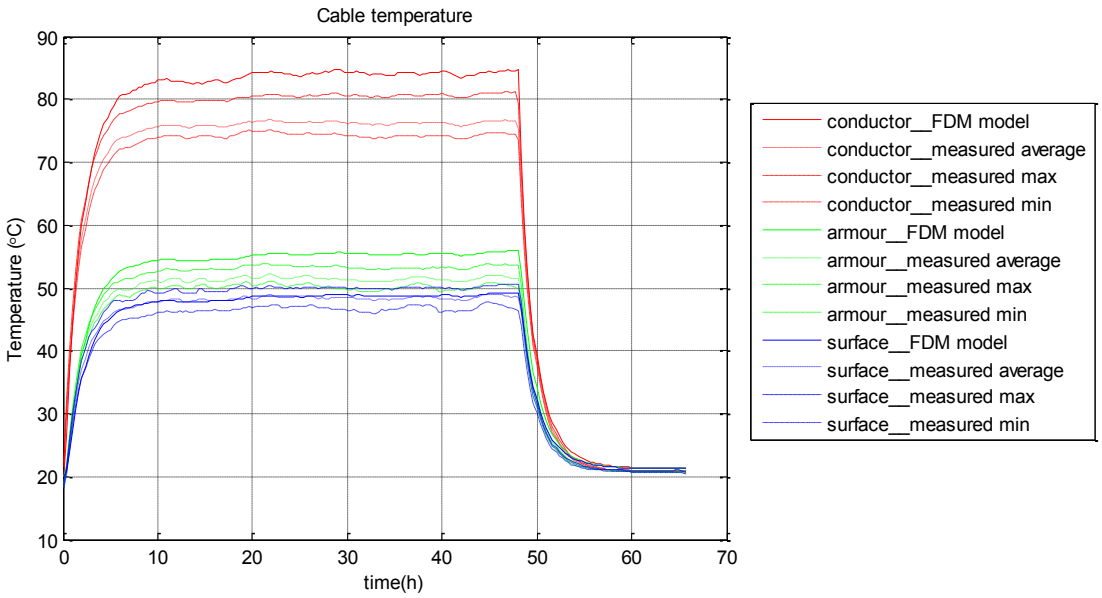

Figure 6.5 – Comparison of FDM 1.0 model and experimental data in Test 1

The temperature difference between the conductor and armour from the model is considerably higher than that measured, suggesting that the thermal resistance within this area has been overestimated and that the heat transfer is better in reality than the model. Two features within the model, geometries and thermal property, which might potentially cause the imprecise result were addressed here to improve the agreement between the FDM model and the lab experimental data.

6.2.1.1 Geometries of the cable

The most uncertain issue which might cause the disagreement between the model and the experiment is the geometry of the cable. The original table given by the manufacturer contains some approximate or minimum values. Thus, the geometries used in FDM 1.0 are the initial adjusted values within manufacturing tolerances. Previous analysis suggests that the thermal resistivity between the conductor and armour of the cable is overestimated in the FDM 1.0 model, which results in a higher conductor temperature in the simulation than in reality. This overestimation might come from overestimating the size of the low conductivity area in the model. Based on this conjecture, the cable has been cut to measure the geometry from the cross-sections at the end of all the experiments. The initial manufacturer data table and the measurement results of the cable geometry are presented in Table 6.2. Three cross-sections have been measured, and 4 measurements for the diameters of each cable layer have been recorded at each cross-section area. The geometry measurement results are taken by calculating the average values from these 12 groups of measurement data.

Table 6.2 – Cable geometry measurement

Component	Initial table		Measurement	
	Thickness (mm)	Outer Diameter (mm)	Thickness (mm)	Outer Diameter (mm)
Conductor		30.40		30.67
Conductor screen	0.60	31.60	1.00	32.67
Dielectric	10.34	52.27	8.50	49.67
Dielectric screen	0.60	53.47	1.04	51.75
Copper tape screen	0.08	53.62	0.17	52.09
Inner sheath	2.76	59.13	2.80	57.69
Fabric tap bedding	0.69	60.51	0.80	59.29
Armour	2.50	65.51	2.50	64.29
Outer Sheath	3.45	72.40	4.00	72.29

Table 6.2 shows that the conductor diameter (not the conductor area) is larger in reality than the value from the original table, while the diameter of the outer surface of the armour reduces from 65.51mm to 64.29mm. Thus, the total thickness between the conductor surface and armour surface is reduced. The thickness of the copper tape screen increases from 0.08mm from original table to 0.17mm from the measurement while the total thickness of the XLPE insulation reduces from 10.34mm to 8.5mm. Thus, the thickness of the layers with high thermal conductivity increase and the thickness of the layers with low thermal conductivity decrease, which result in a lower thermal resistivity between the conductor and the armour (The total thermal resistance between the conductor and the armour reduces from 0.4145 KmW^{-1} to 0.3989KmW^{-1}).

The FDM model after correcting of the cable geometry is named FDM 1.1. The simulation results from FDM 1.1 model are shown in Figure 6.6. Making this correction brings the conductor temperature result from the FDM model closer to the measured conductor from the experiment. The conductor temperature from the FDM 1.1 model is slightly higher (about 2°C) than the maximum measured conductor temperature. The cable armour and surface temperatures from the FDM 1.1 model also match well with the measured values.

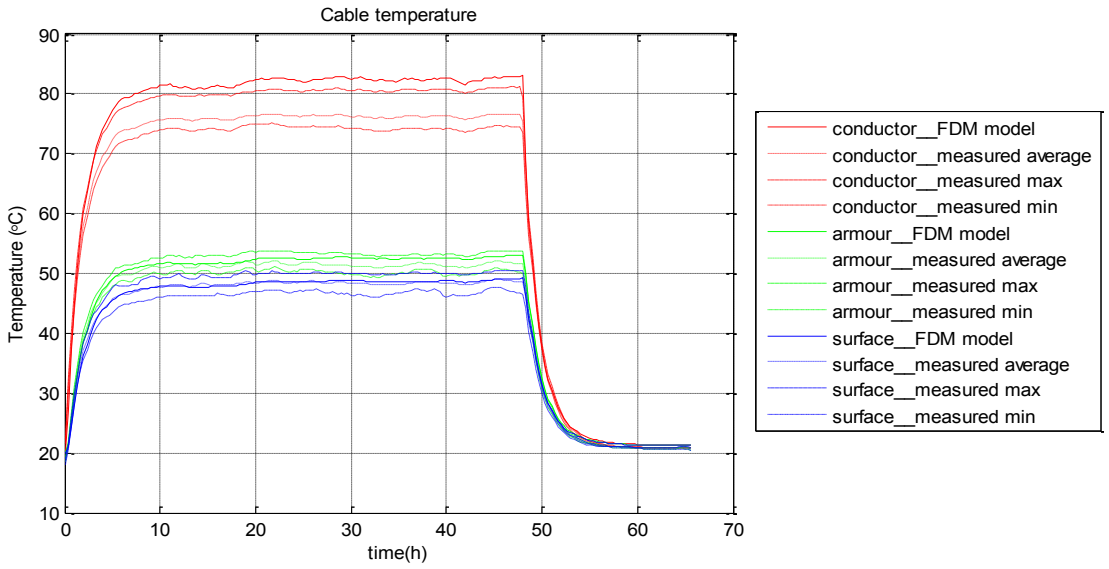

Figure 6.6 – Comparison of FDM 1.1 model and experimental data in Test 1

6.2.1.2 Thermal resistivity of semi conductive material

It should be noted that the conductor temperature from FDM 1.1 model is still higher than the maximum measured conductor temperature during 80°C steady-state. The other possible reason for overestimating the conductor temperature in FDM model is the thermal properties of the materials between conductor and armour. The thermal properties of Copper, XLPE and PVC have been well defined from the IEC 60287 standard. However the thermal properties of the semi-conductive material, which is used as the material of the conductor and dielectric screen, doesn't have standardised values. The common practical assumption (i.e. IEC standard) is to consider the semi-conductive screen as a part of the insulation, which has the same thermal properties as the insulation material (XLPE in this sample). However the two materials are different and the thermal properties might not be the same. Since the electrical conductivity of the semi-conductive material is much higher than the XLPE insulation material, it might be logical to assume a higher thermal conductivity for the semi-conductive material [108]. Particularly, the insulation material with 30% amount of carbon black will result in a 3-4 times higher thermal conductivity than the initial insulation material [109]. The thermal conductivity of typical samples of some elemental and binary compound semiconductors can even range from 1 to 200 $Wm^{-1}K^{-1}$, as shown in [108].

Based on the analysis of the experimental results, the thermal conductivity of the semi-conductive screens are increased from 0.286 $Wm^{-1}K^{-1}$ to 1 $Wm^{-1}K^{-1}$. This value of thermal conductive further reduces the thermal resistance between the conductor and the armour to 0.3574 KmW^{-1}, providing a better agreement between the FDM model and experimental data as

shown in Figure 6.7. The new FDM model with the thermal conductivity of the screen layers being modified is named FDM 1.2 model.

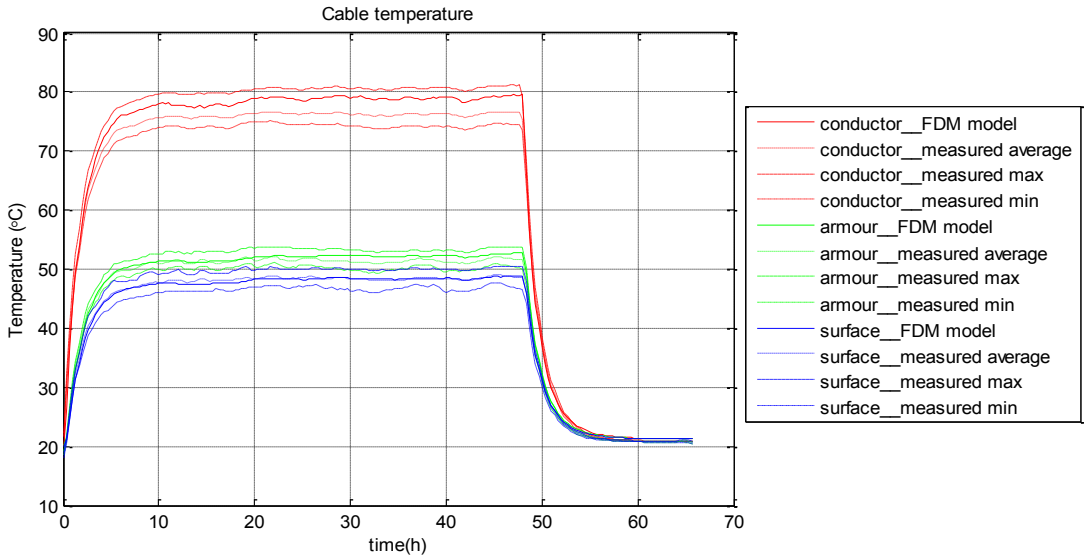

Figure 6.7 – Comparison of FDM 1.2 model and experimental data in Test 1

The conductor temperature from the FDM 1.2 model matches well with the measured value in Test 1, giving results inside the range of measured temperature and about 2.5°C higher than average value during the steady-state. Both the armour temperature and surface temperature results from the FDM 1.2 model have very good agreements with the experimental data, which are located inside the range of measured temperatures and close to the average values.

6.2.2 Thermal response to a given load profile (Test 2)

Since the FDM 1.2 model is able to give accurate temperature results under a step input current, it is used in the Test 2 which is designed to characterize the response of the cable sample to different daily cycles for a week (Figure 6.8).

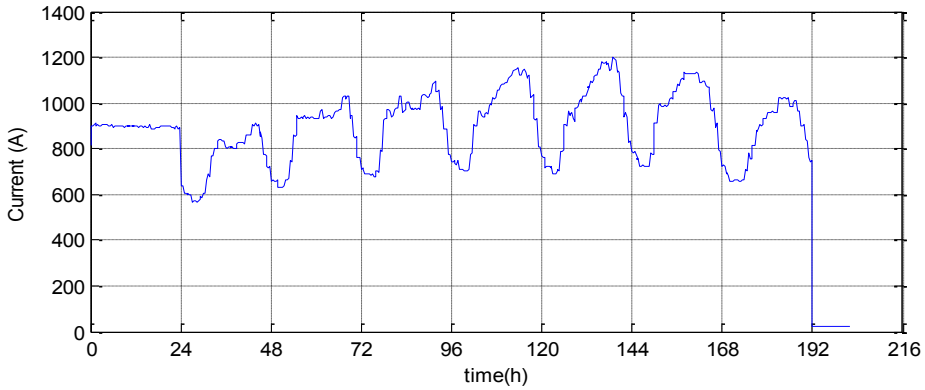

Figure 6.8 – Real-time current applied in Test 2

The load data is obtained from data used in the load prediction in Chapter 4. In order to set up an initial condition, a step current input of the average loading of this week (897A) was applied on the cable sample for 24 hours. This was followed by 7 daily cycles ranging from 572A to 1187A.

The DAQ used in the experiment is set to record the load data every 5 minutes which is the average load value within every 5 minutes. As a result, Figure 6.8 is plotted with the step interval of 5 minutes, which is able to represent the characteristic of the daily cycle sufficiently. Although the ambient air temperature was not absolutely constant throughout the test due to external influences, the variation has been recorded and taken into account in the FDM model.

Figure 6.9 shows the comparison of the temperature results from FDM 1.2 model and the measured temperature from thermocouples in Test 2.

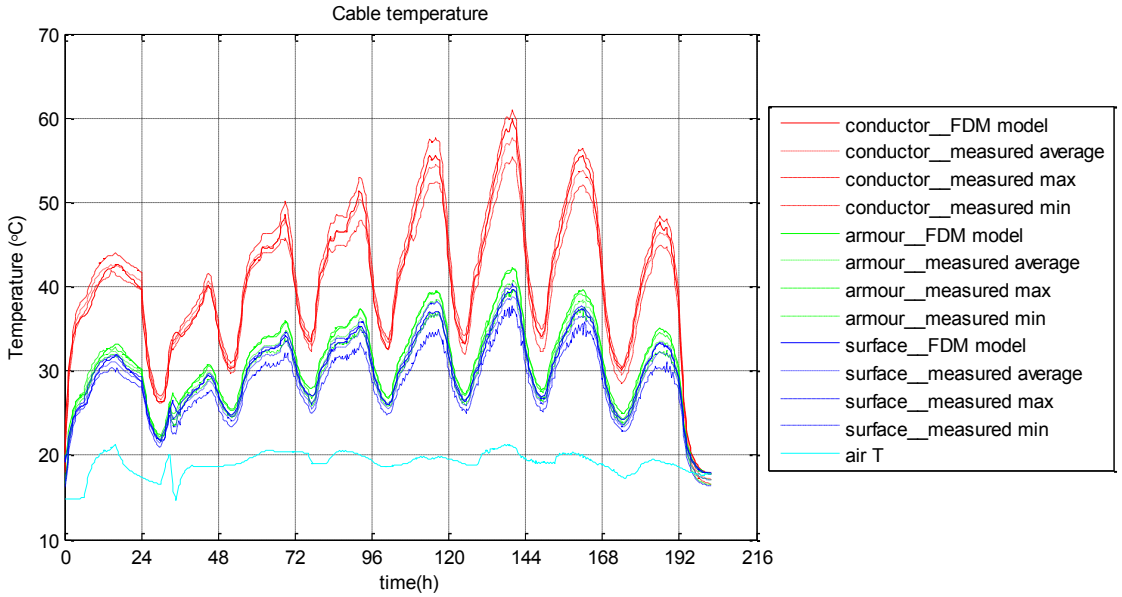

Figure 6.9 - Comparison of FDM 1.2 model and experimental data in Test 2

Good agreements can be observed from Figure 6.9, with all the conductor, armour and surface temperature from FDM 1.2 models following the average measurement data and falling within the boundary of maximum and minimum measured values. These results prove the accuracy of the FDM 1.2 model during the transients of a varying current and ambient temperature environment.

6.3 Demonstration of predicted ratings

In order to test the predicted rating algorithm, the seven days' load data of Test 2 are regarded as real load data. In Test 3, the same current profile in Figure 6.8 of Test 2 for the first six days

(plus one day of constant load of 897A at the beginning) is applied to the cable sample, but the load for the seventh day (168-192 hours in Figure 6.10) is different as it uses the load prediction result. The day-ahead load prediction data from 168 hours to 192 hours are obtained from the SVR load prediction system introduced in Section 4.3. The temperature results in Test 2 (Figure 6.9) will be used as a benchmark to demonstrate the results in Test 3 which applied the load prediction on test cable. Thus, one case of the predicted rating algorithm can be demonstrated.

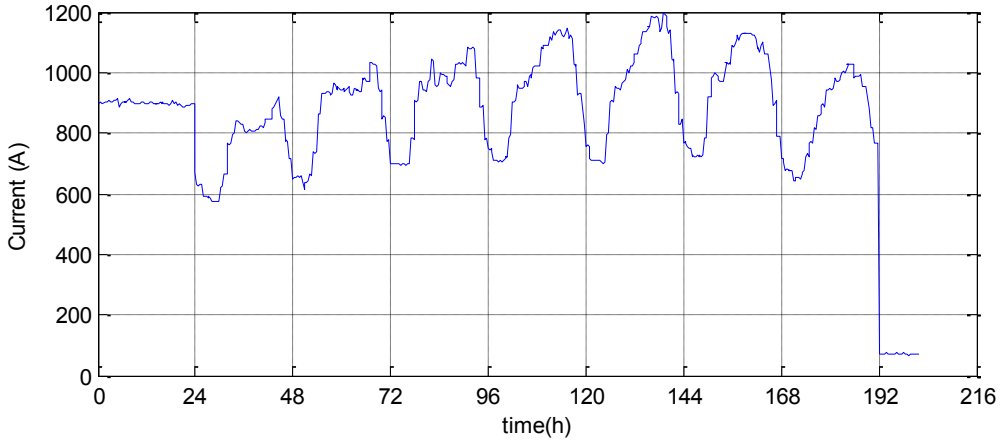

Figure 6.10 – Real-time current applied in Test 3 (with predicted load for 168-192 hours)

As cable ratings are not the values which can be directly measured, instead of testing the predicted rating directly, the following process was applied:

- Task 1, use the model to calculate the cable temperature from both real load data (Test 2) and predicted load data (Test 3).
- Task 2, demonstrate the accuracy of 3hr emergency rating calculations by FDM 1.2 model based on known initial conditions.
- Task 3, calculate and compare the 3hr emergency rating results at each hour within 168 hours to 192 hours for Test 2 and Test 3 to demonstrate the accuracy of predicted rating algorithm.

If the day-ahead predicted cable temperature and the 3hr emergency ratings based on given initial cable temperatures can be calculated precisely by the FDM model, the accuracy of the predicted rating calculations can be guaranteed.

It should be noted that there are two limiting factors in this experiment:

- The experimental setup allows a deviation (±30A) between the actual current on the cable and expected current from the load profile. Thus, the actual current applied on the cable sample in Test 3 (Figure 6.10) is not exactly equal to the current applied in Test 2 (Figure

6.8) from 0-168 hours. However, the deviations are relatively small compared to the applied currents (less than 2%).

- The ambient air temperatures in Test 2 and Test 3 are also not exactly the same as the ambient conditions in the lab fluctuated slightly with time. Figure 6.11 shows that the ambient air temperature during Test 2 and Test 3 have different patterns, but most of the variations are within the range from 16°C to 22°C. The ambient air temperature in Test 2 is assumed to be the actual temperature, and the ambient air temperature in Test 3 is regarded as the day-ahead predicted temperature. Thus, the temperature prediction errors will be taken into account in this predicted rating test.

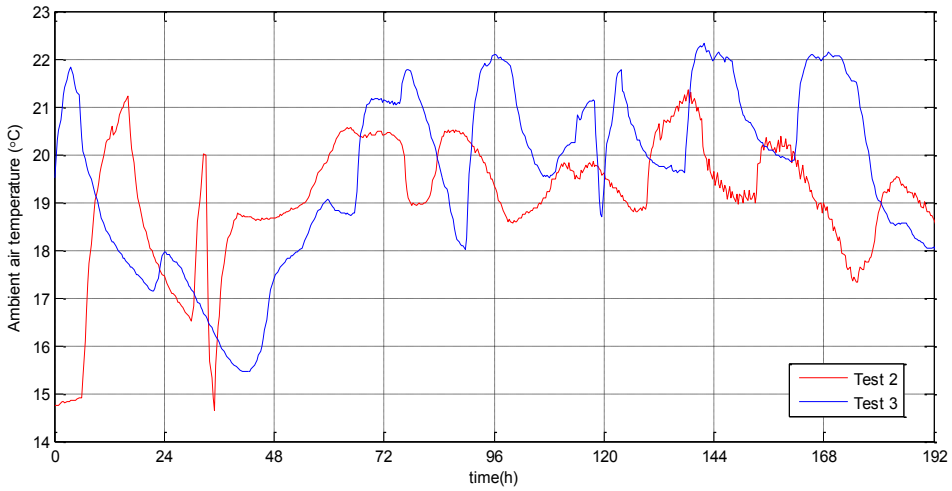

Figure 6.11 – Ambient air temperature in Test 2 and Test 3

6.3.1 Task 1: Predicted cable temperature (Test 3)

Figure 6.12 shows the comparison of the temperature results from FDM 1.2 model and the measured temperature from thermocouples in Test 3. Similar with Test 2, good agreements can be observed for all the conductor, armour and surface temperature between the FDM 1.2 models and measurement data.

As mentioned before, the load applied to the cable sample from 168 hours to 192 hours in Test 3 is the day-ahead load prediction from SVR model. Comparing the cable temperature results from 168 hours to 192 hours between Test 2 (using real load) and Test 3 (using predicted load), the day-ahead temperature prediction errors can be obtained. Figure 6.13 presents the conductor temperature from measured data and the FDM 1.2 model results from 168 hours to 192 hours in Test 2 and Test 3. Although the influences from the Variac and ambient air temperature existed in Test 2 and Test 3, the initial conditions at 168 hours from Test 2 and Test 3 are very close. Only 1.2°C conductor temperature difference is found from the average measured data, which

gives an ideal initial condition for the comparison between Test 2 and Test 3 from 168 hours to 192 hours.

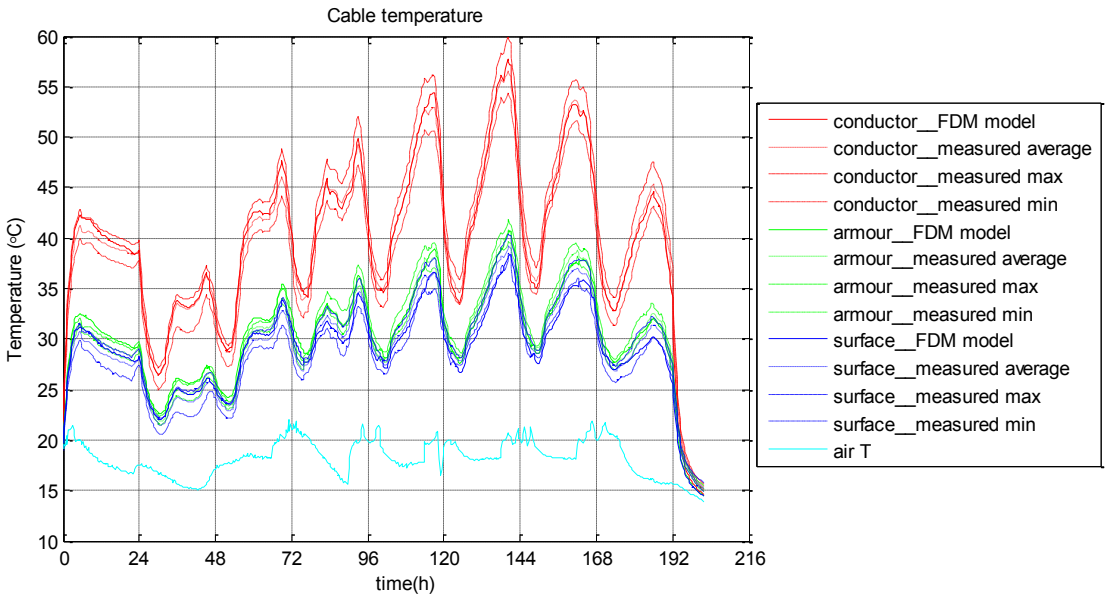

Figure 6.12 – Comparison of FDM 1.2 model and experimental data in Test 3

It should be noted that the load prediction error is not the only factor that influences the accuracy of predicted temperature in this test, the ambient air temperatures during 168 hours to 192 hours are different in Test 2 and Test 3, as shown in Figure 6.13. If we assume the ambient air temperature in Test 2 is the actual temperature, and the ambient air temperature in Test 3 is the day-ahead predicted temperature, large air temperature prediction errors can be found in the first 8 hours (from 168 hours to 176 hours), which mean that the prediction results overestimate the air temperature by 4°C to 5°C. Thus, an overestimation of the conductor temperature prediction (Test 3) can be observed, compared with the real conductor temperature (Test 2) in the first 8 hours.

It is vital for the predicted rating system that a dynamic thermal model can be applied to obtain accurate cable temperature based on real-time data before the emergency ratings being calculated. Figure 6.13 shows that the conductor temperature results from the FDM model follow the average measured result precisely. Although some deviations might exist but all are contained within the ranges between maximum and minimum measured results. Thus, the ability of this FDM model to calculate cable temperature has been demonstrated. Based on the cable temperature calculated by this FDM model and the historical load data, emergency ratings can be obtained.

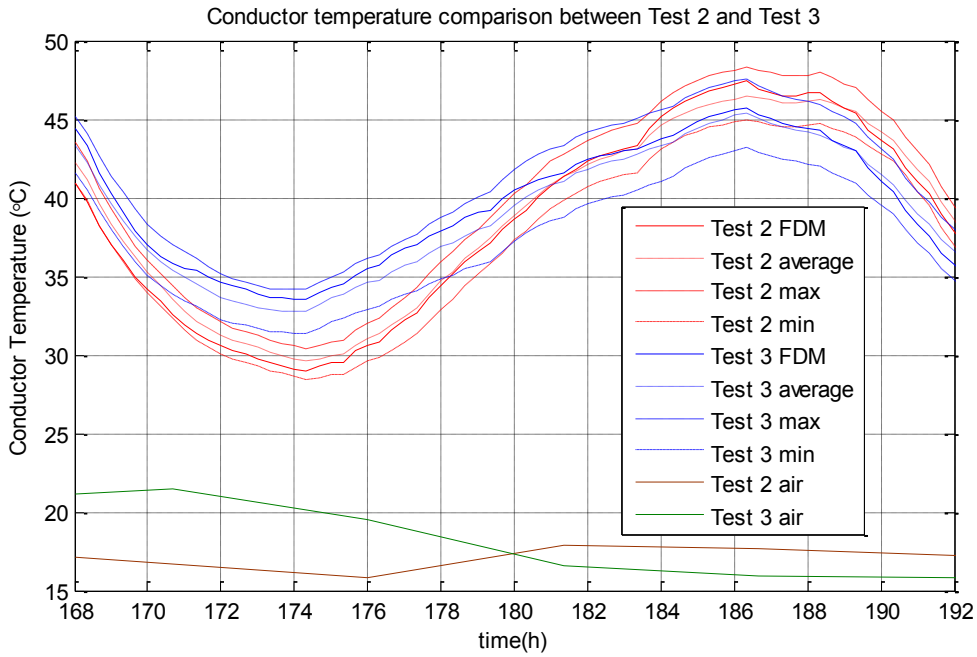

Figure 6.13 – Conductor temperature comparison between Test 2 and Test 3 from measurement and simulation results (from 168 to 192 hours)

6.3.2 Task 2: 3hr emergency rating test (Test 4)

After the initial cable temperature before applying the emergency rating has been obtained, the magnitude of the emergency rating needs to be calculated. In order to test the accuracy of the emergency rating calculation based on a known initial condition, Test 4 is designed to characterize the response of the cable sample during 3hr emergency ratings in the experiment. Twelve 3hr emergency ratings have been applied on the cable sample during the 8 days in Figure 6.14. A constant step current was applied on the cable for the first 24 hours to build up an initial condition and the daily cycles were applied on the cable for the following days. The 3hr emergency ratings were applied during the hours 12-14 and hours 0-2 of every day. These 3hr emergency ratings were calculated by the FDM model in advance under the assumption that the real current applied on the cable matches the expected current profile and the ambient air temperature is constant at 20°C.

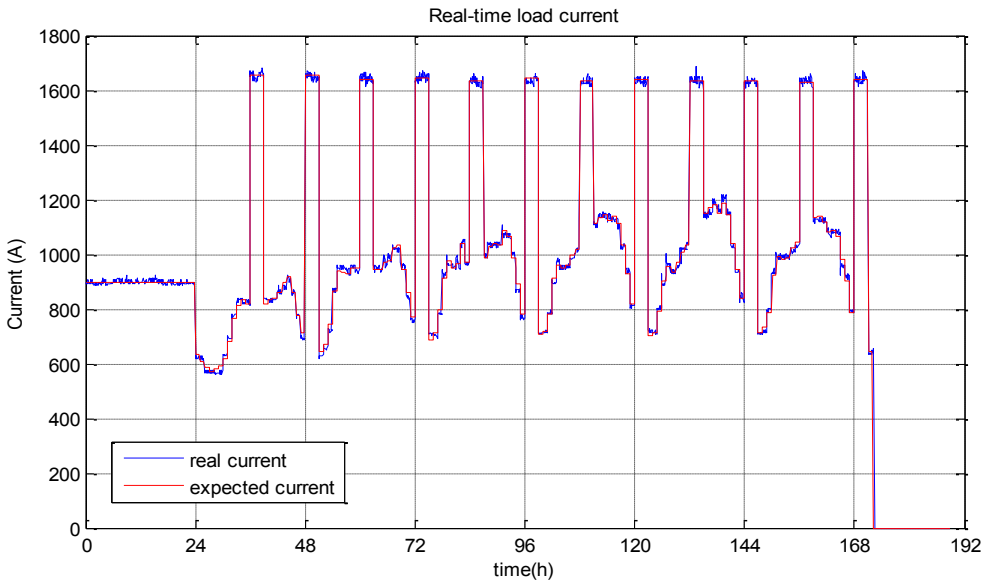

Figure 6.14 – Real-time current in 3hr emergency rating test (Test 4)

Figure 6.15 illustrates the comparison results between the FDM 1.2 model and the experiment in 3hr emergency rating test (Test 4). The conductor temperatures from the FDM 1.2 model follows the track of the maximum measured conductor temperature very well. The cable armour and cable surface temperatures from the FDM 1.2 model are both located in the middle of the measured temperature range. As a result, FDM 1.2 model is able to provide accurate 3hr emergency ratings.

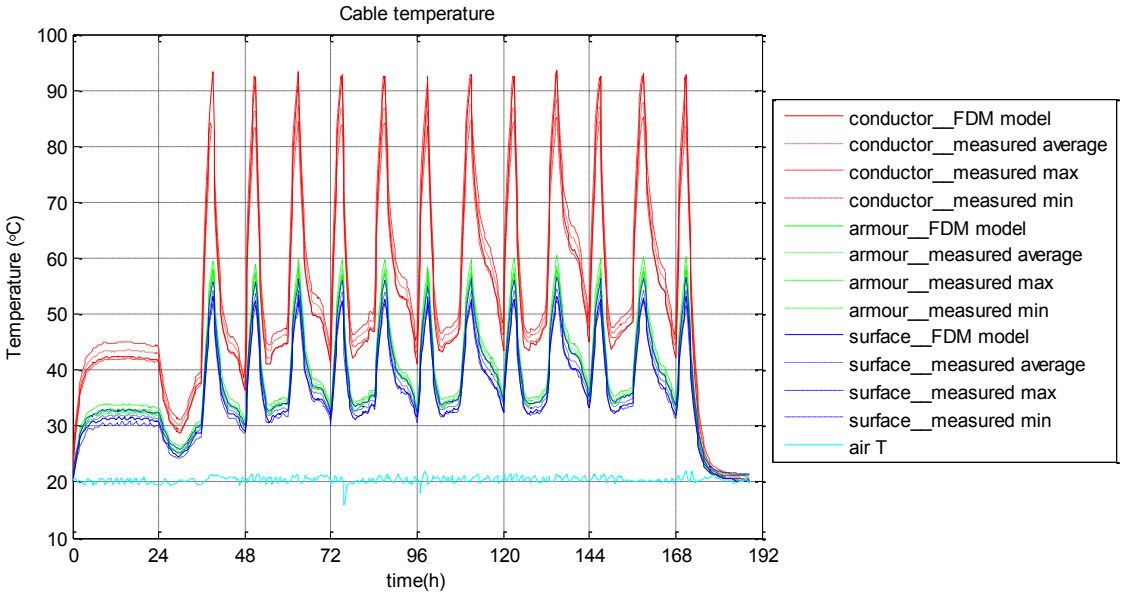

Figure 6.15 – Comparison of FDM 1.2 model and experimental data in Test 4

The ambient air temperature shows that the ambient condition is relatively stable within the range of 19.5°C to 21.5°C, except for a big drop from 20°C to 16°C at 76 hours. As the initial

3hr emergency rating calculations haven't considered the temperature changes and the actual applied currents might have small deviations (less than 30A) from the target values, the conductor temperatures at the end of 3hr emergency ratings are not exactly 90°C. In order to test the accuracy of emergency rating calculated from FDM model, the actual measured maximum conductor temperatures are used as constraint temperatures for 3hr emergency rating (the temperature at the end of 3hr emergency ratings) in FDM model. The 3hr emergency rating currents (for the target temperatures) calculated from the FDM model are then used to compare with the average measured currents during 3hr emergency ratings in the experiment. It should be noted that the FDM model assumes the constant 20°C air temperature during the 3 hours of the emergency rating period.

Table 6.3 shows the comparison results between the average measured current during each 3hr emergency rating in the experiment and the 3hr emergency ratings calculated by FDM model according to the constraint temperature from measurement. The error at the last column is calculated as (Measured avg. current – FDM rating), thus, the positive errors represent the underestimate of emergency rating from the FDM model, and vice versa. It shows that the errors of the 3hr emergency rating from FDM model are all contained within 9A, which is less than 0.5% of the rating values. It proves that the FDM model is able to calculate 3hr emergency ratings accurately. In addition, all of the errors are positive values, showing that the FDM model is still slightly conservative to prevent risk of thermal exceedance.

Table 6.3 – Comparison results of 3hr emergency rating test

No. of 3hr emergency rating	Constraint T in FDM model (°C)	Measured avg. current (A)	FDM rating (A)	Error (A)
1	92.5	1612	1609	3
2	92.6	1604	1604	0
3	92.9	1604	1598	6
4	92.4	1602	1596	6
5	92.6	1594	1592	2
6	91.8	1593	1588	5
7	92.7	1596	1592	4
8	92.4	1594	1593	1
9	93.4	1605	1600	5
10	92.2	1591	1588	3
11	92.6	1598	1589	9
12	92.2	1595	1592	3

6.3.3 Task 3: Predicted rating results

Having demonstrated the accuracy of the FDM model in both the cable temperature and emergency rating calculations, the 3hr emergency ratings for 168 hours to 192 hours in Test 2

and Test 3 can be calculated from this model. The rating results in Test 2 are used to represent the real rating values, and the rating results in Test 3 are used to represent the predicted rating values as they are calculated based on the predicted load and ambient air temperature. The rating results are shown in Table 6.4. As the predicted data resulted in an overestimate of the conductor temperatures in the first ten hours (from 169 hours to 179 hours in Figure 6.13), the 3hr emergency ratings are underestimated by 4A-7A in the first ten hours. After 179 hours, the errors of predicted ratings are all contained within 4A.

The conductor temperature prediction errors in Figure 6.13 show a clear relationship with the ambient air temperature prediction errors. Assuming the ambient temperature predictions are accurate, the predicted rating errors could be reduced. In order to prove this, the ambient temperature prediction from 168 hours to 192 hours is assumed to be accurate by applying the air temperatures in Test 2 within this period to the same period in Test 3. The FDM model is used to calculate the conductor temperature and 3hr emergency rating from 169 hours to 192 hours by using the predicted load and real air temperature data. Thus, the only factor that influences the predicted rating errors is the load prediction error and any inherent error in the thermal model. The results from the FDM model are shown in Figure 6.16 and Table 6.5. It can be seen that the conductor temperature prediction in Test 3, which uses the predicted load and real air temperature, shows much better agreement with Test 2 than that in Figure 6.13. All the conductor temperature prediction errors from 168 hours to 192 hours are contained within 0.8°C in Figure 6.16. Table 6.5 shows good 3hr emergency rating prediction results with all the errors are contained within 1A.

Table 6.4 – Real rating and predicted rating results from Test 2 and Test 3

Number of ahead hour	Hour in Figure 6.13	Real rating (A)	Predicted rating (A)	Number of ahead hour	Hour in Figure 6.13	Real rating (A)	Predicted rating (A)
1	169	1573	1569	13	181	1567	1567
2	170	1577	1572	14	182	1566	1566
3	171	1580	1573	15	183	1565	1565
4	172	1581	1575	16	184	1562	1564
5	173	1582	1576	17	185	1561	1563
6	174	1583	1576	18	186	1560	1562
7	175	1582	1575	19	187	1561	1563
8	176	1581	1574	20	188	1561	1564
9	177	1579	1572	21	189	1562	1566
10	178	1576	1571	22	190	1565	1569
11	179	1573	1570	23	191	1568	1572
12	180	1570	1568	24	192	1572	1575

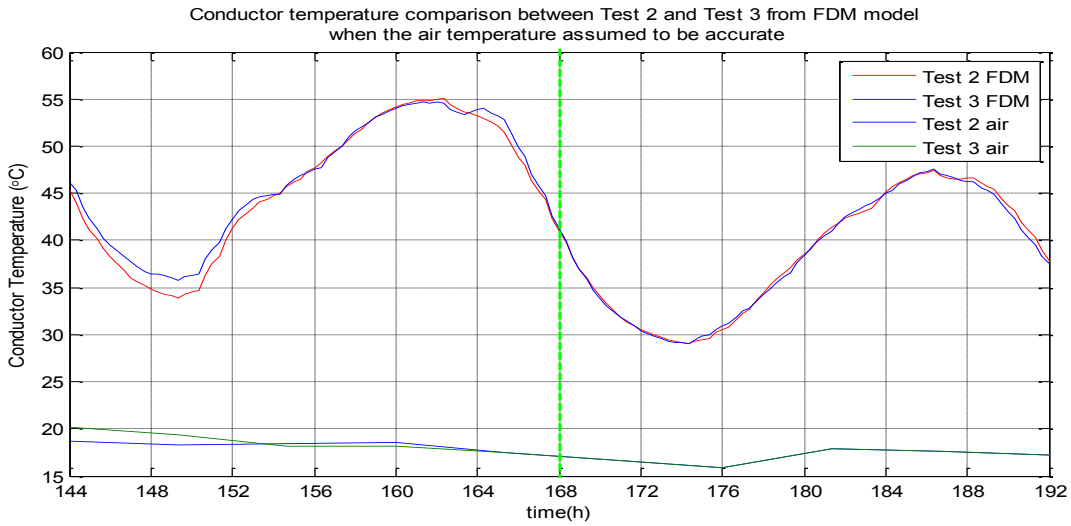

Figure 6.16 – Conductor temperature comparison between Test 2 and Test 3 from FDM 1.2 model (predicted load and real air temperature in Test 3)

Table 6.5 – Real rating and predicted rating results from Test 2 and Test 3 (predicted load and real air temperature in Test 3)

Number of ahead hour	Hour in Figure 6.16	Real rating (A)	Predicted rating (A)	Number of ahead hour	Hour in Figure 6.16	Real rating (A)	Predicted rating (A)
1	169	1573	1574	13	181	1567	1568
2	170	1577	1577	14	182	1566	1565
3	171	1580	1579	15	183	1565	1564
4	172	1581	1581	16	184	1562	1562
5	173	1582	1582	17	185	1561	1561
6	174	1583	1583	18	186	1560	1560
7	175	1582	1582	19	187	1561	1561
8	176	1581	1581	20	188	1561	1561
9	177	1579	1578	21	189	1562	1563
10	178	1576	1576	22	190	1565	1566
11	179	1573	1574	23	191	1568	1569
12	180	1570	1570	24	192	1572	1572

6.4 Summary

The Predicted Rating algorithm was demonstrated in this Chapter by applying it to data from a laboratory experiment. The setup for a thermal test of a cable in air has been introduced, including the heating, thermal measurement, electrical measurement and data acquisition systems. This system is able to control the conductor current according to an expected load profile and measure the temperature response at the conductor, armour and surface of the cable.

The FDM model for the cable in air was built for this test cable and validated by the experimental data. The initial demonstration results show that the FDM 1.0 model overestimates the conductor and armour temperature compared to the experimental data. Two corrections have been made to ensure the model matches better with the experimental data. One is to use the actual measured cable geometry instead of the given table from manufacturer, the other is to increase the thermal conductivity of the semi-conductive screen layers from $0.286 Wm^{-1}K^{-1}$ to 1 $Wm^{-1}K^{-1}$. After these two modifications, the temperature results from the FDM model are all located within the range of measured experimental data. Such experimental experience shows the importance of accurately measuring and surveying the properties of entire cable before applying the algorithm to a real circuit.

The accuracy of the 3hr emergency rating calculation from FDM model have been proved by comparing the temperature results from measurement and FDM model. It shows that the errors of the 3hr emergency rating from FDM model are all contained within 9A, which are less than 0.5% of the rating values. In addition, the results show that the FDM model is conservative to prevent overheating dangers.

One case of day-ahead predicted rating was demonstrated in the experiment and the results of conductor temperature prediction and 3hr emergency rating prediction were presented, showing good prediction accuracy. In this test, the 3hr emergency rating prediction errors can be up to 7A when the air temperature prediction is not ideal, while the predicted rating errors are all contained within 1A when the air temperature prediction is accurate.

Chapter 7: Thermal Status Estimation by Using SVR

Compared with the FEM models, the FDM dynamic thermal models presented in Chapter 3 have shown their ability to deliver accurate real-time cable temperature and rating calculations. Although the solution speed of the FDM models is much faster than the FEM models, it still requires a lot of time when large amount of cable circuits need to be calculated in the whole power transmission system. The most complicated dynamic thermal model in this thesis (the model for tunnel cables) requires about 2.5 seconds to calculate 6hr emergency rating at each step by a PC of 3.40GHz i7 CPU and 16GB RAM and it occupies about 15% of the CPU usage during the calculation. Imagining a transmission system with 200 cable circuits, the rating calculation at each step will require either more than 8 minutes when all the calculations are done sequentially on 1 PC or about 17.5 seconds with the calculations are done concurrently by 29 PCs, which may be too long and unpractical for system operators.

In addition, if the predicted rating algorithm is applied to the system, more ratings need to be calculated at each step, including the real-time dynamic rating and 24 rating predictions for each hour in next 24 hours (the rating calculation number might increase when different time-limited emergency ratings are required). It might require more time or more PCs to calculate all these ratings at each step.

In order to solve this problem, the Support Vector Regression (SVR) technique is applied in this Chapter. The fast solution speed of the SVR models makes them capable to calculate large amount of ratings at the same time. SVR models have been tested for three different kinds of cable installations (buried cable, cable in air and tunnel cables) to calculate the emergency ratings. In addition, instead of using SVR to obtain the load prediction result and then calculating the cable temperature and rating with the load prediction, SVR models are applied to predict the day-ahead cable ratings directly. This idea has been tested for the cable in air installation with the results presented in this Chapter.

The load and ambient temperature data used in this work is from the Global Energy Forecasting Competition 2012 [99]. The cable temperature and rating data used to train the SVR models are from the direct solution of the FDM models. The flow charts in Figure 7.1 and Figure 7.2 display the procedures of the test on SVR models for real-time rating calculation and prediction rating calculation respectively. Real-time load and forecasting load data are input to the dynamic thermal models to obtain the real-time cable ratings and predicted cable ratings from 2004 to 2007 (Figure 7.1(a) and Figure 7.2(a)). The results from 2004 to 2006 are then used as

training data to build the SVR models in Figure 7.1(b) and Figure 7.2(b). The data in 2007 are used to test the SVR models.

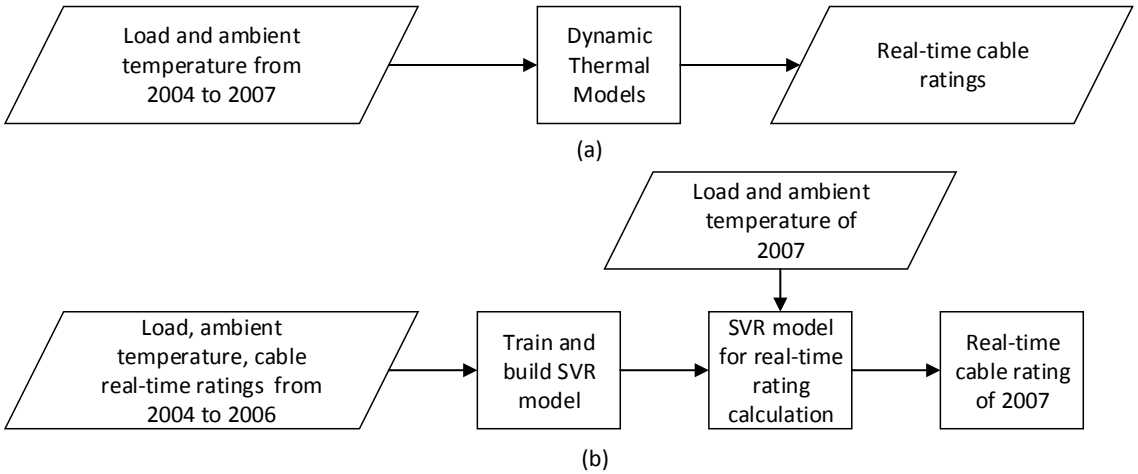

Figure 7.1 – Construction and test procedures of SVR model for real-time rating calculation. (a) Gather data from dynamic thermal model. (b) Build and test SVR model

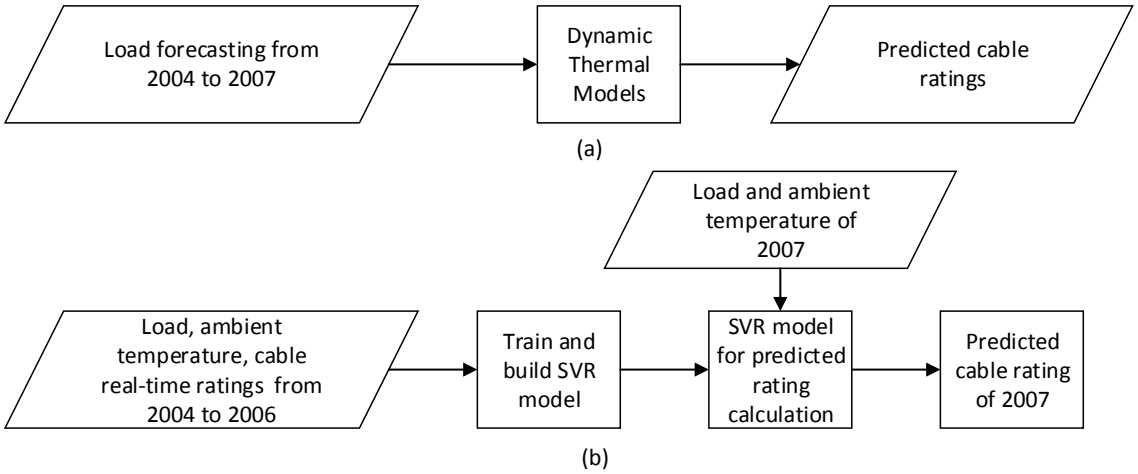

Figure 7.2 – Construction and test procedures of SVR model for predicted rating calculation. (a) Gather data from dynamic thermal model. (b) Build and test SVR model

7.1 General testing processes

To measure the accuracy of 6hr emergency rating calculation and prediction from SVR models, the criteria of mean absolute percentage error (MAPE) have been used in this test as MAPE has been widely used to judge the performance of prediction models [71], [99]. The results of the SVR model are compared with the direct solution from the FDM dynamic thermal model with the input of real load and environmental data. LIBSVM [97] is used to train and predict the 6hr emergency ratings in this Chapter. Two parameters, the cost of error C and the γ in the RBF kernel for each model are allocated during the SVR training.

The procedure known as cross-validation is used in this test. The first 3 years data are used as training data. This data set is firstly split into 3 segments by different year with equal size, and then each year segment is tested by the SVR which was previously trained by the other 2 years' segment sequentially. Using this method, each year subset of the whole data set is predicted once by the SVR trained by other two year subsets which avoids the over-fitting problem and makes the SVR prediction more reliable.

To find the group of C and γ with minimum total error, a 'grid-search' method for C and γ is used in the cross-validation. Various groups of C and γ are tried and the one with minimum error is picked. The author of LIBSVM [97] suggests that trying exponentially growing sequences of C and γ is a practical way to find suitable values. With the best C and γ, the SVR model is trained by the whole dataset including the first three years data and tested by the fourth year data to get a final MAPE.

7.2 Emergency rating calculated by SVR for buried cable

The aim of this section is to build a SVR model to calculate the real-time 6hr emergency rating of the buried cable. The geometry of the buried cable can be referred to Table 7.1. Three single phase 132kV XLPE cables are buried at different depths (0.5m, 1m, 3m, 5m and 8m) with a core-core spacing of 0.4m. The conductor cross-section area is 630mm^2. All the soil around the cables is assumed to have the same thermal parameters and is treated as a uniform medium with thermal resistivity of 1.5KmW^{-1} and volumetric heat capacity of 1MJm^{-3}K^{-1}. The ground surface is assumed to be isothermal.

Table 7.1 – Geometries and properties for 132kV buried cable

Component	Outer Diameter (mm)	Material	Thermal Conductivity (W/mK)	Volumetric Heat Capacity (MJ/m^{3}K)
Conductor	30.5	Copper	400	3.45
Conductor Screen	33.5	XLPE	0.286	2.4
Insulation	67.5	XLPE	0.286	2.4
Insulation Screen	70.5	XLPE	0.286	2.4
Sheath	78.1	Lead	35.3	1.45
Outer Sheath	82.5	Semicon	0.286	2.4

In order to fit the available load data into this buried cable system, all the load data are linearly scaled into the range from 0 to 800A, with an average value of 433A (Figure 7.3). Such load

levels will result in cable temperatures in this buried cable system as observed in practice. The initial condition of the test is the steady state temperature of the average load (433A).

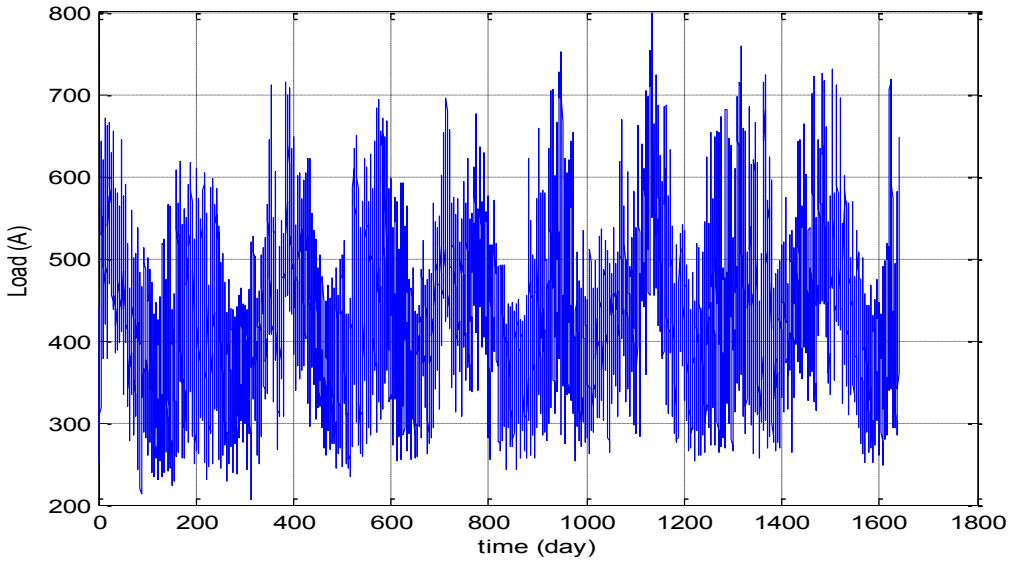

Figure 7.3 - Input load profile for buried cable

7.2.1 Input feature Test 1: historical load

Due to the slow heat dissipation via conduction in the soil, buried cables normally have long thermal time constants. As a result, the historical load has a greater influence on the conductor temperature and cable emergency rating. The thermal time constants for cables with different buried depths are shown in Table 7.2. They are calculated under the condition of 433A constant current (the average current of the real-time input data) and 20°C ambient temperature. The thermal time constants increase dramatically with the deeper installation as the thermal capacity of the ambient environment increases with the buried depth.

Table 7.2 – Thermal time constant for the cable with different buried depths

Buried depth (m)	Steady-state conductor T (°C)	Conductor T at thermal time constant (°C)	Thermal time constant (hour)
0.5	35.75	29.92	102.44
1	40.15	32.69	267.32
3	47.43	37.28	1231.50
5	50.85	39.44	2486.61
8	54.00	41.42	4705.91

In the first SVR model test (Test 1), the category of input features is the historical load data. The length of look back time of the historical load data is gradually increased in the SVR model to test the accuracy of the 6hr emergency rating results for different burial depths of the cable. The MAPE of 6hr emergency ratings calculated by SVR models with different look back time of the historical load and different cable buried depth are shown in Figure 7.4.

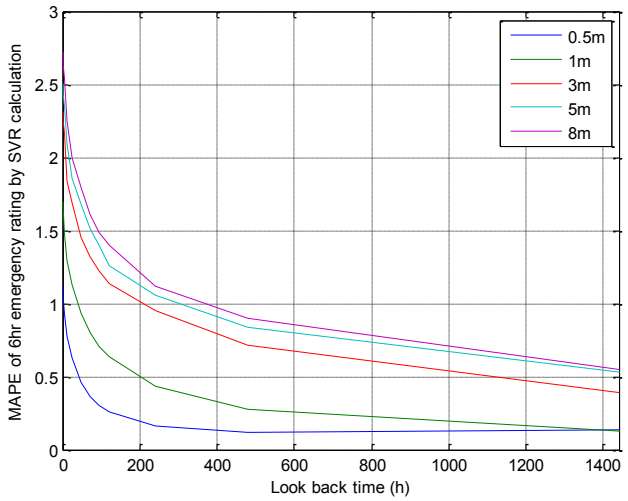

Figure 7.4 - MAPE of Test 1 with different look back time of historical load

The value of MAPE decreases with increasing look back time of the historical load. For the same look back time of historical load, the SVR model with shallower buried depth has smaller MAPE of 6hr emergency rating due to the shorter thermal time constant of the shallower buried cable as shown in Table 7.2. By using one third of these thermal time constants as the lengths of the look back time of historical load data for the cable with different buried depths, the MAPE of 6hr emergency rating by the SVR models are all smaller than 1.

Figure 7.5 presents the cumulative distribution function (CDF) of the 6hr emergency rating errors of the 0.5m depth buried cable in Test 1 SVR models which have different lengths of look back time as input features. The different lengths of look back time are represented as the fractions of the thermal time constant in Figure 7.5. The durations of the considered historical data are from 0.05 to 10 times of the thermal time constant, which correspond to 5 hours to 1000 hours. If the probability of 6hr emergency rating error being contained within ±20A (two red dash line) is calculated as a criteria, the accuracy of SVR models using different look back times can be measured. For the SVR model with 5 hours look back time (about 0.05 times of the thermal time constant) of the historical load, the probability of 6hr emergency rating error being contained within ±20A is lower than 80%. After increasing the look back time to 50 hours (about 0.5 times of the thermal time constant), the probability rises to about 97%. Once the look back time of historical load is longer than 100 hours (about the same with thermal time

constant), almost all the rating errors are within ±20A. It should be noted that the SVR model with 500 hours historical load of input features has smaller error than the SVR model with 1000 hours historical load of input features, which indicates that 1000 hours of lag time of the historical load is too long for the SVR model to calculate 6hr emergency rating for a 0.5m depth buried cable. The time consumption to construct, train and test an SVR model might increase with the complexity of the input features in the model. Figure 7.6 shows the MAPE of 6hr emergency rating in SVR model and the time consumption (including the model construction, training and testing one year's data in this case) for different lengths of the look back time input features in the SVR buried cable model (0.5m burial depth). The MAPE and time consumption have an inverse trend with increasing look back time. Figure 7.6 offers a reference to different requirements of the accuracy and solution time in the practice.

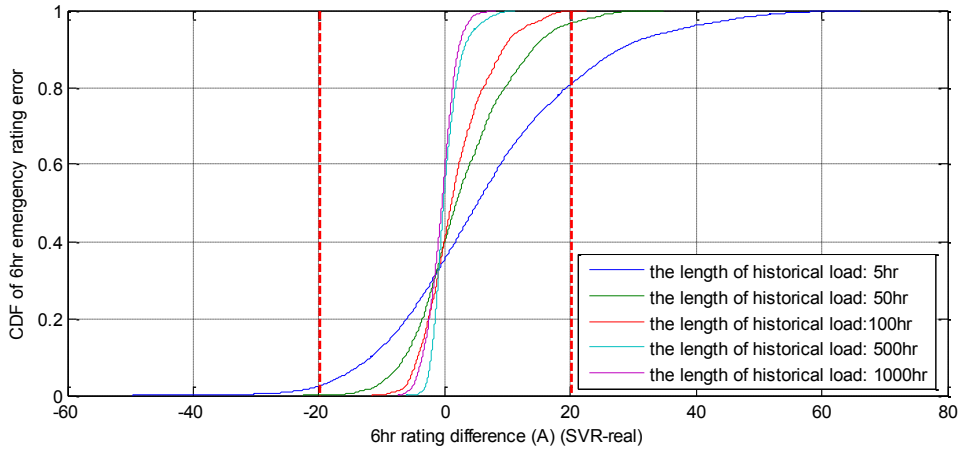

Figure 7.5 - CDF of 6hr emergency rating errors calculated by Test 1 with different look back time of historical load

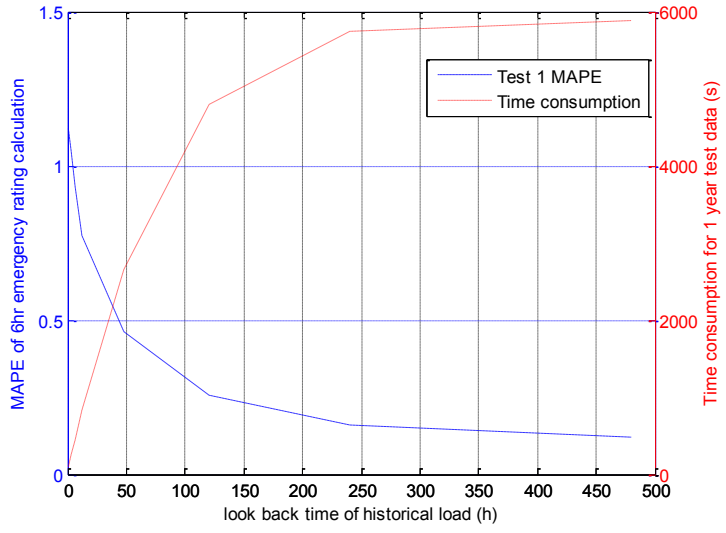

Figure 7.6 - MAPE and the time consumption for SVR buried cable model (0.5m burial depth)

7.2.2 Input feature Test 2: accumulated historical load^2

According to the initial test, the buried cable needs a very long look back time of the historical load which results in a large amount of input features in the SVR model and a long solution time. In order to reduce the number of input features, an exponentially weighted moving average equation is applied to calculate the accumulated historical load^2:

$$Accumulate\_load^2(t_b) = \frac{\sum_{k=1}^{t_b} \alpha^{k-1} load^2\big(t_b - (k-1)\big)}{\sum_{k=1}^{t_b} \alpha^{k-1}} \qquad (7.1)$$

where *Accumulate_load*^{2} *(t_b)* is the accumulated load^2 with the look back time of t_b hour; *load*^{2}(t) is the historical load^2 of t hour ahead and α is the smoothing factor (α<1). By calculating the correlations between the real time conductor temperature and the *Accumulate_load*^{2} with different smoothing factor, the most suitable smoothing factor can be found and used in the moving average equation. According to the tests, the smoothing factors for different look back times of the historical load in 0.5m depth buried cable system are presented in Table 7.3.

Table 7.3 - Smoothing factors for different look back time of historical load

look back time t_b	24	48	72	96	120	240	480
Smoothing factor α	0.90	0.91	0.92	0.93	0.93	0.93	0.93
correlation	0.948	0.954	0.956	0.956	0.956	0.956	0.956

The correlation between *Accumulate_load*^{2} and the conductor temperature stays constant when the look back time is longer than 72 hours. As a result, we chose 72 hours as the look back time t_b and 0.92 as smoothing factor α in (7.1). Based on the input features of the Test 1 (look back time of the historical load), the result of this *Accumulate_load*^{2} will be used as an additional input feature in the new SVR model. The total amount of the input features for the new models in Test 2 are one more than the number of the input features for the corresponding models (with the same look back time of the historical load) in Test 1. The MAPE of 6hr emergency rating results calculated by the models in Test 1 and Test 2 with the input features of different look back time of historical load are presented in Figure 7.7. It shows that, models in Test 2 have better performance than Test 1 when the input features includes less than 120 hours length of the look back time of the historical load. While the differences of the MAPE between these two models reduce with increasing look back time of the historical load (from about 0.5 for 1 hour look back time to almost 0 when look back time is longer than 120 hours). The operators can chose their suitable model from this figure according to the requirement of the accuracy and the solution time. As an example, the Cumulative Distribution Function (CDF) for 6hr emergency

rating calculation errors by SVR model with the input features of 120 hours look back time of historical load data is shown in Figure 7.8. With this SVR model, all the 6hr emergency rating errors are contained within ±20A.

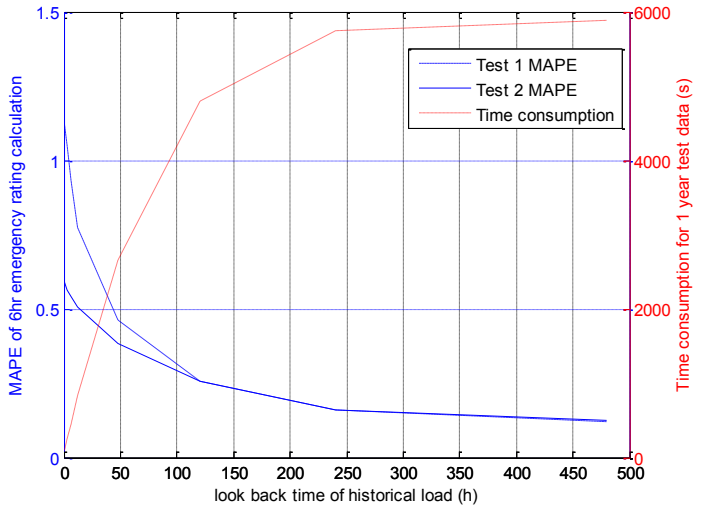

Figure 7.7 – MAPE and the time consumption in input feature Test 1 and Test 2 for buried cable with different look back time of historical load (0.5m burial depth)

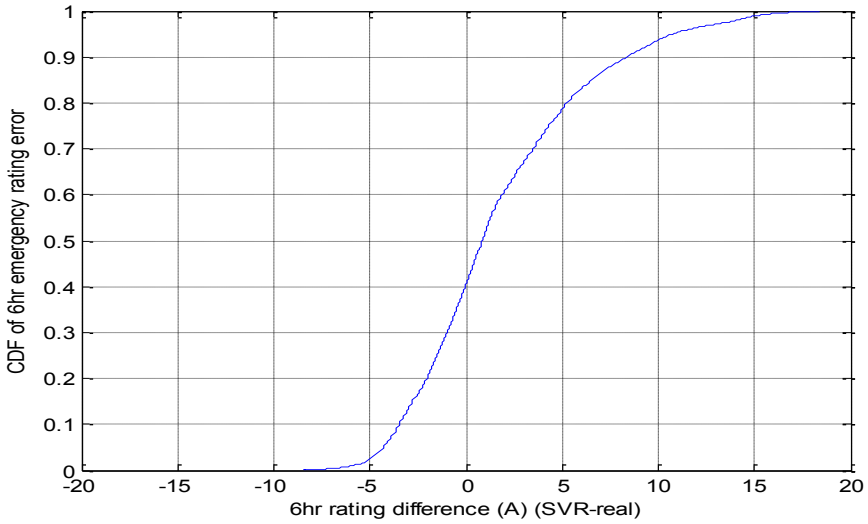

Figure 7.8 – CDF of 6hr emergency rating errors calculated by buried cable SVR model

It should be noted that the model construction and training occupy the majority of time consumption shown in Figure 7.7, while the solution time for one year prediction test by a ready-made model is stable at about 2 seconds as the complexity of SVR model is not related to the number of input features but the number of support vectors. Practically, SVR models only need to be built and trained at the beginning before their application, thus the actual solution

time by the SVR model (2 seconds for 8760 steps) is much faster than FDM model (about 20 minutes for 8760 steps).

7.3 Emergency rating calculated by SVR for cable in air

In this section, the SVR model is used to calculate the 6hr emergency rating for cable in air. The case of a cable protected from solar radiation is considered in this work. The geometries and properties of the cable in air system in this test are as per Table 3.1. It is a 275kV single core XLPE cable with the conductor cross-section area of 2500mm^2. Natural cooling condition is used on the cable surface.

The load data profile is as per Section 7.2, but linearly scaled into the range from 0 to 2000A, with an average value of 1082.5A. The real time ambient air temperature related to the load demand area is shown in Figure 7.9.

The dynamic thermal model is constructed by using the FDM technique and Morgan's heat transfer coefficient to calculate the temperature of cable in air under natural cooling circumstance. The input data presented in this section are used as inputs in this dynamic thermal model to calculate the cable conductor temperature and 6hr emergency ratings. The results associated with all the inputs are used to train and test the SVR model.

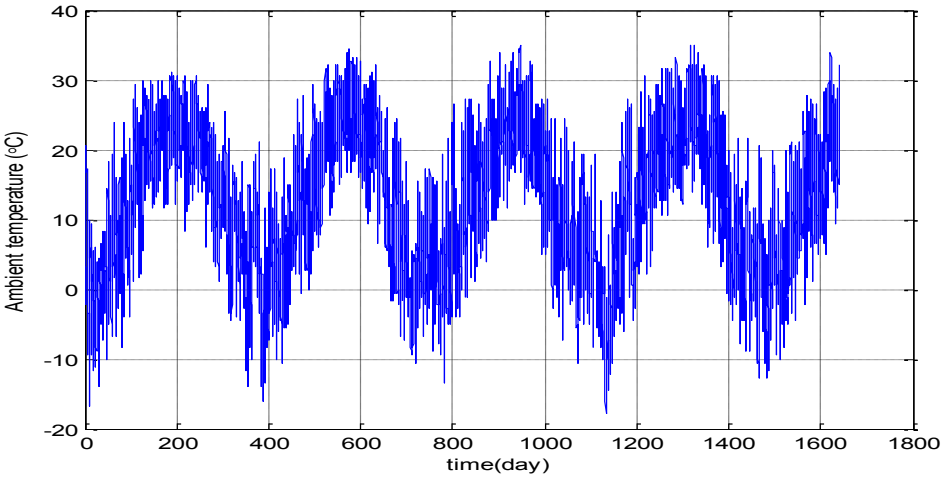

Figure 7.9 - Input ambient air temperature profile for cable in air

7.3.1 Input feature test

The 6hr emergency ratings for cable in air depend on the initial cable temperature at the corresponding points, which is further related to the historical load and ambient temperature. The loads decide the heat generation in the cable and the ambient temperatures decide the

natural heat convection on cable surface, which is the main heat transfer approach for cable in air installation. As a result, the historical load and ambient air temperature are chosen as two input features in the SVR model to calculate the 6hr emergency rating for cable in air.

In order to decide the historical duration of these two variables which need to be consider in the model, the grid search method is applied to find the best look back time of the load and ambient temperature in the rating calculation SVR model. The thermal time constant for this cable installation under 1082.5A constant load (average current of input load profile) and 20°C ambient air temperature is only 2.8 hours. Due to the short thermal time constant of this cable in air installation, only short term historical data are needed in the rating calculation. First, the look back time of 1, 3, 6, 12, 24, 36, 48 hours, which roughly correspond to 1/3, 1, 2, 4, 8, 12 and 16 times of the thermal time constant, for both historical load and ambient air temperature have been tested in the SVR models, thus 49 kinds of combinations are tested with the results shown in Figure 7.10. The minimum MAPE (0.0635) can be found at the 6 hour look back time (2 times of the thermal time constant) for both load and air temperature. According to the initial results in Figure 7.10, we can further locate the search target in the area of 4-12 hour look back time for both load and air temperature. A refined mesh can be set in this area to find a more accurate model. The look back time was increased hourly from 4 hour to 12 hour for both load and air temperature to calculate the MAPE for each case (81 tests), with the results presented in Figure 7.11. The minimum MAPE (0.0550) can be obtained with the 9 hour look back time of load and 11 hour look back time of the air temperature (around 3 to 4 times of the thermal time constant).

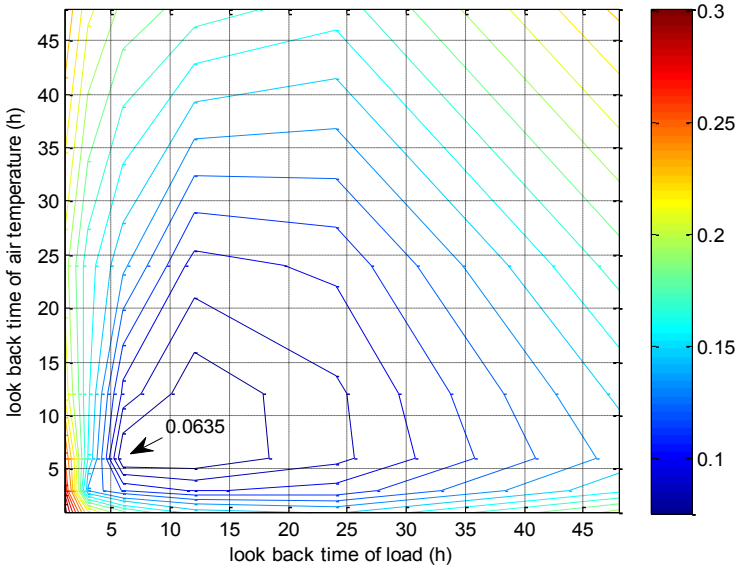

Figure 7.10 – MAPE of rough grid search for different look back time of load and air temperature

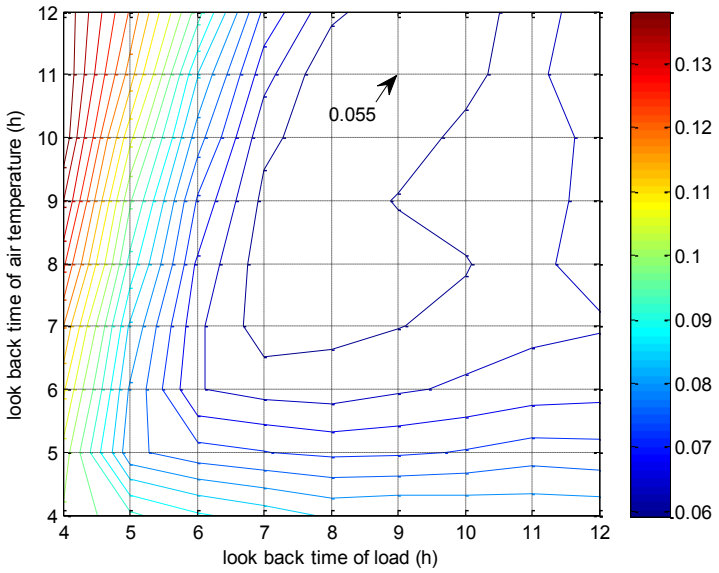

Figure 7.11 – MAPE of fine grid search for different look back time of load and air temperature

7.3.2 Test results

The blue line in Figure 7.12 shows the 6hr emergency rating results calculated by SVR model for the cable in air. It only presents the rating results for about 800 hours due to the size of the figure. Compared with the rating results obtained from the solution of the dynamic thermal model (green line), the results from the SVR model show a high level of accuracy. The 6hr emergency errors of these 800 hours data can be found from Figure 7.13. Most of the errors in this period are smaller than ±4A and all the errors are contained within ±6A.

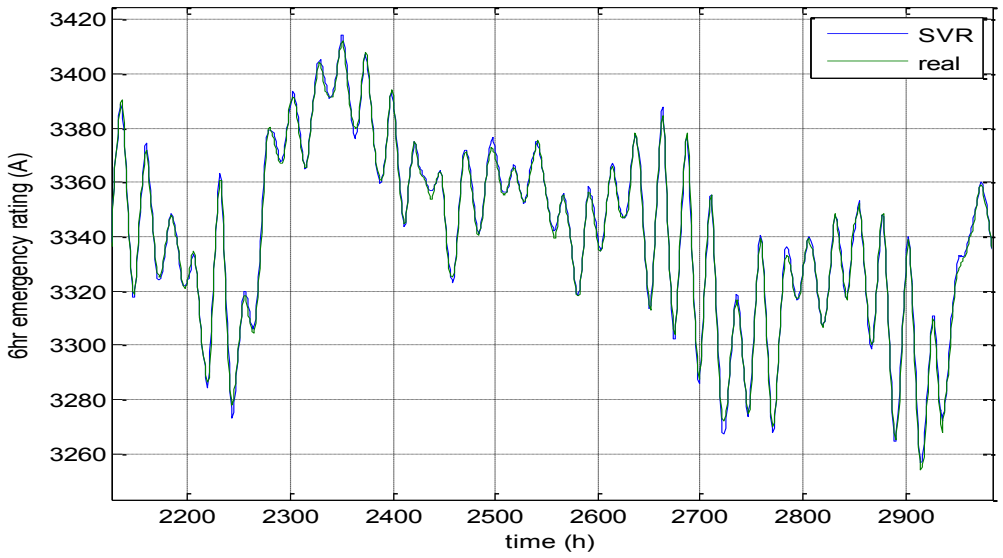

Figure 7.12 - SVR calculation results of 6hr emergency rating for cable in air

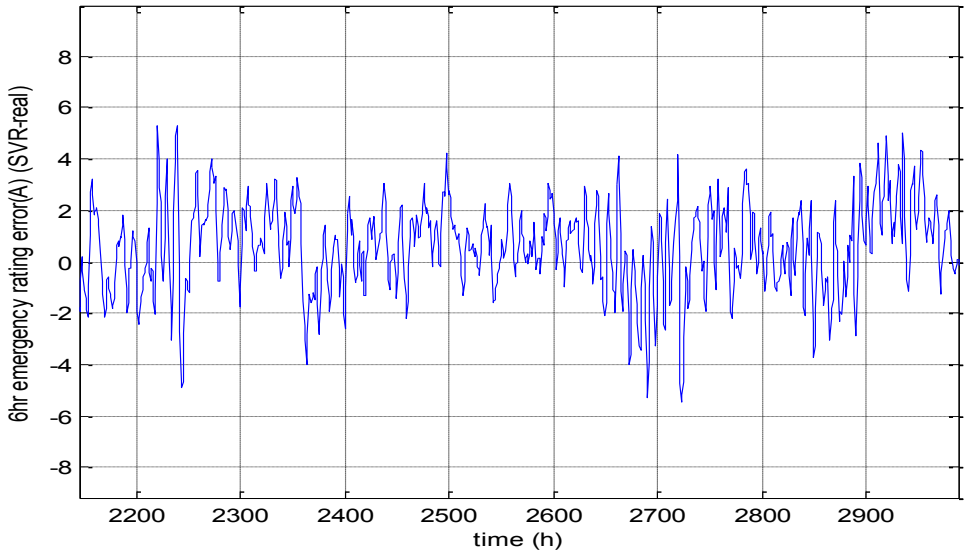

Figure 7.13 - SVR calculation errors of 6hr emergency rating for cable in air

Cumulative distribution function (CDF) of the 6hr emergency rating errors for all the testing data (1 year) is shown in Figure 7.14. For this one year's testing data, 96.7% of the 6hr emergency rating errors are being contained within ±5A and 98.9% of the errors are being contained within ±10A.

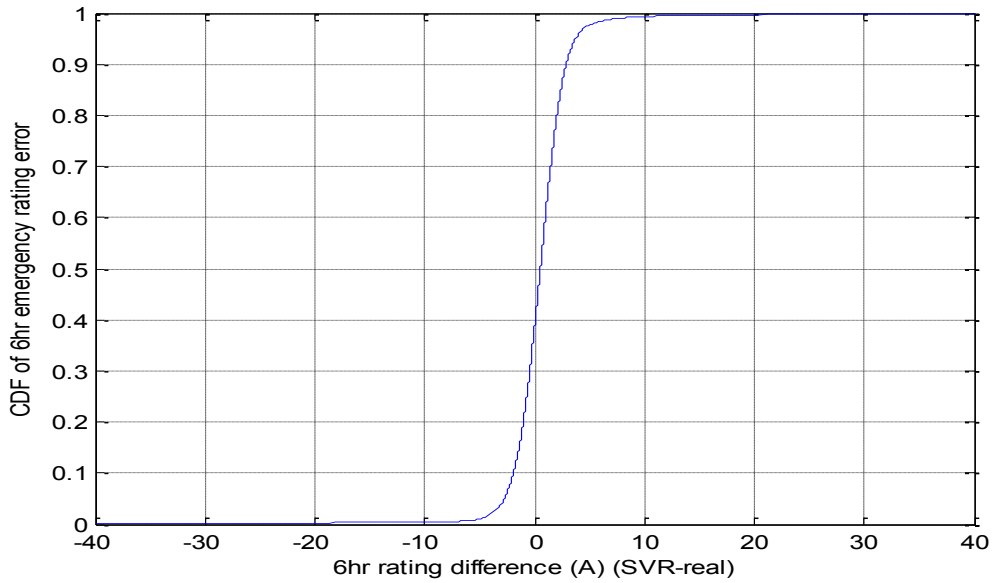

Figure 7.14 - CDF of 6hr emergency rating errors calculated by cable in air SVR model

7.4 Emergency rating calculated by SVR for tunnel cables

In this section, the SVR model is used to calculate the 6hr emergency rating for tunnel cables directly. The input features of historical load and inlet air temperature have been tested to find the most suitable model.

The dynamic thermal model for a three section cable tunnel system is constructed based on the method in Section 3.4. The three section cable tunnel model includes two 40m vertical riser shafts at the two end (Section 1 and Section 3) linked by a 1500m horizontal Section 2. The details of the tunnel installation are presented in Figure 7.15 and Figure 7.16.

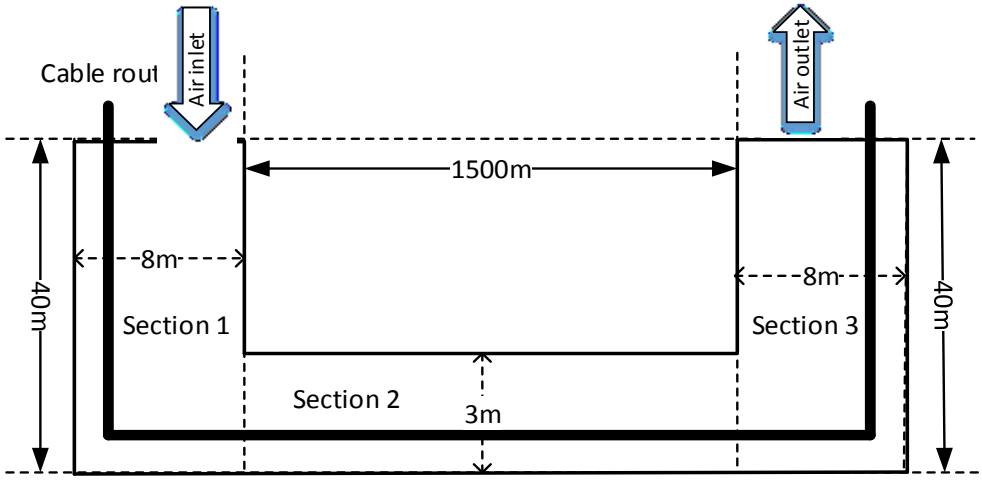

Figure 7.15 – Tunnel geometry with one cable circuit

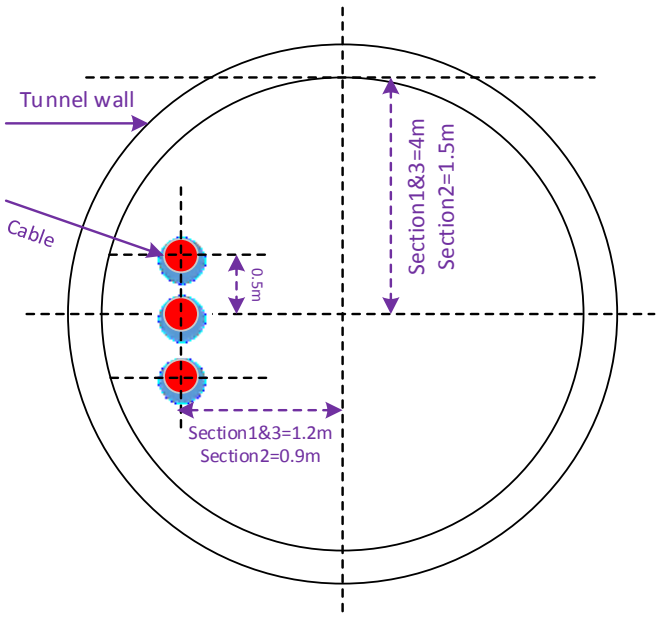

Figure 7.16 – Cable circuit arrangement in the tunnel (one circuit)

Only one cable circuit is installed in the tunnel system for this test. The tunnel wall is assumed to have the same thermal properties as the local soil. The volumetric heat capacity of the soil is $2MJm^{-3}K^{-1}$ and the thermal resistivity is $0.9KmW^{-1}$. An isothermal boundary condition of 10°C is set 15m away from the tunnel centre. The maximum air velocity of this ventilated tunnel is set as $4ms^{-1}$ in section 2. The diameters of the two shaft sections are larger than the main tunnel section, resulting in lower bulk air velocities. The ventilation system is assumed to be running at full speed all the time throughout the test.

In order to fit the initial load data into this cable tunnel system, all the load data are linearly scaled into the range from 0 to 2500A, with an average value of 1352.7A. The real time ambient air temperature for 4 years matches the data used in the cable in air system (Figure 7.9). The resulting conductor temperature in this cable tunnel system is presented in Figure 7.17. It shows the maximum conductor temperature along the cable in tunnel at each time step.

The real-time load and inlet air temperature are the two major factors which influence the conductor temperature of the cable in tunnel. Due to the thermal time constant in the cable tunnel system, the conductor temperature and the emergency ratings are also affected by the preceding historical load and inlet air temperature data. In addition, the maximum conductor temperature might happen in different section of the tunnel in different scenarios. As a result, the historical load and inlet air temperature along with the section of the hot spot in the tunnel will be used in the input features test to find a best SVR model to calculate the 6hr emergency rating in the cable tunnel system.

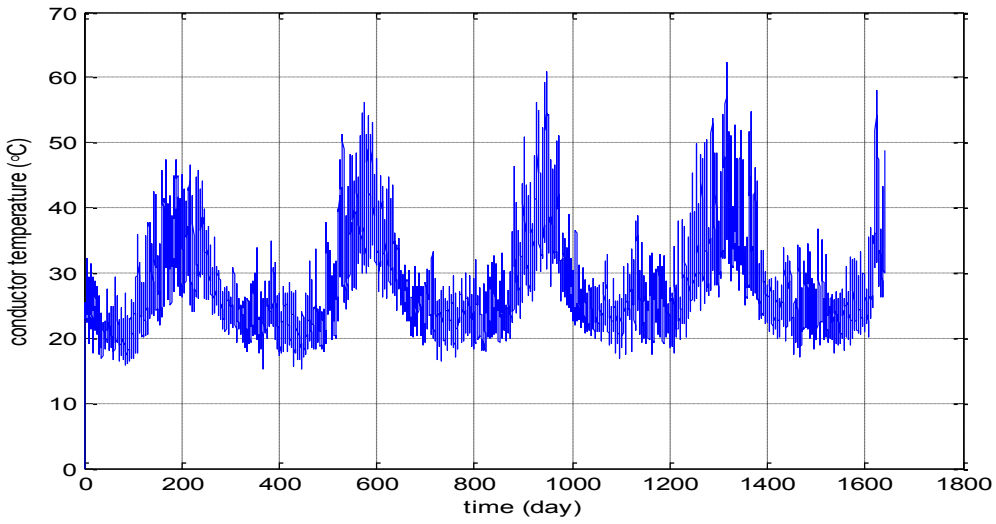

Figure 7.17 - Conductor temperature in cable tunnel system

7.4.1 Input feature Test 1: historical load and air temperature

In Test 1, the historical load and inlet air temperature are chosen as two inputs in the SVR model to calculate the 6hr emergency rating for a cable tunnel system. To test the length of historical data of these two variables which needs to be considered in the model, the grid search method is applied in this work to find the best look back time of the load and inlet air temperature in the SVR model. The thermal time constants under the condition of constant load of 1352.7A (average value of the input load data), 20°C inlet air temperature and full speed ventilation were firstly calculated. The thermal time constants for the tunnel wall of section 3 and air inside this tunnel section, which represent the highest temperature of tunnel wall and air at the steady state condition, are very long (1390 hours for tunnel wall and 179 hours for air inside tunnel) as the tunnel is deeply buried. However, the thermal time constant of the cable is only less than one hour (0.89 hour) as the forced convection, which mainly relates to the ventilation speed, dominate the thermal transfer in ventilated tunnel cables.

Due to the short thermal time constant of the cable, the look back time of 1, 6, 12, 24, 36, 48, 72, 96 and 120 hours for both historical load and inlet air temperature (81 combinations) are chosen for the initial test. A contour plot (Figure 7.18) is used to present the MAPE values for this grid search of different look back time of load and inlet air temperature. The minimum MAPE (0.694) can be found at the 12 hours look back time of historical load and 120 hours look back time of inlet air temperature.

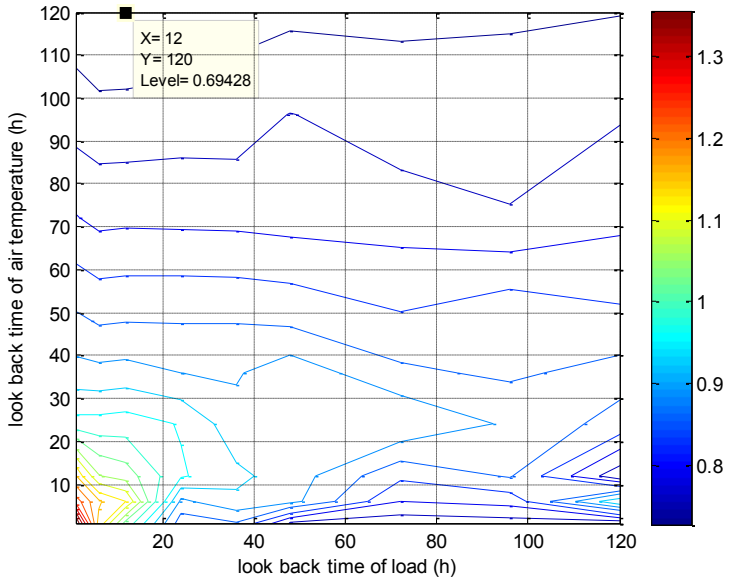

Figure 7.18 - MAPE of the grid search results for different look back time of load and inlet air temperature in Test 1

By using the model obtained from the best result of the grid search, the 6hr emergency rating for the one year test data can be calculated from the SVR model. The SVR rating results are presented in Figure 7.19 with the rating results from the solution of dynamic thermal model. It shows that even with 132 input features in the SVR model (12 hours historical load data and 120 hours historical inlet air temperature data), the rating results from SVR still could not match the results from the dynamic thermal model very well. The CDF in Figure 7.20 presents the details of the distribution of the 6hr emergency rating errors calculated by the SVR model.

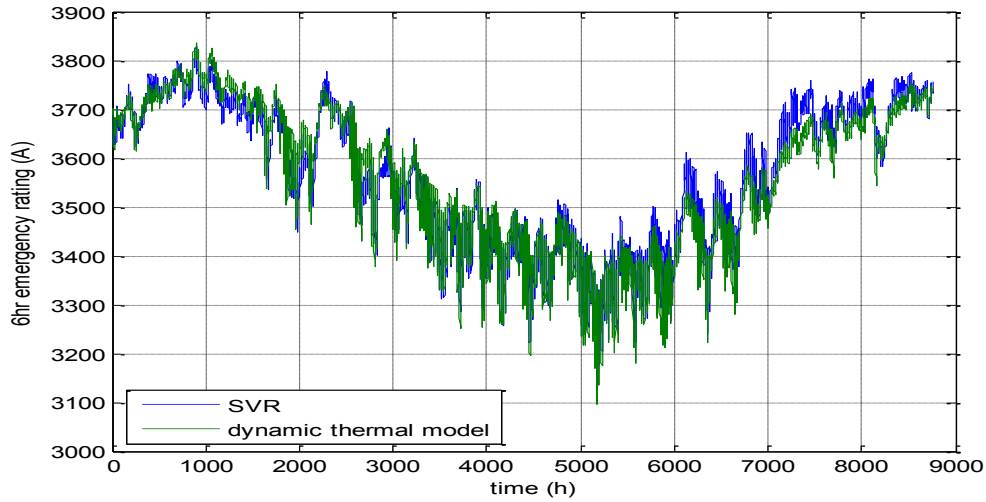

Figure 7.19 - 6hr emergency rating results from the SVR in Test 1 for tunnel cables

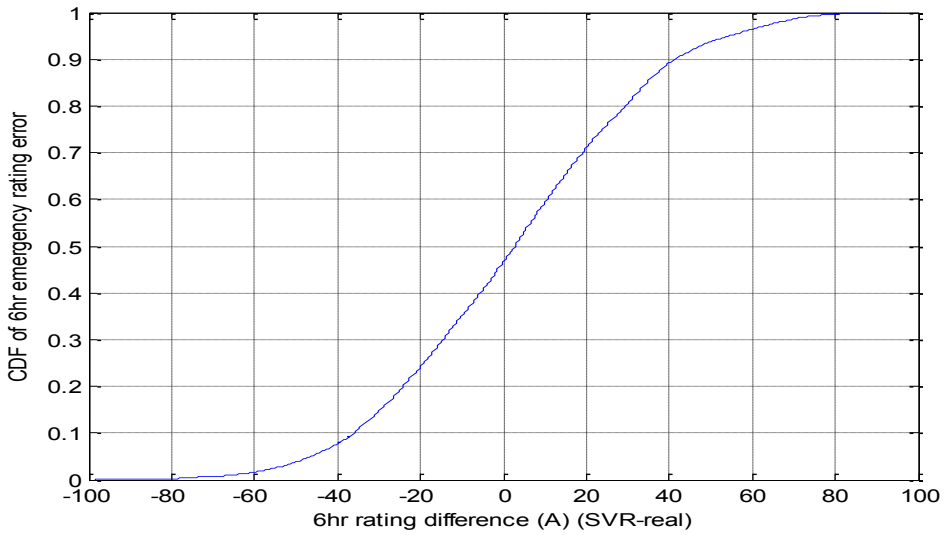

Figure 7.20 - CDF of 6hr emergency rating errors calculated by tunnel SVR model in Test 1

In this one year of test data, the values of 6hr emergency rating range from 3095A to 3835A while nearly 20% of the 6hr emergency rating errors are larger than ±40A, which might cause 2°C-3°C conductor temperature errors within 6 hours in this cable tunnel system. The maximum

6hr emergency rating error in this one year test is close to 100A which might cause up to 5°C conductor temperature errors within 6 hour in this case. As a result, a better SVR model is required to perform better 6hr emergency rating calculation in this cable tunnel system.

7.4.2 Input feature Test 2: section of maximum conductor temperature

In the Test 1, the SVR model could not calculate the 6hr emergency rating for this cable tunnel system accurately. After scrutinizing the 6hr emergency rating error of the SVR model with this cable tunnel system, an interesting relation can be observed between the rating errors and the location of the maximum conductor temperature in the tunnel system at each time step.

7.4.2.1 Error analysis from Test 1

Due to the fluctuation of the input load and inlet air temperature, the location of the maximum conductor temperature in the tunnel may vary at each time step. Figure 7.21 and Figure 7.22 show the rating errors from SVR model and the location (section) of the maximum conductor temperature in the tunnel.

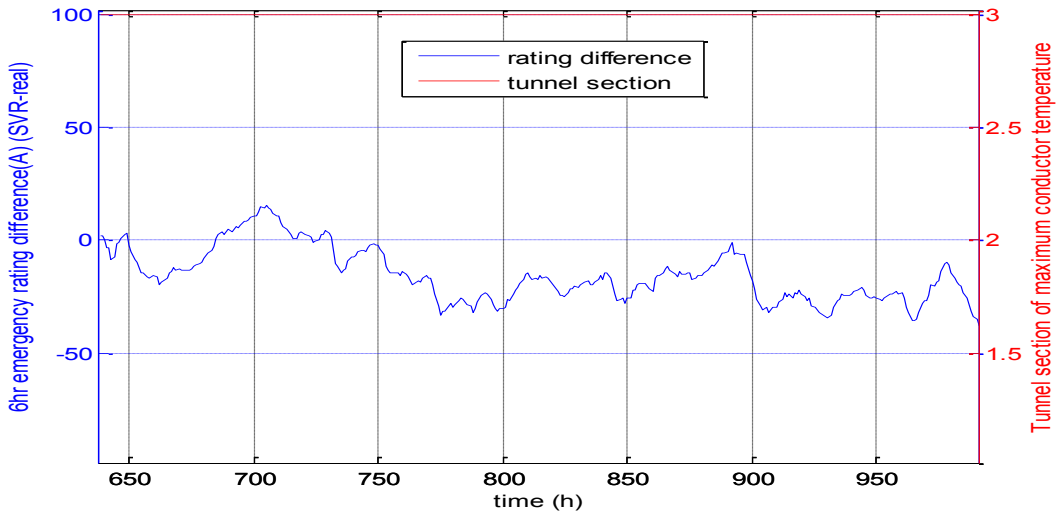

Figure 7.21 - 6hr emergency rating error and the constant section of maximum temperature

During the time period in Figure 7.21, all the maximum conductor temperatures are located in section 3 of the tunnel and the rating errors fluctuate evenly within a small range (-25A to 15A). The SVR model normally underestimates the cable rating which gives a conservative value in the system operation. However, the location of the maximum conductor temperature varied among section one to three in the time period of Figure 7.22, resulted in a sharply fluctuation of the emergency rating errors from SVR model, especially for the time steps where the location of the maximum conductor temperature changes, the rating errors rise dramatically. This is

because the relation of load, inlet air temperature and the conductor temperature is different in each tunnel section of the dynamic thermal model for the cable tunnel system. If the section of maximum conductor temperature is not considered in the SVR model, it is difficult for the SVR model to detect the different relation in each section of the tunnel, thus the model will treat them with the same algorithm and result in a lot of outlying points in the training model when the sections of maximum conductor temperature are different.

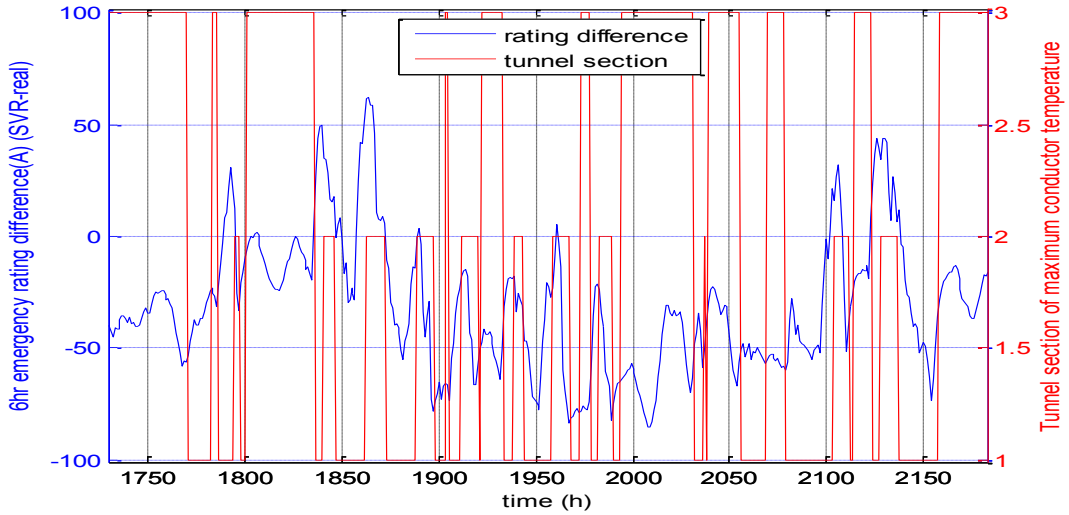

Figure 7.22 - 6hr emergency rating error and the varied section of maximum temperature

In order to remove this shortcoming in the SVR model, an input feature describing the section of maximum conductor temperature in the tunnel will be added in the SVR model in Test 2. However, the tunnel section containing the maximum conductor temperature is unknown unless a Distributed Temperature Sensor system (DTS) is installed in the cable. DTS is not available in some existing cable tunnel systems, thus, other methods should be found to detect the potential location of the hot spot in the cable tunnel system.

7.4.2.2 Classify the data by the sections of maximum conductor temperature

In this test, the Support Vector Machine (SVM) is used to classify the data into three groups according to the different locations of the maximum conductor temperature in the tunnel.

Before building the SVM model, the reason why the maximum conductor temperature can happen in different sections should be analysed. Figure 7.23 shows the location changes of the maximum conductor temperature in each time step for one year. At most of the time steps, the maximum conductor temperature are located in section one and section three due to the slower air movement in these two sections than section two. Figure 7.24 presents the histogram of the locations of maximum conductor temperature. Around 6000 time steps and 2500 time steps of

the total 8760 steps, the maximum conductor temperature occurs in section three and section one respectively, less than 3.5% of the maximum conductor temperature were found in section two.

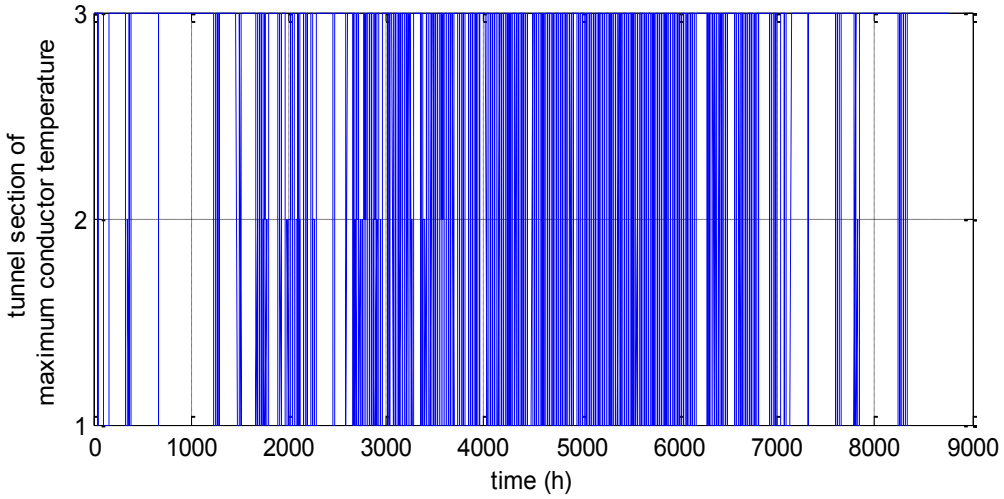

Figure 7.23 - The tunnel section of the maximum conductor temperature at each step

Figure 7.25 shows the clusters of different tunnel sections of the maximum conductor temperature by presenting the relation between load and inlet air temperature data at each time step. Although three patterns can be found in this figure, some overlap regions exist among this three clusters, which means that only looking at the load and inlet air temperature at the current time step is not enough to distinguish the locations of the maximum conductor temperature in the tunnel.

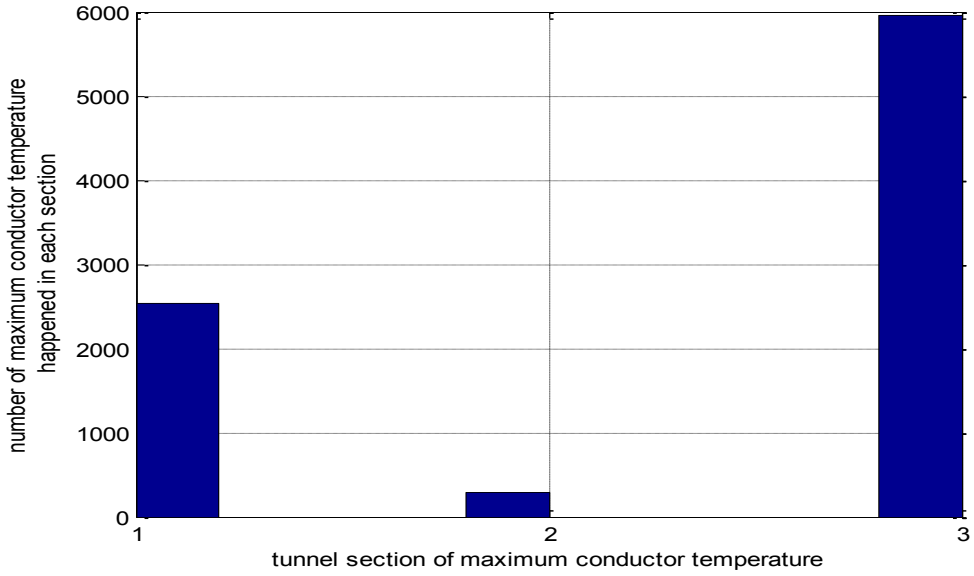

Figure 7.24 - Histogram of the tunnel section with maximum conductor temperature

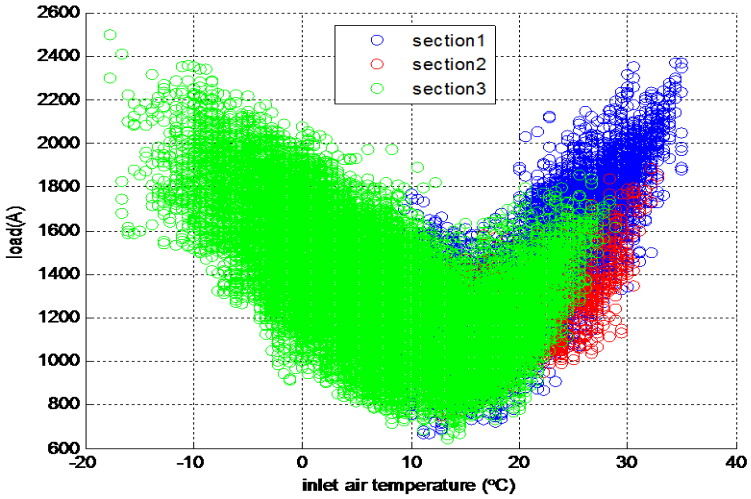

Figure 7.25 - Clusters of different tunnel sections of maximum conductor temperature with different loads and inlet air temperatures

Figure 7.26 shows comprehensive information in the cable tunnel system for 10 days, including the input load data in (a), inlet air temperature data in (b), the maximum conductor temperature in each tunnel section in (c), the maximum air temperature in each tunnel section in (d), the maximum tunnel wall temperature in each tunnel section in (e) and the section of maximum conductor temperature in (f).

From Figure 7.26 (c), we can find that the conductor temperature in section 3 is normally higher than the other two sections during this 10 days. While from 324hr, the conductor temperature in section one is becoming higher than section 2 and 3 due to the rise of the inlet air temperature. At some time steps within 300hr to 320hr, the inlet air temperatures are higher than the air temperature in section 2 and 3, while the differences are very small and the initial temperature in section 3 is higher than other sections, so the conductor temperature in section 3 during this period is still the highest. However, the inlet air temperature rises up to 8°C higher than the air temperature in section 2 and 3 from 324hr which makes the air temperature in section 1 become the hottest through the tunnel and results in less heat being dispatched from the cables in this section. Thus, during 324hr to 352hr, the cable temperature in section 1 is higher than other two sections. From this analysis, it can be concluded that the historical data should be also taken into account to calculate the location of maximum conductor in the tunnel. To decide the length of historical data to be considered in the SVR model, the grid search method is used to test the different lengths of the input features of historical load and inlet air temperature. The results are shown in Figure 7.27, the best SVM model can be found with the 72 hours look back time for both the historical load and inlet air temperature. The accuracy of this SVM model is higher than 91% (713 error points out of total 8760 steps in one year test).

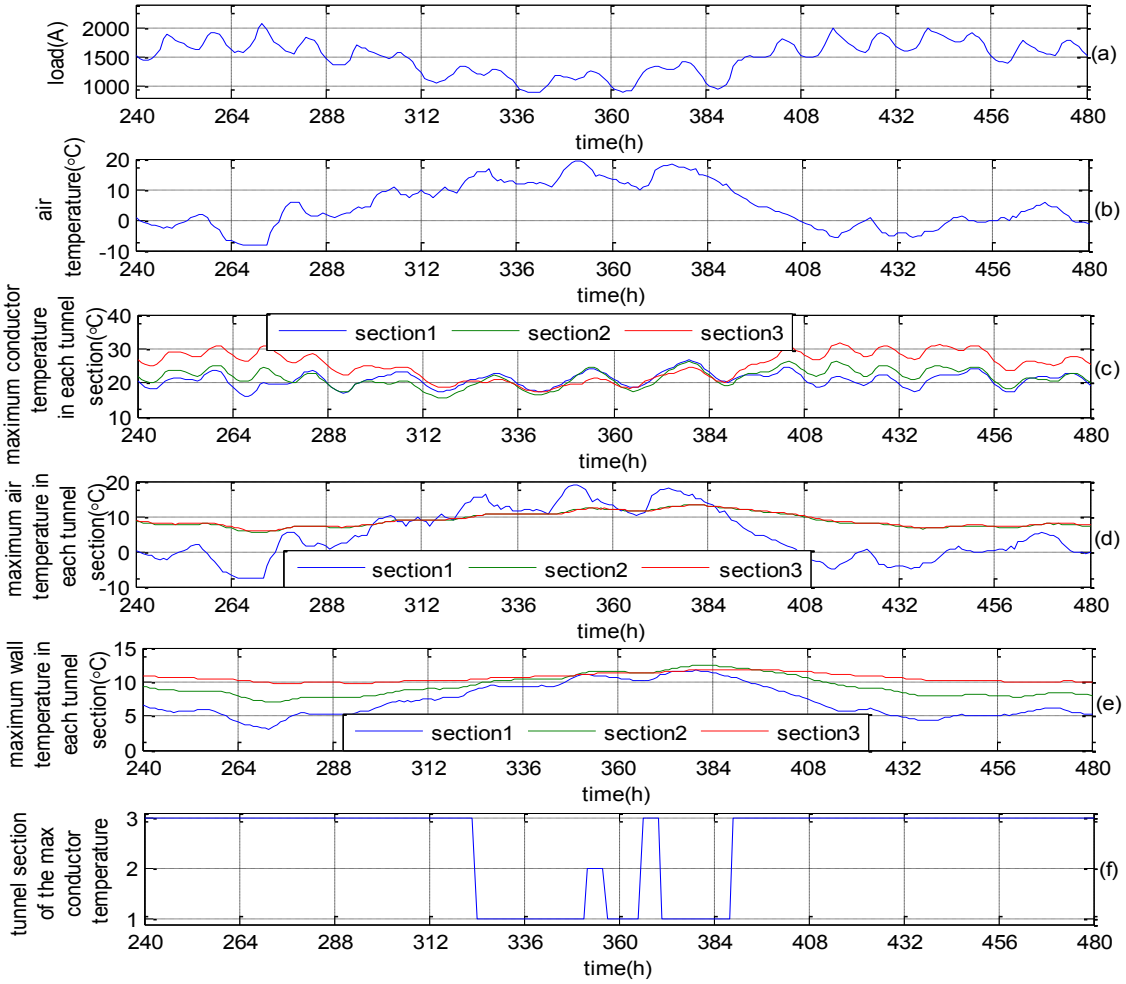

Figure 7.26 - Tunnel information for 240 hours

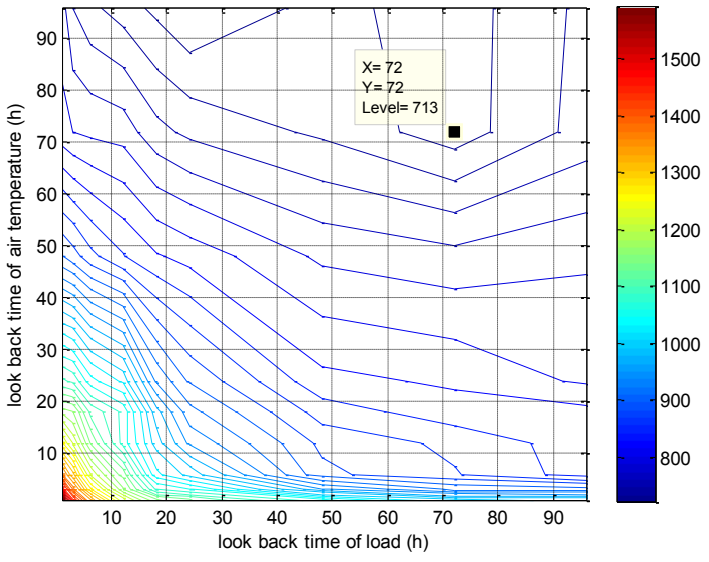

Figure 7.27 - Number of the error steps of tunnel section classification in one year testing data

Figure 7.28 presents some typical results from the SVM model, there are some mistakes at section switching steps made by the SVM model. The SVM model predicts a section switch at 235hr while it doesn't happen. At 278hr and 312hr, the section switch predicted by the SVM model are earlier than the actual situation, while the predicted switches from SVM model is slower at 292hr and 300hr.

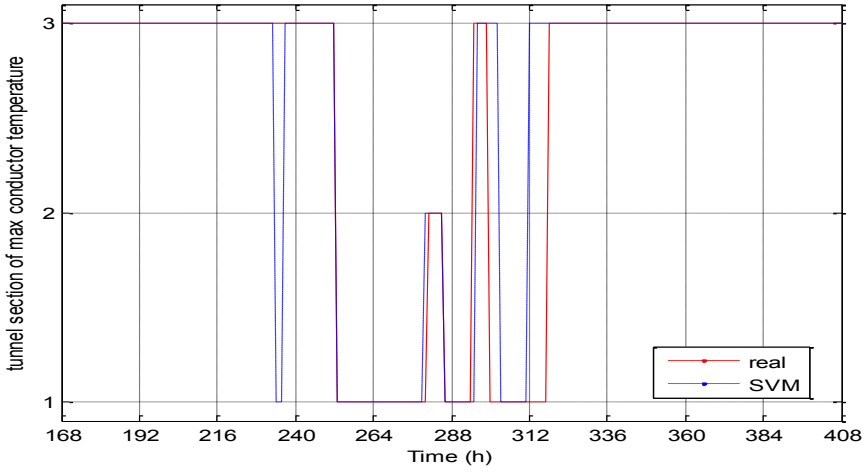

Figure 7.28 - Typical results from SVM model

7.4.2.3 Test 2 results

After the tunnel section of maximum conductor temperature is found from SVM model before each step, the section number can be used as an input feature in the SVR model to calculate the 6hr emergency rating of cable tunnel system (Figure 7.29).

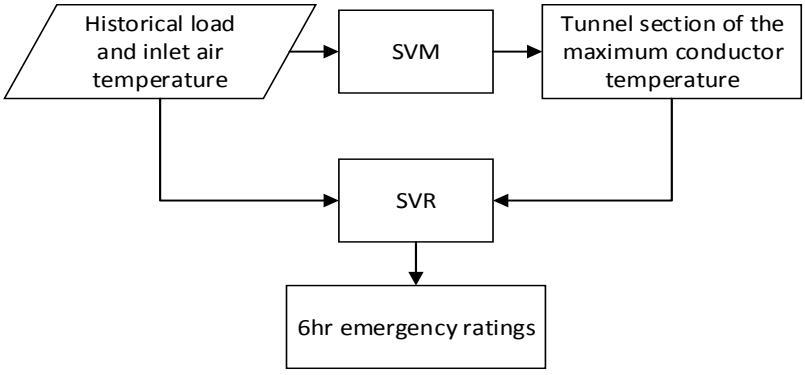

Figure 7.29 - Flow chart of Test 2 for cable tunnel system

The same grid search of different input features of look back time of historical load and inlet air temperature in Test 1 (shown in Figure 7.18) is processed in Test 2, and the results are presented in Figure 7.30. The minimum MAPE value (0.527) can be found when the SVR model is

constructed with the input features of 24 hours look back time of historical load and 120 hours look back time of historical inlet air temperature.

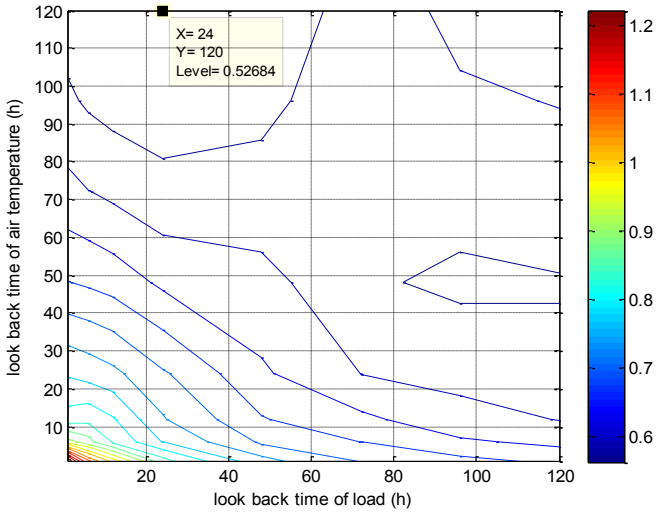

Figure 7.30 - MAPE of the grid search results for different look back time of load and inlet air temperature in Test 2

With this SVR model, the 6hr emergency rating for one year testing data of this cable tunnel system is calculated and compared with the solution from the dynamic thermal model. The Cumulative Distribution Function (CDF) of the 6hr emergency rating difference between the SVR and dynamic thermal model is shown in Figure 7.31. In this one year test data, the probability of 6hr emergency rating errors being contained within ±40A increases from about 80% in the model of Test 1 to higher than 90% in the model of Test 2.

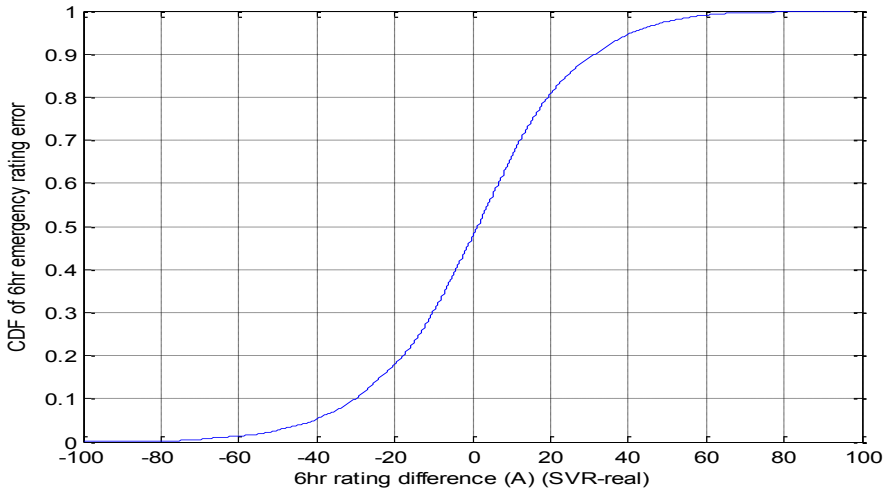

Figure 7.31 - CDF of 6hr emergency rating errors calculated by SVR model in Test 2

Figure 7.32 presents the 6hr emergency rating errors and the section of tunnel which has the maximum conductor temperature at the same time period with Figure 7.22. Compared to the Test 1 SVR model results in Figure 7.22, the results from Test 2 SVR model reduce most of the 6hr emergency rating error into the range of ±50A when the locations of maximum conductor temperature in the tunnel change frequently.

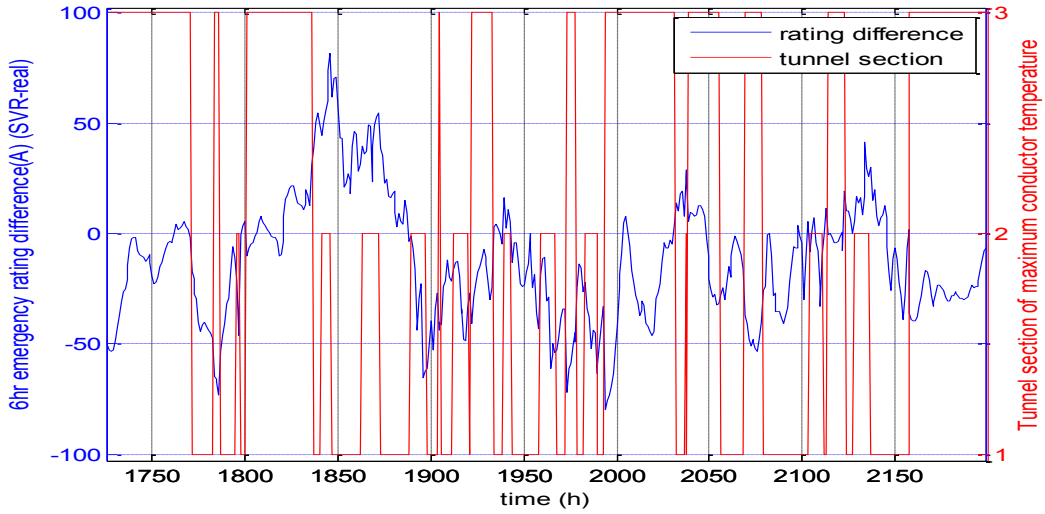

Figure 7.32 - 6hr emergency rating error and the varied tunnel section of maximum conductor temperature in Test 2

7.4.3 Input feature Test 3: multiple SVR models

In Test 3, the 6hr emergency ratings are calculated by three SVR models separately according to the different locations of the maximum conductor temperature (Figure 7.33).

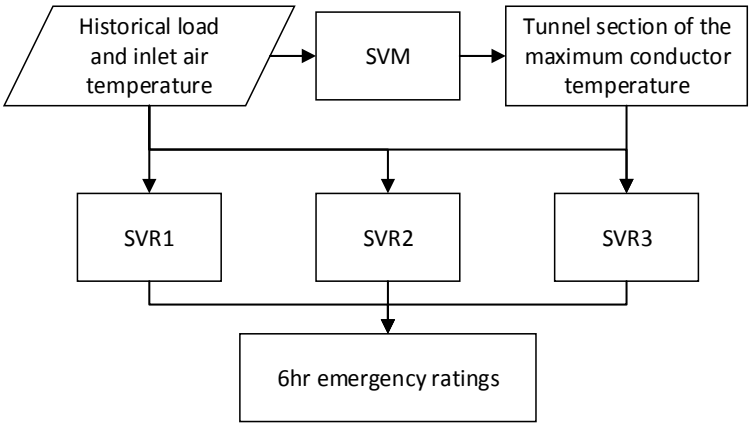

Figure 7.33 - Flow chart of Test Three for cable tunnel system

The four years load and inlet air temperature data have been used in the dynamic thermal model to calculate the cable temperatures and the 6hr emergency ratings. These results are located into

three groups by the locations of maximum conductor temperatures in different tunnel sections. First three years data are used to find the most suitable input features in the SVR model by using the grid search on the look back time of historical load and inlet air temperature. The results of grid search for the SVR models of different tunnel section are shown in Figure 7.34 to Figure 7.36.

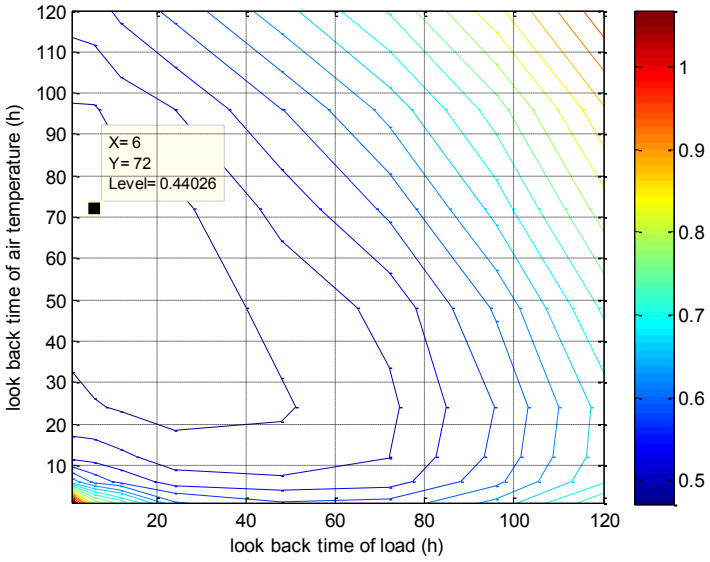

Figure 7.34 - MAPE of the grid search results for different look back time of load and inlet air temperature in tunnel section 1 of Test 3

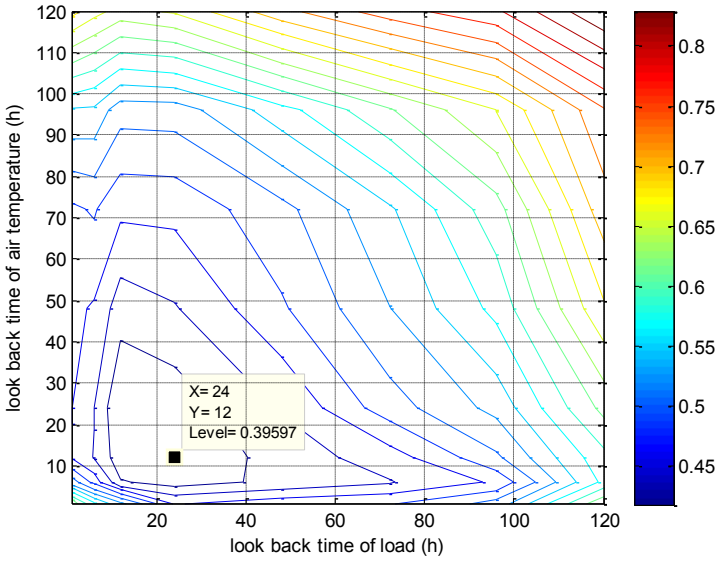

Figure 7.35 - MAPE of the grid search results for different look back time of load and inlet air temperature in tunnel section 2 of Test 3

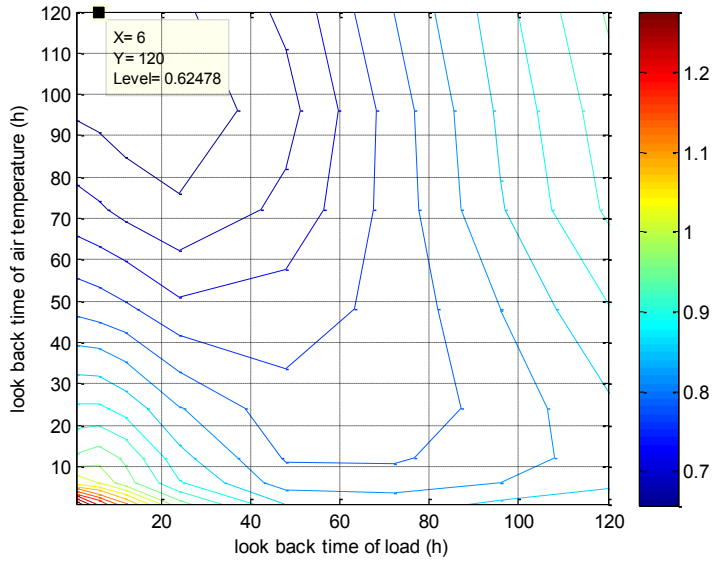

Figure 7.36 - MAPE of the grid search results for different look back time of load and inlet air temperature in tunnel section 3 of Test 3

The best SVR model in tunnel section one can be found from Figure 7.34 with the input features of 6 hours look back time of historical load and 72 hours look back time of the historical inlet air temperature. According to Figure 7.35, the best SVR model for section two contains the input features of 24 hours of historical load and 12 hours of historical inlet air temperature. While for section three, using the data of the look back time of 6 hours of historical load and 120 hours of historical inlet air temperature as input features can best train the SVR model.

The CDF plot of the difference between 6hr emergency rating results calculated by the Test 3 SVR models in different tunnel section and the dynamic thermal model is presented in Figure 7.37. It shows that the large rating errors usually appear in tunnel section three due to the higher complexity of the thermal model in section three than the other two sections. This additional complexity is from the phenomenon that the inlet air temperature in section three depends on the heat transfer between cables, air and the tunnel wall in the first two sections.

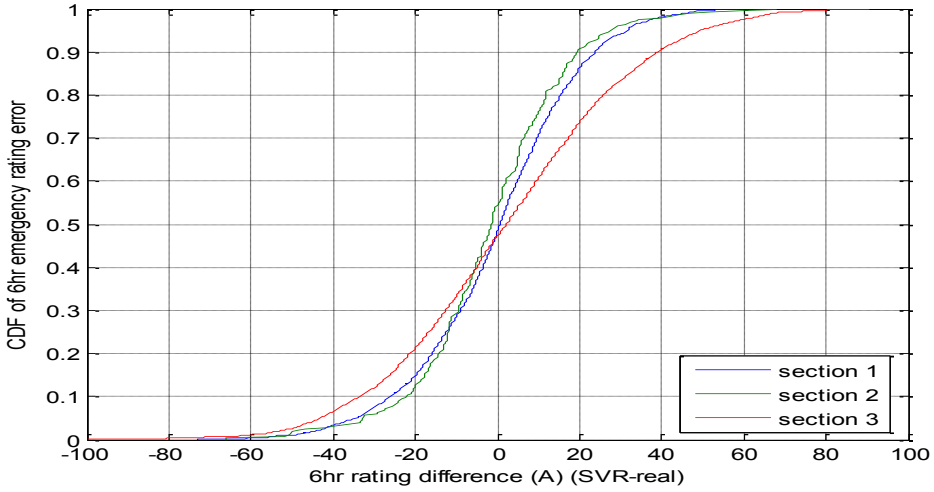

Figure 7.37 - CDF of 6hr emergency rating errors calculated by cable tunnel SVR models for different tunnel sections in Test 3

The three SVR models in Test 3 are combined in one system by using a simple switching operation according to different locations of the maximum conductor temperature. The CDF of 6hr emergency errors for the one year testing data is shown in Figure 7.38.

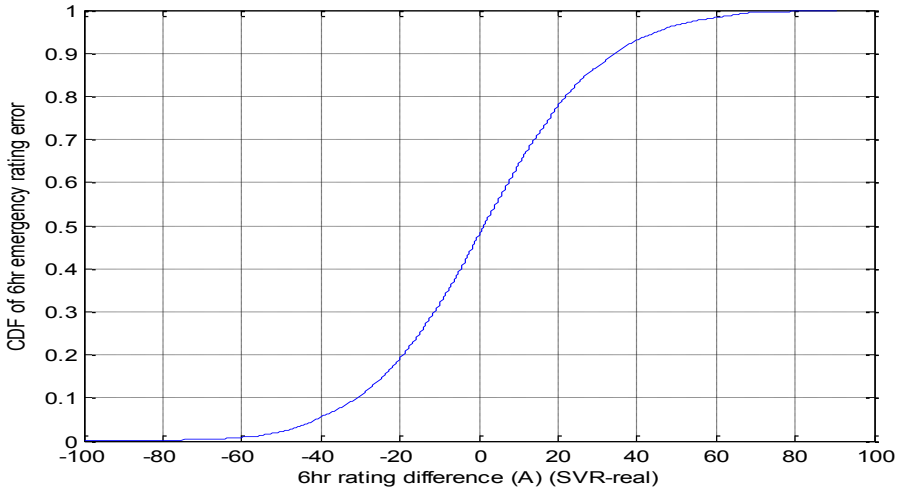

Figure 7.38 - CDF of 6hr emergency rating errors calculated by cable tunnel SVR models in Test 3

The result from Test 3 in Figure 7.38 is almost the same with the results from Test 2 in Figure 7.31. So the SVR model in Test 2 is preferred due to its lower level of complexity.

7.5 Predicted rating calculated directly by SVR for cable in air

Having demonstrated the ability of SVR models to calculate emergency ratings for different kind of cable installation by using proper input features, the models are further developed in this section to directly predict 24hr-ahead emergency ratings.

Instead of using SVR to obtain the load prediction result and then calculating the cable temperature and rating with the load prediction by FDM model, the day-ahead cable ratings are predicted directly by the SVR model, increasing the solution speed. This idea is tested for cable in air installation in this section. Assuming the cable is protected from the solar radiation and the natural convection occurs at the cable surface, historical load and air temperature are the two main parameters that affect the emergency rating results.

According to the test in Section 7.3, to calculate the 6hr emergency rating for cable in air (protected from solar radiation), the best look back times are about 3 times and 4 times of the thermal time constant for historical load (9 hours) and air temperature (11 hours) respectively (Table 7.4). In this work, the day-ahead hourly ambient air temperature forecast is assumed to be available. For the unknown load data, instead of predicting the load first and using the predicted load to calculate the rating, the new SVR model tries to embed both the load prediction and rating calculation to perform the predicted rating directly.

Table 7.4 - Input features for cable in air 6hr emergency rating calculation

Input feature categories	Time of input features
Temperature	t, t-1, t-2, t-3, t-4, t-5, t-6, t-7, t-8, t-9, t-10, t-11
Load	t, t-1, t-2, t-3, t-4, t-5, t-6, t-7, t-8, t-9

7.5.1 Input feature test

The result in Section 7.3 shows that the best look back time of load to calculate 6hr emergency rating in SVR model is 9 hours. For 24hr ahead rating prediction, there are two possible situations shown in Figure 7.39. The x-axis shows the hourly time scale of the prediction, t is the time point of the rating to be predicted, n is the number of ahead hour. If the number of hours ahead n is shorter than 9 hours, it will be the case in Figure 7.39 (a). To predict the 6hr emergency rating at t, there are two parts of load information 9 hour ahead of t, the loads between (t-9) and (t-n) are known and the loads between (t-n) and t are unknown. If the number of hours ahead n is longer or equal to 9 hour, it will be the case in Figure 7.39 (b). All the load information between (t-9) and t are unknown.

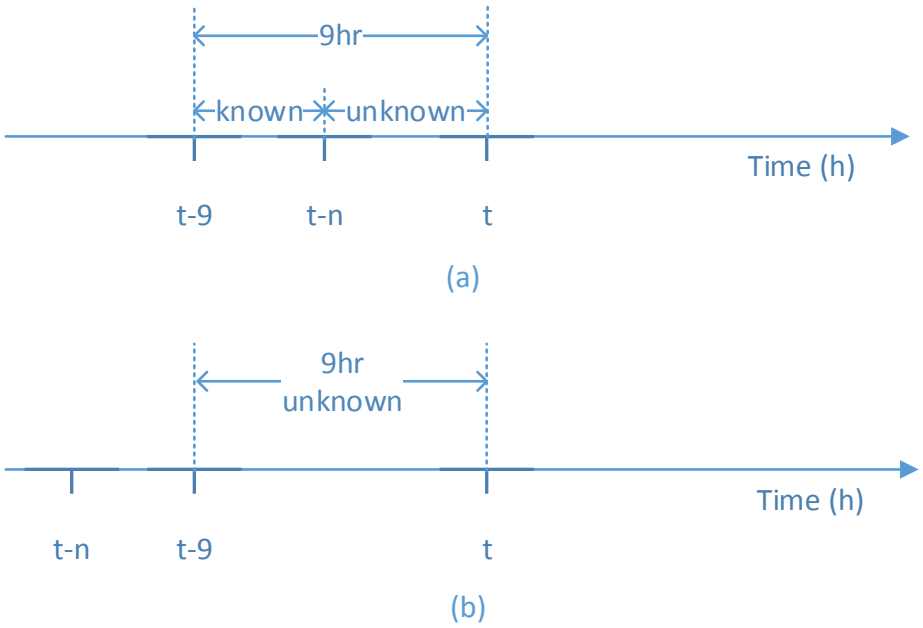

Figure 7.39 – Possible time scale in predicted rating for cable in air

7.5.1.1 Number of ahead hour shorter than 9 hour

For the case of prediction horizons of less than 9 hours, a part of the historical load is already known and can be directly used as input features in the SVR model. However, there is still another unknown part of historical load which needs to be represented by other features related to this part of historical load in the SVR model.

According to the SVR input feature test in Section 4.3.3, the following input features are essential for the 24hr ahead load prediction: the temperature, hour, weekday and season at the time point of rating to be predicted; the same hour load and temperature one and two days before the time point of rating to be predicted; the load 25 and 26 hours before the time point of rating to be predicted; the temperature 1 and 2 hours before the time point of rating to be predicted. These features can be categorized into three groups as shown in Table 7.5.

Table 7.5 - Input features for day-ahead load prediction

Input feature categories	Time of input features
Hour, Weekday, Season	t
Temperature	t, t-1, t-2, t-24, t-25
Load	t-24, t-25, t-26, t-48

By combining Table 7.4 and Table 7.5, the total input features to directly predict 1-8hr ahead 6hr emergency rating can be obtained and shown in Table 7.6.

Table 7.6 - Input features for n hr-ahead 6hr emergency rating prediction (1≤n<9)

Input feature	Time of input features
Hour, Weekday, Season	t
Temperature	t, t-1, t-2, t-3, t-4, t-5, t-6, t-7, t-8, t-9, t-10, t-11, t-24,…, t-24-(n-1), t-48,…, t-48-(n-1)
Load	t-(n+1),…, t-9, t-24,…, t-24-(n-1), t-48,…, t-48-(n-1)

7.5.1.2 Number of ahead hour equal or longer than 9 hour

For the case of prediction horizon equal to or longer than 9 hour, all the load information within 9 hour ahead of the time point to be predicted is unknown. As a result, all the load information needs to be represented by other input features in the SVR model. These input features which are related to the load prediction which can be obtained from Table 7.5. The total input features of 9-24hr ahead emergency rating prediction models are shown in Table 7.7.

Table 7.7 - Input features for nhr-ahead 6hr emergency rating prediction (9≤n≤24)

Input feature	Time of input features
Hour, Weekday, Season	t
Temperature	t, t-1, t-2, t-3, t-4, t-5, t-6, t-7, t-8, t-9, t-10, t-11, t-24,…, t-24-(9-1), t-48,…, t-48-(9-1)
Load	t-24,…, t-24-(9-1), t-48,…, t-48-(9-1)

7.5.2 6hr emergency rating prediction results

Figure 7.40 shows the real values of the 6hr emergency rating for one year. The values fluctuate in the range from 3171A to 3432A.

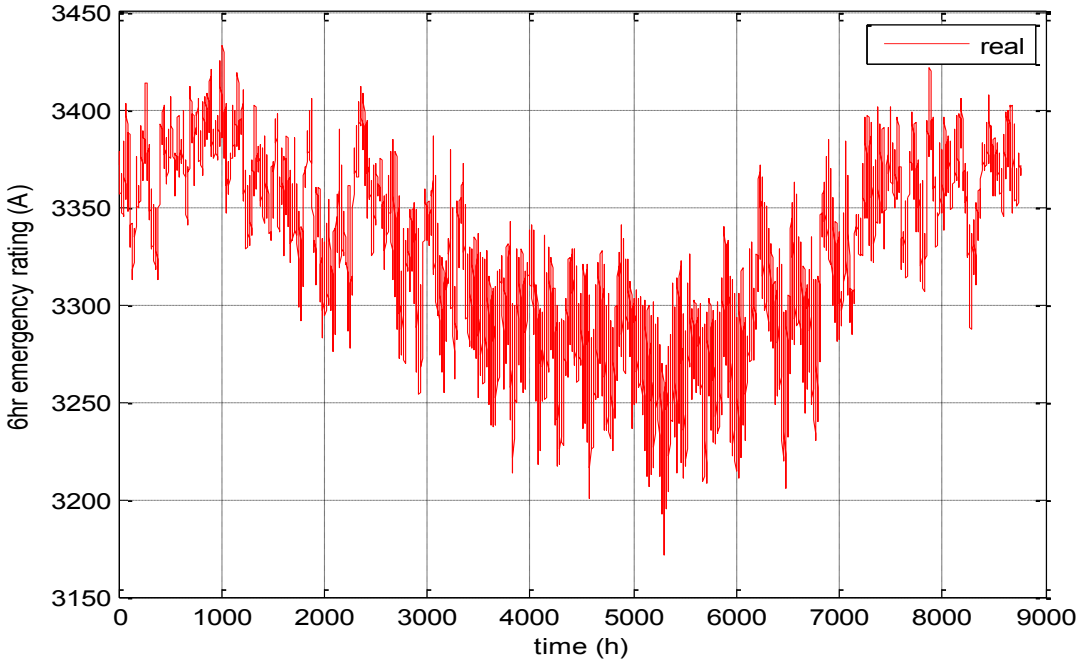

Figure 7.40 – Real 6hr emergency rating values

The 1hr ahead and 24hr ahead prediction results of this year's 6hr emergency ratings are shown in Figure 7.41.

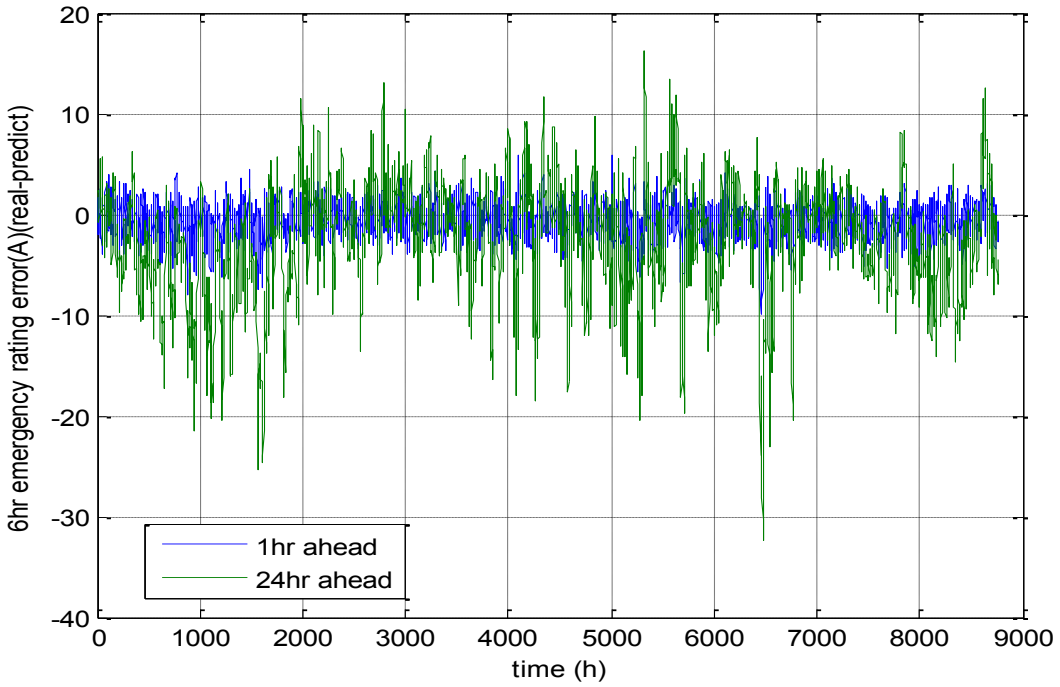

Figure 7.41 - SVR 1hr and 24hr ahead predicted 6hr emergency rating errors

The errors of 1hr ahead prediction are all within the range of -10A to 6A which is smaller than the range of errors for 24hr ahead prediction (-34A to 25A). This is because for 1hr ahead prediction, the load information between 2hr to 9hr before the time point to be predicted are all known and can be directly used as input features in the SVR model. While for 24hr ahead prediction, all the load information between 1hr to 9hr before the time point to be predicted are unknown and need to be represented by other features. Thus, more uncertainties exist in the 24hr ahead prediction than 1hr ahead prediction, resulting in a less accurate prediction.

The cumulative distribution function (CDF) of different hour ahead SVR prediction errors for 6hr emergency rating are shown in Figure 7.42. The predicted 6hr emergency rating error rises with the increasing of the number of ahead hour for the prediction.

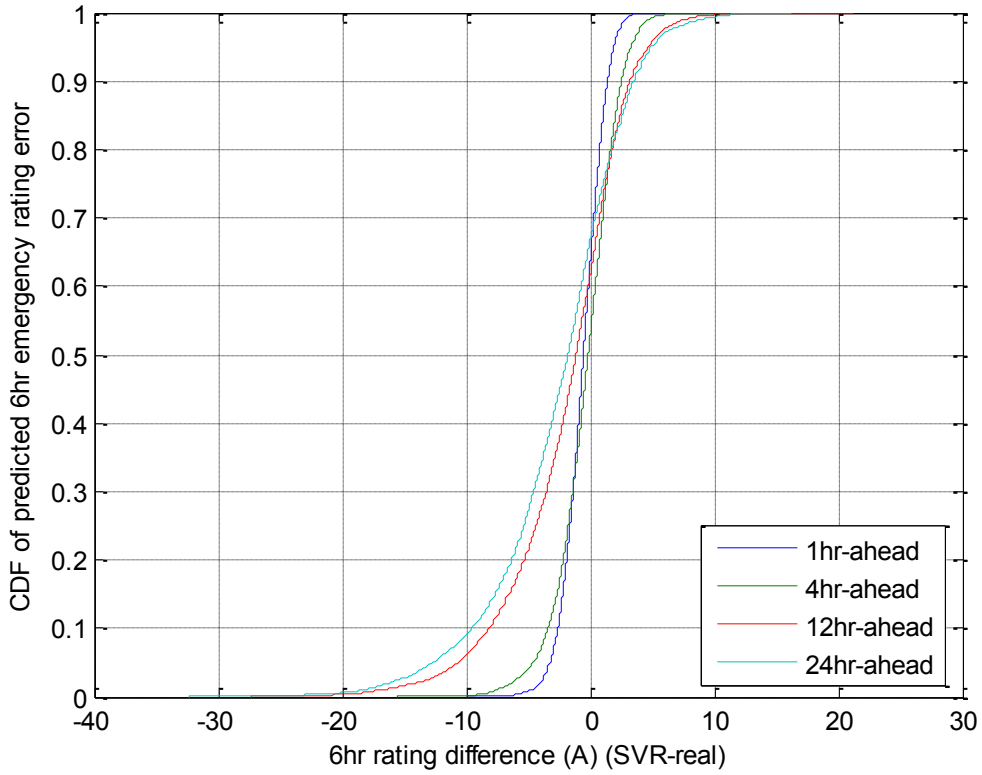

Figure 7.42 - CDF of different hour ahead SVR prediction errors for 6hr emergency rating

To further measure the accuracy of different hour ahead prediction, the probabilities of the predicted rating errors being contained within a certain range for 1hr, 4hr, 12hr and 24hr ahead prediction are calculated and presented in Figure 7.43. The blue, green and red bars show the probabilities of the predicted rating error being contained within ±5A, ±10A, ±20A respectively. For 1hr ahead prediction, 99.19% of the predicted rating errors are within ±5A and all the errors are within ±10A. For 24hr ahead prediction only 67.98% of the predicted rating errors are within ±5A, while most of the errors (99.39%) are within ±20A.

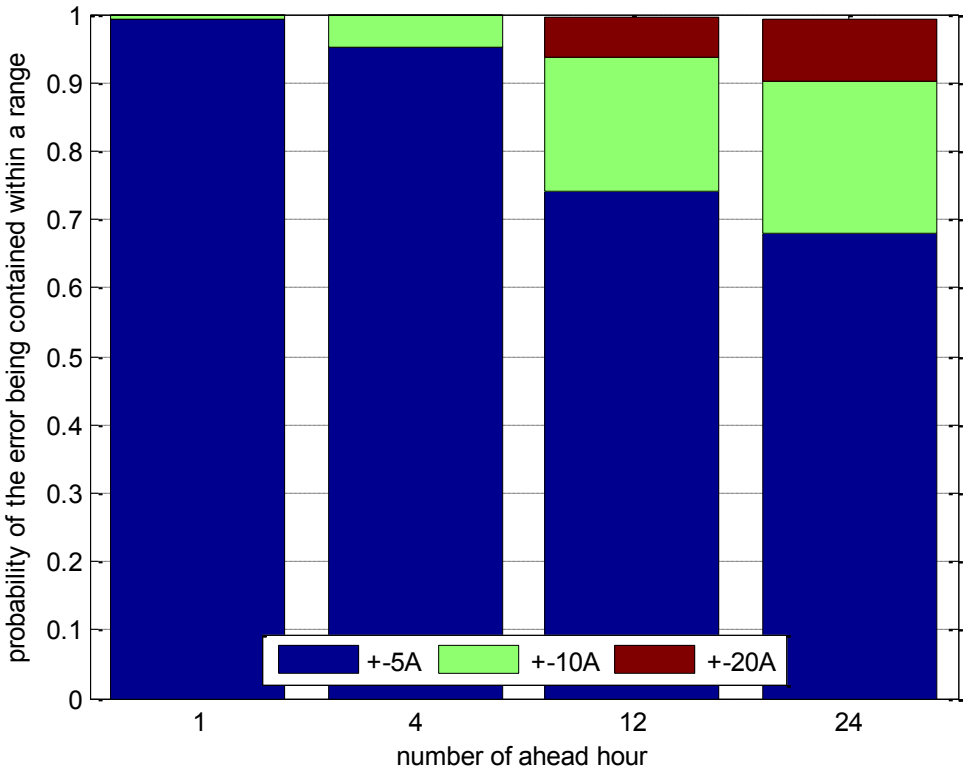

Figure 7.43 - Probability of rating error being contained within a range for different hour ahead prediction

7.6 Summary

With the advantage of fast solution speed, the Support Vector Regression (SVR) technique is applied to build models for the emergency rating calculation and prediction in this Chapter. Such feature makes SVR models capable of calculating large amounts of ratings at the same time.

SVR models have been tested for three different kinds of cable installations to calculate the emergency ratings. For buried cable, the historical load and accumulated historical load^2 data are used as input features, test results showed that all the 6hr emergency rating errors from the SVR model are contained within ±20A. For cable in air, the historical load and ambient air temperature data are used as input features. 96.7% of the 6hr emergency rating errors from the SVR model for cable in air are being contained within ±5A and 98.9% of the errors are being contained within ±10A. For the cable tunnel, the historical load, inlet air temperature and the tunnel section of maximum conductor temperature are used as input features. The probability of 6hr emergency rating errors being contained within ±40A is higher than 90% in this SVR model.

In addition, instead of using SVR to get the load prediction result and then calculating the cable temperature and rating with the load prediction, SVR models are applied to predict the day-ahead cable ratings directly. This idea has been tested for cable in air installation with the results presented in this Chapter. The prediction results from SVR models show that 99.19% of the predicted rating errors are within ±5A and all the errors are within ±10A for 1hr ahead prediction, and most of the errors (99.39%) are contained within ±20A for 24hr ahead prediction.

Chapter 8: Conclusions

This chapter concludes the thesis by summarising and analysing the contributions and the limitations of the developed methodologies. Based on these discussions, future work is proposed, which aims to improve the application of a predicted cable rating system onto the transmission network.

8.1 Research contribution

This thesis has presented a series of new cable rating concepts which are applicable to the operation of existing transmission networks. Potential benefits might be obtained when the penetration of intermittent renewable generation and load demand grows within the network.

The most important contribution in this work is to create a novel cable rating concept, Predicted Cable Rating, which is able to predict the short-term emergency cable rating forward from any point within the next 24 hours. Such accurate short term current ratings at the day ahead stage has double benefits for network operators of reducing variations in the dynamic ratings which makes them difficult to plan with, while reducing the risk of thermally overloading the cable. Such a predicted rating system is built by integrating a day-ahead load forecasting system into the dynamic thermal model.

Dynamic thermal models for a predicted rating system with three kinds of cable circuit installations, including buried cable, cable in air and tunnel cables, were built in Chapter 3. Through the analysis and evaluation of existing methods, it was decided to use the Finite Difference Method (FDM) to build the dynamic thermal model for the cable rating system as FDM shows the best compromise between the accuracy and solution speed among all the investigated models (analytical models and FEA models). Several updates have been implemented of the FDM models to fulfil the requirements in predicted rating system. The dynamic thermal models for buried cable and cable in air were built by using FDM to calculate the transient cable temperature and rating with the consideration of real-time load and environmental conditions. Different convective heat transfer coefficients for different convection conditions have been applied on cable surface when the cable in air model was tested. Good accuracy can be observed by a laboratory experiment validation. The dynamic thermal model for tunnel cables is based on the model proposed by Pilgrim et al. [9], but the heat transfer coefficients on cable surface and tunnel surface were updated to adapt the model to the different ventilation methods and different cable and tunnel installations.

The day-ahead load prediction system presented in Chapter 4 was built by using Support Vector Regression (SVR) technique. With the assumption of only one circuit feeding into a local area without local power generation, a comprehensive test of SVR model has been done to find the best way to predict load 24hrs ahead. Emphasis is placed on selecting inputs to the feature vector to keep computational time as low as possible, while delivering high quality predictions. Such an SVR model is able to predict the load demand from 1 hour ahead to 24 hour ahead at every step with the Mean Absolute Percentage Error (MAPE) within the range of 1.5 (for 1hr-ahead prediction) to 4 (for 24hr-ahead prediction).

With the load being predicted 24 hours ahead at each step, the cable temperature can be predicted 24 hours ahead by applying the load prediction into dynamic thermal model. Thus, the predicted rating system is able to achieve the short-term emergency cable ratings prediction forward from any point within the next 24 hours at each step. During the predicted rating process, the load prediction error will result in a cable temperature prediction error, hence the rating prediction will deviate from the real rating value. In order to give system operator confidence to implement the predicted rating algorithm, an error estimation system has been developed and integrated in the model to quickly detect the possible rating errors. Such a system was built by using the exponentially weighted moving average (EWMA) equation to consider the relation between accumulated load prediction error and cable temperature error, and a Multiple Linear Regression (MLR) model to directly link load prediction error and the predicted rating error. Thus, the predicted rating error can be estimated quickly without using the dynamic thermal model and this information can be used to correct the predicted rating results.

The predicted rating algorithm has been demonstrated by a lab experiment of a cable in air installation with of natural convection and shielded from solar radiation. The comparison shows that the FDM model can provide accurate conductor temperatures with the results located within the range of measurement data. The accuracy of the 3hr emergency rating calculation from FDM model has been proved by showing the errors being contained within 9A, which is less than 0.5% of the rating values. One case of day-ahead predicted rating was demonstrated in the experiment and the results of conductor temperature prediction and 3hr emergency rating prediction showed good accuracy. In this case, the 3hr emergency rating prediction errors were contained within 7A when the air temperature prediction is not ideal, while the predicted rating errors are all contained within 1A when the air temperature prediction is accurate.

SVR models have been built to calculate the dynamic cable rating for different kinds of cable installation in Chapter 7. Instead of calculating the cable temperature and rating by using a dynamic thermal model, the direct calculation of cable ratings by using SVR shows great advantage in solution speed. For directly buried cable, the solution time by the SVR model (2

seconds for 8760 steps) is much faster than FDM model (5.5 hours for 8760 steps). Thus, the solution time for emergency rating calculation can be dramatically reduced when a large number of cable circuits are considered in the transmission network. The predicted rating algorithm requires more solution time by the dynamic thermal model as more ratings need to be calculated at each step. In order to solve this problem, a SVR model has been built to directly predict the cable ratings day-ahead. A test has been done to predict the ratings 24 hour ahead for cable in air by using SVR model directly. The results show that for 1hr ahead prediction, 99.19% of the predicted rating errors are within ±5A and all the errors are within ±10A. For 24hr ahead prediction most of the errors (99.39%) are within ±20A.

8.2 Recommendations for further work

Although several contributions have been made in this work, a number of areas have been identified where potential improvements and applications could be achieved in further work.

The studies of rating calculation in this work only focus on insulated power cable. However, to implement the dynamic rating system and predicted rating system in the whole transmission system, the other parts of the network (transformers, overhead lines, circuit breakers, etc.) should be concerned as they might also be the limitation of the rating for the whole system. In addition, a survey might be necessary for each circuit to detect the potential hot spot along the circuit, as the FDM models used in this work for buried cable and cable in air are only to calculate the temperature of a cross-section. It is unpractical to build a 3D model for the whole circuit as it requires very long time to solve the model. The use of Distributed Temperature Sensor (DTS) systems for some newly installed cables has the advantage to detect the real-time hot spot. Thus, the rating system can be built by several models with typical environments along the circuit and an adaptive control system can be used to choose the suitable model at each step according to the DTS results.

The FDM dynamic thermal models built in this project are basic models for three kinds of cable installations (buried cable, cable in air and tunnel cables). Due to the inherent limitations of the FDM model, several assumptions still exist in order to obtain the best compromise between the accuracy and solution speed. For buried cables, the consideration of moisture migration in the soil and the convection on the ground surface in the future models might have benefit for shallow buried cable. For the cable in air model, although the model results show a good agreement with the average values from measurement data, more advanced methods (for example Computational Fluid Dynamics) might need to be applied to further examine the accuracy FDM model in different ambient environment. In addition, to examine the accuracy of

tunnel cable system, especially the convective heat transfer coefficients on cable surface and tunnel wall, real-time measurement data from experimental validation are required.

The load prediction system in this work is to forecast the local load demand in an area, which is under the assumption of only one circuit feeding into a local area without power generation. However, the loading of one transmission circuit relates to a lot of factors. So a method for predicting load as a function of adjacent circuit and local generation behaviour needs to be further developed.

The predicted rating system developed in this work considers both the load forecasting and air temperature forecasting (assumed to be available) when the cable rating is being predicted. This would be sufficient for some basic cable installation in idea condition. In some cases, the FDM technique is not suitable to simulate the complex thermal condition at the hot spot, for example cable joints or cable crossing. For such situations, FEM techniques might be necessary. In some other cases, only considering the load and air temperature data might not be sufficient to obtain an accurate cable rating. For example, the shallow buried cable or cable in air in a windy area, the wind speed will be essential for the cable rating as the convection on ground surface or cable surface will be an important way of thermal dissipation in the model.

In addition, the predicted rating system can be integrated into the work of power system planning, considering the cost of the prediction uncertainty and the reduction of the tariff by applying this system, an optimization study can be used to find the best way to use the predicted rating algorithm in power system planning and calculate the potential benefit from it.

Appendices

Appendix 1. Test results of forced cooling models for cable in air

Five models have been built to test their performance under the circumstance of forced cooling with real-time input data:

1) FDM model with forced cooling heat transfer coefficient from Electra 143 (FDM_ Electra 143)
2) FDM model with forced cooling heat transfer coefficient from Morgan (FDM_Morgan)
3) FDM model with forced cooling heat transfer coefficient from IEEE 738 (FDM_IEEE738)
4) FEA model with forced cooling heat transfer coefficient from Morgan (FEA_Morgan)
5) FEA model with forced cooling heat transfer coefficient from IEEE 738 (FEA_IEEE738)

The test results of first 14 days are shown in Figure A.8.1:

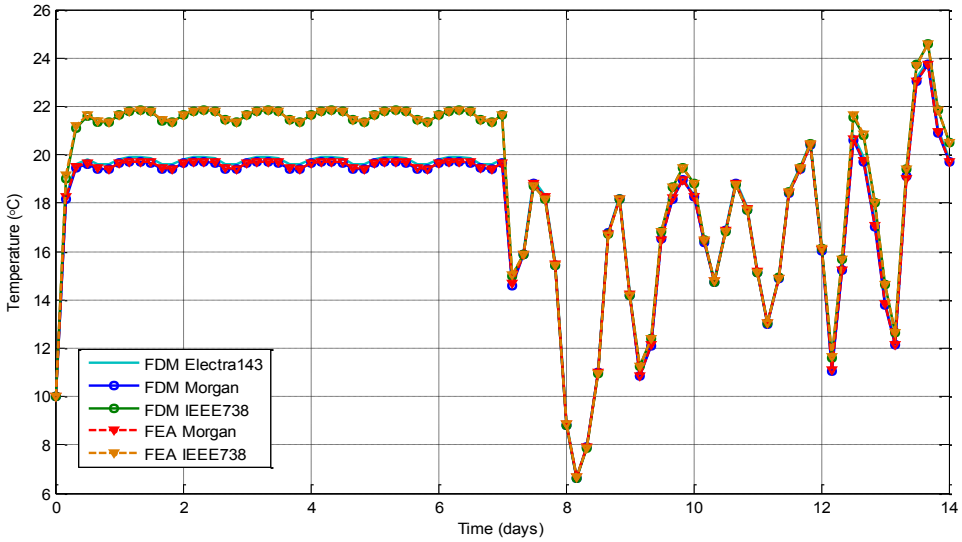

Figure A.8.1 - Conductor temperatures from different forced cooling model

From Figure A.8.1, the following features can be observed:

1) In common with the results from natural cooling model, results from Electra 143 and FEA model with the same heat transfer coefficient match very well. The maximum conductor temperature difference between the Electra 143 model and FEA model using Morgan's heat transfer coefficient and IEEE 738 heat transfer coefficient are 0.38°C and 0.36°C respectively. The Electra 143 based model is thus preferable due to its shorter solution time.
2) Simulation results of the original Electra 143 model and the Electra 143 model with Morgan's heat transfer coefficient also have great similarity degree. The maximum conductor temperature difference is 0.92°C, with a 0.18°C average difference during the 67 days' test.

3) The conductor temperatures calculated by the IEEE 738 model are slightly different to the other models. This is because only the IEEE 738 method considers the wind direction in heat transfer coefficient. Figure A.8.2 shows the conductor temperature difference between the IEEE 738 and the Electra 143 model as well as the real-time wind direction. A tight relation can be found between these two data, when the wind direction changes, the temperature differences fluctuate and when the wind direction equal to 90deg or 270deg, the temperature difference is almost zero.

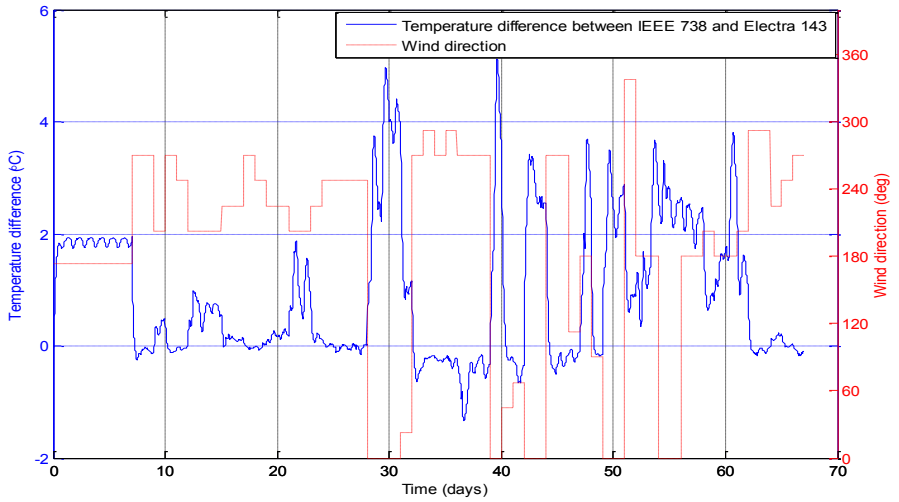

Figure A.8.2 - Temperature difference between IEEE738 and Electra143 model due to wind direction

Three models including FDM_Electra 143 model, FDM_Morgan model and FDM_IEEE 738 model are used to calculate emergency ratings for the forced cooling case. The ambient temperature is assumed as a constant value of 10°C and the intensity of the direct solar beam on a surface normal to the beam is assumed as 1000W·m^{-2}. The wind speed is assumed as 3ms^{-1} and the wind direction is parallel to the cable axis. Emergency rating results for the four points in Figure 3.11 are shown in Table A.1:

Table A.1 - Emergency rating for point 1-4 in forced cooling models

Rating	**1hr rating (A)**			**6hr rating (A)**			**24hr rating (A)**		
Models	IEC	FDM_ Morgan	FDM_ IEEE738	IEC	FDM_ Morgan	FDM_ IEEE738	IEC	FDM_ Morgan	FDM_ IEEE738
Point 1	5584	5586	5554	3578	3596	3359	3451	3475	3146
Point 2	5199	5207	5149	3559	3577	3328	3451	3475	3146
Point 3	5413	5417	5373	3567	3585	3340	3451	3475	3146
Point 4	4921	4937	4804	3547	3567	3304	3451	3475	3146

From Table A.1, it is possible to identify the following features:

I. The result from FDM_Electra143 model and FDM_Morgan model are similar, with the ratings from FDM_Morgan model being slightly. The maximum difference is 16A, 20A and 24A for 1hr, 6hr and 24hr ratings respectively.

II. The result from FDM_IEEE738 model is slightly lower than the other two models. This is because of the wind direction factor in IEEE738 convective heat transfer coefficient equation. When the wind direction is parallel to cable axis, FDM_IEEE738 model will get a higher conductor temperature than other two models. As a result, the emergency ratings will be lower.

III. In common with the natural cooling model, point 2 and point 3 in forced cooling models have different emergency rating with the same preload level due to the different loading history.

Appendix 2. Cable thermal test experiment control system

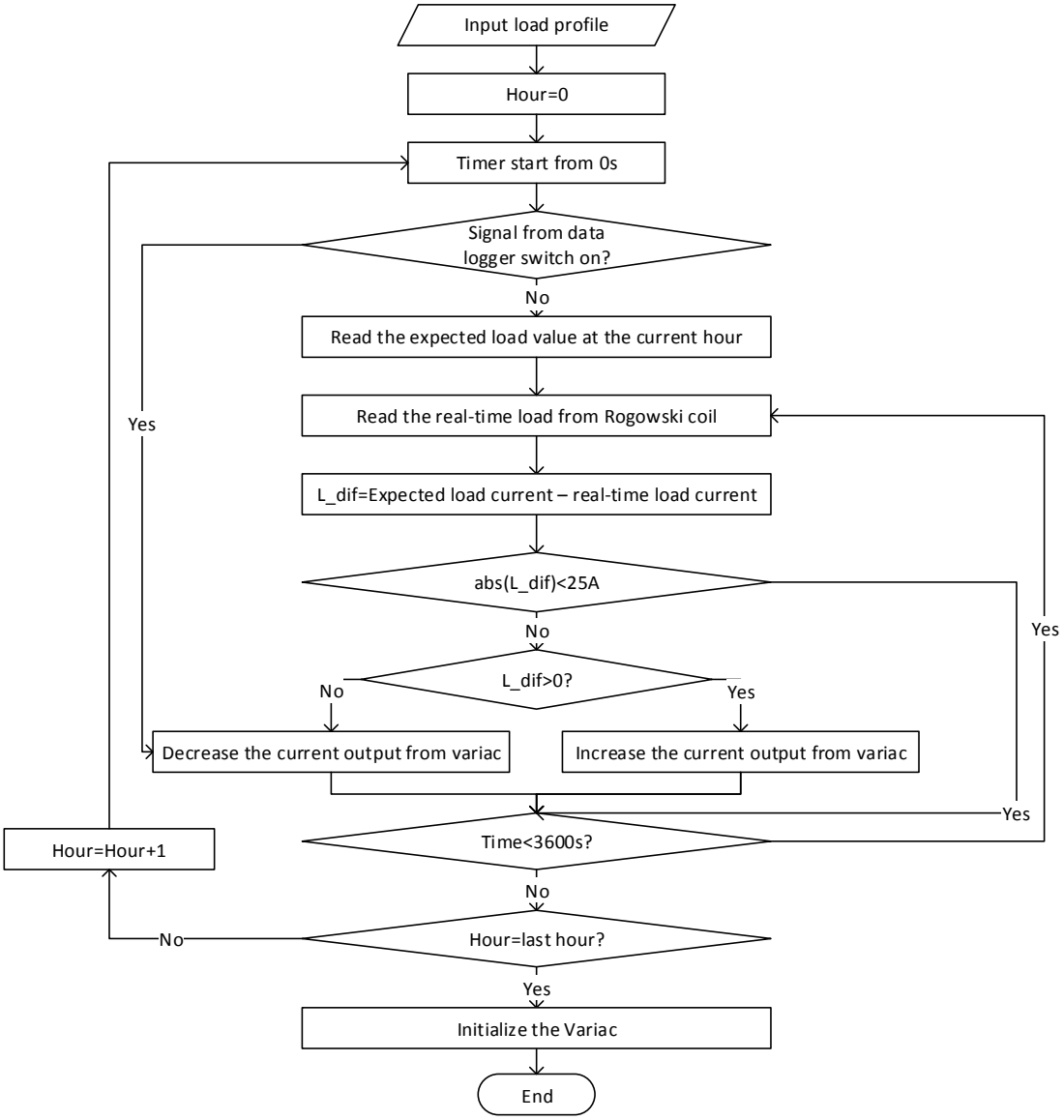

Figure A.8.3 – Flowchart of cable thermal experiment control system

List of References

[1] A. Ipakchi and F. Albuyeh, "Grid of the future," *IEEE Power Energy Mag.*, vol. 7, no. 2, pp. 52–62, Mar. 2009.

[2] Y. Wang, H. Nazaripouya, C.-C. Chu, R. Gadh, and H. R. Pota, "Vehicle-to-grid automatic load sharing with driver preference in micro-grids," in *IEEE PES Innovative Smart Grid Technologies, Europe*, 2014, pp. 1–6.

[3] B. Clairmont, "EPRI Increased Power Flow Gridebook," 2010.

[4] T. Shimakage, K. Wu, T. Kato, T. Okamoto, and Y. Suzuoki, "Economic Evaluation of Cable Replacement Considering Annual Failure Probability," in *Conference Record of the 2002 IEEE International Symposium on Electrical Insulation, Boston, MA USA, April 7-10,* 2002, pp. 472–475.

[5] D. J. Swaffield, P. L. Lewin, and S. J. Sutton, "Methods for Rating Directly Buried High Voltage Cable Circuits," *IET Gener. Transm. Distrib.*, vol. 2, no. 3, pp. 393– 401, 2008.

[6] F. de Leon and G. J. Anders, "Effects of Backfilling on Cable Ampacity Analyzed With the Finite Element Method," *IEEE Trans. Power Deliv.*, vol. 23, no. 2, pp. 537–543, 2008.

[7] G. Anders, *Rating of Electric Power Cable: Ampacity Computations for Transmission, Distribution, and Industrial Applications*. McGRAW-HILL, 1997.

[8] P. L. Lewin, J. E. Theed, A. E. Davies, and S. T. Larsen, "Method for Rating Power Cables Buried in Surface Troughs," *IEE Proc. Gener. Transm. Distrib.*, vol. 146, no. 4, pp. 360–364, 1999.

[9] J. A. Pilgrim, D. J. Swaffield, P. L. Lewin, S. T. Larsen, F. Waite, and D. Payne, "Rating Independent Cable Circuits in Forced-Ventilated Cable Tunnels," *IEEE Trans. Power Deliv.*, vol. 25, no. 4, pp. 2046–2053, 2010.

[10] M. Knights, J. L. R. Mathews, and R. Marshall, "Revealed: London's Network of Power Tunnels," *Proc. ICE Civ. Eng.*, vol. 144, no. 3, pp. 121–127, 2001.

[11] H. J. Li, K. C. Tan, Q. Su, and S. Member, "Assessment of Underground Cable Ratings Based on Distributed Temperature Sensing," *Power Deliv. IEEE Trans.*, vol. 21, no. 4, pp. 1763–1769, 2006.

[12] S. P. Walldorf, J. S. Engelhardt, and F. J. Hoppe, "The Use of Real-Time Monitoring and Dynamic Ratings for Power Delivery Systems and the Implications for Dielectric Materials," *IEEE Electr. Insul. Mag.*, vol. 15, no. 5, pp. 28–33, 1999.

[13] B. Leyland, "Auckland Central and Business District Supply and Failure: the Ministerial Inquiry," *Power Eng. J.*, vol. 12, no. 6, pp. 269–273, 1998.

[14] "IEC 60287. Electric cables. Calculation of the current rating - part 1-1: Current rating equations (100% load factor) and calculation of losses - general," 2006.

[15] "IEEE Std 835 - Standard Power Cable Ampacity Tables," 1994.

[16] G. Moore, *Electric Cables Handbook*, 3rd ed. Blackwell Science, 1997.

[17] A. E. Kennelly, "Current Carrying Capacity of Electric Cables, Submerged, Buried or Suspended in the Air," *Electr. World*, pp. 22–183, 1893.

[18] G. M, "Über die wärmeleitung in einem verteilten kabel," *Elektroteche Zeutscgruft*, p. 137, 1905.

[19] J. Neher and M. McGrath, "The Calculation of the Temperature Rise and Load Capability of Cable Systems," *Power Appar. Syst. Part III. Trans. Am. Inst. Electr. Eng.*, vol. 76, no. 3, pp. 752–764, 1957.

[20] "IEC 60287. Electric cables. Calculation of the current rating - part 2: Thermal resistance. Section 2.1 Calculation of thermal resistance," 1994.

[21] D. A. Douglass and A.-A. Edris, "Real-time Monitoring and Dynamic Thermal Rating of Power Transmission Circuits," *IEEE Trans. Power Deliv.*, vol. 11, no. 3, pp. 1407–1418, Jul. 1996.

[22] K. L. Ho, Y.-Y. Hsu, and C.-C. Yang, "Short Term Load Forecasting Using A Multilayer Neural Network with An Adaptive Learning Algorithm," *IEEE Trans. Power Syst.*, vol. 7, no. 1, pp. 141–149, 1992.

[23] D. S. Freitas and A. T. Prata, "Thermal Performance of Underground Power Cables with Constant and Cyclic Currents in Presence of Moisture Migration in the Surrounding Soil," *Power Deliv. IEEE Trans.*, vol. 11, no. 3, pp. 1159–1170, 1996.

[24] "IEC 60853. Electric cables. Calculation of the cyclic and emergency current rating of cables. part 2: Cyclic rating of cables greater than 18/30 (36)kV and emergency ratings for cables of all voltages," 1989.

[25] H. Goldenberg, "The Calculation of Cyclic Rating Factors and Emergency Loading for One or More Cables Laid Direct or in Ducts," *Proc. IEE - Part C Monogr.*, vol. 105, no. 7, pp. 46–54, 1958.

[26] “Electra 24 - Current Ratings of Cables for Cyclic and Emergency Loads. Part 1 Cyclic Ratings (Load Factor Less Than 100%) and Response to a Step Function,” 1972.

[27] “Electra 44 - Current Rating of Cables for Cyclic and Emergency Loads. Part 2 Emergency Ratings and Short Duration Response to a Step Function.,” 1976.

[28] “Electra 66 - The calculation of continuous ratings for forced-cooled cables,” 1979.

[29] “Electra 87 - Computer method for the calculation of the response of single-core cables to a step function thermal transient,” 1983.

[30] “Electra 104 - Forced cooled cables rating calculation of thermal transients and cyclic loads,” 1986.

[31] “Electra 143 - Calculation of temperatures in ventilated cable tunnels,” 1992.

[32] S.-H. Huang, W.-J. Lee, and M.-T. Kuo, “An Online Dynamic Cable Rating System for an Industrial Power Plant in the Restructured Electric Market,” *IEEE Trans. Ind. Appl.*, vol. 43, no. 6, pp. 1449–1458, 2007.

[33] T. Igi, H. Komeda, and S. Mashio, “Study of the Dynamic Rating of a 138kV XLPE Cable System by Optical Fiber Monitoring,” in *8th International Conference on Insulated Power Cables*, 2011, p. C.9.4.

[34] J. S. Lyall, “Cable On-line Monitoring Analysis,” *Australas. Power Technol. Transm. Distrib.*, pp. 16–18, 2012.

[35] H. C. Zhao, J. S. Lyall, and G.Nourbakhsh, “Probabilistic Cable Rating Based on Cable Thermal Environment Studying,” in *Power System Technology, 2000. Proceedings. PowerCon 2000. International Conference on*, 2000, pp. 1071–1076.

[36] J. S. Lyall, G. Nourbakhsh, and H. C. Zhao, “Underground Power Cable Environment On-line Monitoring and Analysis,” in *2000 Power Engineering Society Summer Meeting Cat No00CH37134*, 2000, vol. 1, pp. 457–462.

[37] G. J. Anders, A. Napieralski, S. M. Zubert, and M. Orlikowski, “Advanced Modeling Techniques for Dynamic Feeder Rating Systems,” *Ind. Appl. Conf. 2002. 37th IAS Annu. Meet. Conf. Rec.*, vol. 2, pp. 1012–1019, 2002.

[38] H. Brakelmann, H. Hirsch, A. Rohrich, H.-P. Scheiffarth, and J. Stammen, “Aadptive Monitoring Program for Dynamic Thermal Rating of Power Cables,” in *7th International Conference on Insulated Power Cables*, 2007, p. C5.2.3.

[39] M. Terracciano, S. Purushothaman, and F. de León, “Calculation of Cable Thermal Rating Considering Non-isothermal Earth Surface,” *IET Gener. Transm. Distrib.*, vol. 8,

no. 7, pp. 1354–1361, Jul. 2014.

[40] J. a Pilgrim, D. J. Swaffield, P. L. Lewin, S. T. Larsen, and D. Payne, "Assessment of the Impact of Joint Bays on the Ampacity of High Voltage Cable Circuits," *IEEE Trans. Power Deliv.*, vol. 24, no. 3, pp. 1029–1036, 2009.

[41] D. J. Swaffield, P. L. Lewin, D. Payne, and S. T. Larsen, "Effects of Modelling Assumptions on the Rating Calculation for Externally Forced Cooled High-voltage Cables," *IET Gener. Transm. Distrib.*, vol. 3, no. 5, pp. 496–507, 2009.

[42] E. F. Steennis, S. M. Berlijn, F. H. de Wild, F. van den Boogaard, C. G. N. de Jong, M. J. M. van Riet, and G. P. T. van de Wijk, "Learning from High-voltage XLPE Cable System Testing and Monitoring," *CIGRE 2000 21-203*, 2000.

[43] B. M. Weedy and J. P. Perkins, "Steady-state Thermal Analysis of A 400 kV-Cable Through Joint," *Proc. Inst. Electr. Eng.*, vol. 114, no. 1, pp. 109–115, Jan. 1967.

[44] S. H. Nam, J. M. Lee, K. Y. Kim, S. K. Lee, S. I. Jeon, H. L. Kim, Y. S. Kim, and H. E. Lim, "Application Results of Rreal-time Ampacity Estimation System and Intelligent Power Cable System," in *7th International Conference on Insulated Power Cables*, 2007, p. C5.2.2.

[45] R. Olsen, J. Holboell, and U. S. Gudmundsdottir, "Electrothermal Coordination in Cable Based Transmission Grids," *IEEE Trans. Power Syst.*, vol. 28, no. 4, pp. 4867–4874, Nov. 2013.

[46] E. Jacobsen, J. F. Nielsen, S. B. Nielsen, W. Nolden, K. Cohnen, A. Mohrs, and S. Seier, "Dynamic Rating of Transmission Cables," *CIGRE 2010 B1_101_2010*, 2010.

[47] R. S. Olsen and U. S. Gudmundsdottir, "Dynamic Temperature Estimation and Real Time Emergency Rating of Transmission Cables," in *2012 IEEE Power and Energy Society General Meeting*, 2012, pp. 1–8.

[48] S. T. Larsen, C. L. Ong-Hall, and P. L. Stephenson, "Cable Rating Methods Applied to A Real Time Cable System Monitor," in *Power Cables and Accessories 10kV - 500kV, 1993., Third International Conference on*, 1993, pp. 203–207.

[49] S. Walldorf, Steven P.; Ernst, A.; Pancholi, S., "A Cost Effective Solution for Increasing Ratings on Underground Transmission Cables-A Case Study," in *Transmission and Distribution Conference, IEEE*, 1999, pp. 32–37.

[50] B. Richard and J. Faires, *Numerical Analysis*, 9th editio. Boston: Cengage Learning, Inc, 2010.

[51] H. J. Li, "Estimation of Soil Thermal Parameters from Surface Temperature of Underground Cables and Prediction of Cable Rating," *Gener. Transm. Distrib. IEE*

Proc., vol. 152, no. 6, pp. 849–854, 2005.

[52] R. Adapa, D. A. Douglass, and N. D. Reppen, "Applying Dynamic Thermal Ratings in System Operations," *CIGRE 2006, C2-306*, pp. 1–8, 2006.

[53] J. M. A. Nuijten, A. Geschiere, J. C. Smit, and G. J. Frijmersum, "Future Network Planning and Grid Control," in *2005 International Conference on Future Power Systems*, 2005, pp. 1–7.

[54] J. C. Smit, R. Trekop, and F. H. D. Wild, "A Dynamic Rating System for An Existing 150kV Power Connection Consisting of An Overhead Line and An Underground Power Cable," *CIGRE 2006 B1-305*, pp. 1–9, 2006.

[55] F. de Wild, G.-J. Meijer, and G. Geerts, "Extracting More Value with Intelligent Cable Systems," *Transm. Distrib. World*, vol. 56, no. 8, pp. 22–29, 2004.

[56] F. de Leon and G. J. Anders, "Effects of Backfilling on Cable Ampacity Analyzed With the Finite Element Method," *IEEE Trans. Power Deliv.*, vol. 23, no. 2, pp. 537–543, Apr. 2008.

[57] H. S. Kim, S. I. Hong, and S. J. Kim, "On the Rule of Mixtures for Predicting the Mechanical Properties of Composites with Homogeneously Distributed Soft and Hard Particles," *J. Mater. Process. Technol.*, vol. 112, no. 1, pp. 109–113, May 2001.

[58] S. Whitehead and E. E. Hutchings, "Current Rating of Cables for Transmission and Distribution," *J. Inst. Electr. Eng.*, vol. 83, no. 502, pp. 517–557, Oct. 1938.

[59] V. T. Morgan, "Effect of Surface-Temperature Rise on External Thermal Resistance of Single-core and Multi-core Bundled Cables in Still Air," *IEE Proc. - Gener. Transm. Distrib.*, vol. 141, no. 3, pp. 215–218, 1994.

[60] V. T. Morgan, "The Thermal Rating of Overhead-line Conductors Part I. The Steady-state Thermal Model," *Electr. Power Syst. Res.*, vol. 5, no. 2, pp. 119–139, Jun. 1982.

[61] V. T. Morgan, "Effect of Mixed Convection on the External Thermal Resistance of Single-core and Multicore bundled Cables in Air," *Gener. Transm. Distrib. IEE Proc.*, vol. 139, no. 2, pp. 109–116, 1992.

[62] "IEEE 738 Standard for Calculating the Current-Temperature of Bare Overhead Conductors." pp. c1–59, 2007.

[63] K. E. House and P. D. Tuttle, "Current-carrying Capacity of ACSR," *Electr. Eng.*, vol. 77, no. 8, pp. 719–719, Aug. 1958.

[64] "Transmission Conductors Thermal Ratings." Transmission Advisory Panel, East

Central Area Reliability Coordination Agreement, p. TAP–28, 2005.

[65] "Ray's Weather Station." [Online]. Available: http://www.riverman.gotdns.com/weather.html. [Accessed: 05-Jan-2013].

[66] "IEC 60287. Electric cables. Calculation of the current rating. part 2. section 2: A method for calculating reduction factors for groups of cables in free air, protected from solar radiation," 1995.

[67] B. M. Weedy, *Thermal Design of Underground Systems*. Southampton: John Wiley & Sons, 1988.

[68] R. K. Rajput, *Heat & Mass Transfer (M.E.)*. S. Chand, 2007.

[69] J. R. Dyer, "Natural-convective Flow Through a Vertical Duct with A Restricted Entry," *Int. J. Heat Mass Transf.*, vol. 21, no. 10, pp. 1341–1354, Oct. 1978.

[70] B.-J. Chen, M.-W. Chang, and C.-J. Lin, "Load Forecasting Using Support Vector Machines: A Study on EUNITE Competition 2001," *IEEE Trans. Power Syst.*, vol. 19, no. 4, pp. 1821–1830, Nov. 2004.

[71] S. Fan and L. Chen, "Short-Term Load Forecasting Based on an Adaptive Hybrid Method," *IEEE Trans. Power Syst.*, vol. 21, no. 1, pp. 392–401, Feb. 2006.

[72] M. Daneshdoost, M. Lotfalian, G. Bumroonggit, and J. P. Ngoy, "Neural Network with Fuzzy Set-based Classification for Short-term Load Forecasting," *IEEE Trans. Power Syst.*, vol. 13, no. 4, pp. 1386–1391, 1998.

[73] R.-H. Liang and C.-C. Cheng, "Combined Regression-Fuzzy Approach for Short-term Load Forecasting," *IEE Proc. - Gener. Transm. Distrib.*, vol. 147, no. 4, pp. 261–266, 2000.

[74] S. H. Ling, F. H. F. Leung, H. K. Lam, and P. K. S. Tam, "Short-term Electric Load Forecasting Based on A Neural Fuzzy Network," *IEEE Trans. Ind. Electron.*, vol. 50, no. 6, pp. 1305–1316, Dec. 2003.

[75] G. Gross and F. D. Galiana, "Short-term Load Forecasting," *Proc. IEEE*, vol. 75, no. 12, pp. 1558–1573, 1987.

[76] P. B. Luh, L. D. Michel, M. A. Coolbeth, P. B. Friedland, and S. J. Rourke, "Short-Term Load Forecasting: Similar Day-Based Wavelet Neural Networks," *IEEE Trans. Power Syst.*, vol. 25, no. 1, pp. 322–330, Feb. 2010.

[77] T. Hong, P. Wang, and H. L. Willis, "A Naïve Multiple Linear Regression Benchmark for Short Term Load Forecasting," in *2011 IEEE Power and Energy Society General*

Meeting, 2011, pp. 1–6.

[78] M. T. Hagan and S. M. Behr, "The Time Series Approach to Short Term Load Forecasting," *IEEE Trans. Power Syst.*, vol. 2, no. 3, pp. 785–791, 1987.

[79] B. Krogh, E. De Llinas, and D. Lesser, "Design and Implementation of An on-Line Load Forecasting Algorithm," *IEEE Trans. Power Appar. Syst.*, vol. PAS-101, no. 9, pp. 3284–3289, Sep. 1982.

[80] J. Y. Fan and J. D. McDonald, "A Real-time Implementation of Short-Term Load Forecasting for Distribution Power Systems," *IEEE Trans. Power Syst.*, vol. 9, no. 2, pp. 988–994, May 1994.

[81] M. Y. Cho, J. C. Hwang, and C. S. Chen, "Customer Short Term Load Forecasting by Using ARIMA Transfer Function Model," in *Proceedings 1995 International Conference on Energy Management and Power Delivery EMPD '95*, 1995, vol. 1, pp. 317–322.

[82] B. Krough, E. S. de Llinas, and D. Lesser, "Design and Implementation of an On-Line Load Forecasting Algorithm," *IEEE Power Eng. Rev.*, vol. PER-2, no. 9, pp. 47–47, Sep. 1982.

[83] T. M. Peng, N. F. Hubele, and G. G. Karady, "Advancement in the Application of Neural Networks for Short-term Load Forecasting," *IEEE Trans. Power Syst.*, vol. 7, no. 1, pp. 250–257, 1992.

[84] H. S. Hippert, C. E. Pedreira, and R. C. Souza, "Neural Networks for Short-term Load Forecasting: A Review and Evaluation," *IEEE Trans. Power Syst.*, vol. 16, no. 1, pp. 44–55, 2001.

[85] A. D. Papalexopoulos, "An Implementation of A Neural Network Based Load Forecasting Model for the EMS," *IEEE Trans. Power Syst.*, vol. 9, no. 4, pp. 1956–1962, 1994.

[86] Y.-Y. Hsu and Chien-Chuen Yang, "Design of Artificial Neural Networks for Short-term Load Forecasting. II. Multilayer Feedforward Networks for Peak Load and Valley Load Forecasting," vol. 138, no. 5. pp. 414–418, 1991.

[87] A. D. Papalexopoulos and T. C. Hesterberg, "A Regression-based Approach to Short-term System Load Forecasting," *IEEE Trans. Power Syst.*, vol. 5, no. 4, pp. 1535–1547, 1990.

[88] Y. Freund, "Boosting a Weak Learning Algorithm by Majority," *Inf. Comput.*, vol. 121, no. 2, pp. 256–285, Sep. 1995.

[89] R. E. Schapire, "The Strength of Weak Learnability," *Mach. Learn.*, vol. 5, no. 2, pp.

197–227, Jun. 1990.

[90] S. Ben Taieb and R. J. Hyndman, "A Gradient Boosting Approach to The Kaggle Load Forecasting Competition," *Int. J. Forecast.*, vol. 30, no. 2, pp. 382–394, Apr. 2014.

[91] J. R. Lloyd, "GEFCom2012 Hierarchical Load Forecasting: Gradient Boosting Machines and Gaussian Processes," *Int. J. Forecast.*, vol. 30, no. 2, pp. 369–374, Apr. 2014.

[92] V. Vapnik and A. Lerner, "Pattern Recognition Using Generalized Portrait Method," *Autom. Remote Control*, no. 24, pp. 774–780, Jan. 1963.

[93] V. Vapnik and A. Chervonenkis, "A Note on One Class of Perceptrons," *Autom. Remote Control*, vol. 25, no. 1, p. 103, Jan. 1964.

[94] V. Vapnik and S. Kotz, *Estimation of Dependences Based on Empirical Data*. Springer Science & Business Media, 2006.

[95] V. Vapnik, *The Nature of Statistical Learning Theory*. Springer Science & Business Media, 2000.

[96] N. Cristianini and J. Shawe-Taylor, *An Introduction to Support Vector Machines and Other Kernel-based Learning Methods*. Cambridge University Press, 2000.

[97] C.-C. Chang and C.-J. Lin, "LIBSVM," *ACM Trans. Intell. Syst. Technol.*, vol. 2, no. 3, pp. 1–27, Apr. 2011.

[98] M. Mohandes, "Support Vector Machines for Short-term Electrical Load Forecasting," *Int. J. Energy Res.*, vol. 26, no. 4, pp. 335–345, Mar. 2002.

[99] T. Hong, P. Pinson, and S. Fan, "Global Energy Forecasting Competition 2012," *Int. J. Forecast.*, vol. 30, no. 2, pp. 357–363, Apr. 2014.

[100] T. Senjyu, H. Takara, K. Asato, K. Uezato, and T. F. Funabashi, "Next Day Load Curve Forecasting Using Hybrid Correction Method," in *IEEE/PES Transmission and Distribution Conference and Exhibition*, 2002, vol. 3, pp. 1701–1706.

[101] ABB, "XLPE Land Cable Systems - User's Guide."

[102] Y. Wang, Q. Xia, and C. Kang, "Secondary Forecasting Based on Deviation Analysis for Short-Term Load Forecasting," *IEEE Trans. Power Syst.*, vol. 26, no. 2, pp. 500–507, May 2011.

[103] T. Hong, "Energy Forecasting : Past , Present , and Future," *Int. J. Appl. Forecast.*, no. 32, pp. 43–48, 2014.

[104] T. Hothorn, P. Bühlmann, T. Kneib, M. Schmid, and B. Hofner, "Model-based Boosting 2.0," *J. Mach. Learn. Res.*, vol. 11, pp. 2109–2113, Mar. 2010.

[105] W. N. Venables; D. M. Smith, "An Introduction to R," *User Man.*, vol. 1, 2009.

[106] X. Yan, *Linear Regression Analysis: Theory and Computing*. World Scientific, 2009.

[107] D. C. Montgomery, E. A. Peck, and G. G. Vining, *Introduction to Linear Regression Analysis*. John Wiley & Sons, 2012.

[108] T. M. Tritt, *Thermal Conductivity: Theory, Properties, and Applications*. Springer Science & Business Media, 2004.

[109] K. Yong Lee, J. Seok Yang, Y. Sung Choi, and D. Hee Park, "Specific Heat and Thermal Conductivity Measurement of XLPE Insulator and Semiconducting Materials," in *2006 IEEE 8th International Conference on Properties and applications of Dielectric Materials*, 2006, pp. 805–809.